FIRST SYNTHESES OF FLUOROMUSCIMOLS

Mohd Abdul Fatah Abdul Manan

A Thesis Submitted for the Degree of PhD
at the
University of St Andrews

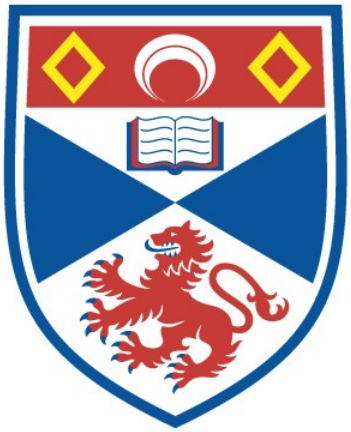

2017

First syntheses of fluoromuscimols

Mohd Abdul Fatah Abdul Manan

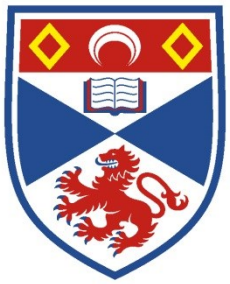

University of
St Andrews

This thesis is submitted in partial fulfilment for the degree of PhD
at the
University of St Andrews

2017

1. Candidate's declarations:

I, Mohd Abdul Fatah Abdul Manan, hereby certify that this thesis, which is approximately 36,800 words in length, has been written by me, and that it is the record of work carried out by me, or principally by myself in collaboration with others as acknowledged, and that it has not been submitted in any previous application for a higher degree.

I was admitted as a research student in September 2013 and as a candidate for the degree of PhD in September 2014; the higher study for which this is a record was carried out in the University of St Andrews between 2013 and 2017.

Date: _____ Signature of Candidate: _____

2. Supervisor's declaration:

I hereby certify that the candidate has fulfilled the conditions of the Resolution and Regulations appropriate for the degree of Doctor of Philosophy in the University of St Andrews and that the candidate is qualified to submit this thesis in application for that degree.

Date: _____ Signature of Supervisor: _____

3. Permission for publication:

In submitting this thesis to the University of St Andrews I understand that I am giving permission for it to be made available for use in accordance with the regulations of the University Library for the time being in force, subject to any copyright vested in the work not being affected thereby. I also understand that the title and the abstract will be published, and that a copy of the work may be made and supplied to any bona fide library or research worker, that my thesis will be electronically accessible for personal or research use unless exempt by award of an embargo as requested below, and that the library has the right to migrate my thesis into new electronic forms as required to ensure continued access to the thesis. I have obtained any third-party copyright permissions that may be required in order to allow such access and migration, or have requested the appropriate embargo below.

The following is an agreed request by candidate and supervisor regarding the publication of this thesis:

No embargo on print copy. No embargo on electronic copy.

Date: _____ Signature of Candidate: _____

Signature of Supervisor: _____

Acknowledgements

I would like to express my sincere thanks to my supervisor Professor David O'Hagan for offering me the opportunity to study and work in his group on such an interesting and challenging project, and for his guidance, comment, encouragement, support and unlimited help. I am very grateful to the entire O'Hagan group for their advice and assistance for chemistry matters were essential.

I also would like to express my appreciation to Dr David Cordes and Professor Alexandra Slawin for their contribution to the single crystal X-ray analyses. Many thanks also go to Dr Thomas Lebl and Mrs Melanja Smith for their help with the NMR. I am also thankful to Mrs Caroline Horsburgh and EPSRC National Mass Spectrometry Service, Swansea for mass spectrometry analyses. Not forgetting, our Australian collaborator at the University of Sydney in Australia, Professor Mary Collins for biological assays of fluoromuscimols and iodomuscimol.

I wish to extend my deepest gratitude to my family for their constant encouragement and support during all the years of my study. Finally, special thanks to Universiti Teknologi MARA and Ministry of Education of Malaysia for awarding me the scholarship.

Table of Contents

Abbreviations

μ	dipole moment
δ	nuclear magnetic resonance chemical shift parts per million downfield from a standard
ρ $GABA_A$	γ-aminobutyric acid type A rho
λ^3	trivalent
λ^5	pentavalent
$\{^{19}F\}$	fluorine decoupled
$\{^{1}H\}$	proton decoupled
18-Crown-6	1,4,7,10,13,16-hexaoxacyclooctadecane
3c-4e	3-centre 4-electron
Ac	acetyl
Ac_2O	acetic anhydride
AcOOH	peracetic acid
ACPCA	aminocyclopropanecarboxylic acid
AmOH	amyl alcohol
APCI	atmospheric pressure chemical ionisation
APS	aminopropanesulfonic acid
aq	aqueous
Ar	aryl
ATR	attenuated total reflectance
BBB	blood brain barrier
BBFO	broad band fluorine observation
BMS	borane dimethyl sulfide
Boc	*tert*-butyloxycarbonyl
Boc_2O	di-*tert*-butyl dicarbonate
br s	broad singlet
Bu	butyl
BuLi	butyl lithium
BZD	benzodiazepine
ca.	approximately
CA1-3	subfield of hippocampus

CACA	*cis*-4-aminocrotonic acid
CACP	*cis*-3-aminocyclopentane-1-carboxylic acid
CAMP	*cis*-2-aminomethylcyclopropane-1-carboxylic acid
CB1	cannabinoid receptor type 1
CB2	cannabinoid receptor type 2
cGMP	current good manufacturing practices
CIF	crystallographic information file
conc.	concentrated
CNS	central nervous system
cRNAs	cloned ribonucleic acids
CSA	camphorsulfonic acid
CT	computerised tomography
d	doublet
DBU	1,8-diazabicycloundec-7-ene
DCE	dichloroethene
DCM	dichloromethane
dd	doublet of doublets
dec.	decomposition
DEPT	distortionless enhancement by polarisation transfer
DHM	dihydromuscimol
dm	doublet of multiplets
DMAP	*N*,*N*-dimethylaminopyridine
DMF	*N*,*N*-dimethylformamide
DMP	Dess-Martin periodinane
DMSO	dimethyl sulfoxide
EC	electron capture
EC_{50}	concentration requires to produce 50% of the response in E_{max}
EDG	electron-donating group
E_{max}	maximal current produced by a saturating concentration of the agonist
eq	equivalent
ESI	electron spray ionisation
Et	ethyl

EWG	electron-withdrawing group
[^{18}F]AH114726	ethyl 7-[^{18}F]fluoro-5-methyl-6-oxo-3a,4,5,6-tetrahydro-3H-benzo[f]imidazo[1,5-a][1,4]diazepine-3-carboxylate
[^{18}F]FAZA	[^{18}F]fluoroazomycinarabinofuranoside
[^{18}F]CB91	*N*-(4-methylcyclohexyl)-1-(4-[^{18}F]fluorobenzyl)-2-oxo-1,2-dihydro-1,8-naphthyridine-3-carboxamide
FDA	the food and drug administration
[^{18}F]DAA1106	*N*-(2,5-dimethoxybenzyl)-*N*-(5-[^{18}F]fluoro-2-phenoxyphenyl)acetamide
[^{18}F]FDG	2-[^{18}F]fluoro-2-deoxy-D-glucose
[^{18}F]FEFMZ	(5-2'-[^{18}F]fluoroethyl)-5-desmethylflumazenil
FEP	fluorinated ethylene propylene
[^{18}F]FFMZ	(3-2'-[^{18}F]fluoro)-flumazenil
F-GABA	fluoro-γ-aminobutyric acid
[^{18}F]GEH120348	*tert*-butyl 7-[^{18}F]fluoro-5-methyl-6-oxo-3a,4,5,6-tetrahydro-3H-benzo[f]imidazo[1,5-a][1,4]diazepine-3-carboxylate
FIBX	2-iodoxy-3,4,5,6-tetrafluorobenzoic acid
[^{18}F]FLT	3'-deoxy-3'-[^{18}F]fluorothymidine
[^{18}F]MFBG	*meta*-[^{18}F]fluorobenzylguanidine
[^{18}F]FMZ	[^{18}F]flumazenil
FT-IR	fourier transform infrared spectroscopy
[^{18}F]UCB-H	(*R*)-1-((3-[^{18}F]fluoropyridin-4-yl)methyl)-4-(3,4,5-trifluorophenyl)pyrrolidin-2-one
GABA	γ-aminobutyric acid
$GABA_{A/B/C}$	γ-aminobutyric acid subclass A/B/C
GABARc	γ-aminobutyric acid subclass C receptors
GABA-T	γ-aminobutyric acid transaminase
GAD	glutamic acid decarboxylase
GAT-1	γ-aminobutyric acid transporter 1
h	hour
HEK293	human embryonic kidney cells 293
HEPES	4-(2-hydroxylethyl)piperazine-1-ethanesulfonic acid
HMBC	heteronuclear multiple bond correlation
HMPA	hexamethylphosphoramide
HPLC	high performance liquid chromatography

HRMS	high resolution mass spectrometry
HSQC	heteronuclear single quantum correlation
IBX	2-iodoxybenzoic acid
i-Pr	isopropyl
IR	infrared
IUPAC	the international union of pure and applied chemistry
J	coupling constant
K_{222}	4,7,13,16,21,24-hexaoxa-1,10-diazabicyclo[8.8.8]hexacosane
KHMDS	potassium hexamethyldisilazide
L	ligand
Lit.	literature
Max.	maximum
m/*z*	mass to charge ratio
*m*CBA	*meta*-chlorobenzoic acid
*m*CPBA	*meta*-chloroperoxybenzoic acid
Me	methyl
MFSDA	methylfluorosulfonyl difluoroacetate
Min.	minimum
min	minute
mp	melting point
MRI	magnetic resonance imaging
MTBE	methyl *tert*-butyl ether
m	multiplet
MW	microwave
N	number of valence electrons
NBS	*N*-bromosuccinimide
NCA	no-carrier-added
n_{exp}	number of repeats
NFSI	*N*-fluorobenzenesulfonimide
NIS	*N*-iodosuccinimide
NSI	nanospray ionisation
Nu	nucleophile
OAc	acetate

OTf	triflate
Oxone	potassium peroxymonosulfate
P4S	piperidine-4-sulfonic acid
PET	positron emission tomography
Ph	phenyl
4-PIOL	5-(4-piperidyl)-3-isoxazolol
PLP	pyridoxal-5'-phosphate
PMA	phosphomolybdic acid
PMP	pyridoxamine-5'-phosphate
ppm	parts per million
py	pyridine
quant.	quantitative
R	substituent
RCY	radiochemical yield
R_f	retention factor
rt	room temperature
s	singlet
sec	second
sept	septet
SET	single electron transfer
S_NAr	nucleophilic aromatic substitution
SPB	sodium perborate tetrahydrate
SPECT	single-photon emission computed tomography
SSADH	succinic semialdehyde dehydrogenase
SV2A	synaptic vesicle glycoprotein 2A
t	triplet
TACA	*trans*-4-aminobut-2-enoic acid
TACP	*trans*-3-aminocyclopentane-1-carboxylic acid
TBAF	tetrabutylammonium fluoride
TFA	trifluoroacetic acid
TfOH	triflic acid
THF	tetrahydrofuran
THIP	4,5,6,7-tetrahydroisoxazolo-[5,4-c]pyridin-3-ol

$TiCpCl_3$	cyclopentadienyl(IV) titanium trichloride
t_R	retention time
Ts	tosyl
UDEFT	uniform driven equilibrium fourier transform
uv	ultraviolet
v/v	volume per volume
W	Watt
ZAPA	Z-3-[(aminoiminomethyl)thio]prop-2-enoic acid

Abstract

Chapter 1 provides a general introduction on the role of bioisosterism of fluorine aiming to improve the pharmacokinetics properties of lead compounds. $GABA_A$ receptors specifically, synaptic $GABA_A$ receptors, extrasynaptic $GABA_A$ receptors and $GABA_A$ rho receptors are then presented. Compounds that exhibit agonist and partial agonist effects at these receptors are also discussed. The applications of some compounds as $GABA_A$ receptor PET radiotracers are also described.

Chapter 2 details the synthesis of two fluorinated analogues of muscimol, fluoromuscimol and trifluoromethylmuscimol. Fluoromuscimol was obtained from the lithiation of a Boc-protected isoxazole followed by *in-situ* fluorination using NFSI, whereas trilfuoromethylmuscimol was obtained from the coupling of a heteroaryl iodide with trifluoromethylcopper species, which was generated *in-situ* from MFSDA in the presence of CuI. Fluoromuscimol and trifluoromethylmuscimol were assessed on human synaptic ($\alpha_1\beta_2\gamma_2$), extrasynaptic ($\alpha_4\beta_2\delta$) and ρ_1 subunits of the $GABA_A$ receptor. The biological results show that fluoromuscimol exhibits greater maximum response in comparison to GABA at the extrasynaptic $GABA_A$ receptors ($\alpha_4\beta_2\delta$), but lower overall potency, whereas trifluoromethylmuscimol was inactive at all the tested $GABA_A$ receptors.

Chapter 3 discusses the synthesis and late stage fluorination of diaryliodonium salts as precursors to fluoromuscimol. Application of iodonium salts as precursors for nucleophilic fluorination in PET studies are also highlighted. The last part of this chapter focuses on the synthesis of iodomuscimol as a potential alternative SPECT radiotracer to fluoromuscimols in probing GABA binding sites on $GABA_A$ receptors.

Chapter 1: Small molecule agonists of GABA receptors

1.1 Introduction

Elemental fluorine was first isolated in 1886 by Henri Moissan. His historic and courageous efforts focused on its isolation earned him a Nobel Prize in 1906.[1] Fluorine (van der Waals radius of 1.47 Å) (Table 1) is the smallest atom after hydrogen (van der Waals radius of 1.20 Å) and the most electronegative element in periodic table. The substitution of hydrogen with fluorine has proved to be a good replacement as it causes a minimal steric change to the host motif. Thus, fluorine is a good hydrogen mimic and has been widely employed in medicinal chemistry in this regard.[2,3]

Atom	I	Br	Cl	O	F	H
Van der Waals radii (Å)	1.98	1.85	1.75	1.52	1.47	1.20

Table **1**: Fluorine van der Waals radii relative to other electronegative elements.[4]

The high electronegativity (4.0, Pauling scale)[5] and strong dipole moment (μ C-F = 1.4 D)[6] of fluorine result in a significant ionic character to the C-F bond, which makes the C-F bond the strongest single bond that carbon can form with any other element.[7] Table 2 summarises the bond length and bond dissociation energy of some common elements bound to carbon. This property increases the chemical and thermal stability of a fluorinated compound, a feature that is widely used to improve drug half-life.[8,9]

Bond	**C-F**	C-H	C-O	C-C	C-Cl	C-N
Length (Å)	**1.35**	1.09	1.43	1.54	1.77	1.47
Energy (kcal/mol)	**105.4**	98.8	84.0	83.1	78.5	69.7

Table **2**: Bond length and bond dissociation energy of some common elements in organic compounds.[7]

Bioisosterism is an important concept and strategy in medical chemistry. It refers to the capacity of subunits or functional groups with similar sizes or shapes to be interchanged without significant perturbation in biological activity,[10] but may have a significant role in the alteration of pharmacokinetics.[11] Due to the similar steric parameters described above, fluorine acts as a bioisostere of hydrogen and the incorporation of fluorine into molecules can significantly affect physiochemical properties such as electronegativity, steric size and lipophilicity.[12]

The application of monovalent substitution of hydrogen by fluorine is demonstrated by synthetic cannabinoids (Figure 1). Replacement of hydrogen in (**1a**), (**2a**) and (**3a**) to give (**1b**), (**2b**) and (**3b**) respectively, resulted in enhanced affinity and efficacy towards the CB1 receptor. This greater binding affinity and efficacy could be attributed to the activation of the CB1 receptor by the terminal fluorine atom of the *N*-pentyl substituent of these cannabinoids resulting in a stronger interaction with the receptor.[13]

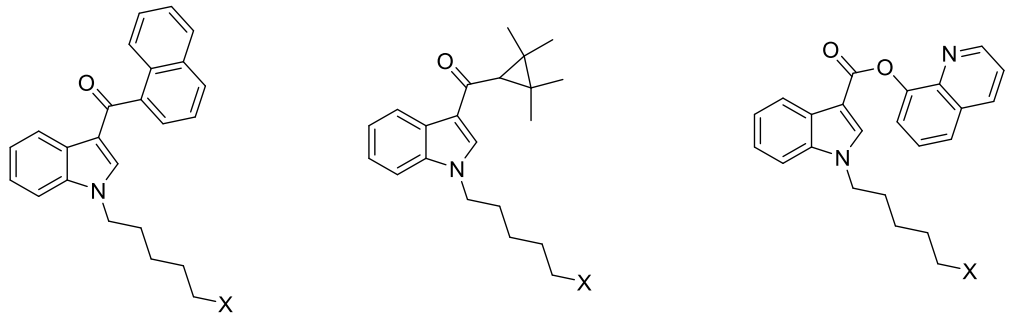

1a, x = H, EC_{50} = 102 nM
1b, x = F, EC_{50} = 38 nM

2a, x = H, EC_{50} = 421 nM
2b, x = F, EC_{50} = 98 nM

3a, x = H, EC_{50} = 26 nM
3b, x = F, EC_{50} = 51 nM

Figure **1**: Effects of bioisosteric fluorine in synthetic cannabinoids.

1.2 Fluorine in medicinal chemistry

Because of its extreme chemical properties, fluorine has been exploited extensively in drug design and development.[14,15] The discovery of the first fluorinated bioactive compound by Fried in 1954 was a major breakthrough in medicinal chemistry. Fludrocortisone (**4**) was found to possess a remarkable glucocorticoid activity and has been employed ever since in the treatment of Addison's and congenital adrenal hyperplasia diseases.[16] A few year later, Heidelberger *et al.*, reported the first synthesis of 5-fluorouracil (**5**), a drug which exhibits profound antitumor-inhibiting activity and one that has been widely used in the treatment of solid malignant tumors.[17] Since then, fluorine has become an important and essential tool in drug discovery and has been incorporated to numerous blockbuster drugs.

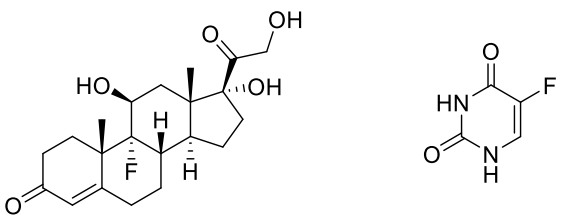

4 **5**

1.2.1 Some drugs containing isoxazole moiety acting on the central nervous systems (CNS)

Atypical antipsychotic drugs are a class of compounds that are used as medication for the treatment of schizophrenia and other related central nervous system disorder. They operate by decreasing the dopamine levels in brain.[18] Among these structurally diverse compounds, the 6-fluoro-3-(piperidin-4-yl)benzo[d]isoxazole moiety has received much attention, with risperidone (**6**) being the first compound of this family when it was approved by the FDA in 1993 for the treatment of schizophrenia and bipolar disorder.[19] Risperidone exhibits comparable efficacy and is less toxic than haloperidol.[20] Subsequent studies by Janssen,[21] led to the discovery of its hydroxyl analogue, paliperidone (9-hydroxyrisperidone) (**7**) which appears to be the primary active metabolite of risperidone. With less side effects and better pharmacokinetic properties, paliperidone has been regarded as an improved drug of risperidone.[22] It is marketed in tablets form as a racemic mixture and was approved by the FDA in 2006 for the treatment of schizophrenia.

Moreover, paliperidone palmitate (**8**), an injectable new-generation of antipsychotic drug has been developed and approved by the FDA in 2009 and in Europe in 2011.[23] It serves as an alternative to oral delivery of paliperidone and offers better efficacy and tolerability due to improved adherence and more stable pharmacokinetics.[24] Another member of this family of compound is iloperidone (**9**), which was developed by Vanda Pharmaceuticals for the treatment of acute schizophrenia in adults.[25]

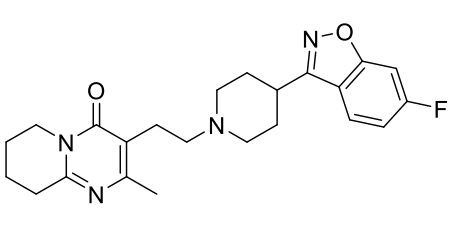

6

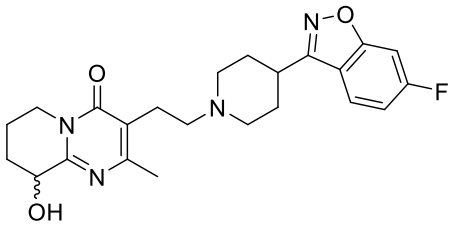

7

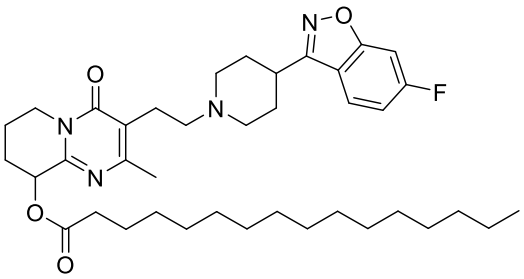

8

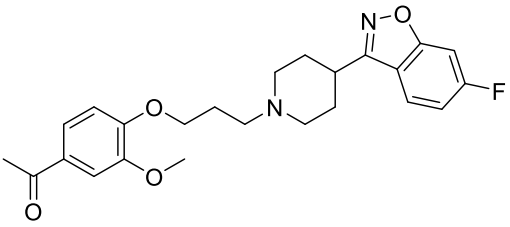

9

1.3 Muscimol: active compound of *Amanita muscaria*

The mushroom *Amanita muscaria* (Figure 2) also known as fly agaric has powerful psychotropic and hallucinogenic effects. Because of its important effects on brain activity, it was one of the first psychoactive drugs used by man.[26]

Figure **2**: *Amanita muscaria* (fly agaric) (Photo by Onderwijsgek is licenced under CC BY-SA 3.0 NL) adapted from https://commons.wikimedia.org/wiki/File:Amanita_muscaria_3_vliegenzwammen_op_rij.jpg, (accessed June 2016).[27]

Numerous efforts have been made to identify and isolate the psychoactive constituents of *Amanita muscaria*. The first active chemical species of *Amanita muscaria* were isolated in 1964 by Takemoto *et al*.[28] These compounds, exist in zwitterionic form and were shown to be ibotenic acid (**10**) and muscimol (**11**). Ibotenic acid is biosynthesised by the mushroom, whereas muscimol is formed as a consequence of decarboxylation, a process that proceeds without an enzyme catalyst. [26] Later, two groups independently reported the isolation and structure determination of the active amino acids of *Amanita muscaria*.[29,30]

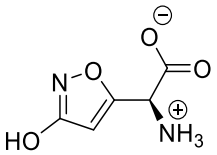

10

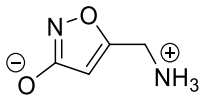

11

Muscimol (**11**) is a more potent $GABA_A$ receptor agonist than GABA (γ-aminobutyric acid) (**12**) and is used as a tool in neurobiology. It binds and is capable of activating GABA receptors in a similar mode to that of GABA, altering the normal function of the neurones and leading to psychoactive effects. By contrast to GABA, muscimol can cross the blood brain barrier on systemic administration affecting the central nervous system in various ways. It has also been widely used as a selective $GABA_A$ receptor agonist of high efficacy. Unfortunately, despite its proven efficacy, muscimol is not clinically useful as it is toxic and rapidly decomposes *in vivo* and produces metabolites which may contribute to the pronounced toxicity of muscimol.[26,31,32] Chemically, muscimol

belongs to the isoxazol-3-one family of alkaloids. It contains an electron-rich isoxazole ring with a OH at the C-3 and an amino methyl group at C-5.

The protolytic properties of muscimol are comparable to GABA (**12**) with pK_a values of 4.8 and 8.4 for muscimol and 4.0 and 10.7 for GABA respectively. Therefore, at neutral pH these compounds exist as zwitterions. Unlike GABA, the conformational mobility of muscimol (**11**) is more constrained due to the ring (Figure 3).[26]

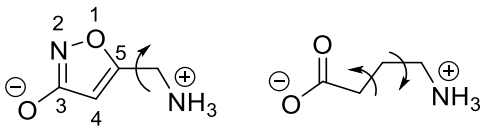

11 **12**

Figure **3**: Conformational restriction of muscimol (**11**) compared to GABA (**12**).

Gaboxadol (THIP) (**13**), a more conformationally rigid and restricted analogue of muscimol is a partial agonist at the synaptic $GABA_A$ receptors. Although less potent than muscimol, THIP was shown to be a super agonist at extrasynaptic $GABA_A$ receptors.[33,34] Moreover, THIP is comparatively non-toxic in animals and can cross the blood brain barrier (BBB) after systemic administration.[35,36]

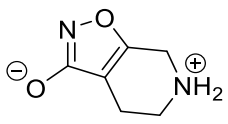

13

1.4 GABA: The inhibitory neurotransmitter in CNS

Neurotransmitters can be placed in two classes, excitatory and inhibitory. Excitatory neurotransmitters are exemplified by acetylcholine and glutamic acid, whereas GABA and glycine serve as major inhibitory neurotransmitters. Binding of these neurotransmitters to the ligand-gated ion channels receptors can lead to either excitatory postsynaptic potentials, resulting in depolarisation or inhibitory postsynaptic potentials, resulting in hyperpolarisation.[37] GABA (**12**) is the major fast inhibitory neurotransmitter in the mammalian central nervous system. It is essential in maintaining the overall balance between neuronal excitation and inhibition of normal brain. Disturbing the balance between excitatory and inhibitory neurotransmission can lead to a range of conditions which include convulsions, anxiety, high blood preassure, restlessness and insomnia. Extreme imbalance of neurotransmission can result in death.[36]

GABA acts at receptors that can be classed as either ionotropic (receptors that are ligand-gated ion channels-$GABA_A$ and $GABA_C$ receptors) or metabotropic (G-protein coupled receptors-$GABA_B$ receptors). Cognitive disorder, epilepsies, mood disorders, schizophrenia and sleep disorders are all associated with GABA imbalances.[38–40]

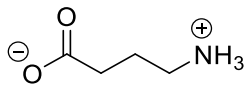

12

1.4.1 Synthesis and degradation of GABA *via* GABA shunt

Since GABA cannot cross the blood brain barrier, its supply is biosynthesised in the brain through a closed-loop process known as the GABA shunt pathway.[41] The first step in GABA biosynthesis involves the transamination of α-ketoglutarate (**14**) which is formed from glucose metabolism in the Krebs cycle into L-glutamic acid (**15**) by the enzyme GABA transaminase (GABA-T) (Scheme 1). Glutamic acid decarboxylase (GAD), a PLP-dependent enzyme then catalyses the decarboxylation of glutamic acid to form GABA (**12**). GABA is further metabolised by GABA-T, which is also a PLP-dependent enzyme to form succinic semialdehyde (**16**). This process converts PLP to PMP, then PMP is recycled back to PLP *via* transamination with α-ketoglutarate (**14**), regenerating L-glutamic acid (**15**). Succinic semialdehyde (**16**) is then oxidised by succinic semialdehyde dehydrogenase (SSADH) to succinic acid (**17**). It can then re-enter the Krebs cycle to complete the loop (Scheme 1). In order to conserve the supply of GABA, transamination only occurs when the parent compound, α-ketoglutarate (**14**), is present to accept the amino group removed from GABA to form glutamic acid (**15**). In other words, GABA only can be metabolised in the presence of α-ketoglutarate (**14**).

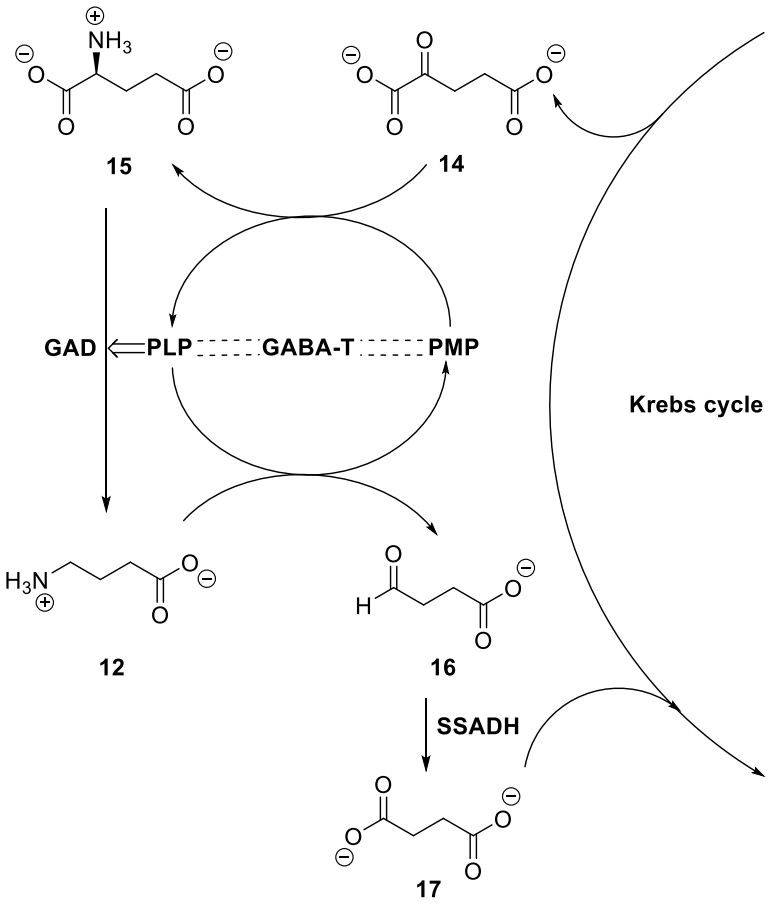

Scheme **1**: Synthesis of GABA (**12**) from Krebs cycle.[41]

1.4.2 $GABA_A$ receptors: Synaptic and extrasynaptic receptors

$GABA_A$ receptors are mostly heteropentameric proteins (Figure 4) that are assembled from a family of 19 homologous subunits, six α subunits (α_{1-6}), three β subunits (β_{1-3}), three γ subunits (γ_{1-3}), three ρ subunits (ρ_{1-3}) and one each of the δ, ε, π, and θ subunits. Most $GABA_A$ receptors are constituted from two copies of α-subunits, two copies of β-subunits and one copy of another subunit (γ, δ, or ε).[32,33] The diversity of these subunit compositions gives rise to a substantial, anatomical, functional and pharmacological heterogeneity. The fast signalling of

brain mediated by $GABA_A$ receptors can be classified into two main groups, synaptic $GABA_A$ receptors and extrasynaptic $GABA_A$ receptors.[33]

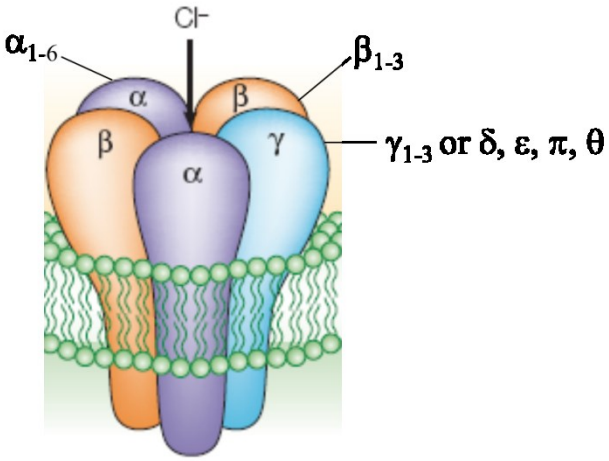

Figure **4**: Heteropentameric $GABA_A$ receptor.[42]

Synaptic $GABA_A$ receptors consist of two α subunits (α_1-α_4 or α_6), two β subunits and one γ subunit (usually γ_2) and have a relatively low sensitivity to GABA. They can be activated by a high concentration of GABA. Extrasynaptic $GABA_A$ receptors are constituted from two α subunits (α_1, α_4, or α_6), two β subunits and one δ subunit. They are highly sensitive to GABA can respond to low concentrations of spill-over GABA.[37,43] In addition, the α_5 subunit $GABA_A$ receptors which do not include the δ subunit are also present in the extrasynaptic membranes. The δ subunit is only found in the extrasynaptic population, which distinguish the two receptors classes.[44] Both synaptic and extrasynaptic subunit combinations are shown to be exclusively localised in the brain in various neuronal cells (Table 3).[45]

Subunit composition	Brain location	GABA potency (EC_{50})[a] (μM)
Synaptic		
$\alpha_1\beta_2\gamma_2$	Ubiquitous[46–48]	6.6
$\alpha_1\beta_3\gamma_2$	Ubiquitous	2.1
$\alpha_2\beta_3\gamma_2$	Hippocampus, amygdala, lateral septum caudate putamen[46–48]	13.4
$\alpha_3\beta_{2/3}\gamma_2$	Cerebral cortex, thalamus	12.5
$\alpha_4\beta_{2/3}\gamma_2$	Hippocampus, thalamus[49]	2.1
$\alpha_6\beta_3\gamma_2$	Cerebellum	0.17
Extrasynaptic		
$\alpha_4\beta_{2/3}\delta$	Dentate gyrus granule layer,[50,51] hippocampus,[50,51] thalamus[51]	0.91-1.7
$\alpha_1\beta\delta$	Dentate gyrus molecular layer,[45,52] hippocampal interneurons[52]	3.7
$\alpha_5\beta_3\gamma_2$	Cerebral cortex,[53] CA1-3 hippocampus[53,54]	1.4
$\alpha_6\beta_{2/3}\delta$	Cerebellum granule layer[55]	0.17

[a]Potency data based on recombinantly expressed receptors HEK293 cells.[56]

Table **3**: $GABA_A$ receptor subunit compositions and distribution in the brain.

Figure 5 illustrates GABA signalling in the brain. The GABA molecules are packaged in small vesicles in the neuronal axon terminus. Activation of exocytosis by neuronal activity leads to the release GABA into the synaptic cleft, the gap between presynaptic and postsynaptic membrane. Some of these molecules bind to synaptic $GABA_A$ receptors and activate the receptor, allowing the migration of the chloride ions into the neuron. This results in the hyperpolarisation of the cell and inhibition of the neuronal activity.[57] The majority of the GABA released is taken up by GABA Transporter 1 (GAT 1), the primary reuptake protein and mechanism responsible for transport of the released GABA. A lower concentration of GABA molecules diffuse out of the synaptic cleft to bind and activate the extrasynaptic $GABA_A$ receptors.[43]

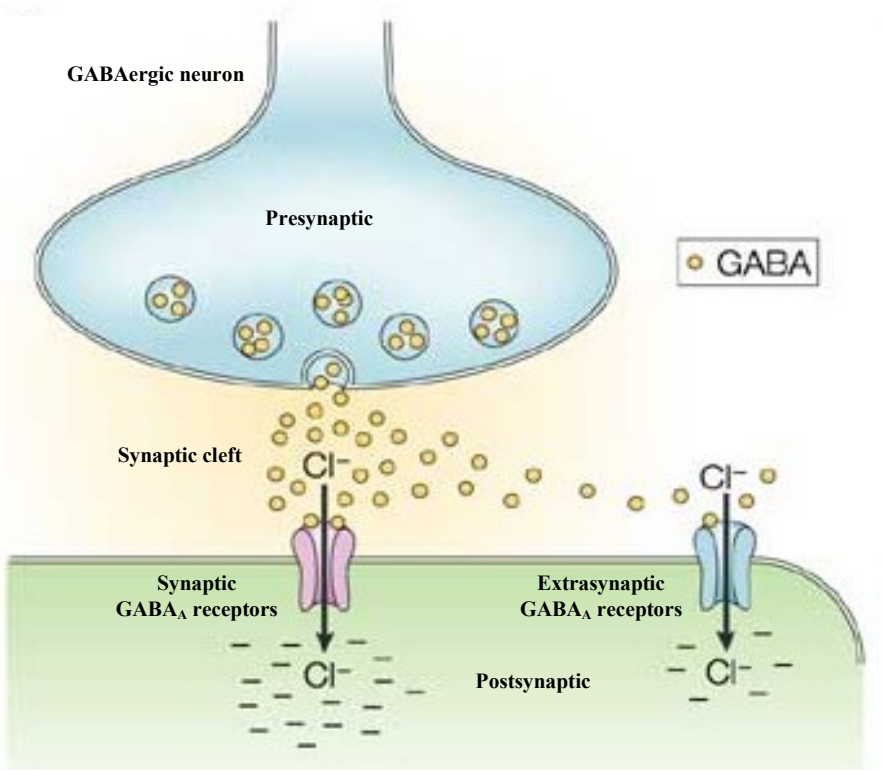

Figure **5**: GABA signalling in the brain (adapted from U. Rudolph and B. Antkowiak*, Nat. Rev. Neurosci.*, 2004).[58]

1.4.3 Phasic and tonic inhibition of $GABA_A$ receptors

Two modes of $GABA_A$ mediated inhibition have been identified, phasic and tonic inhibition. These are mediated by activation of the synaptic and extrasynaptic $GABA_A$ receptors respectively. Activation of the synaptic $GABA_A$ receptors by a high concentration of GABA mediates transient phasic inhibitory currents that cease within miliseconds as GABA is mopped up by GABA transporter 1 (GAT-1) from the synaptic cleft, whereas activation of the extrasynaptic $GABA_A$ receptors on exposure to a low concentration of GABA, leads to a persistent or tonic inhibitory current (Figure 6).[33,59]

Although the concentration of GABA in the synaptic cleft is high (1-10 mM), its low affinity for the synaptic $GABA_A$ means it only occupies the receptor for a very short duration before being taken up by the primary reuptake mechanism, GAT-1. This event results in a fast rise and slow decay waveform that varies depending upon the subunit composition and the transmitter profile of the synaptic $GABA_A$ receptors within the cleft (Figure 6a). On the other hand, an exposure to low ambient concentration of GABA, enables the activation of the high affinity extrasynaptic $GABA_A$ receptors to generate a persistent tonic inhibitory potential which sets the threshold for activation and regulates excitatory and inhibitory balance in the brain (Figure 6b). This is a fine tuning mechanism which the brain uses to discriminate signal from noise.[43,44,59]

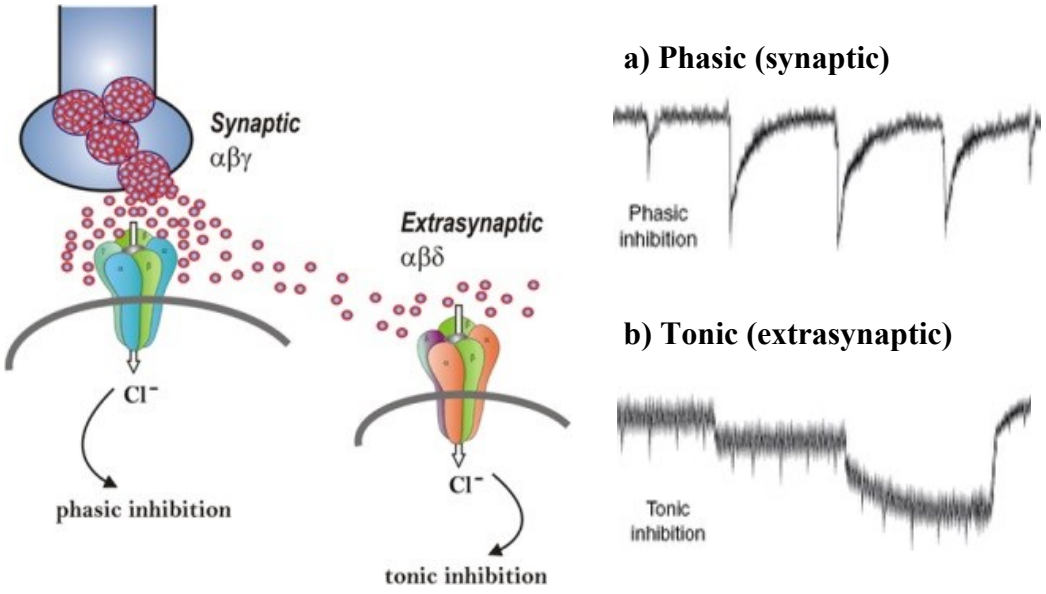

Figure **6:** Activation of the synaptic and extrasynaptic lead to phasic and tonic inhibition (adapted from D. S. Reddy, *Front. Endocrinol.*, 2011).[60]

1.4.4 $GABA_A$ rho receptors

$GABA_C$ receptors (GABARc) also known as γ-aminobutyric acid type A rho (ρ $GABA_A$) receptors, belong to a subclass of ligand-gated chloride channel that mediate fast synaptic inhibition. GABARc receptors can be distinguished from $GABA_A$ receptors on the basis of their five protein subunits. Unlike $GABA_A$ receptors, GABARc or (ρ $GABA_A$) are formed from five identical homomeric ρ subunits (ρ_{1-3}) or pseudo-heteromeric ρ subunits comprising a combination of (ρ_1 and ρ_2 or ρ_1 and ρ_3 subunits) to assemble a single ion channel (Figure 7).[61–63]

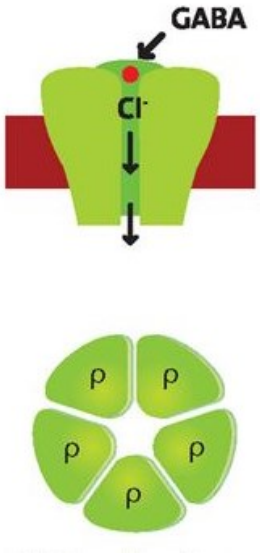

Figure **7**: Homomeric or pseudo-heteromeric GABA A rho receptors (adapted from B. Frølund *et al., Lægemiddelforskning*, 2006).[64]

$GABA_C$ have distinct different properties to $GABA_A$ receptors in term of potency and electrophysiological properties. $GABA_C$ receptors have higher potency and sensitivity for GABA with lower current and they do not desensitise. On the single-channel level, these receptors are activated and closed more slowly with longer mean channel opening time and lower chloride conductance than $GABA_A$ ion channels. GABAc receptors are mainly expressed in the retina (strong ρ_1 subunit expression), hippocampus (strong ρ_2 subunit expression), superior colliculus, cerebellum and lateral amygdala.[34,38,39] Table 4 shows the differences between $GABA_A$ and $GABA_C$ receptors.

Property	$GABA_A$ receptors	$GABA_C$ receptors
GABA EC_{50}	5-100 μM	1-4 μM
GABA concentrations	10-100 μM	1 μM
Channel type	Anion (Cl^- channel)	Anion (Cl^- channel)
Channel composition	Heterooligomeric	Homo/pseudo-homooligoemeric
Subunit composition	α_{1-6}, β_{1-3}, γ_{1-3}, δ, ε, π, θ	ρ_{1-3}
Conductance	27-30 pS	7-8 pS
Mean channel open time	25-30 ms	150-200 ms
Activation/deactivation	Fast	Slow
Desensitisation	Strong	Weak
Pore size	5.6 Å	5.1 Å

Table **4:** Comparisons between $GABA_A$ and $GABA_C$ receptors.[38,39]

1.5 GABA receptor agonists and partial agonists

A variety of compounds can bind to the GABA receptors and regulate the opening or closing of gated chloride ion channels. Agents that induce chloride ion flux are GABA receptor agonists, whereas agents that block the flux are antagonists. With such important pharmacological properties and therapeutic efficacy, GABA receptors have been extensively studied by molecular biologists and medicinal chemists.[65,66]

This has led to design and development of a diversity of GABA receptor agonists and partial agonists (Figure 8).

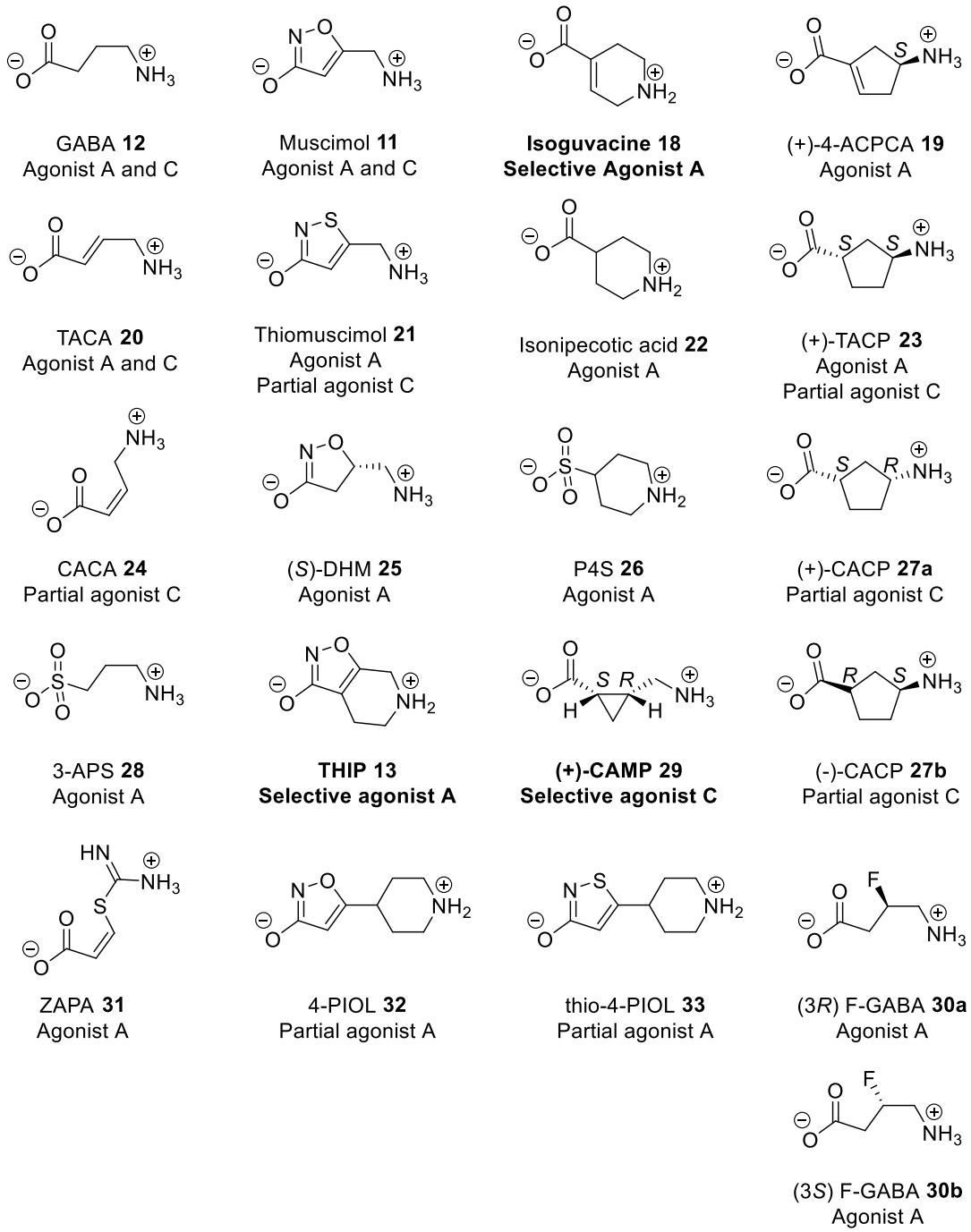

Figure **8**: Structures of GABA analogues that have agonist and partial agonist effects at $GABA_A$ and $GABA_C$ receptors.

Muscimol (**11**) and GABA (**12**) are potent agonists at $GABA_A$ and $GABA_C$ receptors, however, muscimol is the more potent $GABA_A$ receptor agonist. Although, the action of muscimol on different subunits of the $GABA_A$ receptor is relatively uniform, it acts as a super agonist at the extrasynaptic GABA ($\alpha_4\beta_3\delta$).[67] Like muscimol, THIP (**13**) appears to act as super agonist at the $\alpha_4\beta_3\delta$ extrasynaptic GABA receptors. Although THIP (EC_{50} values of 13 μM) is less potent than both muscimol (EC_{50} values of 0.20 μM) and GABA (EC_{50} values of 0.35 μM), it is more efficacious (E_{Max} values of 224%) compared to muscimol (E_{Max} = 120%) and GABA (E_{Max} = 98%), which is in agreement with the data for the $\alpha_4\beta_2\delta$ (Table **5**).[44] The super agonist activity of THIP on these receptors can be explained by the reduced desensitisation and increase in the frequency and duration of channel opening, resulting in longer burst durations. On the other hand, THIP is a partial agonist at the synaptic $\alpha_1\beta_3\gamma_2$ $GABA_A$ receptors (EC_{50} values of 107 μM, E_{Max} values of 85%) compared to muscimol (EC_{50} values of 0.92 μM, E_{Max} values of 101%) and GABA (3.4 μM, E_{Max} values of 100%) respectively (Table 5).[44,67]

Agonist	$\alpha_1\beta_3\gamma_2$ Synaptic		$\alpha_4\beta_3\delta$ Extrasynaptic		$\alpha_4\beta_2\gamma_2$ Synaptic		$\alpha_4\beta_2\delta$ Extrasynaptic	
	EC_{50} (μM)	E_{Max} (%)	EC_{50} (μM)	E_{Max} (%)	EC_{50} (μM)	E_{Max} (%)	EC_{50} (μM)	E_{Max} (%)
GABA (**12**)	3.4	100	0.35	98	12	100	1.6	97
Muscimol (**11**)	0.92	101	0.20	120	2.6	120	0.12	120
THIP (**13**)	107	85	13	224	190	76	17	190

Table **5**: GABA (**12**), muscimol (**11**) and THIP (**13**) responses at synaptic and extrasynaptic $GABA_A$ receptors.[44,67]

The 3-fluoro enantiomers of GABA, (3*R*)-F-GABA (**30a**) (EC_{50} values of 240 μM, E_{Max} values of 77%) and (3*S*)-F-GABA (**30b**) (EC_{50} values of 380 μM, E_{Max} values of 82%) displayed similar agonistic potency at the $\alpha_1\beta_2\gamma_2$ synaptic receptors but an overall reduced potency relative to GABA (EC_{50} values of 49 μM).[68] Based on the structure of THIP and muscimol, several heterocyclic $GABA_A$ agonists have been developed. Isoguvacine (**18**), isonipecotic acid (**22**), P4S (**26**) and 4-PIOL (**32**) are derived from THIP whereas, thiomuscimol (**21**) and (*S*)-DHM (**25**) are derived from muscimol. Isoguvacine is slightly less potent than GABA in mediating chloride flux but was found to exhibit approximately the same potency as GABA in competing for the binding of [^{3}H]GABA.[40,69] On the other hand, 4-PIOL is a partial agonist at $GABA_A$ receptors with an EC_{50} value of 91 μM and it is approximately 200 times less potent than isoguvacine as an agonist. As with THIP (**13**), thio-4-PIOL (**33**), an analogue of 4-PIOL (**32**), exhibits differences in activity at the synaptic and extrasynaptic $GABA_A$ receptors. It is a partial agonist with maximal responses up to 30% at the extrasynaptic but only 0-4% maximal responses at the synaptic $GABA_A$ receptors.[70,71]

Both thiomuscimol (**21**) and (*S*)-DHM (**25**) retained the agonism of muscimol, despite certain structural modifications. Thiomuscimol was found to be approximately equipotent with muscimol whereas, (*S*)-DHM exhibits the most potent agonist activity so far demonstrated in both functional and binding assays.[72] In contrast, replacement of the carboxylic acid group in GABA by a sulfonic acid to give 3-APS (**28**) led to a decrease in potency at inducing $^{36}Cl^-$ influx than its parent compound.[73] However (**28**) is more potent than GABA

in competing for the binding of [^{3}H]GABA suggesting that high-affinity binding may not always correlate well with the agonist potency.[74] On the other hand, the conformationally restricted analogues of GABA, ZAPA (**31**) and TACA (**20**) are potent $GABA_A$ agonists. ZAPA (EC_{50} values of 10.3 μM) was found to be more potent than GABA on low-affinity GABA banding sites, compared to GABA (EC_{50} value of 12.8 μM).[36,75]

The cylopentane (+)-TACP (**23**) and cylopentene (+)-4-ACPCA (**19**) analogues of GABA, are also potent $GABA_A$ agonists.[66] The *cis* isomer of TACA, CACA (**24**) serves as a partial but selective agonist at the $GABA_C$ receptors. CACA is a partial agonist at both ρ_1 (EC_{50} values of 74 μM) and ρ_2 (EC_{50} values of 70 μM) with 70-80 efficacy of GABA and weaker agonist at ρ_3 (EC_{50} values of 139.4 μM) receptors expressed in *Xenopus* oocytes (Table 6). Although TACA is not a selective agonist for GABA receptors, it is the most potent $GABA_C$ agonist described so far. The (+)-isomer of CAMP (**29**), can be regarded as a superior $GABA_C$ receptor agonist. (+)-CAMP was found to be a selective agonist at both ρ_1 (EC_{50} values of 40 μM) and ρ_2 (EC_{50} values of 17 μM) and it has been widely used as a better tool in neurobiology compared to CACA due to its low effect on GABA transporters. (+)-CACP (**27a**), (-)-CACP (**27b**) and (+)-TACP (**23**) are also partial agonists at $GABA_C$ receptors.[66,76]

Agonist	ρ_1 (EC_{50}) (μM)	ρ_2 (EC_{50}) (μM)	ρ_3 (EC_{50}) (μM)
GABA (**12**)	1.0	0.8	4
CACA (**24**)	74	70	139.4
TACA (**20**)	0.6	0.4	3.8
(+)-CAMP (**29**)	40	17	-

Table **6**: GABA (**12**), CACA (**24**), TACA (**20**) and (+)-CAMP (**29**) responses at $GABA_C$ receptors.[76]

1.6 Positron Emission Tomography (PET) and fluorine-18 in nuclear medicine

PET is a non-invasive molecular imaging technique and one of the most powerful imaging modalities used to study the fundamental biochemical and physiological processes in living organism. It operates by the detection of emitted positrons. Unlike other molecular imaging techniques such as MRI, CT, X-rays or ultrasound, which only provide limited or no information at all on metabolic or molecular events, PET relies on detectable exogenous radioactive probes that have the ability to monitor metabolic processes in living patients.[77] These probes can be designed to be tissue or receptor-specific, useful in the diagnosis and early detection of diseases such as cancer, heart malfunctioning and disorders of brain or neurogenic origin such as epilepsy, stroke and dementia.[78] Table 7 shows the key characteristics of several complementary non-invasive imaging techniques.

Imaging technique	Mode	Spatial resolution [ranges]	Target sensitivity [ranges]
X-ray/CT	Anatomical	300.0 μm	Low [>mM]
MRI	Anatomical	800.0 μm	Low [>mM]
Ultrasound	Anatomical	800.0 μm	Medium [nM]
SPECT	Functional + molecular	5.0 – 10.0 mm	High [nM-pM]
PET	Functional + molecular	2.0 – 8.0 mm	High [nM-pM]

Table **7**: Key characteristics of several complementary non-invasive imaging techniques.[79,80]

There are four radionuclides which have been used widely as positron emitters. These are carbon-11, nitrogen-13, oxygen-15 and fluorine-18. The wide historical use of these isotopes in the field of radiochemistry is due to the fact that they can be produced in relatively high yields by commercially available cyclotrons and their decay mode is close to 100% positron emission (Table 8).[78]

Radionuclide	Half-life (min)	Decay mode
Fluorine-18	110	97% β^+, 3% EC
Carbon-11	20.4	100% β^+
Nitrogen-13	9.97	100% β^+
Oxygen-15	2.04	100% β^+

Table **8**: Physical characteristics of fluorine-18, carbon-11, nitrogen-13 and oxygen-15.[78]

Among these four PET isotopes, fluorine-18 is the most widely used, especially for clinical application. This is because fluorine-18 has ideal properties for high-resolution PET imaging.[81] It has a short and manageable 110 minutes half-life which allows sufficient time for multistep synthesis labelling reactions and then transportation of doses to sites several hours away. Secondly, the positron decay of fluorine-18 (97% β^+), lower energy (640 keV maximum) and short travel distance (2.4 mm positron linear range in tissue) before its annihilation with an electron, are particularly advantageous in term of spatial resolution compared to other available positron emitters.[82]

Additionally, the higher achievable specific activity of fluorine-18 produced by proton irradiation of ^{18}O-enriched water is very important, especially for high affinity receptor and gene-expression related PET studies.[81]

Table 9 shows the theoretical and specific activity values of carbon-11 compared to fluorine-18. One of the important advancements in scanner technology is the incorporation of PET and CT (X-ray) into one device which allows the complementary data of metabolism and anatomy to be merged into a unique image to form the final result.[83]

Nuclide	Common production method	Max energy (keV)	Mean energy (keV)	Max. range in water (mm)	Theoretical and (practical) radioactivity (GBq/μmol)
C-11	$^{14}N(p,\alpha)^{11}C$	960	386	4.1 mm	3.4×10^5 (110-2600)
F-18	$^{18}O(p,n)^{18}F$	640	250	2.4 mm	6.3×10^4 (180-3700)

Table **9**: The relationship of positron energy and positron travel range of carbon-11 and fluorine-18.[84–86]

1.7 Fluorine-18 labelling methods

Direct and indirect fluorination methods offer two distinct strategies which can be employed for fluorine-18 labelling. Direct fluorination requires the fluorine-18 isotope to be introduced directly into the target molecule in one step, whereas indirect fluorination requires so-called fluorine-18 prosthetic groups (small fluorine-18 labelled alkyl or aryl groups) in a multistep synthetic approach. Direct fluorine-18 can be divided into nucleophilic and electrophilic approaches. Of these two methods, nucleophilic fluorine-18 reactions have been found to be very important due to the ease of access to ^{18}F-fluoride and its high specific activity.[78]

1.7.1 Nucleophilic fluorination

Nucleophilic fluorination is the most common and routinely used approach to produce radiolabelled [^{18}F]-organofluorine compounds. [^{18}F]-Fluoride is generated through the nuclear reaction of $^{18}O(p,n)^{18}F$, in which ^{18}O-enriched water is irradiated with a high energy beam of protons. This nuclear reaction is intrinsically high yielding at low proton energies (<16 MeV) and produces the

fluorine-18 as $[^{18}F]F^-$ ion in aqueous solution. This "no-carrier-added" (NCA) method produces $[^{18}F]F^-$ ion with a high specific radioactivity (exceeding 5 Ci/μmol).[81] In order to render the fluoride ion as a reactive nucleophilic, several pre-activation steps are required. The first step is to remove the bulk [^{18}O]water and solubilise the fluoride-18 in organic solvent. This can be achieved by adsorption of the $[^{18}F]F^-$ onto an ion exchange column which allows the recovery of expensive [^{18}O]water. The trapped $[^{18}F]F^-$ is then eluted from the column with a small volume of aqueous potassium carbonate. The aqueous fluoride is a poor nucleophile because of a high degree of solvation, therefore addition of a phase transfer reagent (e.g.: aminopolyether kryptofix K_{222}), followed by removal of water improves the reactivity of $[^{18}F]F^-$ in two ways. First, the aminopolyether forms a strong complex with potassium cation, consequently exposing the $[^{18}F]F^-$. Second, the complex is readily soluble in organic solvents, where the $[^{18}F]F^-$ is not solvated and remains reactive.[81] Alternatively, the irradiated target [$H_2{}^{18}O$] can be directly subjected to azeotropic evaporation cycles in the presence of base and kryptands or other phase-transfer catalysts. However, this method is unable to recycle the ^{18}O-enriched water for further use (Figure 9).[81]

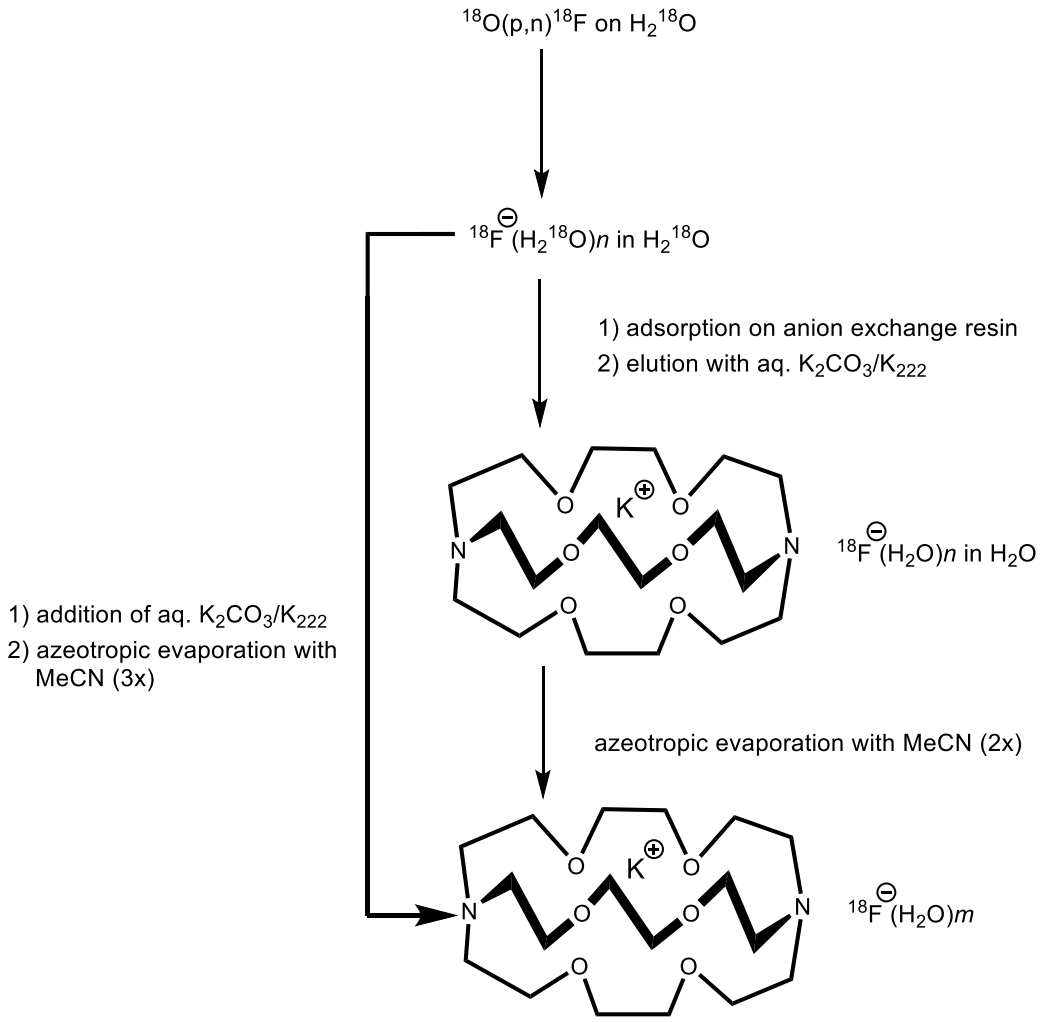

Figure **9**: Two alternative methods for the preparation of reactive $[^{18}F]F^-$ through the formation of $[^{18}F]F^-/K_{222}/K^+$-complex ("kryptofix-complex");[81] *n* may be as great as 15 in fully hydrated fluoride ion;[87] *m* is expected to be < *n*.

1.7.2 Electrophilic fluorination

Electrophilic fluorine-18 labelling can be achieved through the nuclear reaction of $^{20}Ne(d,\alpha)^{18}F$ carried out in a neon gas target with carrier addition of $[^{19}F]F_2(g)$ at a pressure up to 25 bar in a nickel target. This approach is less favorable nowadays for several reasons.[82] The nuclear reaction only gives labelled products with low achievable specific radioactivities (Table 10) due to the highly exothermic reaction, and electrophilic fluorine-18 may exchange with added fluorine or diffuse to the target wall to be adsorbed as nickel fluoride.[88,89] Moreover, the high reactivity of the generated $[^{18}F]F_2(g)$, resulting in poor selectivity giving mixtures of ^{18}F-labelled products. One of the advantages of this approach is that the resultant radiolabelled $[^{18}F]F_2$ can be used directly without any pre-activation procedures.[81]

	Nucleophilic fluorine-18 approach	Electrophilic fluorine-18 approach
Nuclear reaction	$^{18}O(p,n)^{18}F$	$^{20}Ne(d,\alpha)^{18}F$
Target	Enriched $H_2{}^{18}O_{(aq)}$	$Ne_2(g)$ (0.1% F_2)
Main product form	$[^{18}F]F^-_{(aq)}$	$[^{18}F]F_{2(g)}$
Specific activity [MBq/μmol]	~600×10^3	~100

Table **10**: Nucleophilic and electrophilic approaches for fluorine-18 labelling.[80,84,90]

Intravenous injection or inhalation is required in order to introduce the PET probe into the subject (animal or human). During decay, ^{18}F emits a positron (β^+) with a maximum energy of 640 keV. The emitted positrons travel at a specific range before colliding with an electron (annihilation event) in the surrounding tissue. The collision of positron and electron results in an annihilation to give rise to two gamma ray photons (γ) of equal energy (511 keV), that travel at 180° to each other. The simultaneous detection of these two gamma ray photons allows the radioactive events and PET probe in the body to be located (Figure 10). The raw data is then converted into quantified data such as flow, consumption tracer, affinity and/or density of receptor information using a mathematical model.[77,82]

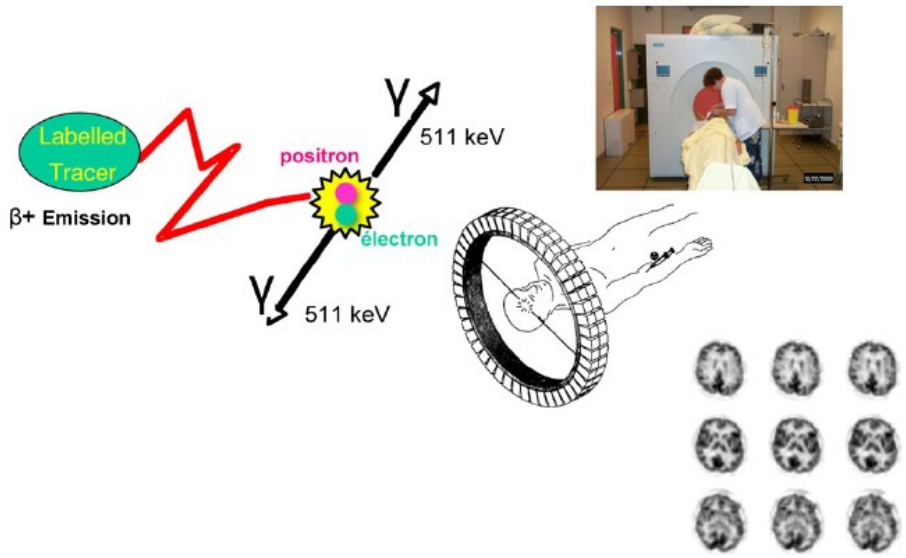

Figure **10**: Positron emission tomography (adapted from D. Le Bars, *J. Fluor. Chem.*, 2006).[82]

For example, some of the most important fluorine-18 PET radiotracers (Figure 11) produced from nucleophilic 18 fluorination reactions include [^{18}F]FDG (**34**) and 3'-deoxy-3'-[^{18}F]fluorothymidine ([^{18}F]FLT) (**35**). These tracers are used in oncology investigations.[91–93] [^{18}F]Fallypride (**36**),[94] [^{18}F]haloperidol (**37**) and [^{18}F]spiperone (**38**) are used in dopamine receptor studies,[95,96] while [^{18}F]fluoroazomycinarabinofuranoside ([^{18}F]FAZA (**39**) and [^{18}F]fluoromisonidazole ([^{18}F]FMISO (**40**) are used for imaging tissue hypoxia.[97,98]

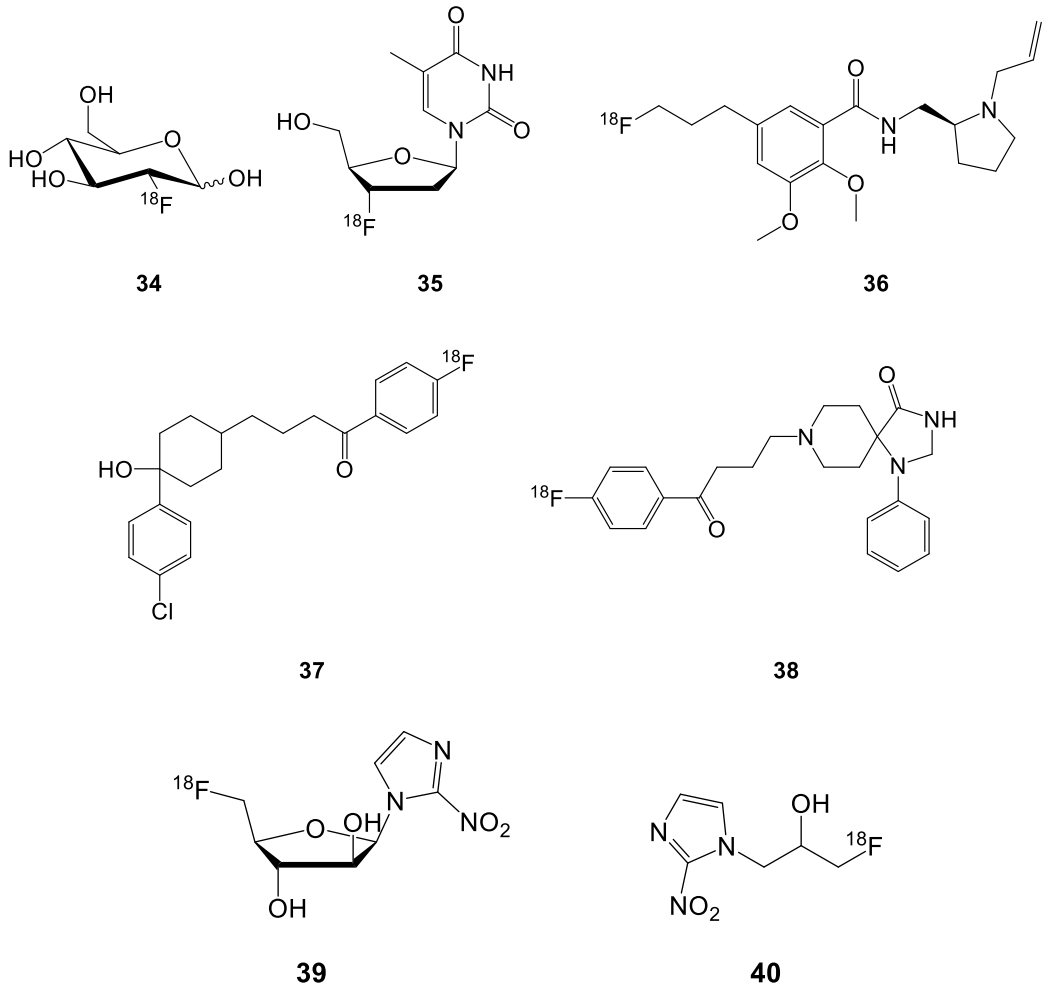

Figure **11**: Some of the most important clinical [^{18}F]-PET radiotracers.

1.8 Synthesis and use of [^{18}F]FDG in nuclear medicine

The development of the first PET tracer [^{18}F]FDG (**34**) was a major breakthrough in the field of radiopharmaceuticals.[99] This glucose mimic has been employed in neurological, cardiovascular and oncology investigations. Unlike glucose, the phosphorylation of FDG generates FDG-6-phosphate by the action of hexokinase, which cannot be further metabolised and accumulates in cells at a rate proportional to glucose. This allows the identification and characterisation of diseases related to the alterations in the metabolism of glucose. For example, the uptake of FDG in cancerous cells correlates with the rate of tumour growth and degree of metastasis. Therefore, [^{18}F]FDG (**34**) plays an important role in locating a tumor prior to surgery or radiotherapy.[82,99]

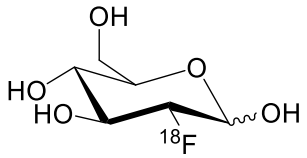

34

1.8.1 Synthesis of [^{18}F]FDG *via* nucleophilic fluorination

The most reliable method for producing [^{18}F]FDG (**34**) in a high radiochemical yield (RCY) is through nucleophilic fluorination.[78,100,101] With the current methods available, the radiochemical yield (purified product radioactivity over total starting radioactivity) of this procedure could reach up to 70-73%.[78,101]

The modified glucose, mannose triflate (**41**) serves as a substrate for a nucleophilic reaction. Displacement of the tiflate by [$^{18}F^-$] ion through nucleophilic substitution leads to formation of tetra-acetylated fluorodeoxyglucose (**42**) which is then treated with HCl affording the ^{18}F labelled FDG (**34**) (Scheme 2).[100]

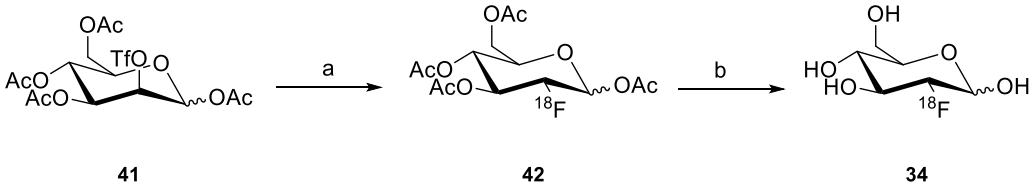

41 **42** **34**

Scheme **2**: Synthesis of [^{18}F]FDG (**34**) *via* nucleophilic fluorination.[100] Reagents: a) [^{18}F]F^-, kryptofix K_{222}/K_2CO_3, MeCN; b) HCl.

[^{18}F]FDG is by far the most commonly employed radiotracer in PET imaging. The ability of [^{18}F]FDG PET to quantify *in vivo* pathological processes allows the early detection of some neurodegenerative diseases before clinical symptoms appear. Thus this technique appears to be an ideal tool in neurobiology for monitoring the efficiency of drugs to the targeted pathological sites and could serve as a platform and starting point for future research in drug development to treat neurological diseases.

1.9 $GABA_A$ receptor radiotracers

Due to the role of GABA as the major inhibitory neurotransmitter in CNS and taking advantage of PET as a powerful imaging tool, various radiotracers that specifically bind and target the GABA receptors have been designed and developed as useful tools in neurobiology.

1.9.1 PET radioligands binding to the GABA binding site

Despite extensive research on the pharmacology of $GABA_A$ receptors, there are only a few examples in the literature of GABA radiotracers that have been reported.[102] [4-^{11}C]GABA (**45**) was labelled starting with hydrogen [^{11}C]cyanide prepared from [^{11}C]CO_2. Michael addition with ethyl acrylate (**43**) followed by a selective reduction and hydrolysis of the resulting amino ester (**44**) afforded [4-^{11}C]GABA (**45**) (Scheme 3).[103]

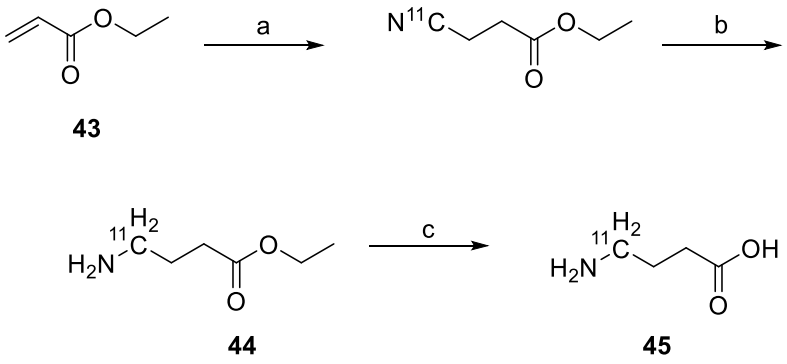

Scheme **3**: Radiosynthesis of [4-^{11}C]GABA (**45**).[103] Reagents: a) K^{11}CN, kryptofix K_{222}, THF; b) $CoCl_2$/$NaBH_4$, MeOH; c) NaOH.

Schiff bases of benzophenone derivatives have been reported to displace GABA from the $GABA_A$ receptor by mimickling the binding properties of GABA. In this category, [^{11}C]methoxyprogabidic acid (**47**) was radiolabelled by reacting 5-fluoro-2-hydroxy-4'-hydroxybenzophenone (**46**) with [^{11}C]methyl iodide through a Schiff reaction with an excess of GABA (**12**) in the presence of sodium methoxide as a catalyst (Scheme 4). Although the biodistribution of this radioligand in mice has been reported, no human PET data is reported.[104]

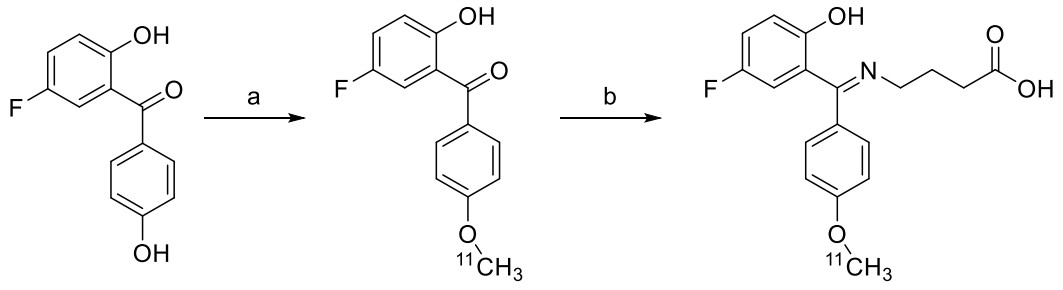

46 **47**

Scheme **4**: Radiosynthesis of [^{11}C]methoxypropagidic acid (**47**).[104] Reagents: a) $^{11}CH_3I$; b) GABA (**12**), NaOMe.

1.9.2 PET radioligands binding to the benzodiazepine binding site

Benzodiazepines have been prescribed as psychotropic drugs for the treatment of epilepsy, sleep disorders, anxiety and symptoms of depression for more than four decades.[105] Chemically, benzodiazepines are a class of compound that contain an aryl ring fused to a seven membered diazepine (often 1,4-diazepine) ring. Some of the most common benzodiazepine psychotropic drugs are illustrated in Figure 12.

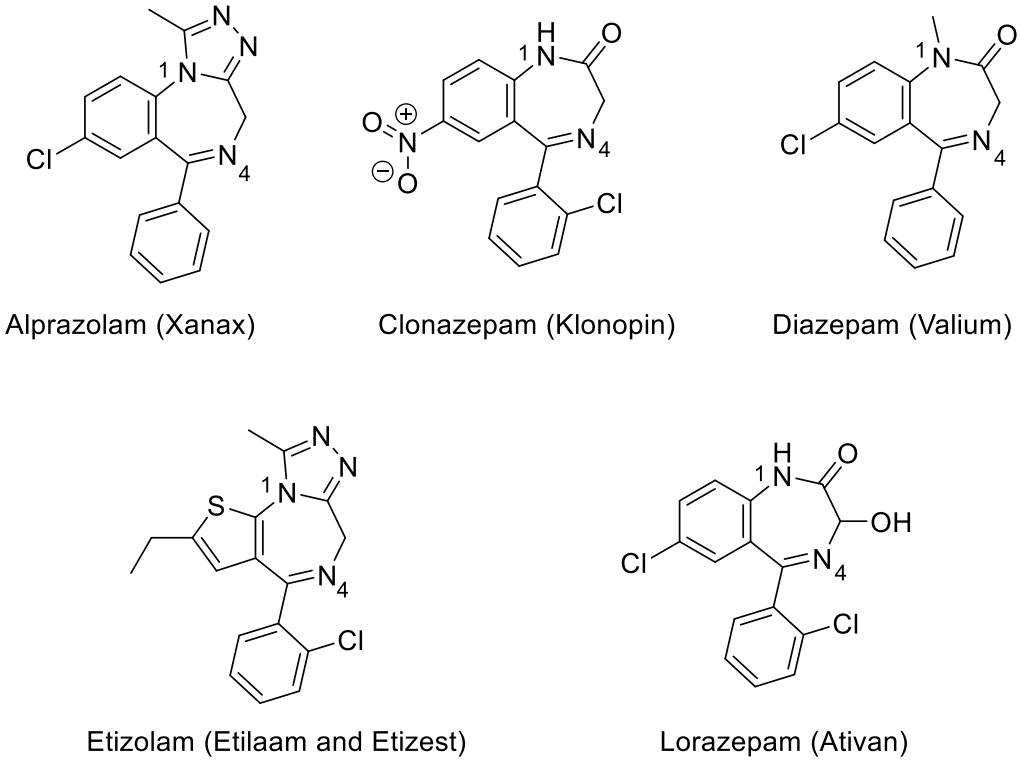

Figure **12**: Common benzodiazepine psychotropic drugs.[105]

The classical benzodiazepines are agonists with similar affinity to GABA for $GABA_A$ receptors. The binding site of benzodiazepines, however, is slightly different. In GABA, the binding site is located between the α and β subunits, whereas the binding site of benzodiazepines is located between the α and γ subunits (Figure 13).[42] Due to this different location, benzodiazepines do not trigger chloride ion channel opening, but they enhance the activity of the channel once it is opened. Therefore, benzodiazepines are inactive without the presence of GABA.[42]

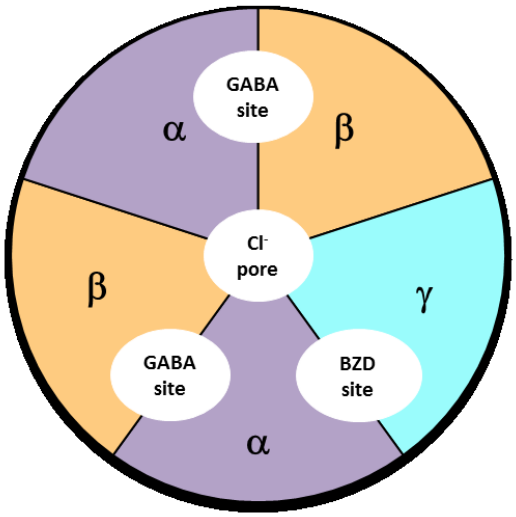

Figure **13:** Binding sites of GABA and benzodiazepine on $GABA_A$ receptor.

[^{11}C]Flunitrazepam (**48**) and [^{11}C]diazepam (**49**) were the first examples of radiolabelled benzodiazepines.[106,107] Both of these compounds were labelled by *N*-[^{11}C]-methylation on the amide nitrogen using [^{11}C]methyl iodide. Later, [^{11}C]fludiazepam (**50**), which is the 2'-fluoro analogue of [^{11}C]diazepam, was also labelled using the same approach (Scheme 5). The low specificity and binding affinity of these compounds on the benzodiazepine receptors was a major drawback for progressing them for PET imaging.[108]

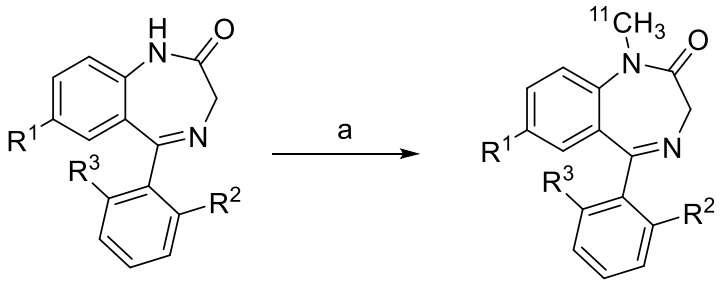

Scheme **5**: Radiosyntheses of [^{11}C]flunitrazepam (**48**) ($R^1 = NO_2$, $R^2 = F$, $R^3 = H$), [^{11}C]diazepam (**49**) (R^1=Cl, R^2=R^3=H), and [^{11}C]fludiazepam (**50**) (R^1 = Cl, $R^2 = F$, $R^3 = H$). Reagent: a) $^{11}CH_3I$.

As benzodiazepines are prone to be metabolised by 3-hydroxylation,[109] 3-[^{18}F]fluorodiazepam (**53**) was explored as a potential tracer. It was prepared from diazepam (**51**) by electrophilic fluorination of [^{18}F]F_2 or using the milder fluorinating agent [^{18}F]acetyl hypofluorite.[110] It was suggested that the radiolabelled compound is formed through a concerted cyclic mechanism from the enol form of diazepam (**52**) as illustrated in Scheme 6.[110]

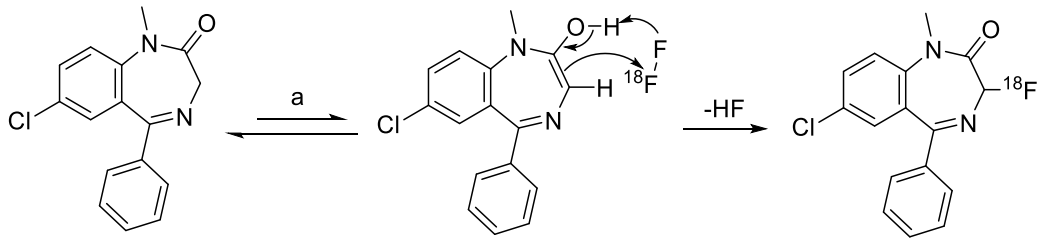

51 **52** **53**

Scheme **6**: Radiosynthesis of 3-[^{18}F]fluorodiazepam (**53**). Reagent: a) [^{18}F]F_2.

Due to accumulated pharmacological problems associated with the classical benzodiazepines such as [^{11}C]flunitrazepam (**48**) and [^{11}C]diazepam (**49**), a potent benzodiazepine antagonist bearing an imidazole ring system was designed. The imidazobenzodiazepine flumazenil (Ro 15-1788) (**54**) was labelled with carbon-11 on the *N*-methyl carbon using [^{11}C]methyl iodide[111–113] or [^{11}C]methyl triflate[114] (Scheme 7). [^{11}C]-*N*-Methyl-flumazenil (**55**) has been extensively used to quantify benzodiazepine binding in the human brain,[115] to measure changes in GABA levels,[116,117] as well as to investigate some neurological disorders such as epilepsy and neuronal loss in stroke.[118,119]

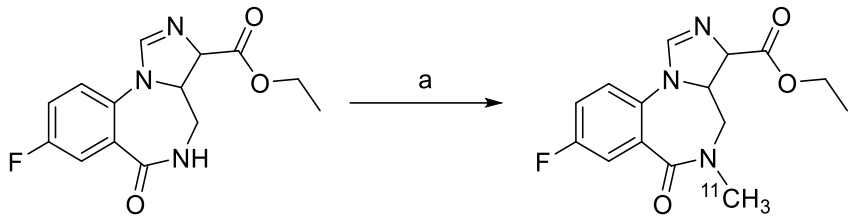

54 **55**

Scheme **7**: Radiosynthesis of [^{11}C]flumazenil (**55**). Reagents: a) $^{11}CH_3I$ or $^{11}CH_3OTf$, acetone, NaOH.

Incorporating fluorine 18 into the structure of flumazenil was challenging because of the unactivated aromatic ring. The first reported synthesis of [^{18}F]flumazenil (**57**) involved nucleophilic substitution of [^{18}F] fluoride ion with the nitro precursor (**56**), under both conventional and microwave irradiation heating methods (Scheme 8).[120,121]

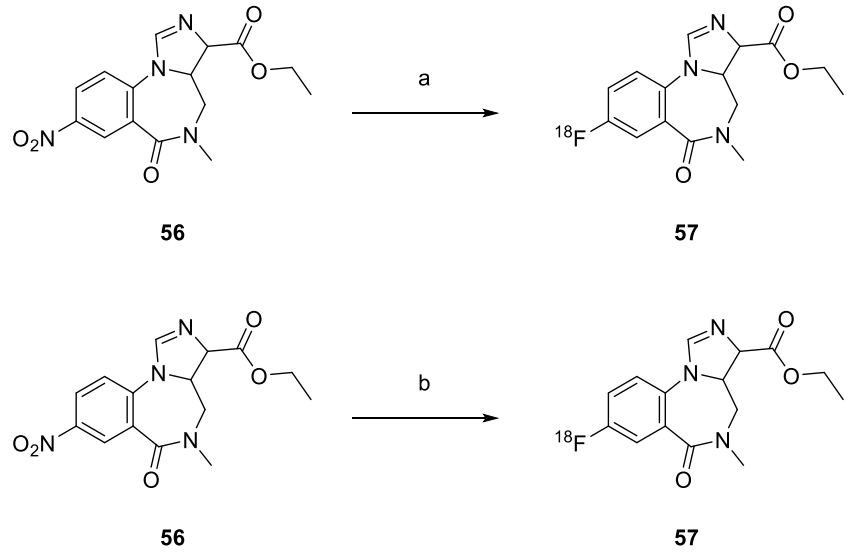

56 **57**

56 **57**

Scheme **8**: Synthetic routes to obtain [^{18}F]flumazenil (**57**). Reagents and conditions: a) [^{18}F]F$^-$, kryptofix K_{222}/K_2CO_3, DMF, 160 °C, 30 min; b) [^{18}F]F$^-$, kryptofix K_{222}/K_2CO_3, DMF, 160 °C, 5 min.

More recently, Rodnick *et al*.,[122] introduced the new flumazenil analogue radiotracers [^{18}F]AH114726 (**60**) and [^{18}F]GEH120348 (**61**) with high chemical and radiochemical purities and high specific activities. The syntheses of these radiotracers were carried out by nucleophilic aromatic substitution using [^{18}F] fluoride ion with the nitro aromatic precursors (**58**) and (**59**) (Scheme 9). Both radiotracers showed good activities on $GABA_A$/benzodiazepines receptors, and are comparable to [^{11}C]flumazenil (**55**), offering an option for imaging the $GABA_A$ receptor.[122]

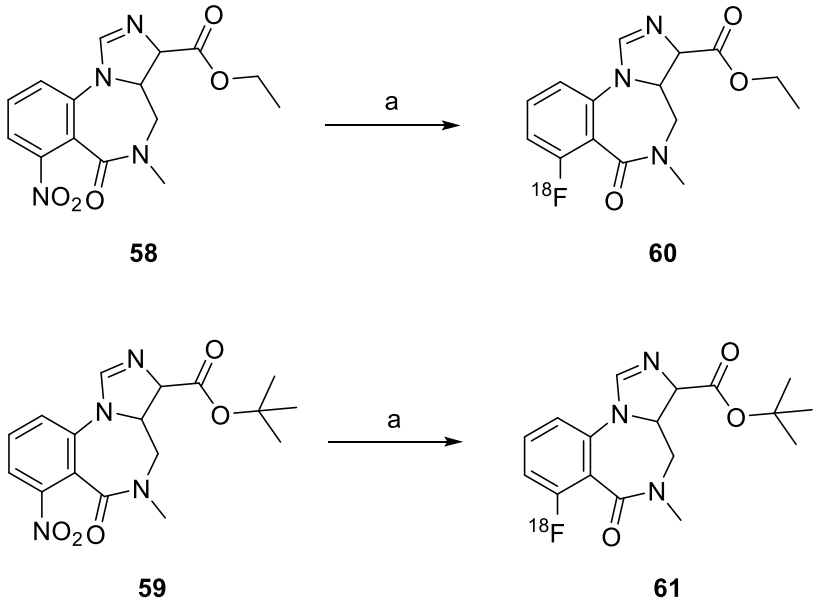

58 **60**

59 **61**

Scheme **9**: Radiosynthesis of [^{18}F]AH14726 (**60**) and[^{18}F]GEH120348 (**61**). Reagents and conditions: a) [^{18}F]F$^-$, kryptofix K_{222}/K_2CO_3, DMF, 130 °C, 30 min.

Some other examples of the [^{18}F] labelled radiotracers of the flumazenil analogues include [^{18}F]FFMZ (**62**) and [^{18}F]FEFMZ (**63**). However, neither of these labelled radiotracers exhibited satisfactory *in vivo* properties compared to [^{18}F]FMZ (**57**).[123,124]

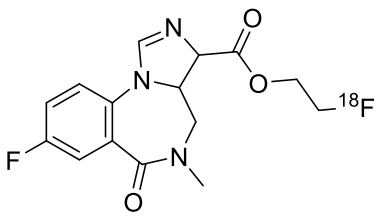

62

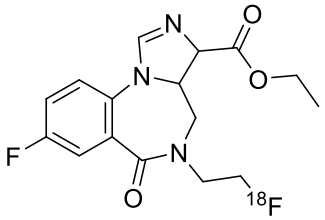

63

Since the fluorination of muscimol has never been achieved before, fluoromuscimol would be of great interest for its agonist activity against $GABA_A$ receptors. A first synthesis of fluoromuscimol and its biological effect on $GABA_A$ receptors is the subject of Chapter 2.

1.10 References

1 A. Tressaud, *Angew. Chem. Int. Ed.*, 2006, **45**, 6792–6796.

2 J. Swinson, *Pharmaceuticals*, 2005, **1**, 26–30.

3 B. K. Park, N. R. Kitteringham and P. M. O'Neill, *Annu. Rev. Pharmacol. Toxicol.*, 2001, **41**, 443–470.

4 A. Bondi, *J. Phys. Chem.*, 1964, **68**, 441–451.

5 L. Pauling, *The nature of the chemical bond and the structure of molecules and crystals: an introduction to modern structural chemistry*, Cornell University Press, New York, 3rd ed., 1960, pg. 90.

6 B. S. Chauhan, *Principles of biochemistry and biophysics*, University Science Press, New Delhi, 2008, pg. 8.

7 D. O'Hagan, *Chem. Soc. Rev.*, 2008, **37**, 308–319.

8 T. Furuya, C. A. Kuttruff and T. Ritter, *Curr. Opin. Drug Discov. Devel.*, 2008, **11**, 803–819.

9 T. Furuya, A. S. Kamlet and T. Ritter, *Nature*, 2011, **473**, 470–477.

10 G. A. Patani and E. J. LaVoie, *Chem. Rev.*, 1996, **96**, 3147–3176.

11 R. B. Silverman and M. W. Holladay, *The organic chemistry of drug design and drug action*, Academic press, London, 3rd edn., 2014, pg. 29.

12 B. E. Smart, *J. Fluor. Chem.*, 2001, **109**, 3–11.

13 S. D. Banister, J. Stuart, R. C. Kevin, A. Edington, M. Longworth, S. M. Wilkinson, C. Beinat, A. S. Buchanan, D. E. Hibbs, M. Glass, M. Connor, I. S. McGregor and M. Kassiou, *ACS Chem. Neurosci.*, 2015, **6**, 1445–1458.

14 J. Wang, M. Sánchez-Roselló, J. L. Aceña, C. del Pozo, A. E. Sorochinsky, S. Fustero, V. A. Soloshonok and H. Liu, *Chem. Rev.*, 2014, **114**, 2432–2506.

15 C. Isanbor and D. O'Hagan, *J. Fluor. Chem.*, 2006, **127**, 303–319.

16 J. Fried and E. F. Sabo, *J. Am. Chem. Soc.*, 1954, **76**, 1455–1456.

17 C. Heidelberger, N. K. Chaudhuri, P. Danneberg, D. Mooren, L. Griesbach, R. Duschinsky, R. J. Schnitzer, E. Pleven and J. Scheiner, *Nature*, 1957, **179**, 663–666.

18 M. Rowley, L. J. Bristow and P. H. Hutson, *J. Med. Chem.*, 2001, **44**, 477–501.

19 J. T. Strupczewski, K. J. Bordeau, Y. Chiang, E. J. Glamkowski, P. G. Conway, R. Corbett, H. B. Hartman, M. R. Szewczak, C. A. Wilmot and G. C. Helsley, *J. Med. Chem.*, 1995, **38**, 1119–1131.

20 C. S. Carter, B. H. Mulsant, R. A. Sweet, R. A. Maxwell, K. Coley, R. Ganguli and R. Branch, *Psychopharmacol. Bull.*, 1995, **31**, 719–725.

21 *Us*. *Pat*., US005158952A, 1992.

22 B. Green, *Curr. Drug Ther.*, 2009, **4**, 7–11.

23 A. M. Nussbaum and T. S. Stroup, *Schizophr. Bull.*, 2012, **38**, 1124–1127.

24 S. Zhornitsky and E. Stip, *Schizophr. Res. Treatment*, 2012, **2012**, 1–12.

25 S. Caccia, L. Pasina and A. Nobili, *Drug Des. Devel. Ther.*, 2010, **4**, 33–48.

26 P. Krogsgaard-Larsen, L. Brehm and K. Schaumburg, *Acta Chem. Scand. B*, 1981, **35**, 311–324.

27. *Amanita muscaria*, https://commons.wikimedia.org/wiki/File:Amanita_muscaria_3_vliegenzwammen_op_rij.jpg, (accessed June 2016).

28 T. Takemoto, T. Nakajima and T. Yokobe, *J. Pharm. Soc. Jpn.*, 1964, **84**, 1232–1233.

29 C. H. Eugster, G. F. R. Müller and R. Good, *Tetrahedron Lett.*, 1965, **6**, 1813–1815.

30 K. Bowden and A. Drysdale, *Tetrahedron Lett.*, 1965, **6**, 727–728.

31 G. Karimi and B. M. Razavi, *Toxinology Clin. Toxinology Asia Pacific Africa*, 2015, 578–636.

32 D. Chandra, L. M. Halonen, A.-M. Linden, C. Procaccini, K. Hellsten, G. E. Homanics and E. R. Korpi, *Neuropsychopharmacology*, 2010, **35**, 999–1007.

33 P. Meera, M. Wallner and T. S. Otis, *J. Neurophysiol.*, 2011, **106**, 2057–2064.

34 N. Gavande, H.-L. Kim, M. R. Doddareddy, G. A. R. Johnston, M. Chebib and J. R. Hanrahan, *ACS Med. Chem. Lett.*, 2013, **4**, 402–407.

35 P. Krogsgaard-Larsen, G. A. R. Johnston, D. Lodge and D. R. Curtis, *Nature*, 1977, **268**, 53–55.

36 G. A. R. Johnston, *Pharmacol. Ther.*, 1996, **69**, 173–198.

37 K. Egawa and A. Fukuda, *Front. Neural Circuits*, 2013, **7**, 1–15.

38 M. Chebib and G. A. R. Johnston, *J. Med. Chem.*, 2000, **43**, 1427–1447.

39 J. Bormann, *Trends Pharmacol. Sci.*, 2000, **21**, 16–19.

40 P. Krogsgaard-Larsen, B. Frølund, F. S. Jørgensen and A. Schousboe, *J. Med. Chem.*, 1994, **37**, 2489–2505.

41 R. W. Olsen and H. Betz, in *Basic Neurochemistry: Molecular, Cellular and Medical Aspects*, eds. G. J. Siegel, R. W. Albers, S. Brady and D. Price, Elsevier Science, Amsterdam, 7th edn., 2005, pp. 291–293.

42 D. Belelli and J. J. Lambert, *Nat. Rev. Neurosci.*, 2005, **6**, 565–575.

43 S. G. Brickley and I. Mody, *Neuron*, 2012, **73**, 23–34.

44 P. K. Ahring, L. H. Bang, M. L. Jensen, D. Strøbæk, L. Y. Hartiadi, M. Chebib and N. Absalom, *Pharmacol. Res.*, 2016, **111**, 563–576.

45 C. Sun, W. Sieghart and J. Kapur, *Brain Res.*, 2004, **1029**, 207–216.

46 E. Persohn, P. Malherbe and J. G. Richards, *J. Comp. Neurol.*, 1992, **326**, 193–216.

47 D. J. Laurie, W. Wisden and P. H. Seeburg, *J. Neurosci.*, 1992, **12**, 4151–4172.

48 S. Pirker, C. Schwarzer, A. Wieselthaler, W. Sieghart and G. Sperk, *Neuroscience*, 2000, **101**, 815–850.

49 W. Wisden, A. Herb, H. Wieland, K. Keinänen, H. Lüddens and P. H. Seeburg, *FEBS Lett.*, 1991, **289**, 227–230.

50 G. Sperk, C. Schwarzer, K. Tsunashima, K. Fuchs and W. Sieghart, *Neuroscience*, 1997, **80**, 987–1000.

51 Z. Peng, B. Hauer, R. M. Mihalek, G. E. Homanics, W. Sieghart, R. W. Olsen and C. R. Houser, *J. Comp. Neurol.*, 2002, **446**, 179–197.

52 J. Glykys and I. Mody, *Neuron*, 2007, **56**, 763–770.

53 V. B. Caraiscos, E. M. Elliott, K. E. You-Ten, V. Y. Cheng, D. Belelli, J. G. Newell, M. F. Jackson, J. J. Lambert, T. W. Rosahl, K. a Wafford, J. F. MacDonald and B. A. Orser, *Proc. Natl. Acad. Sci. U. S. A.*, 2004, **101**, 3662–3667.

54 K. Quirk, P. Blurton, S. Fletcher, P. Leeson, F. Tang, D. Mellilo, C. I. Ragan and R. M. McKernan, *Neuropharmacol.*, 1996, **35**, 1331–1335.

55 E. R. Korpi, T. Kuner, P. H. Seeburg and H. Lüddens, *Mol. Pharmacol.*, 1995, **47**, 283–289.

56 M. Mortensen, B. Patel and T. G. Smart, *Front. Cell. Neurosci.*, 2012, **6**, 1–10.

57 G. A. R. Johnston, *Curr. Pharm. Des.*, 2005, **11**, 1867–1885.

58 U. Rudolph and B. Antkowiak, *Nat. Rev. Neurosci.*, 2004, **5**, 709–720.

59 M. Farrant and Z. Nusser, *Nat. Rev. Neurosci.*, 2005, **6**, 215–229.

60 D. S. Reddy, *Front. Endocrinol.*, 2011, **2**, 1–11.

61 R. Enz and G. R. Cutting, *Vision Res.*, 1998, **38**, 1431–1441.

62 G. A. R. Johnston, M. Chebib, J. R. Hanrahan and K. N. Mewett, *Curr. Drug Targets-CNS Neurol. Disord.*, 2003, **2**, 260–268.

63 M. M. Naffaa, N. Absalom, V. R. Solomon, M. Chebib, D. E. Hibbs and J. R. Hanrahan, *PLoS One*, 2016, **11**, 1–21.

64 B. Frølund, C. Madsen, A. J. Anders, U. Kristiansen and T. Liljefors, *Lægemiddelforskning*, 2006, 32–33.

65 S. Braat and R. F. Kooy, *Neuron*, 2015, **86**, 1119–1130.

66 G. A. R. Johnston, *Curr. Top. Med. Chem.*, 2002, **2**, 903–913.

67 M. Mortensen, B. Ebert, K. Wafford and T. G. Smart, *J. Physiol.*, 2010, **588**, 1251–1268.

68 G. Deniau, A. M. Z. Slawin, T. Lebl, F. Chorki, J. P. Issberner, T. van Mourik, J. M. Heygate, J. J. Lambert, L. A. Etherington, K. T. Sillar and D. O'Hagan, *ChemBioChem*, 2007, **8**, 2265–2274.

69 J. R. Bloomquist, R. E. Grubs, D. M. Soderlund and D. C. Knipple, *Comp. Biochem. Physiol. Part C Comp. Pharmacol.*, 1991, **99**, 397–402.

70 U. Kristiansen, J. D. C. Lambert, E. Falch and P. Krogsgaard-Larsen, *Br. J. Pharmacol.*, 1991, **104**, 85–90.

71 K. Hoestgaard-Jensen, R. M. O'Connor, N. O. Dalby, C. Simonsen, B. C. Finger, A. Golubeva, H. Hammer, M. L. Bergmann, U. Kristiansen and P. Krogsgaard-Larsen, *Br. J. Pharmacol.*, 2013, **170**, 919–932.

72 P. Krogsgaard-Larsen, B. Frølund and T. Liljefors, *Adv. Pharmacol.*, 2006, **54**, 53–71.

73 A. Cupello and H. Hydén, *Int. J. Neurosci.*, 1986, **30**, 297–301.

74 R. J. Breckenridge, S. H. Nicholson, A. J. Nicol, C. J. Suckling, B. Leigh and L. Iversen, *J. Neurochem.*, 1981, **37**, 837–844.

75 R. D. Allan, H. W. Dickenson, B. P. Hiern, G. A. R. Johnston and R. Kazlauskas, *Br. J. Pharmacol.*, 1986, **88**, 379–387.

76 C. K. L. Ng, H. L. Kim, N. Gavande, I. Yamamoto, R. J. Kumar, K. N. Mewett, G. A. R. Johnston, J. R. Hanrahan and M. Chebib, *Futur. Med. Chem.*, 2011, **3**, 197–209.

77 G. B. Saha, *Basics of PET Imaging Basics of PET Imaging*, Springer, New York, 2nd edn., 2010.

78 P. W. Miller, N. J. Long, R. Vilar and A. D. Gee, *Angew. Chem. Int. Ed.*, 2008, **47**, 8998–9033.

79 R. Pither, *Expert Rev. Mol. Diagn.*, 2003, **3**, 703–713.

80 L. K. Mien, PhD Thesis, University of Vienna, 2007.

81 L. Cai, S. Lu and V. W. Pike, *Eur. J. Org. Chem.*, 2008, 2853–2873.

82 D. Le Bars, *J. Fluor. Chem.*, 2006, **127**, 1488–1493.

83 T. B. Lynch, *PET/CT in Clinical Practice*, Springer, London, 2007.

84 O. Jacobson, D. O. Kiesewetter and X. Chen, *Bioconjugate Chem.*, 2015, **26**, 1–18.

85 R. Finn and D. Schlyer, *Production considerations for the "classical" PET nuclides*, Brookhaven National Laboratory report BNL-68381, Upton, New York, 2001.

86 A. Fredriksson, PhD Thesis, Karolinska Insttitute Stockholm, 2002.

87 D. D. Kemp and M. S. Gordon, *J. Phys. Chem. A*, 2005, **109**, 7688–7699.

88 R. J. Nickles, S. J. Gatley, J. R. Votaw and M. L. Kornguth, *Int. J. Radiat. Appl. Instrumentation. Part A. Appl. Radiat. Isot.*, 1986, **37**, 649–661.

89 M. Guillaume, A. Luxen, B. Nebeling, M. Argentini, J. C. Clark and V. W. Pike, *Int. J. Radiat. Appl. Instrumentation. Part A. Appl. Radiat. Isot.*, 1991, **42**, 749–762.

90 H. H. Coenen, in *PET Chemistry*, Springer, Berlin Heidelberg, 2007, pp. 15–50.

91 L. B. Been, A. J. H. Suurmeijer, D. C. P. Cobben, P. L. Jager, H. J. Hoekstra and P. H. Elsinga, *Eur. J. Nucl. Med. Mol. Imaging*, 2004, **31**, 1659–1672.

92 J. R. Grierson and A. F. Shields, *Nucl. Med. Biol.*, 2000, **27**, 143–156.

93 A. F. Shields, J. R. Grierson, B. M. Dohmen, H. J. Machulla, J. C. Stayanoff, J. M. Lawhorn-Crews, J. E. Obradovich, O. Muzik and T. J. Mangner, *Nat. Med.*, 1998, **4**, 1334–1336.

94 J. Mukherjee, B. T. Christian, K. A. Dunigan, B. Shi, T. K. Narayanan, M. Satter and J. Mantil, *Synapse*, 2002, **46**, 170–188.

95 A. Katsifis, K. Hamacher, J. Schnitter and G. Stöcklin, *Appl. Radiat. Isot.*, 1993, **44**, 1015–1020.

96 K. Hamacher and W. Hamkens, *Appl. Radiat. Isot.*, 1995, **46**, 911–916.

97 M. Piert, H.-J. Machulla, M. Picchio, G. Reischl, S. Ziegler, P. Kumar, H.-J. Wester, R. Beck, A. J. B. McEwan, L. I. Wiebe and M. Schwaiger, *J. Nucl. Med.*, 2005, **46**, 106–113.

98 J. G. Rajendran, D. C. Wilson, E. U. Conrad, L. M. Peterson, J. D. Bruckner, J. S. Rasey, L. K. Chin, P. D. Hofstrand, J. R. Grierson, J. F. Eary and K. A. Krohn, *Eur. J. Nucl. Med. Mol. Imaging*, 2003, **30**, 695–704.

99 T. Ido, C.-N. Wan, V. Casella, J. S. Fowler, A. P. Wolf, M. Reivich and D. E. Kuhl, *J. Label. Compd. Radiopharm.*, 1978, **14**, 175–183.

100 K. Hamacher, H. H. Coenen and G. Stocklin, *J. Nucl. Med.*, 1986, **27**, 235–239.

101 B. Beuthien-Baumann, K. Hamacher, F. Oberdorfer and J. Steinbach, *Carbohydr. Res.*, 2000, **327**, 107–118.

102 J. D. Andersson and C. Halldin, *J. Label. Compd. Radiopharm.*, 2013, **56**, 196–206.

103 G. Antoni, P. Malmborg and B. Langström, *J. Label. Compd. Radiopharm.*, 1989, **26**, 400–401.

104 F. De Vos and G. Slegers, *J. Label. Compd. Radiopharm.*, 1994, **34**, 643–652.

105 M. Defrancesco, J. Marksteiner, W. Wolfgang Fleischhacker and I. Blasko, *Int. J. Neuropsychopharmacol.*, 2015, **18**, 1–11.

106 D. Comar, M. Maziere, G. J. M, G. Berger, F. Soussaline, C. H. Menini, G. Arfel and R. Naquet, *Nature*, 1979, **280**, 329–331.

107 M. Maziere, J.-M. Godot, G. Berger, C. Prenant and D. Comar, *J. Radioanal. Chem.*, 1980, **56**, 229–235.

108 K. Ishiwata, K. Yanai, T. Ido, Y. Miura-Kanno and K. Kawashima, *Int. J. Radiat. Appl. Instrumentation. Part B. Nucl. Med. Biol.*, 1988, **15**, 365–371.

109 A. Acikgöz, N. Karim, S. Giri, W. Schmidt-Heck and A. Bader, *Toxicol. Appl. Pharmacol.*, 2009, **234**, 179–191.

110 A. Luxen, N. Satyamurthy, M. E. Phelps and L. Angeles, *J. Fluor. Chem.*, 1987, **36**, 83–92.

111 M. Maziere, P. Hantraye, C. Prenant, J. Sastre and D. Comar, *Int. J. Appl. Radiat. Isot.*, 1984, **35**, 973–976.

112 K. Suzuki, O. Inoue, K. Hashimoto, T. Yamasaki, M. Kuchiki and K. Tamate, *Int. J. Appl. Radiat. Isot.*, 1985, **36**, 971–976.

113 C. Halldin, S. Stone-Elander, J.-O. Thorell, A. Persson and G. Sedvall, *Int J Radiat Appl Instrum A*, 1988, **39**, 993–997.

114 K. Nagren and C. Halldin, *J. Label. Compd. Radiopharm.*, 1998, **41**, 831–841.

115 A. Persson, S. Pauli, C. Halldin, S. Stone-Elander, L. Farde, I. Sjögren and G. Sedvall, *Hum. Psychopharmacol. Clin. Exp.*, 1989, **4**, 21–31.

116 W. G. Frankle, R. Y. Cho, R. Narendran, N. S. Mason, S. Vora, M. Litschge, J. C. Price, D. A. Lewis and C. A. Mathis, *Neuropsychopharmacology*, 2009, **34**, 624–633.

117 W. G. Frankle, R. Y. Cho, N. S. Mason, C.-M. Chen, M. Himes, C. Walker, D. A. Lewis, C. A. Mathis and R. Narendran, *PLoS One*, 2012, **7**, 1–9.

118 P. L. Pearl, K. M. Gibson, Z. Quezado, I. Dustin, J. Taylor, S. Trzcinski, J. Schreiber, K. Forester, P. Reeves-Tyer and C. Liew, *Neurology*, 2009, **73**, 423–429.

119 I. Savic, P. Roland, G. Sedvall, A. Persson, S. Pauli and L. Widen, *Lancet*, 1988, **332**, 863–866.

120 N. N. Ryzhikov, N. Seneca, R. N. Krasikova, N. A. Gomzina, E. Shchukin, O. S. Fedorova, D. A. Vassiliev, B. Gulyás, H. Hall, I. Savic and C. Halldin, *Nucl. Med. Biol.*, 2005, **32**, 109–116.

121 K. S. Mandap, T. Ido, Y. Kiyono, M. Kobayashi, T. G. Lohith, T. Mori, S. Kasamatsu, T. Kudo, H. Okazawa and Y. Fujibayashi, *Nucl. Med. Biol.*, 2009, **36**, 403–409.

122 M. E. Rodnick, B. G. Hockley, P. Sherman, C. Quesada, M. R. Battle, A. Jackson, K. E. Linder, S. Macholl, W. J. Trigg, M. R. Kilbourn and P. J. H. Scott, *Nucl. Med. Biol.*, 2013, **40**, 901–905.

123 G. Gründer, T. Siessmeier, C. Lange-Asschenfeldt, I. Vernaleken, H. G. Buchholz, P. Stoeter, A. Drzezga, H. Lüddens, F. Rösch and P. Bartenstein, *Eur. J. Nucl. Med.*, 2001, **28**, 1463–1470.

124 M. Mitterhauser, W. Wadsak, L. Wabnegger, L.-K. Mien, S. Tögel, O. Langer, W. Sieghart, H. Viernstein, K. Kletter and R. Dudczak, *Nucl. Med. Biol.*, 2004, **31**, 291–295.

Chapter 2: Syntheses and biological studies of fluoromuscimols

2.1 Introduction

As discussed in Chapter 1, despite extensive research on the development of novel radiotracers that target the $GABA_A$ receptor, most do not locate at the GABA binding site.[1–5] In addition, there are currently no suitable radiotracers that have been specifically designed to locate at the synaptic and extrasynaptic $GABA_A$ receptors. Therefore, the fluoro analogues of a compound known to locate at the GABA binding site of $GABA_A$ receptors could be of value. If the fluoro analogues retained similar properties to its non-fluorinated parent, it could then serve as a starting point for the development of a PET radiotracer for GABA receptors. In this context, the fluorination of muscimol (**11**), a naturally occurring toxin isolated from the mushroom *Amanita muscaria,* was chosen as a research focus. Specifically, syntheses of fluoromuscimol (**64**) and trifluomethylmuscimol (**65**) were addressed.

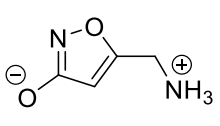

11

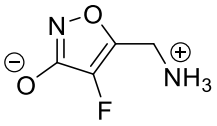

64

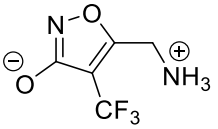

65

2.2 Previous syntheses of muscimol

Since the isolation of muscimol from *Amanita muscaria*, a number of syntheses have been reported.[6–11] However, the preparation and investigations of muscimol and its derivatives have been restricted due to the limited availability of both natural and synthetic material. Despite a number of approaches, the synthesis of muscimol suffers from the number of steps, availability of starting materials, and poor reproducibility of yields.

Among the several synthetic approaches, the route reported by Pevarello and Varasi is one of the most convenient,[6] particularly for large scale synthesis of muscimol (Scheme 10). In this synthesis, the bromo(chloromethyl)isoxazole (**69**) intermediate was obtained in a high yield (81%) through a 1,3-dipolar cycloaddition reaction between bromonitrile oxide (**68**) generated *in situ* from stable and easily available dibromoformaldoxime (**66**) and 2,3-dichloropropene (**67**). Substitution reactions with ammonia and methanol afforded methyl ether protected muscimol (**70**), which was then deprotected using HBr in AcOH furnishing muscimol (**11**).

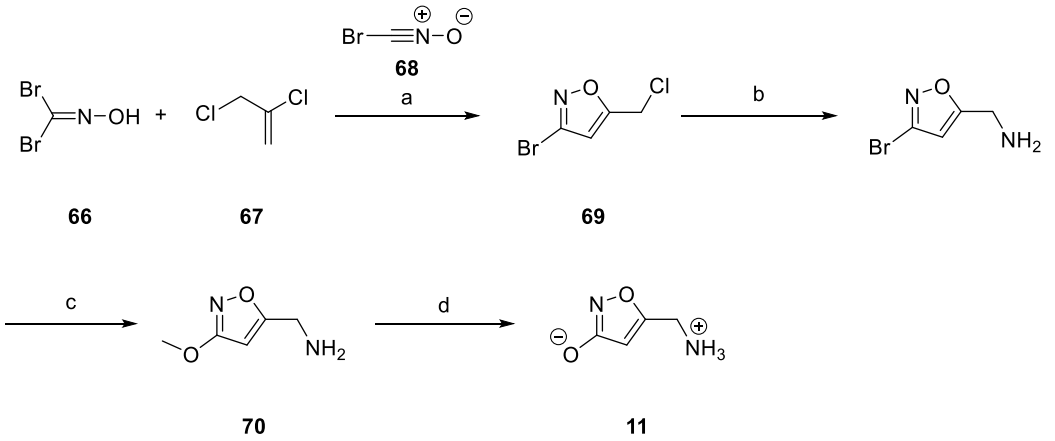

Scheme **10**: Pevarello and Varasi synthesis of zwitterionic muscimol (**11**).[6] Reagents and conditions: a) $KHCO_3$, EtOAc, H_2O, 25 °C, 20 h, 81%; b) 30% NH_3, H_2O, dioxane, 0→25 °C, 5 h; 90%; c) MeOH, KOH, H_2O, reflux, 48 h, 66%; d) 33% HBr, AcOH, reflux, 15 min, 62%.

On the other hand, McCarry and Savard reported a facile approach to the synthesis of muscimol starting from propargyl chloride (**71**) (Scheme 11).[7] The first step of this reaction involved the deprotonation of propargyl chloride by methyllithium and then treatment with ethyl chloroformate, to generate ethyl chlorotetrolate (**72**). Further reaction with hydroxylamine in basic methanolic solution produced hydroxamic acid (**73**) which underwent *in situ* cyclisation to afford 5-chloromethyl hydroxyisoxazole (**74**). Finally, the conversion to muscimol (**11**) was accomplished by heating (**74**) in a methanolic solution of anhydrous ammonia.

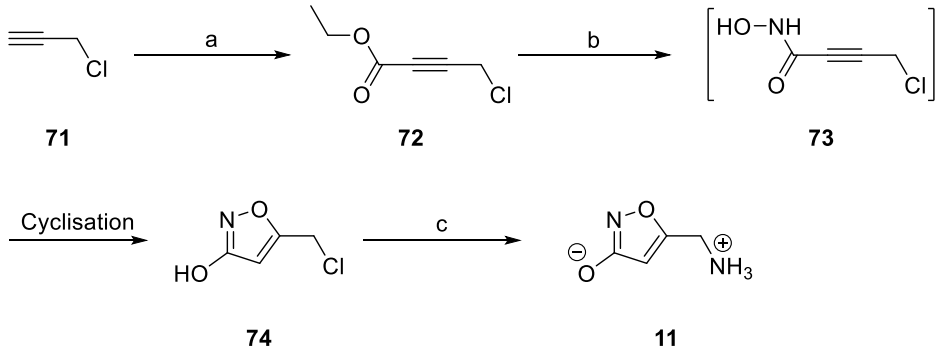

Scheme **11:** McCarry and Savard synthesis of muscimol (**11**).[7] Reagents and conditions: a) CH_3Li, $ClCO_2Et$, Et_2O, -40 °C, 70%, b) NH_2OH, MeOH (aq), -35 °C, 15 min, 41%; c) NH_3, MeOH, 0→50 °C, 5 h, 65%.

The shortest and convenient synthesis of muscimol was reported by Frey and Jäger (Scheme 12).[8] The reaction involved three straightforward steps, progressing through stable crystalline intermediates. The synthesis began with a DBU induced condensation of hydroxyurea (**75**) and dimethyl acetylenedicarboxylate (**76**) to form methyl 3-hydroxyisoxazole-5-carboxylate (**77**). Treatment of (**77**) with ammonia, followed by amide reduction of (**78**) using borane dimethyl sulfide (BMS), furnished muscimol (**11**) as a white crystalline solid after acidic ion-exchange resin work up.

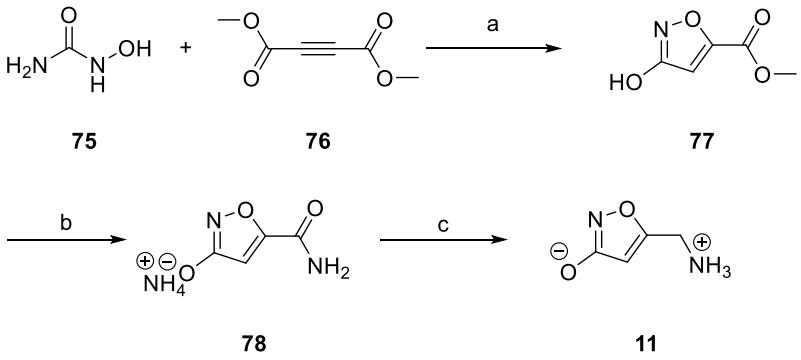

Scheme **12:** Frey and Jäger synthesis of muscimol (**11**).[8] Reagents and conditions: a) DBU, MeOH, 0-10 °C, 60%; b) NH_3(aq), MeOH, 1 h, quant.; c) BMS, THF, reflux, 8 h, 51%.

A proposed mechanism for the formation of methyl ester (**77**) in Scheme 13 involves an initial deprotonation of the OH group of hydroxyurea (**75**) by DBU forming (**79**). Michael addition of (**79**) to dimethyl acetylenedicarboxylate (**76**) results in the formation of intermediate (**80**), which then undergoes intramolecular cyclisation through nucleophilic displacement of the methoxyl group, to generate the five-membered heterocycle (**81**). The final product (**77**), is obtained *via* the loss of methyl carbamate and subsequent enolisation of (**82**).[12]

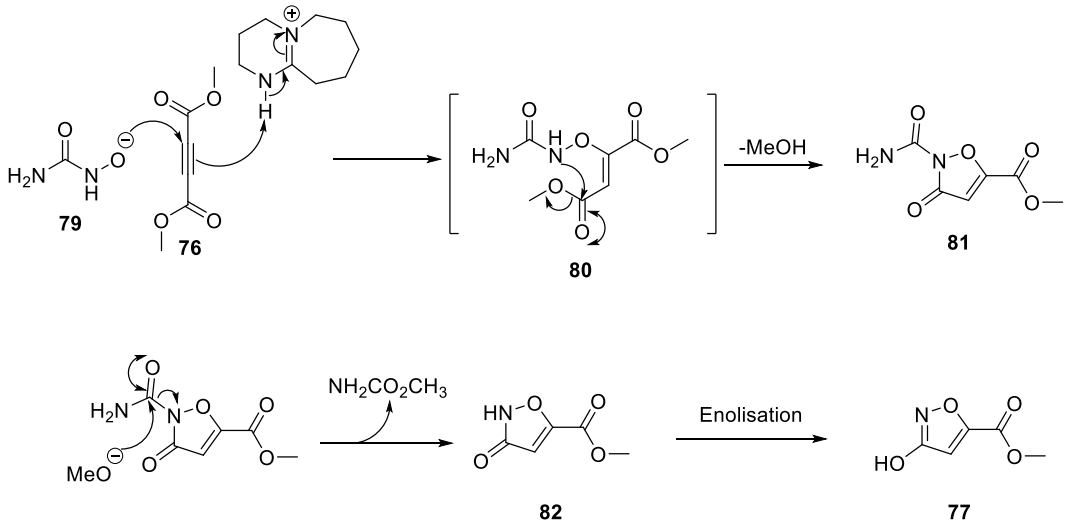

Scheme **13**: Proposed mechanism for the formation of the heterocycle (**77**).[12]

2.3 Aims of this project

The objective of this project was to prepare two fluorinated analogues of muscimol and, subsequently, assay their agonist activities against the $GABA_A$ receptors in order to study their relative efficacy compared to muscimol itself. If the interesting properties of muscimol, such as the ability to cross the blood brain barrier[13] and high affinity[14] for the GABA binding site are preserved in fluoromuscimol (**64**) and trifluoromethylmuscimol (**65**), this opens opportunities for future PET application, specifically [^{18}F]-fluoromuscimol and [^{18}F]-trifluoromethylmuscimol. They could indeed serve as a starting point to probe GABA binding sites on $GABA_A$ receptors; something that remains unresolved with the current $GABA_A$ receptor radiotracers, as they bind almost exclusively at the benzodiazepine binding site.[15–18] If such properties are conserved in these fluorine containing compounds, a synthesis suitable for PET will require development.

2.4 Results and discussion

2.4.1 Approach A-Retrosynthetic approach

Our first approach towards the synthesis of fluoromuscimol (**64**) envisioned the retrosynthetic route shown in Scheme 14. According to the proposed retrosynthetic route, the desired fluoromuscimol (**64**) could be approached through azide (**83**). This intermediate might be formed by cyclisation of α-fluoro-β-keto-hydroxamic acid (**84**). The reactive β-ketohydroxamic acid (**84**) could be obtained from the corresponding fluorinated ketoester (**85**) which is accessible *via* fluorination of ketoester (**86**).

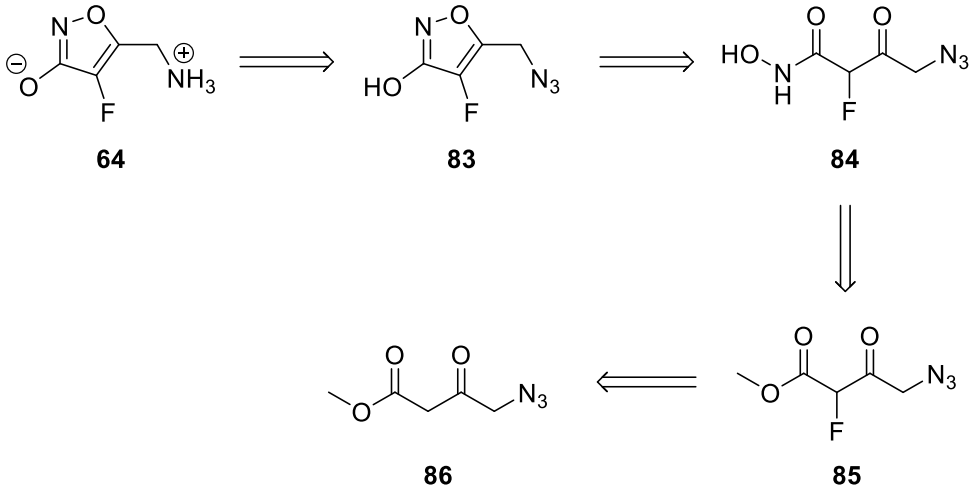

Scheme **14**: Retrosynthetic approach to fluoromuscimol (**64**).

In order to address this approach, ketoester (**86**) was synthesised through nucleophilic substitution on the commercially available chloroacetoaetate (**87**) with sodium azide in THF/water mixture (Scheme 15). Fluorination of (**86**) was carried out at room temperature using Selectfluor™ as an electrophilic fluorination reagent, as shown in Scheme 15. The reaction used a catalytic amount of cyclopentadienyl(IV) titanium trichloride ($TiCpCl_3$) in acetonitrile. The catalyst was chosen on the basis of the previously reported fluorination reactions on several β-ketoesters which showed that the use of $TiCpCl_3$ induced a clean fluorination with high selectivity towards the monofluorinated product.[19,20] The reaction was not clean and purification by column chromatography proved to be challenging as some impurities co-eluted together with ketoester (**85**). However, after careful chromatography, the desired fluorinated product (**85**) was successfully isolated, albeit in low yield (37%). A control experiment indicated that the reaction did not occur in the absence of catalyst.

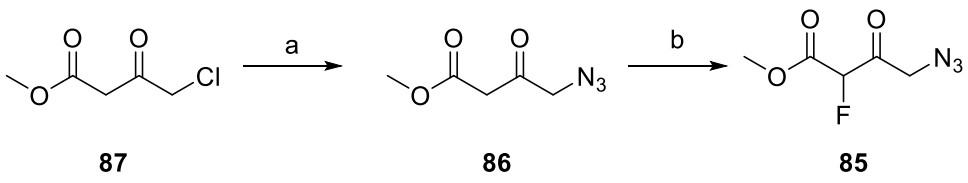

87 **86** **85**

Scheme **15:** Synthesis and fluorination method of (**85**). Reagents and conditions: a) NaN_3, THF/water, 0 °C→rt, overnight, 67%, b) Selectfluor™, $TiCpCl_3$, MeCN, 15 h, 37%.

The mechanism proposed for this fluorination reaction is depicted in Scheme 16 and starts with the coordination of substrate (**86**) to $TiCpCl_3$ (**88**) followed by enolisation within the coordination sphere of the catalyst. Subsequent SET interaction with Selectfluor™ (**89**) gives rise to the formation of radical cation intermediate (**90**), which then captures a fluorine atom from the reagent forming the new C-F bond.[21] Displacement of product (**85**) from the catalyst by exchange with another molecule of substrate (**86**) completes the catalytic cycle.[22,23]

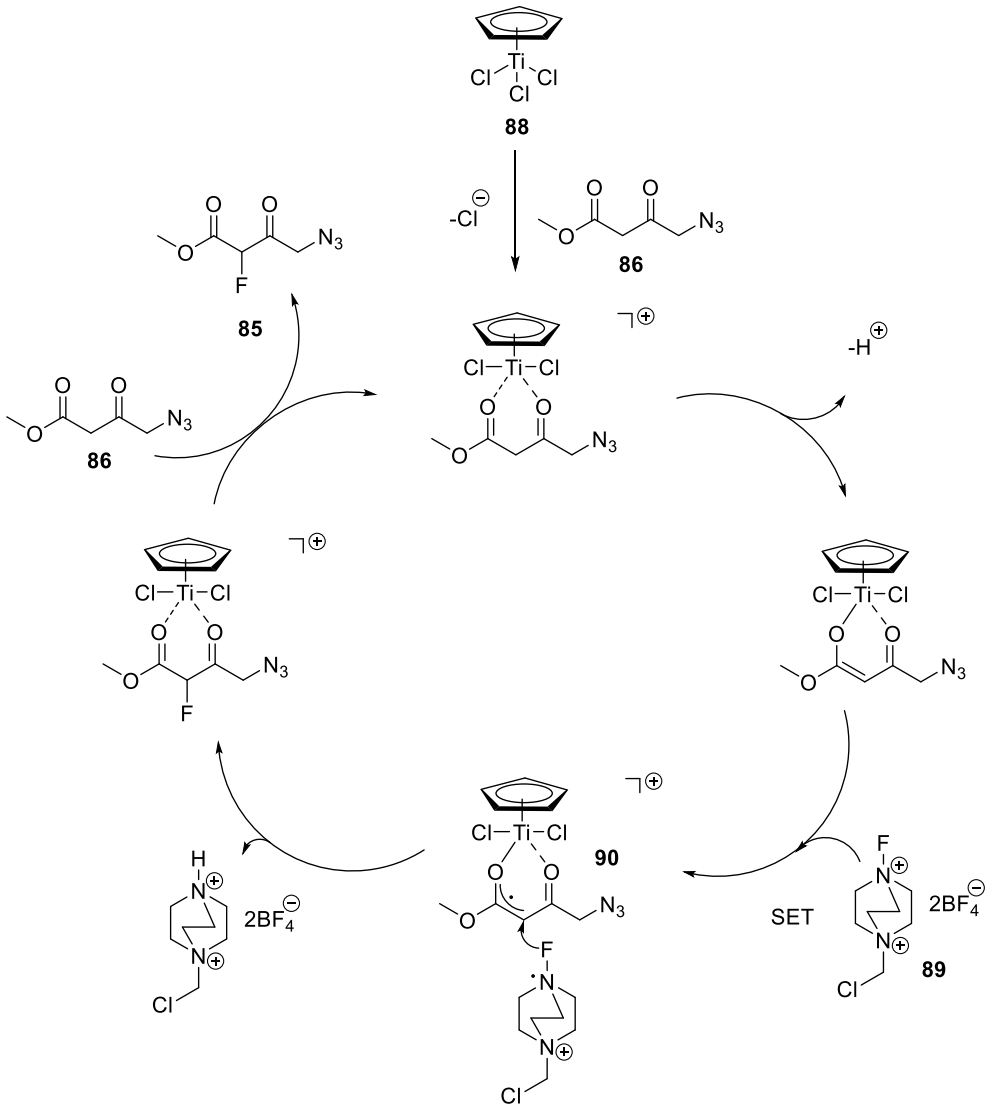

Scheme**16**: Proposed catalytic cycle for the fluorination of (**86**).[22,23]

As shown in Figure 14, the ^{1}H NMR spectrum of (**85**) exhibits three proton signals. The methyl group at 3.88 ppm is assigned to H-5 and the methine proton H-2 appears as a doublet at 5.39 ppm, with a geminal fluorine coupling constant of $^{2}J_{HF}$ = 48.4 Hz. The methylene protons (H-4) are diastereotopic and display an AB-pattern at 4.31 ppm ($^{2}J_{HH}$ = 19.2 Hz, $^{4}J_{HF}$ = 2.2 Hz) and at 4.26 ppm ($^{2}J_{HH}$ = 19.2 Hz, $^{4}J_{HF}$ = 1.6 Hz) respectively.

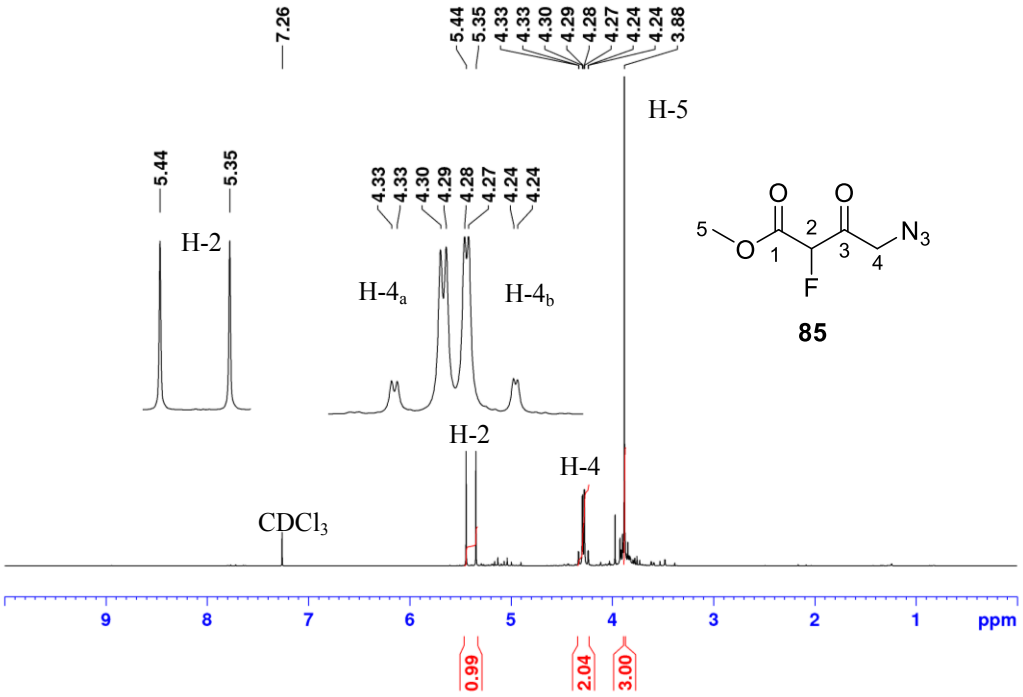

Figure **14**: ^{1}H NMR spectrum of (**85**).

A representative fluorine decoupled ^{1}H{^{19}F}experiment of (**85**) is shown in Figure 15. The spectrum clearly shows that the doublet for the H-2 collapses to a singlet, while that of the AB-pattern simplifies with the removal of fluorine coupling.

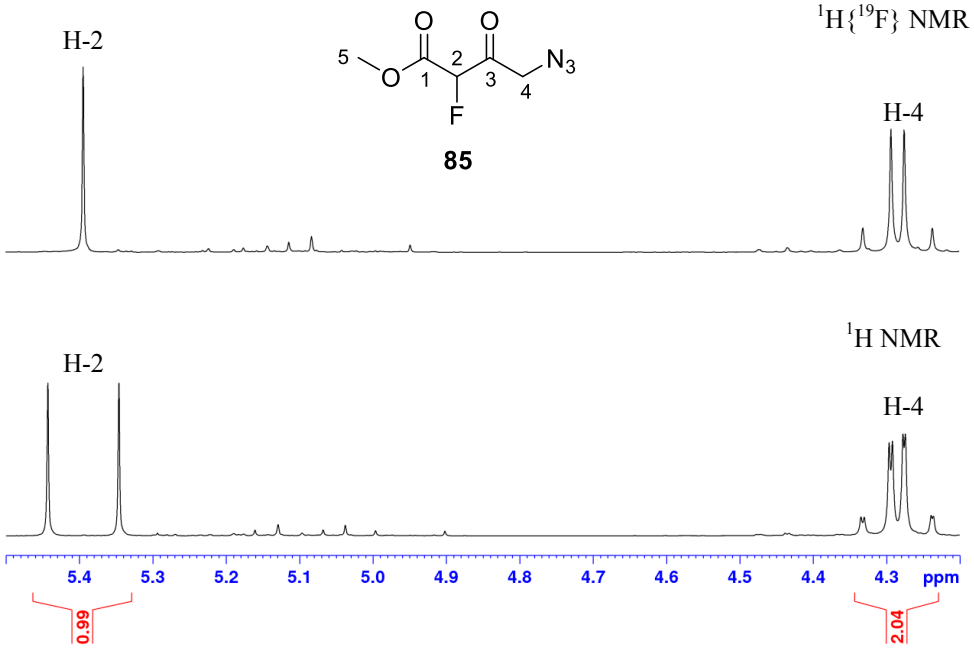

Figure **15**: Partial ^{1}H NMR spectra of (**85**) with and without {^{19}F}.

The ^{19}F-NMR spectrum of (**85**) (Figure 16) has a signal at -199.5 ppm. It appears as doublet of multiplets with a geminal coupling constant of $^2J_{HF}$ = 48.4 Hz. This signal becomes a singlet in the proton-decoupled ^{19}F{^{1}H} NMR spectrum, as expected.

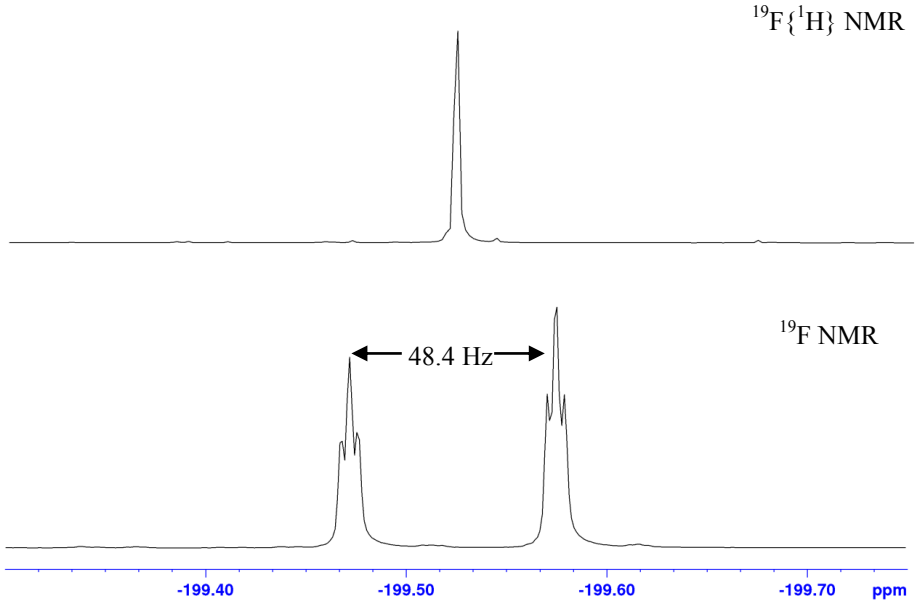

Figure **16**: Partial ^{19}F NMR spectra of (**85**) with and without {^{1}H}.

The ^{13}C NMR analysis of (**85**) (Figure 17) reveals three sets of doublets. The signals at 199.5 ppm and 163.7 ppm have coupling constants of $^{2}J_{CF}$ 24.2 Hz and $^{2}J_{CF}$ 23.6 Hz, are assigned to C-3 and C-1 carbonyl carbons respectively, whereas that at 90.5 ppm with a large $^{1}J_{CF}$ coupling constant of 197.4 Hz is assigned to the CHF C-2.

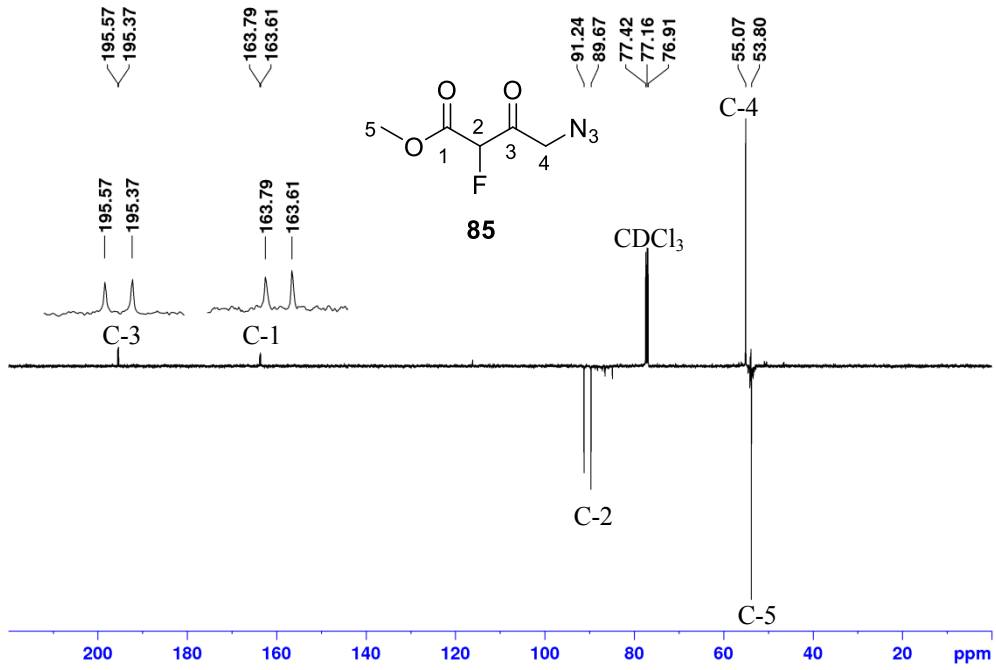

Figure **17**:^{13}C NMR spectrum of (**85**).

With compound (**85**) in hand, a conversion to β-ketohydroxamic acid (**84**) was required. Since the carbonyl group of a ketone is more susceptible to nucleophilic attack than that of an ester, it was necessary to protect this group in order to avoid formation of hydroxyl-imine (**91**) rather than the desired ketohydroxamic acid (**84**).

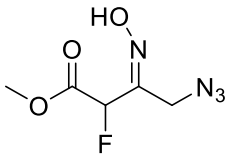

91

Protection of ketone (**85**) as an acetal (Scheme 17) was attempted using ethylene glycol. However, despite exploring various sets of conditions (boron trifluoride diethyl etherate, or tosic acid as catalyst, molecular sieves or Dean-Stark apparatus), none of the desired acetylated product (**92**) was formed, and only starting material was recovered at the end of the reaction period. An attempt to protect ketone (**85**) as dimethyl acetal (**93**) was carried out using trimethyl orthoformate in DCM in the presence of a catalytic amount of CSA (Scheme 17). However, again, this reaction was unsuccessful and no new organic fluorine signals were apparent in ^{19}F NMR spectrum beyond the starting material (**85**). It is not clear why the protection α-fluoro-β-ketoester (**85**) did not proceed as expected.

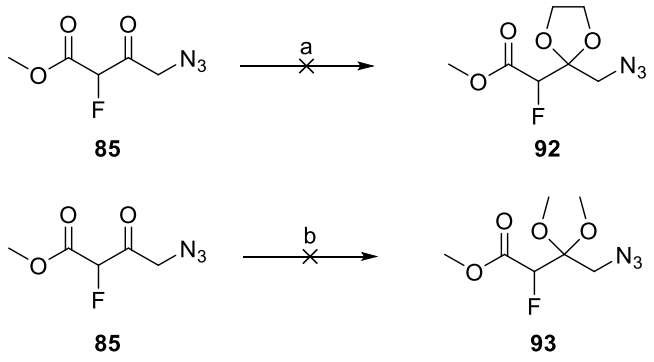

Scheme **17:** Attempted protection of (**85**) as acetal (**92**) and dimethyl acetal (**93**). Reagents and conditions: a) Ethylene glycol, $BF_3{\cdot}OEt_2$ or TsOH, DCM, b) $HC(OMe)_3$, CSA, DCM.

Since the attempted syntheses of (**92**) and (**93**) failed, this route was discontinued, and a new synthetic strategy for the synthesis of fluoromuscimol was explored.

2.4.2 Approach B–Direct fluorination using fluorine gas at Durham University

An alternative approach towards the fluorinated isoxazole was envisaged *via* direct fluorination using fluorine gas of an already-formed isoxazole ring. Similar fluorination has been reported for pyrazole derivative.[24] These compounds were obtained in acceptable yields (40–46%) after purification (Scheme 18).

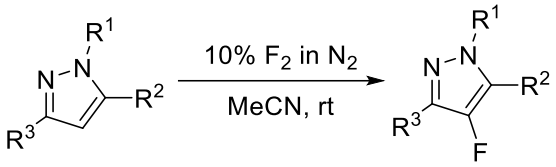

R^1 = H, R^2 = CH_3, R^3 = Ph, 45%
R^1 = H, R^2 = CF_3, R^3 = Ph, 46%
R^1 = Ph, R^2 = R^3 = CH_3, 40%

Scheme **18**: Synthesis of monofluoropyrazoles using fluorine gas.[24]

Three isoxazole precursors (**77**), (**94**) and (**96**) were chosen as representative substrates for this investigation. These substrates were prepared according to the synthetic route outlined in Scheme 19. Treatment of hydroxyurea (**75**) with dimethyl acetylenedicarboxylate (**76**) under basic conditions, afforded 3-hydroxyisoxazole-5-carboxylate (**77**), which was subsequently converted to methyl ester (**94**) with methyl iodide and potassium carbonate. Ester (**94**) was obtained as a colourless crystalline solid in good yield (66%) after column chromatography. Reduction of (**94**) with $NaBH_4$ in MeOH afforded alcohol (**95**) in good yield and then conversion of (**95**) to its methyl-ether derivative (**96**) was carried out with methyl iodide and sodium hydride. This reaction afforded (**96**) in acceptable yield (57%).

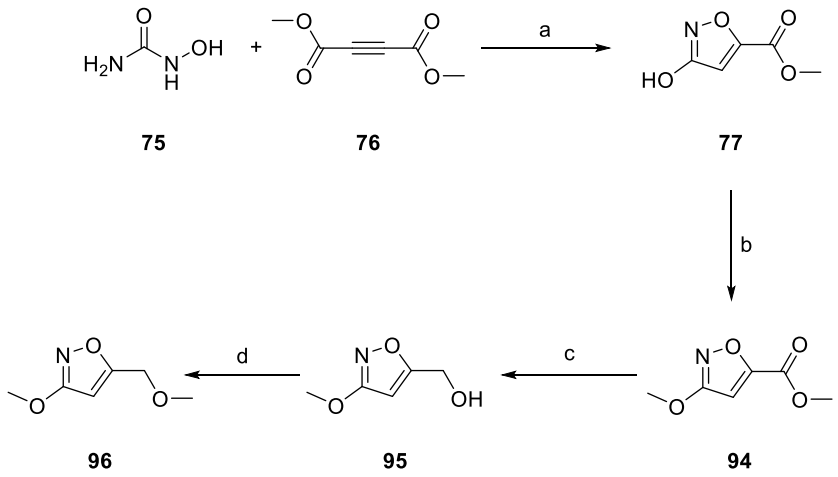

75 76 77 94 95 96

Scheme **19**: Synthesis of isoxazole derivatives (**77**), (**94**) and (**96**): Reagents and conditions: a) DBU, MeOH, 41%; b) MeI, K_2CO_3, DMF, 14 h, 66%; c) $NaBH_4$, MeOH rt, overnight, 85%; d) NaH (60% dispersion oil), MeI, THF, 0 °C→rt, 1h, 57%.

These compounds were subjected to direct fluorination conditions using formic acid as a solvent and were carried out at the University of Durham. An image from the experimental setup is shown in Figure 18. Accordingly, in a glass reaction vessel fitted with a mechanical stirrer, an FEP thermocouple well, an FEP gas delivery tube and an exit tube to a scrubber filled with soda lime was charged with substrate (1.0 eq) and formic acid (4 ml) before being cooled to *ca*. 10 °C. The vessel was purged with nitrogen, and then fluorine gas (4.0 eq) diluted at 10% v/v in nitrogen, was passed through the stirred solution over 1 h. When the fluorine supply had been turned off, the reaction vessel was purged with nitrogen.[25,26] The reaction mixture was poured into water and extracted with ethyl acetate. The extracts were dried and the solvent was removed under reduced pressure to afford dark brown oil.

Figure **18**: Experimental setup for direct fluorination using elemental F_2 (the reaction was carried out with assistance from Dr Tony Harsanyi at the University of Durham).

Unfortunately, all three reactions afforded a complex mixture of products that could not readily be characterised (Scheme 20). These findings clearly indicated that fluorine gas was too reactive, resulting in significant decomposition of substrates (**77**), (**94**) and (**96**), particularly when the reagent is present in excess. This approach was not pursued.

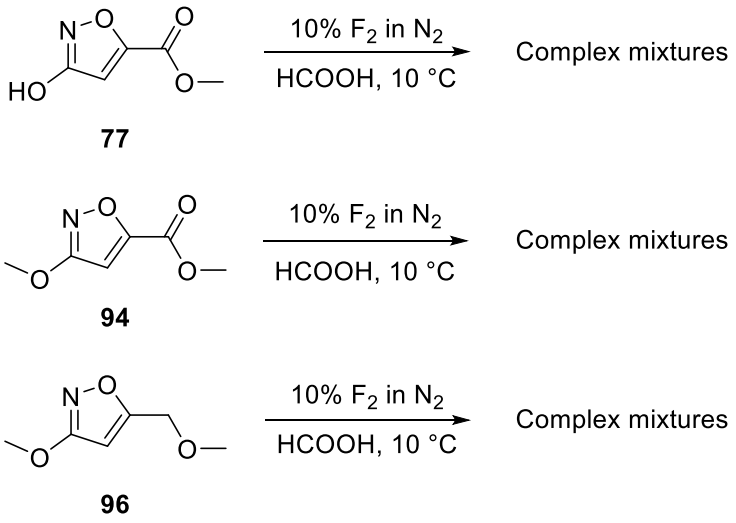

Scheme **20**: Direct fluorination of (**77**), (**94**) and (**96**) using elemental F_2.

In order to tackle the drawback associated with the apparent reactivity of fluorine gas, the use of less reactive electrophilic fluorinating agents such as Selectfluor™ (**89**) and NFSI (**97**) was explored.

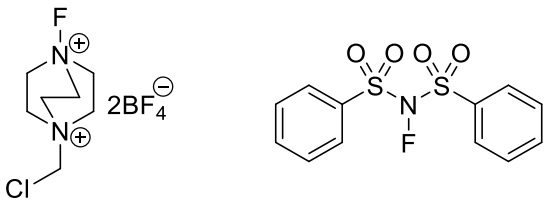

2.4.3 Approach C–Direct fluorination of isoxazole motifs using electrophilic N-F reagents and nucleophilic fluoride sources

Direct C-4 fluorination of a series of 3,5-diphenylisoxazoles by electrophilic fluorination using the N-F reagent, Selectfluor™ has been reported by Stephens *et al.*,[27] (Scheme 21) and Sato *et al.*,[28] (Scheme 22). Following these successful examples, it was decided to investigate the fluorination of (**94**) and (**96**) using the N-F electrophilic fluorination agents, as these class of reagents are commonly employed by medicinal chemists due to ease of handling and are commercially available.[29–34]

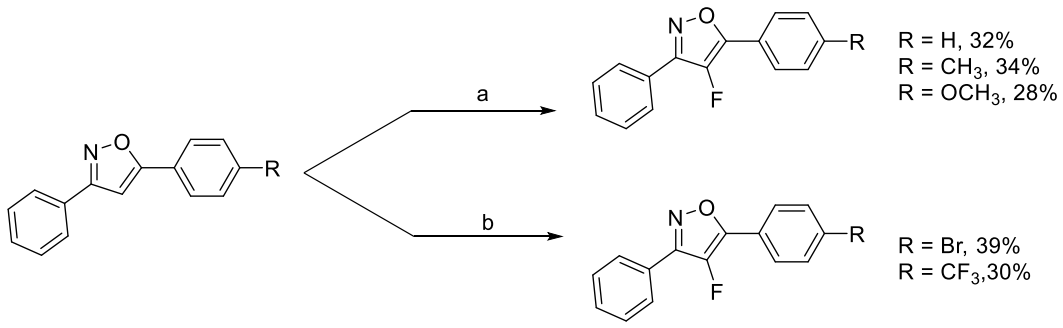

Scheme **21**: Direct C-4 fluorination of series of 3,5-diphenylisoxazoles as reported by Stephens *et al.*[27] Reagents and conditions: a) Selectfluor™ (1.05 eq), MeCN, reflux, overnight; b) Selecfluor™ (1.05 eq), sulfolane, 120 °C, 3→96 h.

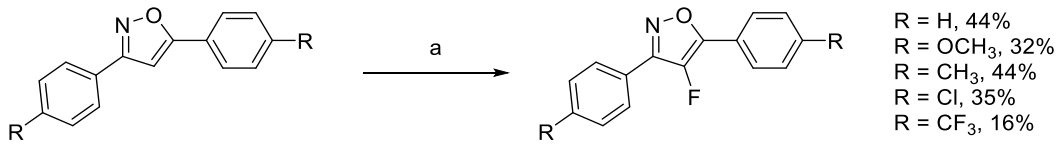

Scheme **22**: Direct C-4 fluorination of series of 3,5-diphenylisoxazoles as reported by Sato *et al.*[27] Reagents and conditions: a) Selectfluor™ (1.0 eq), sulfolane, 120 °C (oil bath), 1 h.

2.4.3.1 Fluorination attempts on ester (94)

The first attempt to fluorinate methyl ester (**94**) was carried out according to a protocol reported in the literature.[27,28] Accordingly, a mixture of methyl ester (**94**) (1.0 eq) and Selectfluor™ (1.0 eq) in dry acetonitrile was heated under reflux (Scheme 23). However, the reaction failed to produce any new organofluorine products. Increasing the amount of Selectfluor™ to 4.0 equivalents, or changing the solvent to sulfolane did not improve the outcome of the reaction. There was no apparent consumption of starting material and no fluorinated products were observed by ^{19}F NMR.

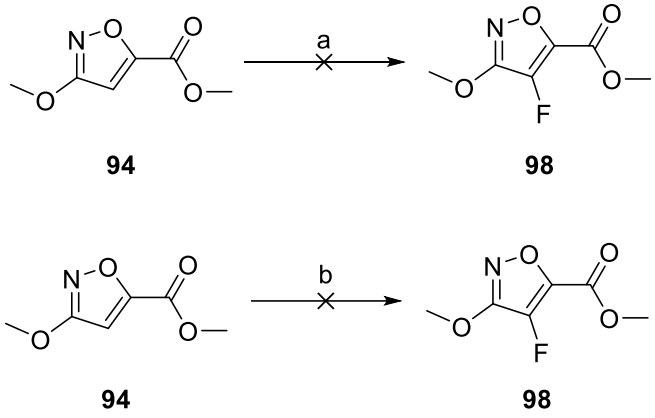

Scheme **23**: Fluorination attempts of (**94**) with Selectfluor™. Reagents and conditions: a) Selectfluor™, MeCN, reflux; b) Selectfluor™, sulfolane, 130 °C.

Heating the compound under forcing conditions in a microwave assisted reaction in both acetonitrile and sulfolane (Scheme 24) was also investigated. Again, these strategies did not afford any fluorinated compound, and only the unreacted starting material was recovered at the end of the reaction.

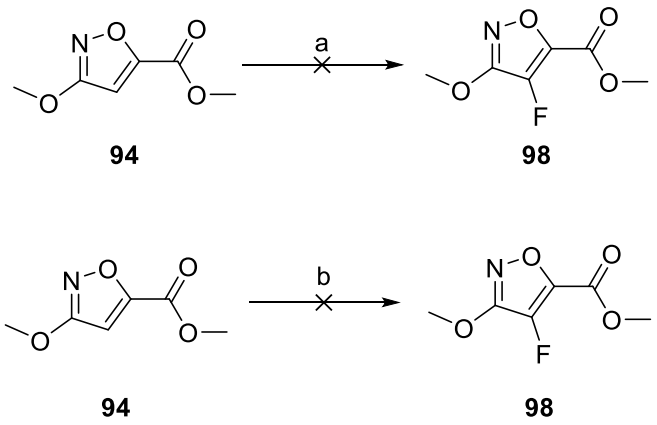

Scheme **24**: Fluorination attempts of (**94**) *via* microwave assisted reaction. Reagents and conditions: a) Selectfluor™, MeCN, MW, 50 W, 90 °C; b) Selectfluor™, sulfolane, MW, 50 W, 150 °C.

It has been reported that the reactivity of the 4-position of the isoxazole ring towards electrophilic reagents is sensitive to the electronic properties of its neighbouring substituents.[27,28,35,36] The presence of electron withdrawing groups at C-3 or C-5 of the isoxazoles leads to a decrease in their nucleophilicity.[35,36] A possible approach to circumvent this problem is to replace the ester moiety with an ether group. This should increase reactivity towards electrophilic fluorination reagents such as Selectfluor™ and NFSI. Attempts to fluorinate (**96**) (Schemes 25 and 26) were carried out according to the conditions described in Schemes 23 and 24. However again, this reaction was unsuccessful and no new organic fluorine signals were apparent in the ^{19}F NMR, except for those of the tetrafluoroborate groups of Selectfluor™.

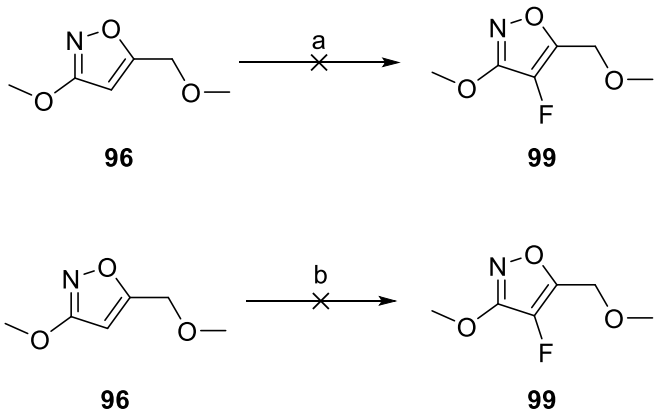

Scheme **25**: Fluorination attempts of (**96**) with Selectfluor™. Reagents and conditions: a) Selectfluor™, MeCN, reflux; b) Selectfluor™, sulfolane, 130 °C.

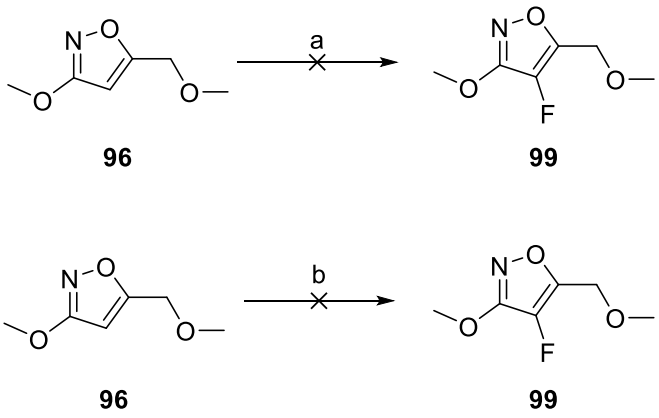

Scheme **26**: Fluorination attempts of (**96**) *via* microwave assisted reaction. Reagents and conditions: a) Selectfluor™, MeCN, MW, 50 W, 90 °C; b) Selectfluor™, sulfolane, MW, 50 W, 150 °C.

2.4.3.2 Nitration of methyl ester (94)

It was hypothesised that the fluorination of the 4-position of (**94**) could be achieved using a nucleophilic fluorination reagent *via* addition-elimination reaction by taking advantage of the electron withdrawing effect of methyl ester (**94**). In order to facilitate nucleophilic attack by fluoride, a suitable activating group with good leaving ability required to be placed at C-4. It was therefore decided to explore the introduction of a nitro group at this position. Moreover, the nitro group of (**100**) also has the potential to be converted to a reactive cationic quaternary ammonium species such (**102**) as shown in Scheme 27.

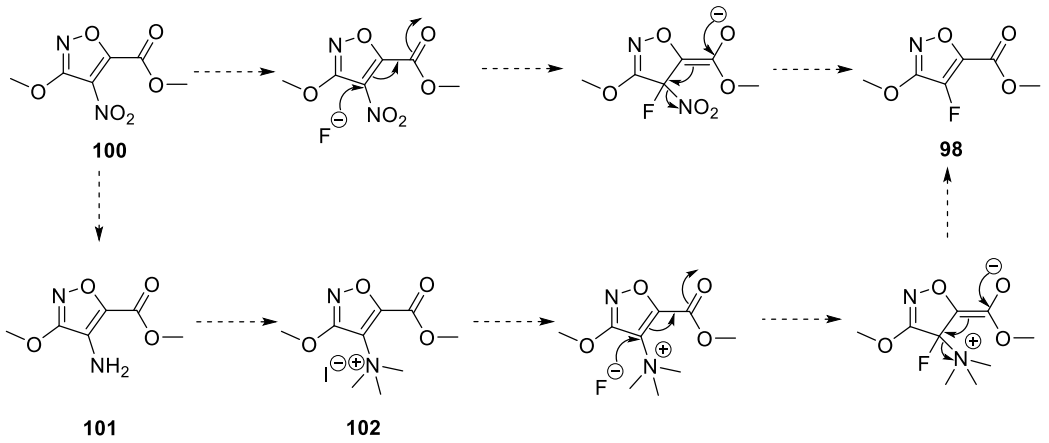

Scheme **27**: C-4 fluorination strategies of nitro (**100**) and quaternary ammonium salt (**102**) using nucleophlic fluorination reagents.

Nitration of methyl ester (**94**) was accomplished in a one-pot procedure using the nitronium triflate reagent (**103**). This reagent was generated *in situ* from tetramethylammonium nitrate and triflic anhydride in DCM (Scheme 28).[37]

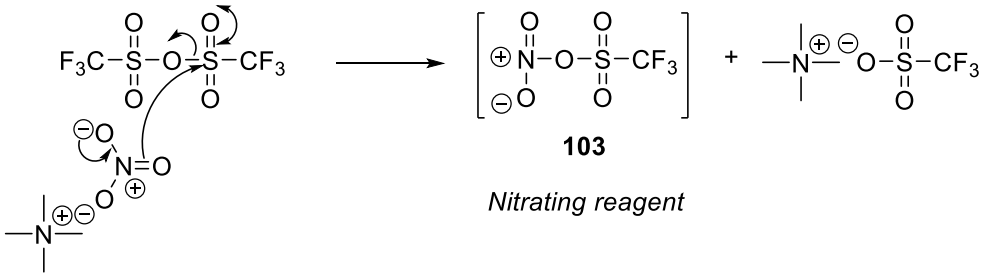

Scheme **28**: *In situ* formation of, nitronium triflate (**103**).[37]

Addition of substrate (**94**) to the *in situ* generated nitronium triflate (**103**), furnished the corresponding nitro product (**100**) as a yellow oil, in acceptable yield (70%) (Scheme 29).

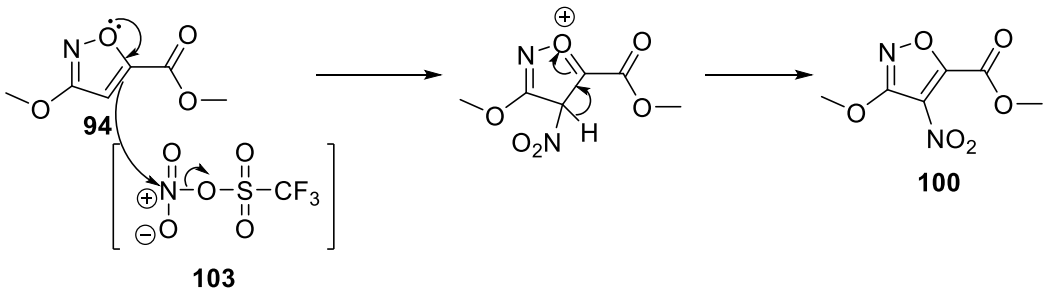

Scheme **29**: One-pot nitration of (**94**).

2.4.3.3 Fluorination attempts on nitro isoxazole (100)

Fluorinations of nitro isoxazole (**100**) were attempted using CsF and KF as fluoride sources (Scheme 30). These reagents were dried under vacuum at 150 °C prior to use. Accordingly, a mixture of nitro (**100**) (1.0 eq) and fluoride reagent (2.0 eq) in dry DMF were heated under reflux. However, despite exploring various conditions (increasing fluoride to 4.0 equivalents, heating under microwave, and addition of the phase transfer reagent kryptofix K_{222} to KF), none of the attempted procedures furnished the desired fluorinated heterocycle (**98**). Moreover, there was no new signal observed by ^{19}F NMR and the starting material did not react. Thus the nitro group was not sufficient to induce the addition-elimination reaction.

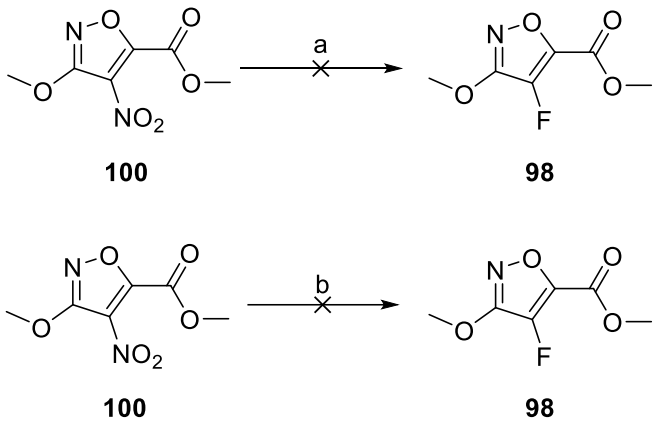

Scheme **30**: Fluorination attempts of (**100**) using nucleophlic fluorination reagents. Reagents and conditions: a) CsF, DMF, 150 °C; b) KF, DMF, 150 °C.

Although the fluorination of (**100**) was disappointing, the fact that quaternary ammonium salts are widely employed as precursors for nucleophilic fluorinations, particularly in PET studies, prompted further investigation.[38–40] Reduction of the nitro group of (**100**) to the corresponding free amine (**101**) was achieved using iron powder under acidic conditions (Scheme 31). Purification by column chromatography afforded (**101**) as a colourless crystalline solid in good yield (83%). The structure of (**101**) was confirmed by X-ray crystallography (Figure 19).

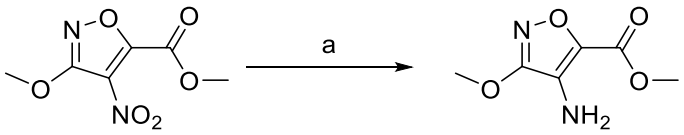

100 **101**

Scheme **31**: Reduction of nitro (**100**) to free amine (**101**). Reagents and conditions: a) Fe powder, AcOH/H_2O, 50 °C, 2 h, 83%.

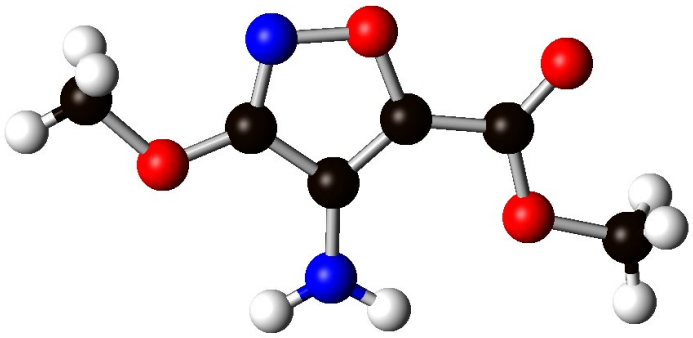

Figure **19**: X-ray structure of (**101**).

An attempt to transform the free amine (**101**) into the *N*-methylated quaternary ammonium salt (**102**) was carried out using an excess methyl iodide in basic methanolic solution (Scheme 32). Disappointingly, even after a prolonged reaction time of 24 hour and elevated temperature (reflux), the reaction failed to produce the desired product (**102**), and only the unreacted starting material was recovered at the end of reaction period. The lack of success is presumably due to the mesomeric electron-withdrawing effect of the ester moiety, resulting in a poorly nucleophilic amine.

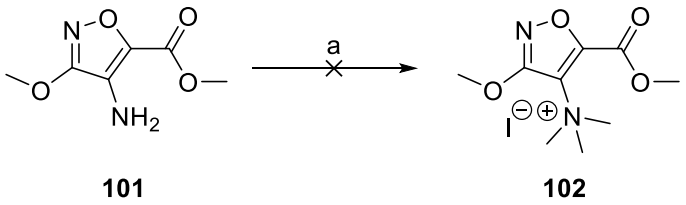

101 **102**

Scheme **32**: Unsuccessful synthesis of quaternary ammonium salt (**102**) from free amine (**101**). Reagents and conditions: a) MeI, Ca_2CO_3, MeOH.

2.4.3.4 Bromination of methyl ester (94)

It was decided to explore further the fluorination of methyl ester (**94**). Therefore, a lithium-halogen exchange reaction was envisaged. In order to facilitate carbanion formation at C-4, a halogen substituent, in this case bromine was introduced at the 4-position. Bromination of methyl ester (**94**) proved to be straightforward and was achieved using NBS in TFA. TFA enhances the electrophilicity of the Br through NBS protonation (**104**) (Scheme 33).[41] Moreover, TFA was shown to be an effective and useful solvent for bromination and iodination of very unreactive aromatic compounds.[36,42–44]

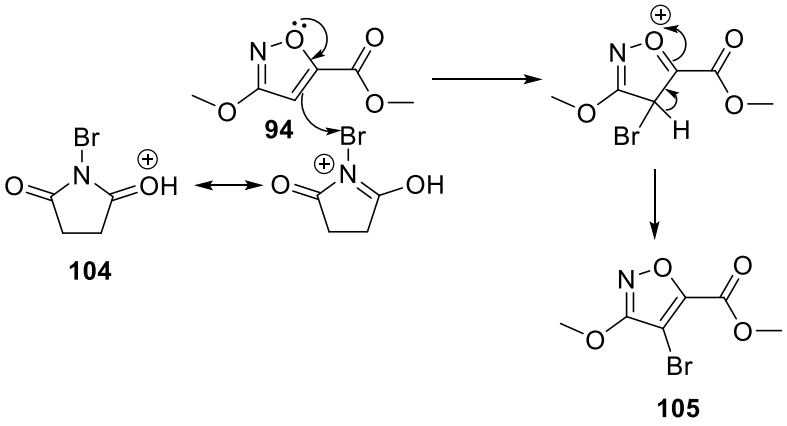

Scheme **33**: Strategy to introduce a bromine atom at C-4 of (**94**).

Accordingly, a solution of ester (**94**) in TFA was treated with an excess of NBS under reflux. A relatively long reaction time (>24 h) was required to achieve an acceptable conversion, suggesting that the presence of an electron withdrawing group at the 5 position of the isoxazole ring decreases its nucleophilicity. In order to expedite the reaction, substrate (**94**) was subjected to microwave irradiation at 150 °C for 3 hours, affording clean and complete conversion to the desired product (**105**) (Scheme 34). Compound (**105**) was obtained as a colourless crystalline solid in 85% yield after column chromatography and its structure was confirmed by single crystal X-ray crystallography (Figure 20).

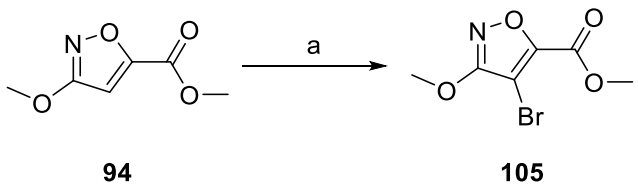

Scheme **34**: Synthesis of (**105**) *via* microwave assisted reaction. Reagents and conditions: a) NBS, TFA, MW, 50 W, 150 °C, 3 h, 85%.

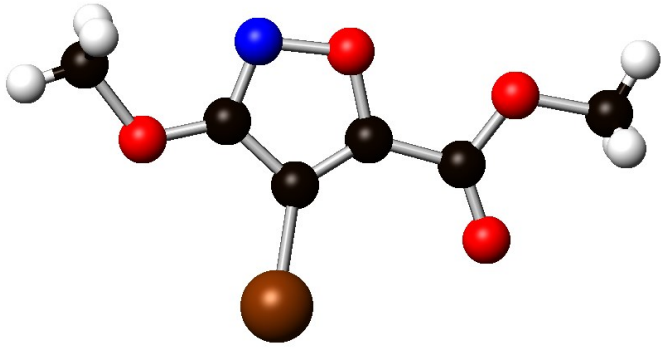

Figure **20**: X-ray structure of (**105**).

2.4.3.5 Fluorination attempts on brominated ester (105)

With compound (**105**) in hand, an attempt to fluorinate the 4 position of isoxazole ring (**105**) in two stages *via* a lithium-halogen exchange reaction using *t*-BuLi and NFSI as an electrophilic source of fluorine, was made. As shown in Scheme 35, *t*-BuLi (2.0 eq) was added at -78 °C to a solution of substrate (**105**) in THF. The mixture was stirred for 1 h and a solution of NFSI in THF was added. TLC and ^{19}F NMR analyses of the product showed a complex mixture of products containing several fluorine signals. Due to the poor yield and low concentration of the fluorinated product, no further attempt was made at isolation. Furthermore, the ^{1}H NMR analysis showed evidence for the presence of ketone (**106**) as a major product, which could clearly arise from direct nucleophilic attack of the *t*-butylithium to the ester carbonyl.

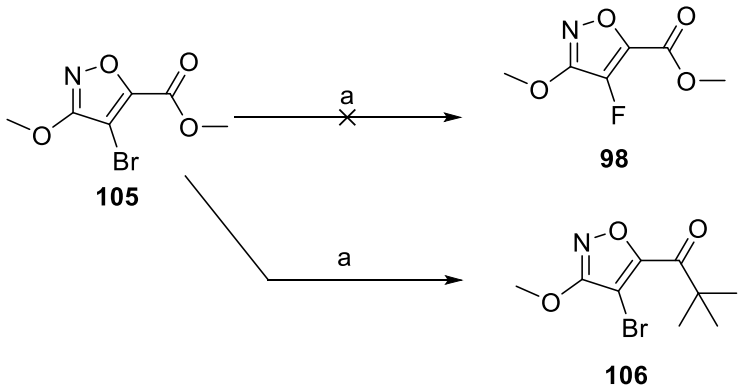

Scheme **35**: Attempt to fluorinate (**105**) using *t*-BuLi and NFSI. Reagents and conditions: a) *n*-BuLi, NFSI, THF, -78 °C.

In order to avoid direct nucleophlic attack by the base at the ester moiety of (**105**), a reaction was carried out using a weaker non nucleophilic base, KHMDS on ester (**94**) (Scheme 36). Analysis of the ^{1}H NMR of the product showed unreacted starting material. However, ^{19}F NMR analysis indicated a new organofluorine product at δ_F = -166.1 ppm. An attempt to isolate this product for further characterisation was not possible due to its low concentration in the resulting mixture.

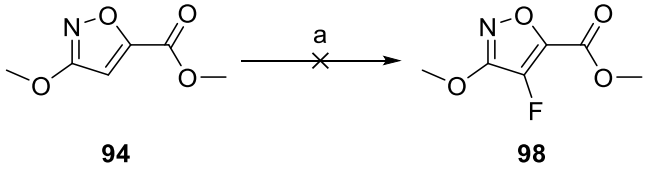

Scheme **36**: Attempt to fluorinate (**94**) using non nucleophilic base, KHMDS and NFSI. Reagents and conditions: a) KHMDS, NFSI, THF, -78 °C.

2.4.3.6 Bromination of methyl ether (96)

The bromination of ether (**96**) represents a possible strategy to overcome the limitation of direct fluorination of C-H. Moreover, this approach allows the fluorination reaction *via* two stages using organolithium bases followed by the addition of NFSI, to be fully utilised without having to consider the complication of direct nucleophilic attack of these reagents to the electrophilic carbon. Methyl ether (**96**) was brominated, as outlined in Scheme 33. This was achieved by adding an excess NBS to a solution of ether (**96**) in TFA. Purification by column chromatography afforded (**107**) as a colourless crystalline solid in 85% yield (Scheme 37). The structure of (**107**) was confirmed by X-ray crystallography (Figure 21).

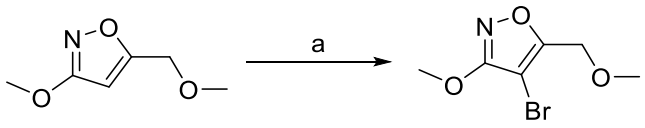

96 **107**

Scheme **37**: Synthesis of brominated compound (**107**). Reagents and conditions: a) NBS, TFA, rt, 48 h, 85%.

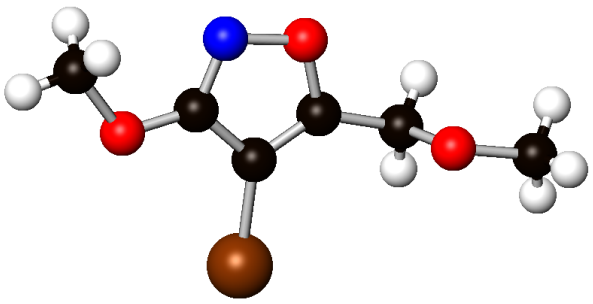

Figure **21**: X-ray structure of (**107**).

2.4.3.7 Fluorination of (107) *via* a lithium-halogen exchange reaction

The fluorination of (**107**) *via* a lithium-halogen exchange reaction was investigated using *n*-BuLi and NFSI (Scheme 38). Ether (**107**) was subjected to lithiation with *n*-BuLi (1.1 eq) at -78 °C in THF, followed by quenching with NFSI (2.0 eq). This afforded a complex mixture of products containing several fluorine signals (^{19}F NMR). Of these, one was of particular interest in that the ^{19}F NMR signal (δ_F = -187.4 ppm), appeared in the expected region (from $\delta_F(CDCl_3)$ = -173 ppm to $\delta_F(CDCl_3)$ = -185 ppm)[27,45] for fluorination at the C-4 of the isoxazole.

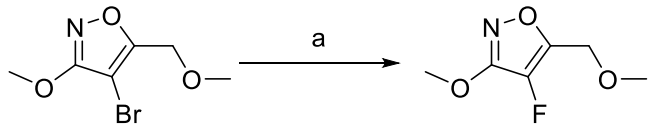

107 **99**

Scheme **38**: Fluorination approach of (**107**) *via* halogen-exchange reaction. Reagents and conditions: a) *n*-BuLi, NFSI, THF, -78 °C→rt, overnight, <10%.

An attempt to isolate this compound was performed by careful chromatography. In the event, the desired fluorinated methyl ether (**99**) was isolated, albeit in very low yield (<10%).

The ^{1}H NMR spectrum of (**99**) (Figure 22) shows that the methylene signal of H-6 is coupled to fluorine, as a doublet (J = 1.6 Hz), consistent with $^{4}J_{HF}$ coupling.[45] This signal collapses to a singlet in the fluorine-decoupled ^{1}H{^{19}F} NMR spectrum. Moreover, the proton signal assigned to the 4-position of (**96**) is not present in the ^{1}H NMR spectrum, suggesting the successful incorporation of fluorine atom into the isoxazole ring.

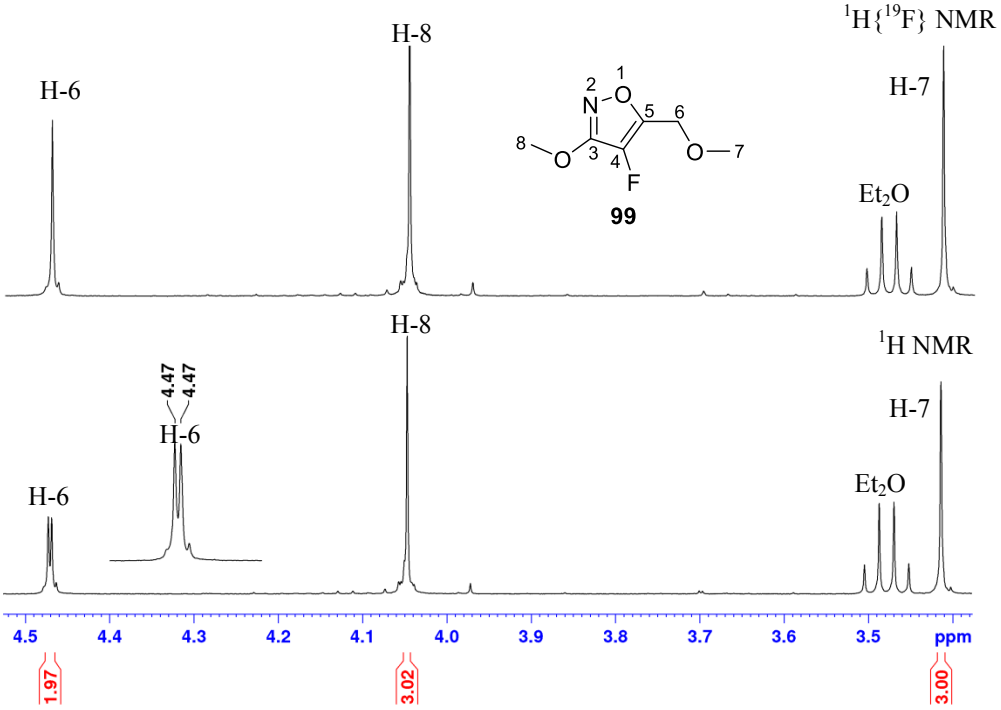

Figure **22**: Partial ^{1}H NMR spectra of (**99**) with and without {^{19}F}.

The incorporation of fluorine at the 4-position was further confirmed by ^{19}F NMR (Figure 23). The ^{19}F NMR exhibits a triplet at -187.4 ppm, with a $^{4}J_{HF}$ coupling constant of 1.6 Hz. A proton-decoupled ^{19}F{^{1}H} NMR experiment resulted in the collapse of this signal.

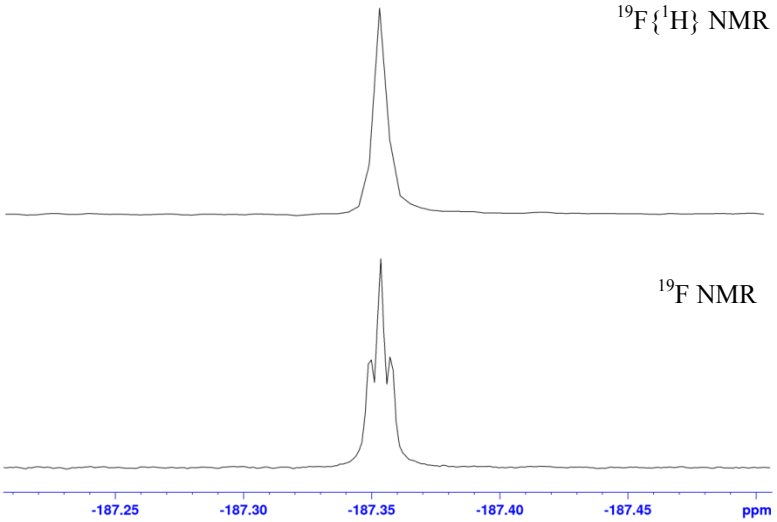

Figure **23**: Partial ^{19}F NMR spectra of the (**99**) with and without $\{^{1}H\}$.

In view of this promising result, it was decided to prepare compound (**108**) in order to optimise the metal exchange and fluorination reactions. Moreover, (**108**) is structurally closer to the desired fluoromuscimol (**64**) and thus, fewer steps are required to complete the synthesis, if fluorination is successful.

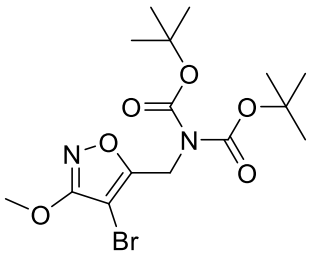

108

2.4.3.8 Synthesis of brominated di-Boc (108)

As illustrated in Scheme 39, the synthesis of (**108**) was achieved in 8 steps starting from (**77**). It is worth mentioning that, initially (**77**) was synthesised *via* the method reported by Frey and Jäger.[12] However, upon becoming commercially available, it was subsequently purchased from Fluorochem. The methylation of (**77**) followed by reduction of (**94**) to alcohol (**95**) was carried out under similar conditions as described in Scheme 19. Alcohol (**95**) was brominated using Appel conditions, in DCM at 0 °C to yield (**109**) in 83% yield after column chromatography. The latter was then subjected to nucleophilic substitution using NaN_3 in DMF at 80 °C to obtain (**110**) in 90% yield. Bromination of intermediate (**110**) was accomplished according to the standard conditions outlined in Scheme 37, adding an excess of NBS to a solution of the substrate in TFA at 30 °C to acquire (**111**) in 85%. Reduction of the azide using Staudinger's conditions produced the corresponding protected bromomuscimol (**112**), as a yellowish oil after purification by column chromatography. The route was progressed by monoprotection of the amine moiety of bromoisoxazole (**112**) by treatment with Boc anhydride under basic conditions at room temperature. This afforded (**113**) as a colourless crystalline solid in good yield (72%). The second Boc group was introduced by dissolving (**113**) in the aprotic solvent, MeCN and heating the mixture under reflux after addition of Boc anhydride and a catalytic amount of DMAP. Di-Boc protected (**108**) was obtained as a colourless crystalline solid in excellent yield (91%). Structure (**108**) was confirmed by X-ray crystallography (Figures 24).

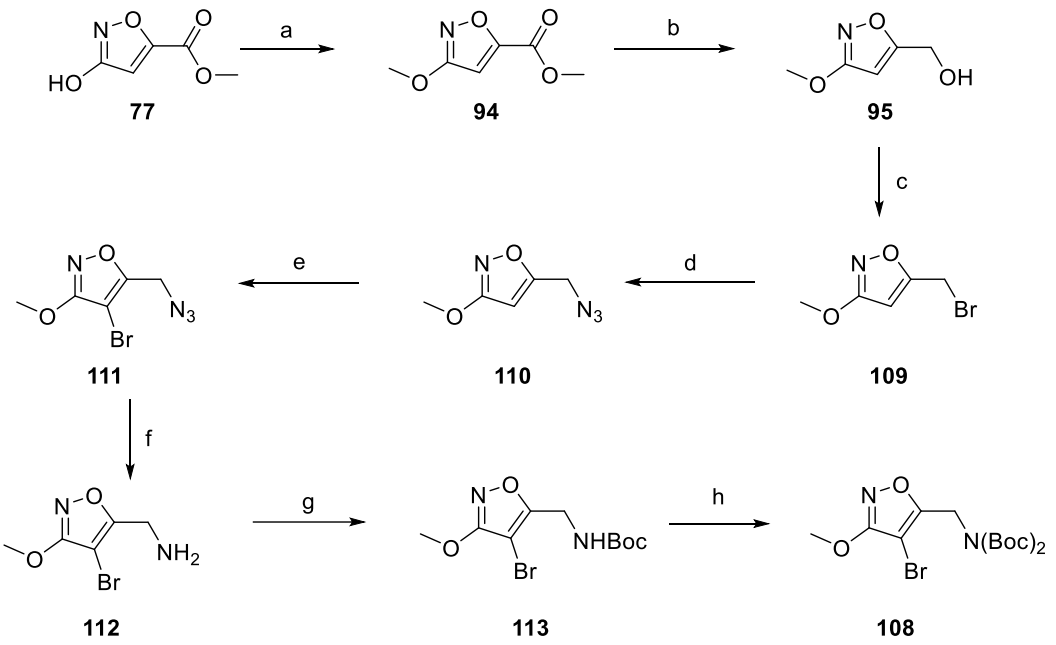

Scheme **39**: Synthetic route to (**108**). Reagents and conditions: a) MeI, K_2CO_3, DMF, rt, 14 h, 66%; b) $NaBH_4$, MeOH, 0 °C→rt, overnight, 85%; c) PPh_3, CBr_4, DCM 0 °C, 2 h, 83%; d) NaN_3, DMF, 80 °C, 3.5 h, 90%; e) NBS, TFA, 30 °C, 27 h, 85%; f) PMe_3, THF, H_2O, 0 °C, 30 min, 66%; g) Boc_2O, Et_3N, DCM, rt, 15 h, 72%; h) Boc_2O, DMAP, MeCN, reflux, 3 h, 91%.

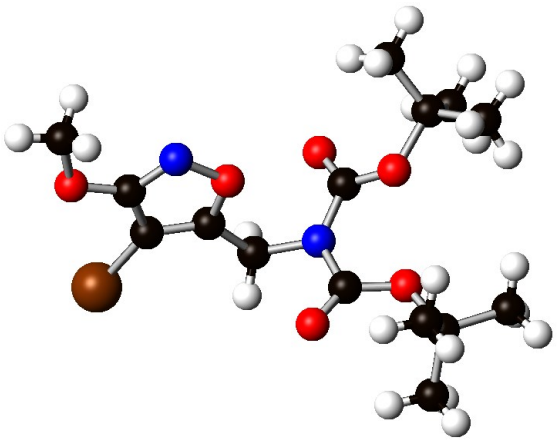

Figure **24**: X-ray structure of (**108**).

2.4.3.9 Fluorination of (108) *via* a lithium-halogen exchange reaction

Fluorination of (**108**) was conducted in a similar manner to that illustrated in Scheme 38, by adding *n*-BuLi (1.1 eq) into a solution of (**108**) in THF at -78 °C, followed by quenching with NFSI (2.0 eq) (Scheme 40). This reaction was not clean and gave rise to a complex mixture of products as evidenced by TLC analysis. Nevertheless, the crude material showed a clear fluorine signal, which was found to be consistent with fluorination at C-4 of the isoxazole, as it appeared in the same region to that observed in the fluorinated methyl ether (**99**). Despite the difficulty of separation by column chromatography, the desired product (**114**) was isolated cleanly, but in low yield, <10%.

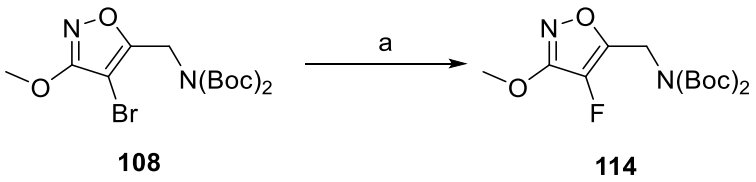

108 **114**

Scheme **40**: Fluorination approach of (**108**) *via* a halogen-exchange reaction. Reagents and conditions: a) *n*-BuLi, NFSI, THF, -78 °C→rt, overnight, <10%.

Analysis of the ^{1}H NMR spectrum (Figure 25) shows that the methylene proton (H-6) of (**114**) resonates as a doublet at 4.84 ppm with a $^{4}J_{HF}$ coupling constant of 1.8 Hz. This collapses to a singlet upon ^{19}F decoupling. Moreover, the fluorine signal (Figure 26), which appears as a triplet at δ_F -187.9 ppm has a similar coupling constant ($^{4}J_{HF}$ = 1.8 Hz) to that observed in the ^{1}H NMR spectrum. This signal becomes a singlet in the proton-decoupled ^{19}F{^{1}H} experiment and in agreement with previous results on the fluorination of methyl ether (**99**).

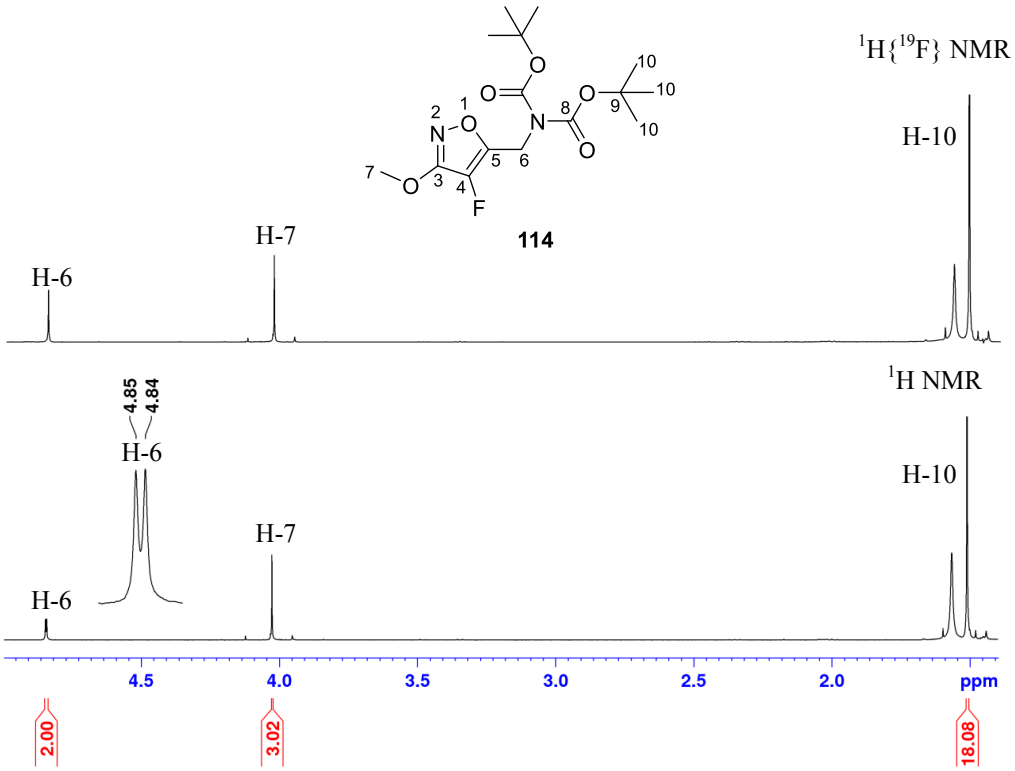

Figure **25**: Partial ^{1}H NMR spectra of (**114**) with and without $\{^{19}F\}$.

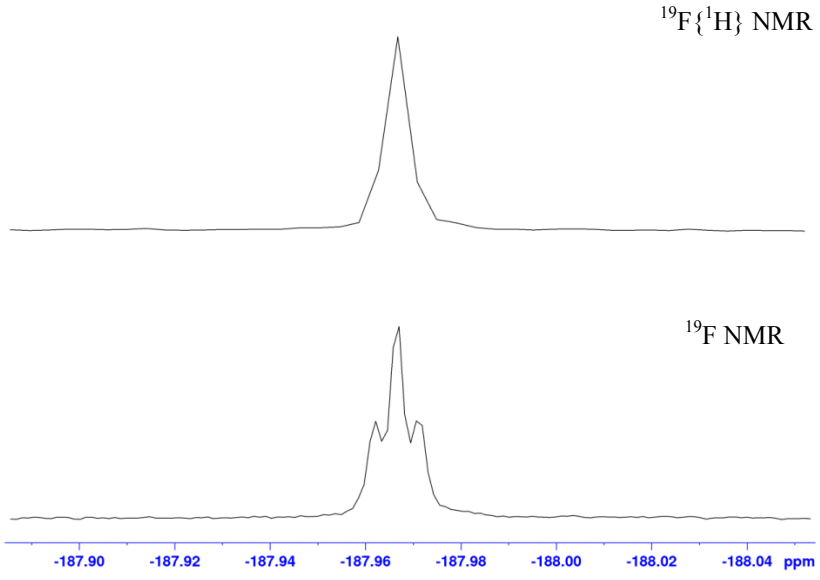

Figure **26**: Partial ^{19}F NMR spectra of (**114**) with and without $\{^{1}H\}$.

The formation of (**114**) was further confirmed by HRMS (NSI^+) analysis (Figure 27), with the appearance of characteristic peaks at *m/z* 369.1435 and 715.2965, assigned to the $[M+Na]^+$ and $[2M+Na]^+$ respectively.

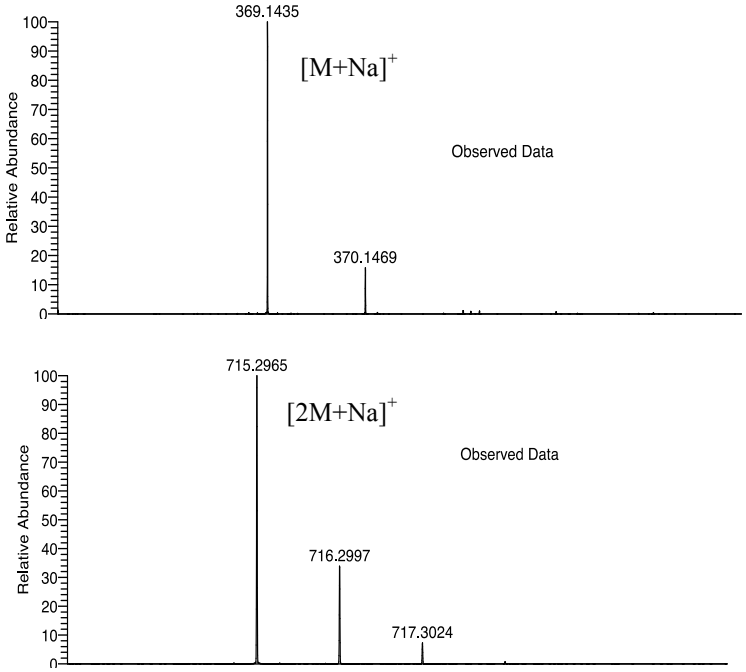

Figure **27**: HRMS (NSI^+) analysis of (**114**).

Although fluorination of (**108**) was successful, due to the large number of steps and the poor overall yield, this route was abandoned. Once again, a new approach to fluoromuscimol was required. This time, it was decided to begin the synthesis by switching the protecting group of the 3-position of (**94**) from methyl to isopropyl (**115**), as it appeared that it may be easier to deprotect this ether.[46–48]

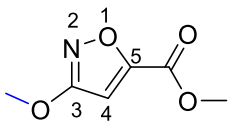

94

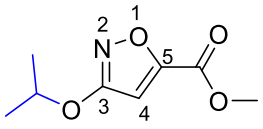

115

2.4.4 Successful route to fluoromuscimol (64)

The successful route to fluoromuscimol (**64**) built on previous experience involved nine steps (Scheme 41), starting from the protection of (**77**) as an isopropyl ether (**115**). Reduction of the ester group of (**115**) was achieved using an excess of $NaBH_4$ and gave alcohol (**116**). Bromination of (**116**) using the Appel reaction generated bromide (**117**), which was subjected to nucleophilic substitution with sodium azide affording (**118**). The resultant azide was transformed into the desired amine (**119**) *via* a Staudinger reaction using PMe_3 at 0 °C in water/THF mixture. Protection of the amino group was achieved by addition of Boc anhydride and Na_2CO_3 to a solution of the free amine (**119**) in dioxane/water mixture. The mono-Boc protected product (**120**) was then isolated in excellent yield (90%) as a colourless viscous oil that crystallised in time. Its structure was confirmed by X-ray crystallography (Figure 28).

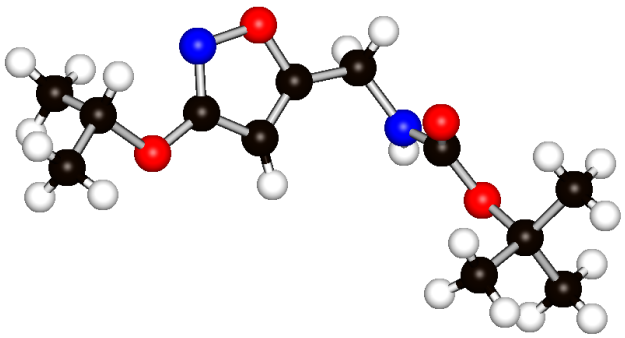

Figure **28**: X-ray structure of (**120**).

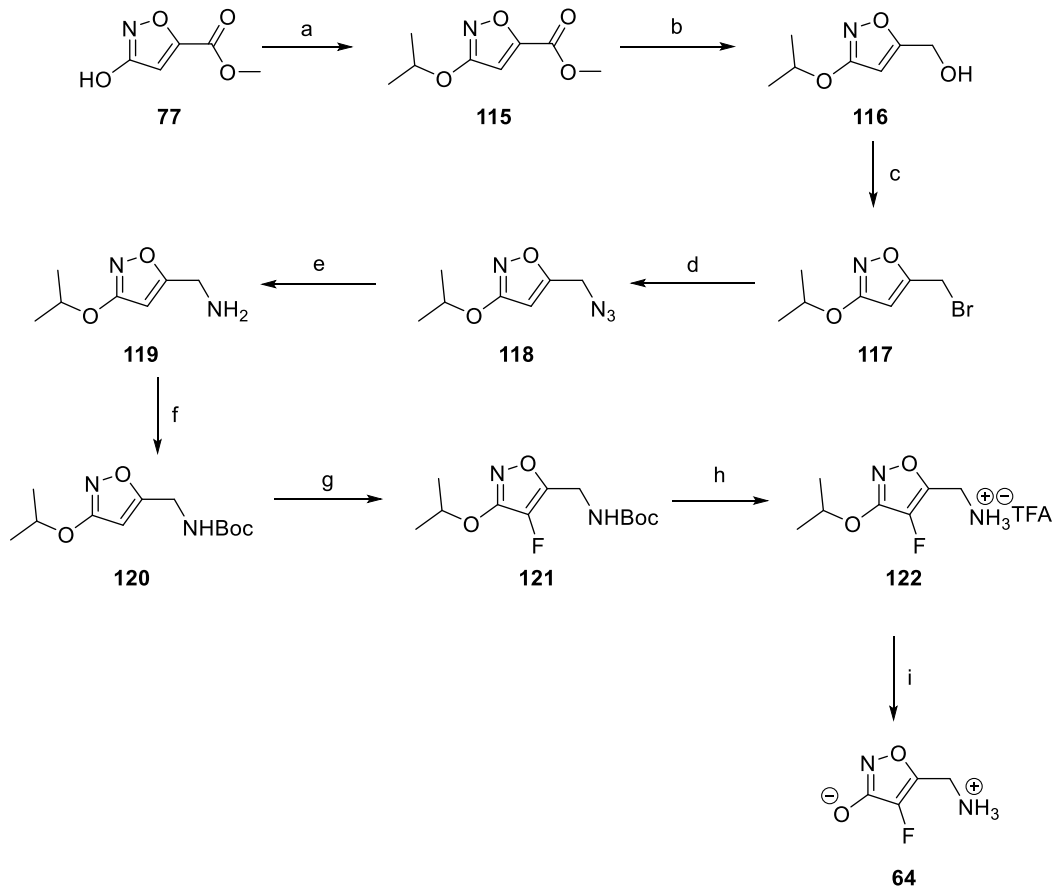

Scheme **41**: Successful route to fluoromuscimol (**64**). Reagents and conditions: a) *i*-PrBr, K_2CO_3, DMF, 55 °C, overnight, 77%; b) $NaBH_4$, MeOH, 0 °C→rt, overnight, 90%; c) PPh_3, CBr_4, rt, 12 h, 58%; d) NaN_3, DMF, 80 °C, 3.5 h, 91%; e) PMe_3, THF, H_2O, 0 °C, 1 h, 65%; f) Boc_2O, Na_2CO_3, dioxane/H_2O, rt, overnight, 90%; g) *n*-BuLi, NFSI, THF, -78 °C→rt, overnight, 30%; h) TFA, DCM, rt, 98%; i) 33% HBr in AcOH, 60 °C, 17 h, 36%.

The key fluorination step of (**120**) was successfully achieved by addition of *n*-BuLi (2.2 eq) to a solution of (**120**) in THF at -78 °C followed by addition of NFSI (1.1 eq). The proposed mechanism of this reaction is outlined in Scheme 42 and starts with abstraction of a proton from carbamate (**120**) by the first equivalent of *n*-BuLi to generate lithium enolate (**123**). The nitrogen of (**123**) then acts as a ligand and coordinates to the second equivalent of *n*-BuLi *via* ortho-directed lithiation, thus facilitating the deprotonation at the 4-position of the ring

and formation of a pseudo five-membered di-lithio chelate (**124**).[49] This latter carbanion is more reactive towards electrophiles and results in the formation of intermediate (**125**) after addition of NFSI (**97**). Intermediate (**125**) then collapses to furnish the desired fluoro compound (**121**) upon warming to room temperature. After work-up and purification, (**121**) was obtained in 30% yield as a colourless viscous oil that crystallised in time. The structure of (**121**) was confirmed by X-ray crystallography (Figure 29).

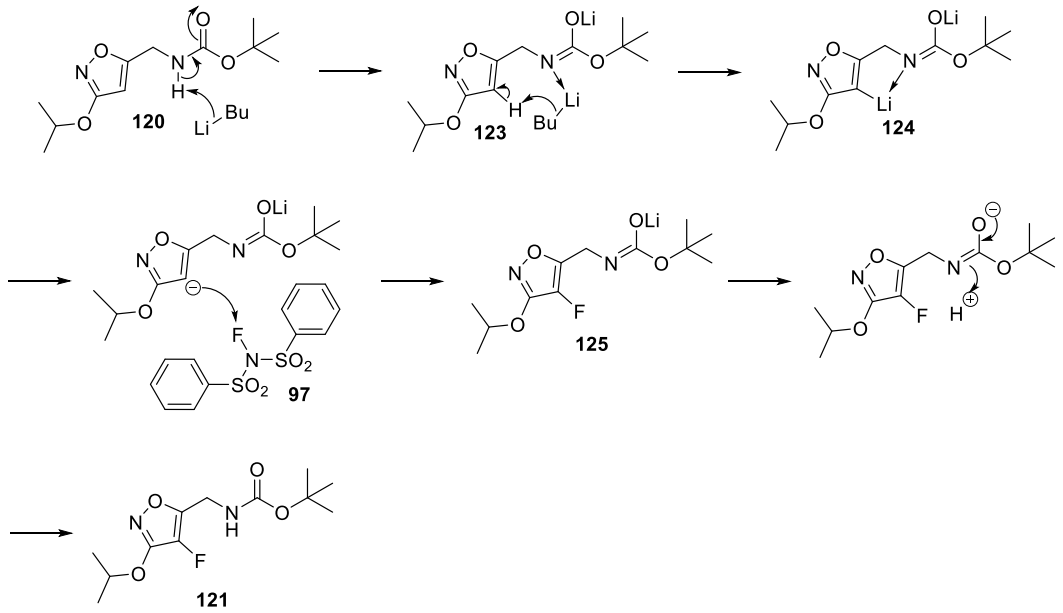

Scheme **42**: Proposed mechanism for the fluorination of (**120**).

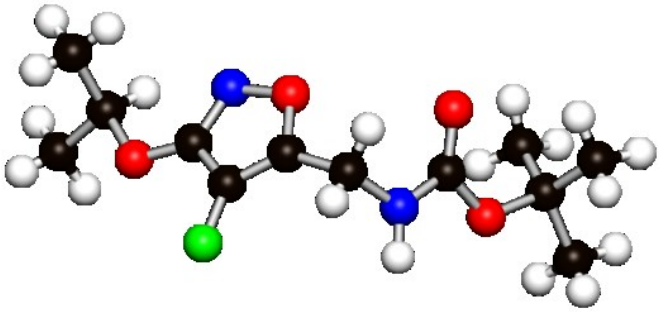

Figure **29**: X-ray structure of (**121**).

Analysis of the ^{1}H NMR spectrum of (**121**) (Figure 30) is not straightforward, as the chemical shift of the NH proton cannot be properly assigned due to overlapping of its broad signal with the septet of the isopropyl group H-7 at 4.92 ppm. Moreover, the 4-J ($^{4}J_{HF}$) coupling between the methylene group of H-6 and fluorine is not observed due to the strong and more intense 3-J ($^{3}J_{HH}$) vicinal coupling of this group with the adjacent NH moiety. Nevertheless the ^{19}F NMR (Figure 31) gives clear evidence for the formation of the desired compound with the presence of a singlet at -188.0 ppm.

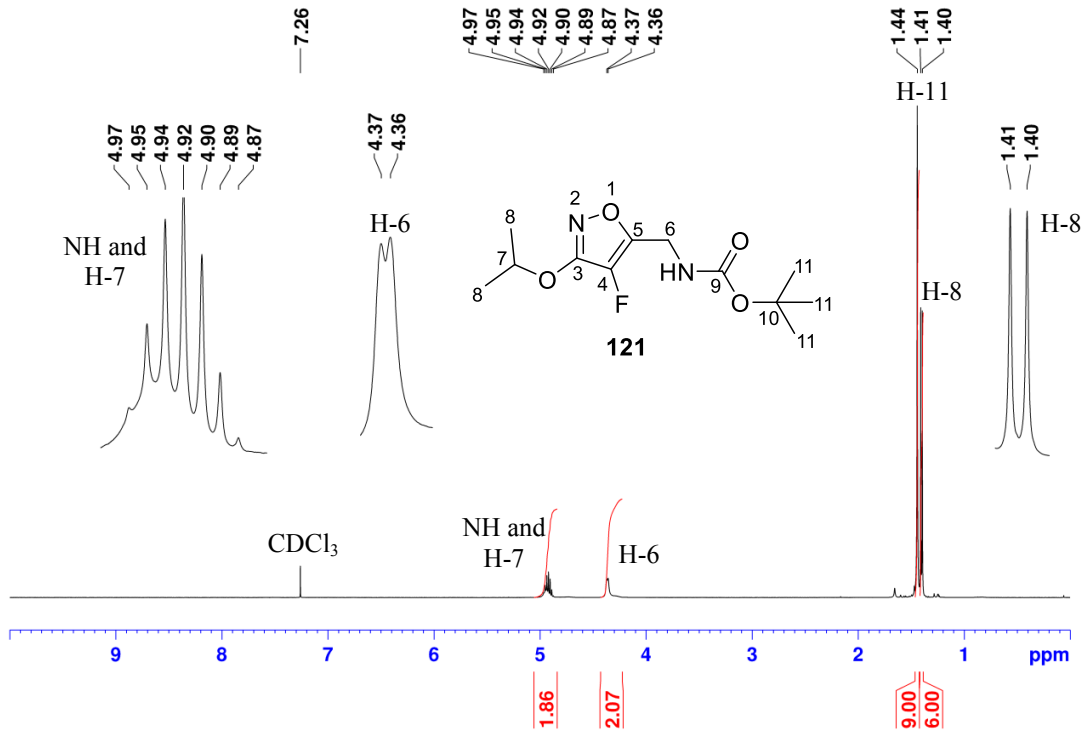

Figure **30**: ^{1}H NMR spectrum of (**121**).

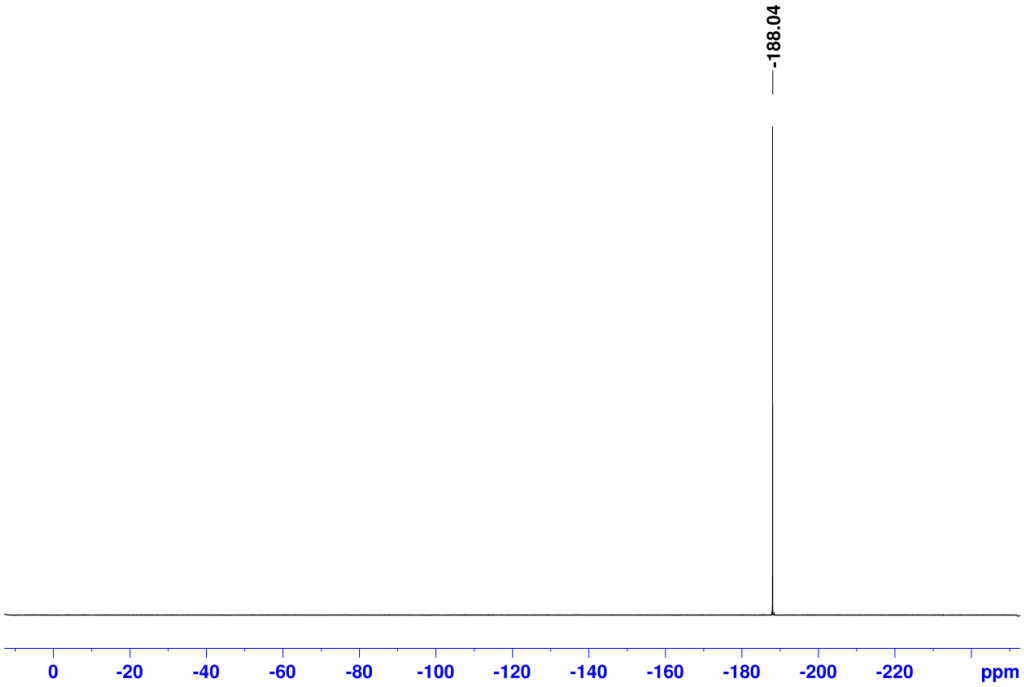

Figure **31**: ^{19}F NMR spectrum of (**121**).

Further characterisation by ^{13}C NMR (Figure 32) reveals that compound (**121**) exhibits three distinct doublets at 161.5 ppm (C-3), 152.3 ppm (C-5) with $^{2}J_{CF}$ coupling constants of 12.5 and 19.2 Hz respectively, while the third doublet signal appears much further upfield at 134.3 ppm (C-4) with a large $^{1}J_{CF}$ coupling constant of 254.6 Hz. The carbonyl carbon (C-9) and one sp^3 quaternary carbon (C-10) appear at 155.5 ppm and 80.5 ppm respectively. Two upfield signals resonate at 28.4 ppm and 22.0 ppm are assigned to the methyl carbons of C-11 and C-8 respectively. The remaining signals at 74.6 ppm and 35.0 ppm are attributed to methine carbon of C-7 and methylene carbon of C-6 respectively.

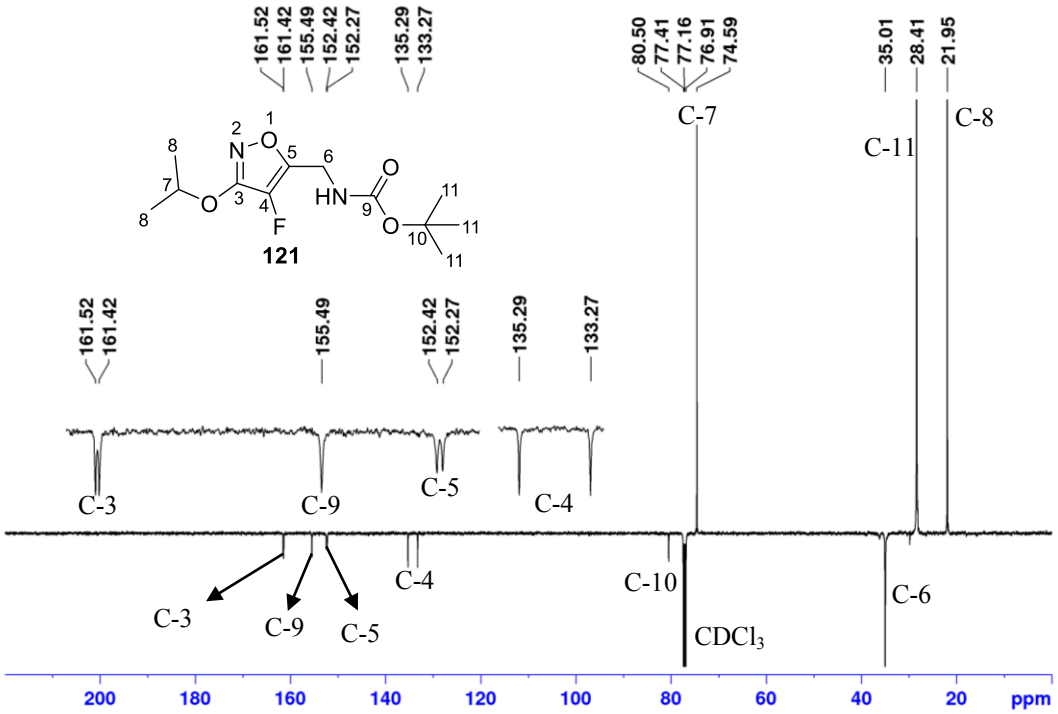

Figure **32**: ^{13}C NMR spectrum of (**121**).

Removal of the Boc protecting group of (**121**) with TFA furnished the TFA salt of (**122**) in excellent yield (98%), after purification by column chromatography. A single crystal suitable for X-ray diffraction studies was grown from DCM and Et_2O and the resultant structure is shown in Figure 33.

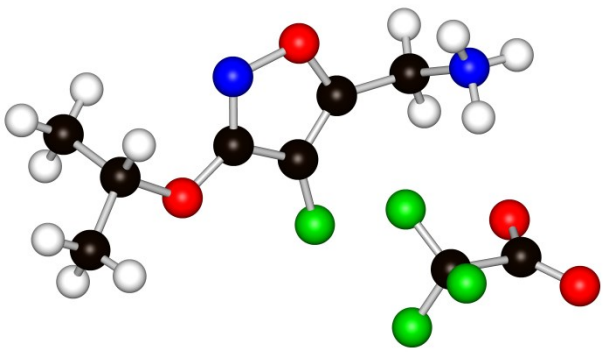

Figure **33**: X-ray structure of (**122**).

Final deprotection of the isopropyl group of (**122**) with 33% HBr in acetic acid, followed by subsequent preparative HPLC purification afforded (**64**) as a colourless solid in 36% yield after freeze-drying. A suitable crystal for X-ray diffraction was grown from water and Et_2O. The structure is shown in Figure 34.

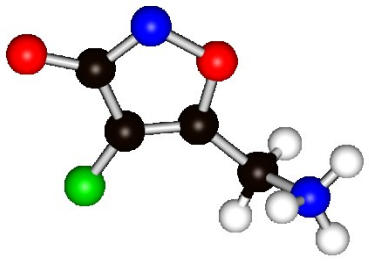

Figure **34**: X-ray structure of fluoromuscimol (**64**).

The purity of fluoromuscimol (**64**) was determined by analytical HPLC on a reverse phase column. HPLC gave a single peak (t_r = 1.97 min) corresponding to fluoromuscimol (**64**), and indicating a high purity (>99%) (Figure 35).

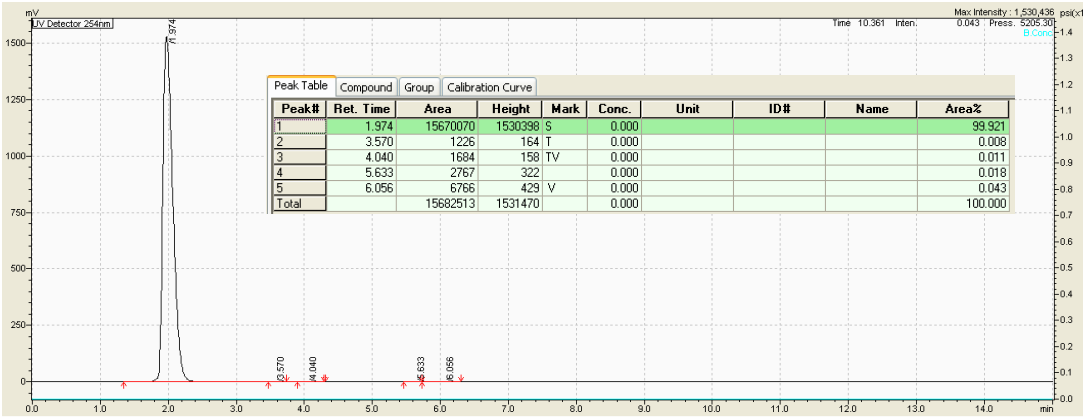

Figure **35**: HPLC chromatogram of fluoromuscimol (**64**) showing greater than 99% purity.

In the ^{1}H NMR spectrum of fluoromuscimol (**64**) (Figure 36), the methylene proton of H-6 appears as a doublet at 4.21 ppm with a $^{4}J_{HF}$ coupling constant of 1.5 Hz, which collapses to a singlet upon ^{19}F decoupling, while the ^{19}F NMR spectrum exhibits a singlet resonance at -185.2 ppm (Figure 37).

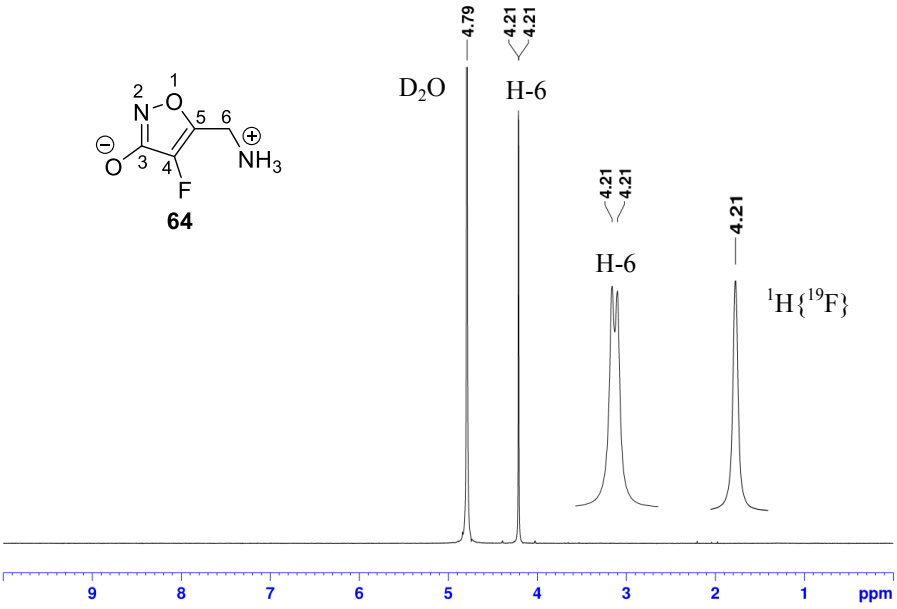

Figure **36**: ^{1}H NMR spectra of fluoromuscimol (**64**).

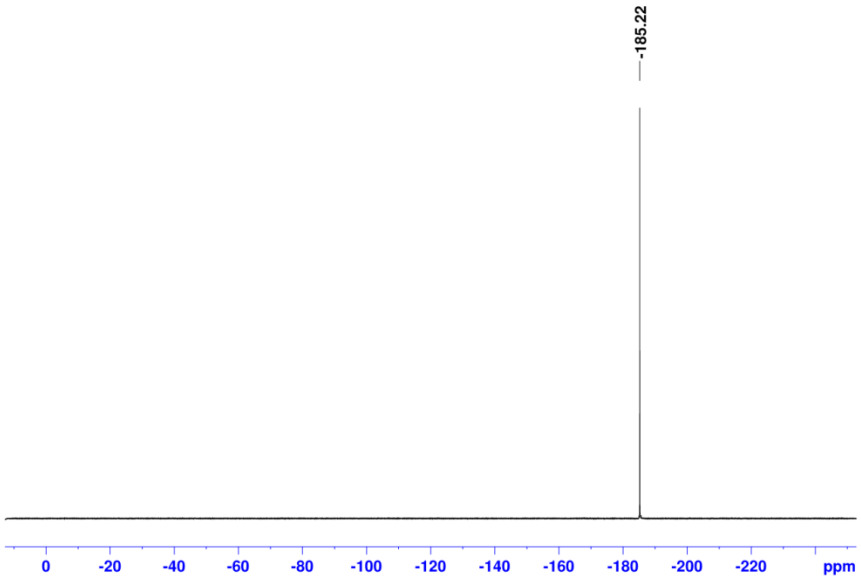

Figure **37**: ^{19}F NMR spectrum of fluoromuscimol (**64**).

The ^{13}C NMR spectrum of fluoromuscimol (**64**) (Figure 38) exhibits four sets of doublets corresponding to ^{13}C-^{19}F couplings, whose coupling constants are for one bond $^{1}J_{CF}$ 257.1 Hz, two bonds $^{2}J_{CF}$ 21.8 Hz, 11.0 Hz and three bonds $^{3}J_{CF}$ 3.1 Hz. These are assigned to 139.1 ppm (C-4), 145.6 ppm (C-5), 167.8 ppm (C-3) and 32.5 (C-6) respectively. Analysis of the ^{1}H-^{13}C HMBC spectrum (Figure 39) indicates that H-6 has a ^{4}J correlation with δ_C 167.8 ppm (C-3), a ^{3}J correlation with δ_C 139.1 (C-4) and a ^{2}J correlation with δ_C 145.6 ppm (C-5) respectively.

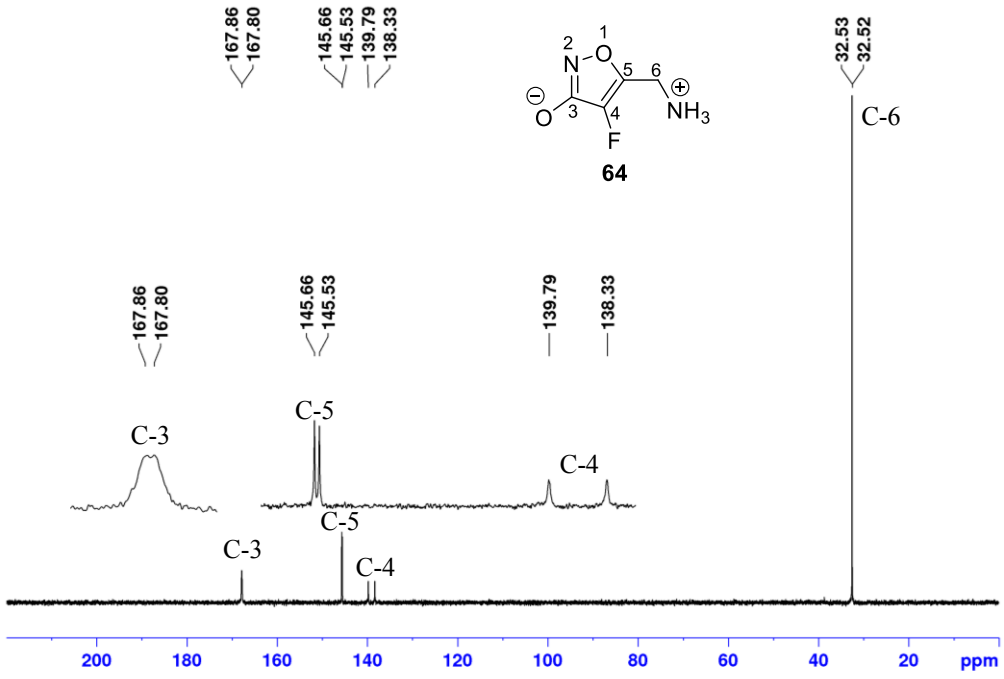

Figure **38**: ^{13}C NMR spectrum of fluoromuscimol (**64**).

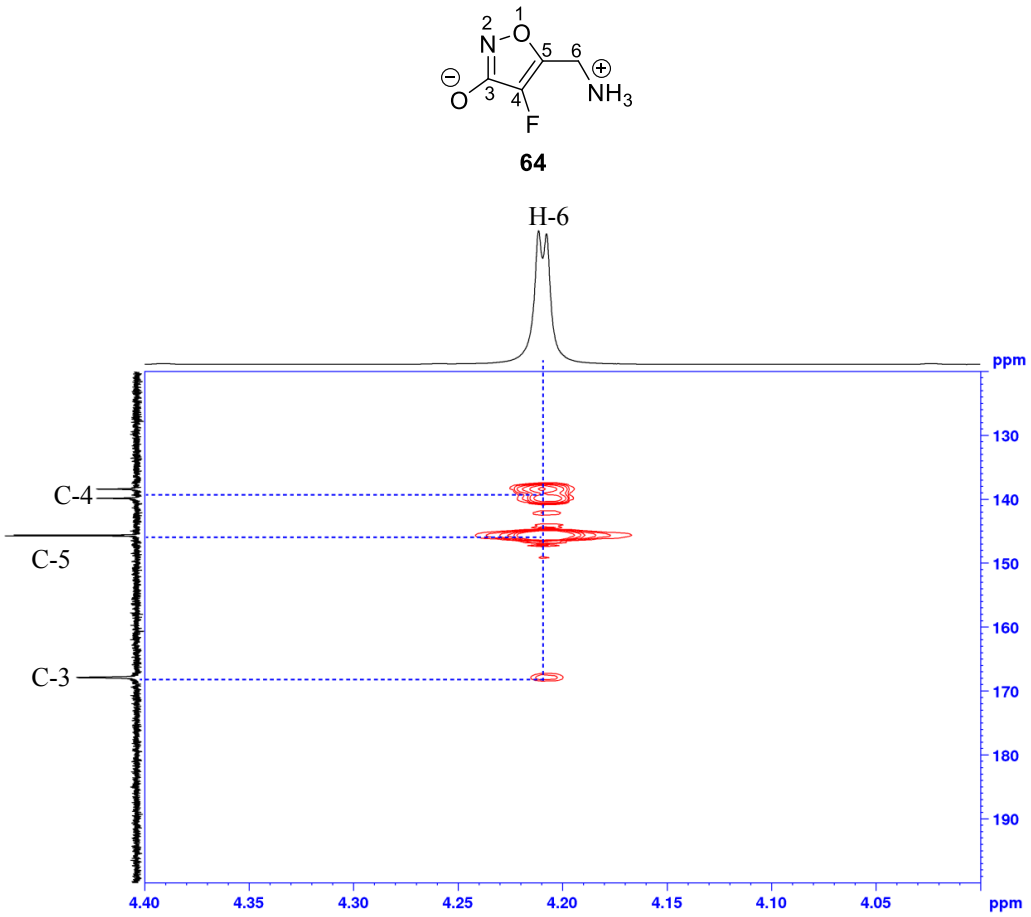

Figure **39**: ^{1}H-^{13}C HMBC spectrum of fluoromuscimol (**64**).

A synthesis of muscimol (**11**) was carried out as a control for biological assessment. Deprotection of the isopropyl group of (**119**) with 33% HBr in acetic acid, followed by purification using preparative HPLC afforded muscimol (**11**) as colourless solid in 34% yield after freeze-drying (Scheme 43).

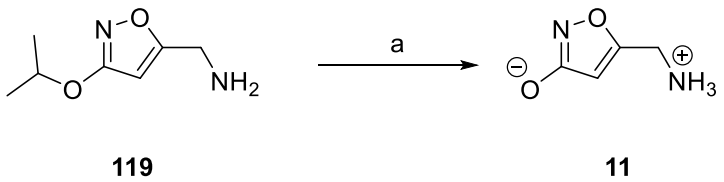

119 **11**

Scheme **43**: Synthesis of muscimol (**11**) from (**119**). Reagents and conditions: a) 33% HBr in AcOH, 60 °C, 17 h, 34%.

2.4.5 Synthesis of trifluoromethylmuscimol (65)

Introduction of trifluoromethyl (CF_3) group to an organic molecule has attracted much interest particularly in the field of pharmaceuticals and agrochemicals.[50–56] In addition, this structural moiety presents in a range of commercially available drugs and is known to dramatically alter the solubility, lipohilicity, bioavailability, metabolic stability etc of organic molecules.[57–59] Importantly, due to the lipophilic nature of the trifluoromethyl group, it can increase the lipid solubility of drugs, thus enhancing their ability to penetrate the blood-brain barrier, an important structural feature that has to take into account when designing novel CNS drugs.[60–63] Hence, it was of interest to synthesise the trifluoromethyl analogue of muscimol and evaluate its agonist activities against $GABA_A$ receptors. It is anticipated that replacing the fluorine for trifluoromethyl group should significantly increase the lipophilicity of the muscimol analogue.

The synthetic route to trifluoromethylmuscimol (**65**) is illustrated in Scheme 44, a synthesis which took eleven steps, starting from the commercially available (**77**). The first four steps of the route were similar to that previously described for the synthesis of fluoromucimol (**64**) outlined in Scheme 41. Iodination at C-4 of isopropyl azido (**118**) was accomplished in a similar manner to that described in Scheme 37, replacing NBS with NIS as the electrophilic halogen source. Reduction of the azide group of (**126**) to amine (**127**) *via* the Staudinger process followed by direct protection with Boc anhydride afforded the *N*-doubly protected amino (**129**) in 87%. With this compound in hand, the next task was to install the trifluoromethyl group at C-4 of intermediate (**129**). The key step for

triflurомethylation was achieved using methyl fluorosulfonyldifluoroacetate (MFSDA) as a nucleophilic triluoromethylating reagent. This approach enabled the incorporation of the trifluoromethyl group at a late stage in the synthetic sequence, an aspect which is attractive for PET studies.

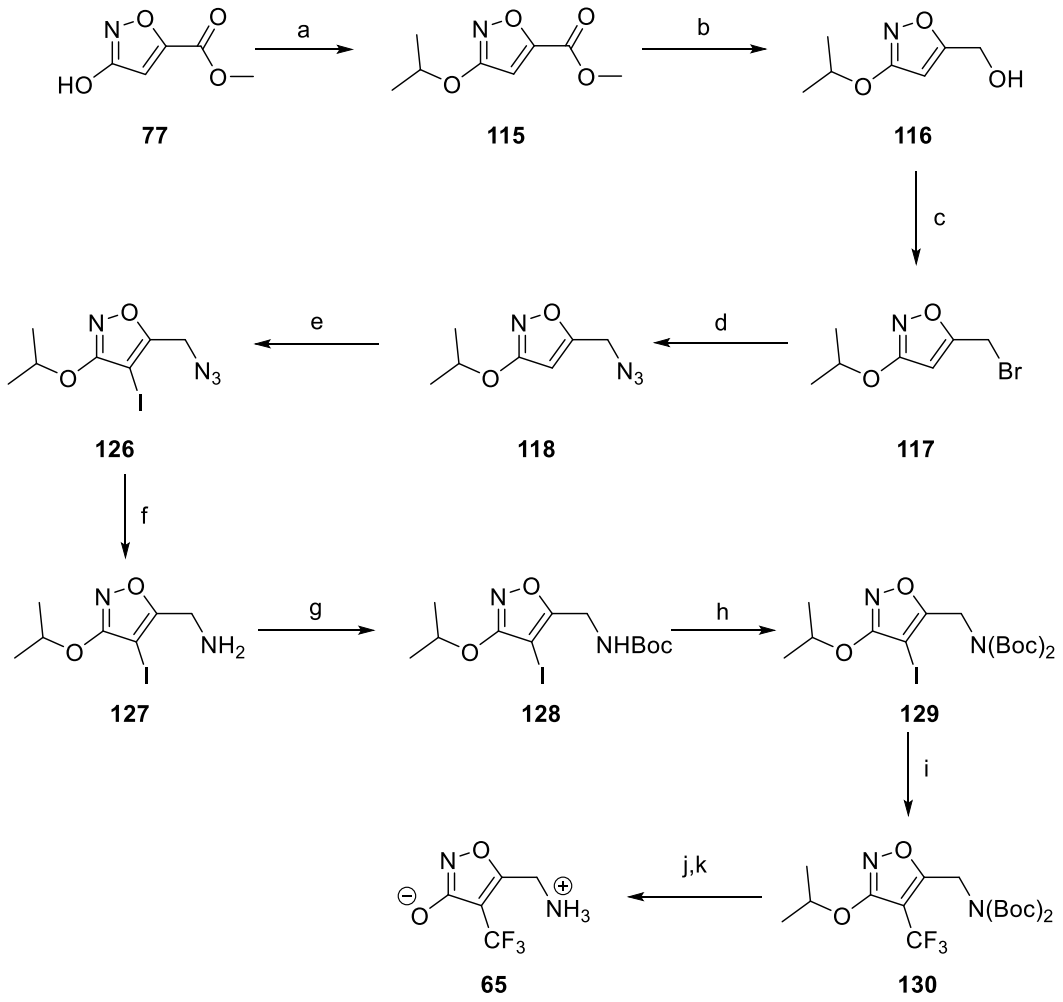

Scheme **44**: Successful route to trifluoromethylmuscimol (**65**). Reagents and conditions: a) *i*-PrBr, K_2CO_3, DMF, 55 °C, overnight, 77%; b) $NaBH_4$, MeOH, 0 °C→rt, overnight, 90%; c) PPh_3, CBr_4, rt, 12 h, 58%; d) NaN_3, DMF, 80 °C, 3.5 h, 91%; e) NIS, TFA, rt, overnight, 86%; f) PMe_3, THF, H_2O, 0 °C, 1 h, 83%; g) Boc_2O, Na_2CO_3, dioxane/H_2O, rt, overnight, 81%; h) Boc_2O, DMAP, MeCN, reflux, 3 h, 87%; i) MFSDA, CuI, HMPA/DMF, 80 °C, 24 h, 34%; j) TFA, DCM, rt, 6 h; k) 33% HBr in AcOH, 60 °C, 48 h, 36% over two steps.

The proposed mechanism for the trifluoromethylation of (**129**) is shown in Scheme 45. The process starts with the reaction of MFSDA (**131**) with CuI by elimination of methyl iodide to generate copper salt (**132**). Decarboxylation of salt (**132**) leads to the formation of difluorocarbene and a fluoride ion, which are in equilibrium with trifluoromethyl anion (**133**). In the presence of CuI, the equilibrium shifts to afford the active cuprate species (**134**).[60,64,65] Subsequently, the oxidative addition to the cuprate (**134**) of aryl iodide (**129**), followed by reductive elimination gives the desired cross-coupling triflоromethylated product (**130**) along with the release of CuI and iodide ion, thus completing the catalytic cycle.[66]

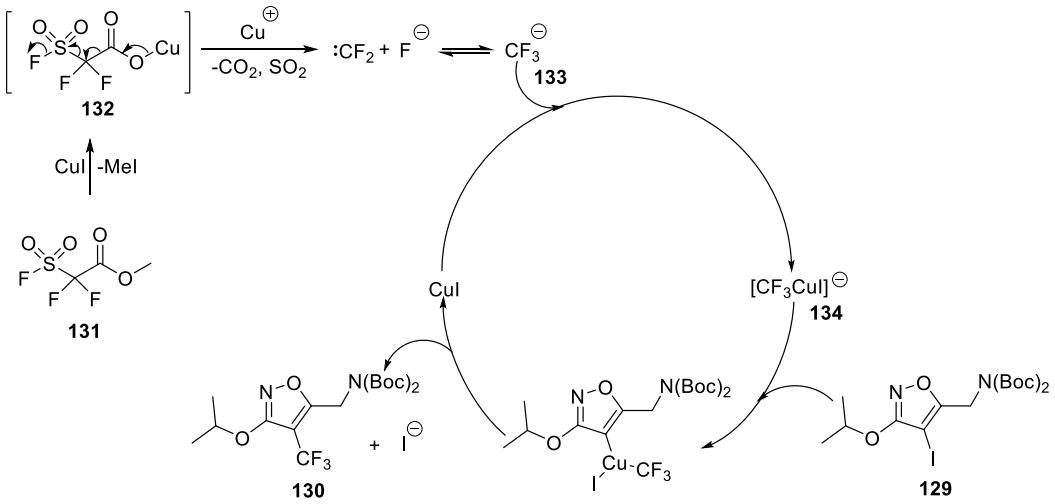

Scheme **45**: Proposed mechanism for the trifluoromethylation of (**129**).[60,64–66]

The structure of trifloromethylated product (**130**) was elucidated by NMR analyses. As can be seen in Figure 40, the methylene proton of H-6 resonates as a quartet at 4.97 ppm and shows a coupling to the trifluormethyl group ($^{5}J_{HF}$ = 1.0 Hz). This signal collapses to a singlet in the $^{1}H\{^{19}F\}$ NMR spectrum. In the ^{19}F NMR (Figure 41), the trifluoromethyl group is found to resonate as a triplet at -57.7 ppm with the same $^{5}J_{HF}$ coupling constant of 1.0 Hz. This triplet collapses to a singlet in the $^{19}F\{^{1}H\}$ experiment confirming the presence of coupling between the trifluoromethyl group and methylene proton H-6.

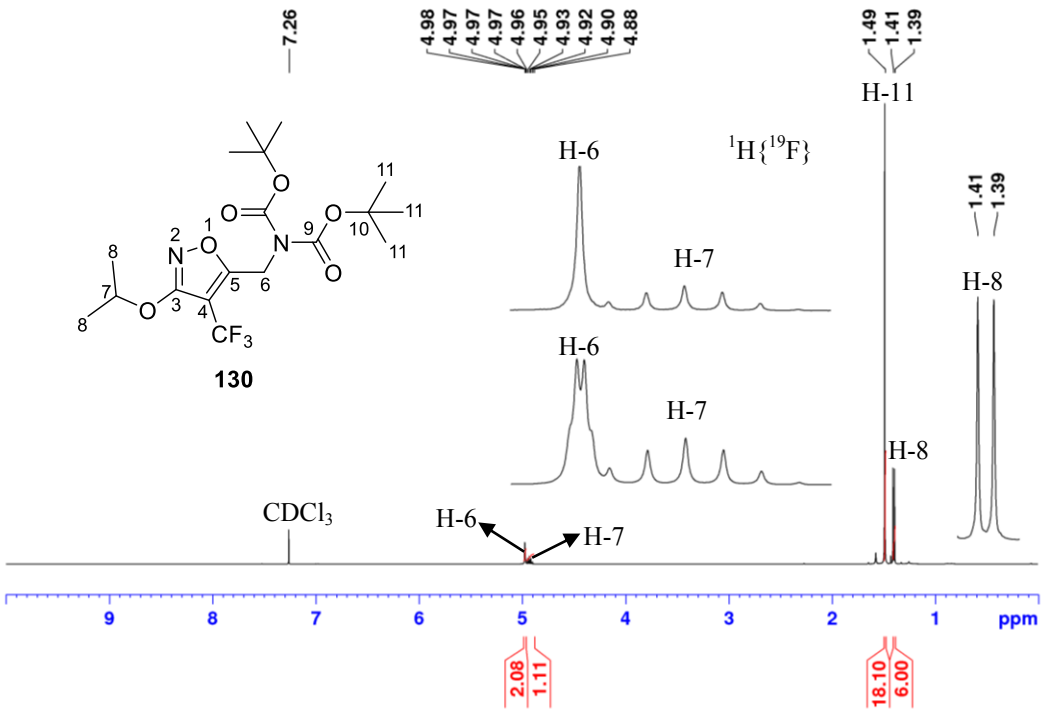

Figure **40**: ^{1}H NMR spectra of (**130**) with and without $\{^{19}F\}$.

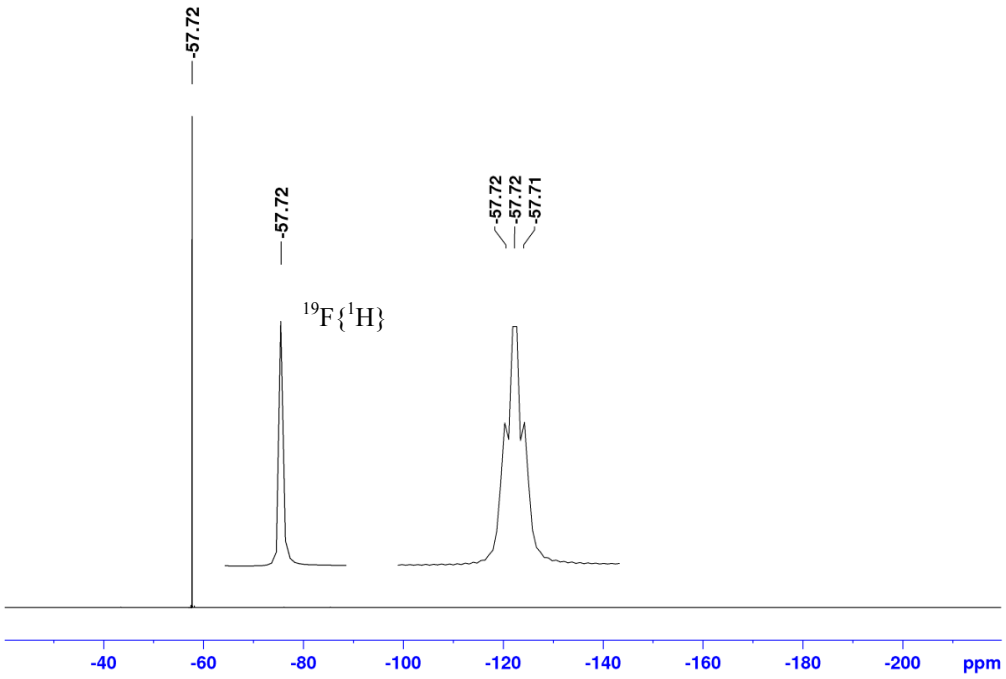

Figure **41**: ^{19}F NMR spectra of (**130**) with and without $\{^{1}H\}$.

^{13}C NMR analysis of compound (**130**) is shown in Figure 42. Two quartets appear at 121.2 ppm ($^{1}J_{CF}$ = 254.6 Hz) and 99.2 ppm ($^{2}J_{CF}$ = 39.4 Hz) are attributed to ^{13}C-^{19}F coupling associated with the trifluoromethyl group. These signals are assigned to the CF_3 carbon and C-4 respectively. The carbonyl group of C-9 is assigned to 169.4 ppm, while the other three quaternary carbons of C-3, C-5 and C-10 which appear more upfield are assigned to 167.4 ppm, 151.6 ppm and 83.8 ppm respectively. Other signals such as that 28.1 ppm and 21.8 ppm correspond to methyl carbons of C-11 and C-8. The rest of the signals at 74.9 ppm and 42.2 ppm are attributed to the methine carbon of C-7 and methylene carbon of C-6 respectively.

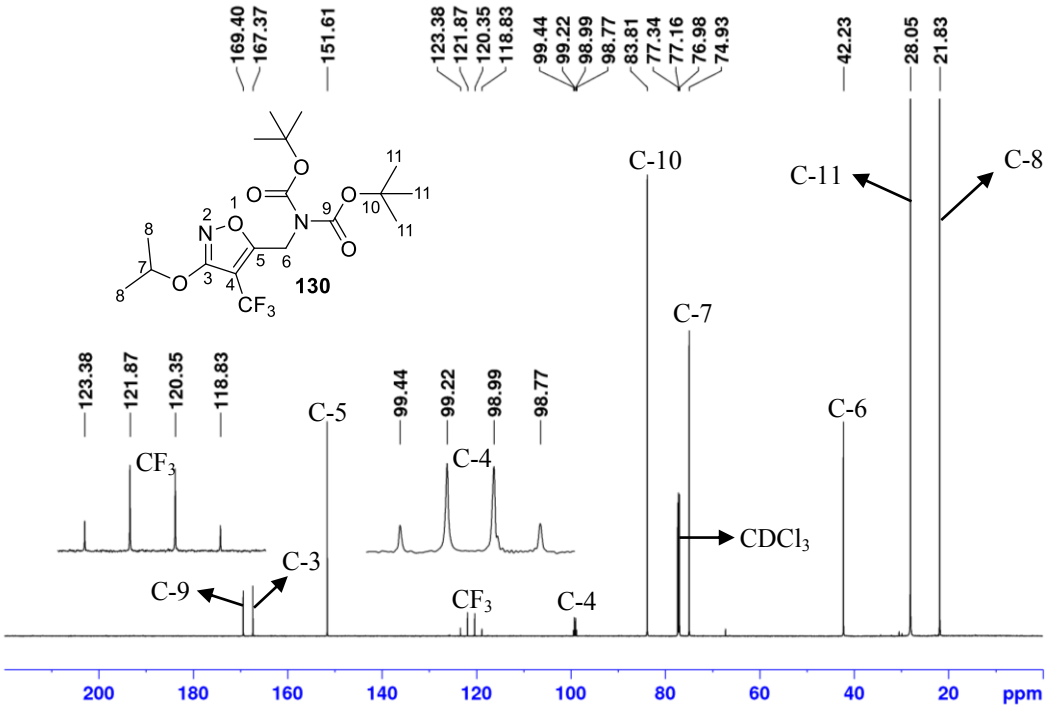

Figure **42**: ^{13}C NMR spectrum of (**130**).

Deprotection of the Boc protecting groups was conducted according to the standard protocol, adding an excess TFA to a solution of substrate (**130**) in DCM. This reaction afforded a colourless crystalline solid containing the TFA salt (**135**) upon removal of solvent under reduced pressure. Unfortunately, attempts to purify the product by chromatography were unsuccessful due to its instability on silica gel. Nevertheless, the crystalline material was found to be stable enough to perform single-crystal X-ray diffraction analysis (Figure 43), thus confirming the formation of the desired compound.

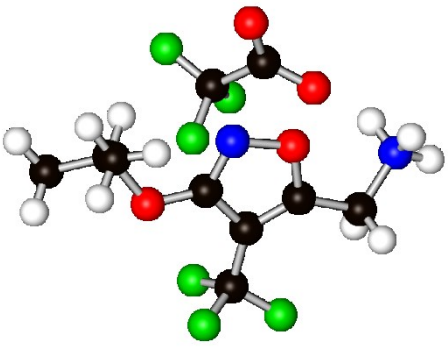

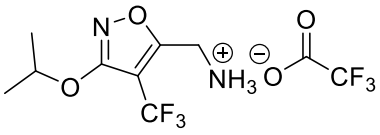

135

Figure **43**: X-ray structure of (**135**).

Due to the suspected instability of (**135**) it was submitted directly to further deprotection conditions in order to remove the isopropyl group. Thus the colourless crystalline solid was treated with an excess of HBr (33% in acetic acid) for 48 hours at 60 °C. The final trifluoromethylmuscimol (**65**) was obtained as a colourless solid in 36% yield after purification by preparative HPLC. The purity of (**65**) was assessed by analytical HPLC on a reverse phase column. HPLC gave a single peak (t_r = 2.27 min) corresponding to (**65**), and indicating a high purity (>98%) (Figure 44).

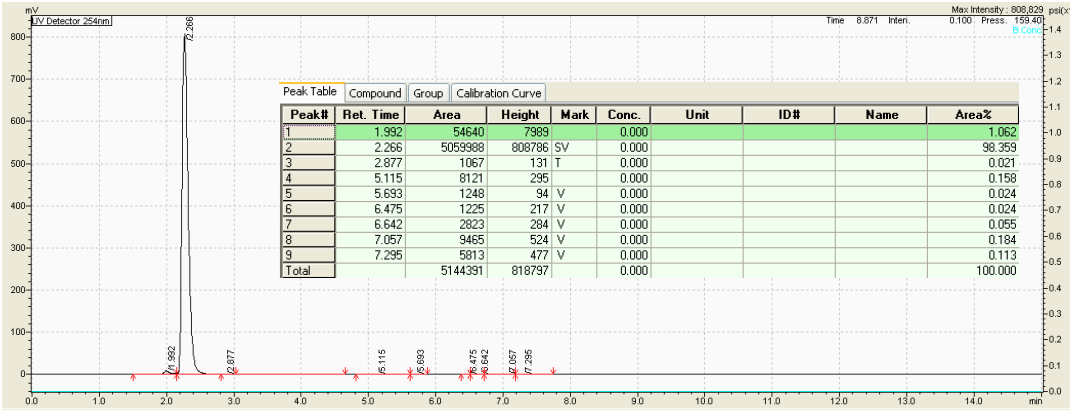

Figure **44**: HPLC chromatogram showing greater than 98% purity of trifluoromethylmuscimol (**65**).

As shown in Figures 45 and 46, both ^{1}H NMR and ^{19}F NMR spectra of trifluoromethylmuscimol (**65**) exhibit one sharp singlet resonating at 4.38 ppm and -58.9 ppm respectively, readily recognisable as arising from methylene proton H-6 and trifluoromethyl CF_3 group respectively. With respect to ^{13}C NMR (Figure 47), the signal corresponding to the trifluoromethyl CF_3 group appears as a quartet at 121.6 ppm, showing clear ^{13}C-^{19}F coupling ($^{1}J_{CF}$ of 267.8 Hz), whereas the quaternary sp^2 carbon (C-4) adjacent to the trifluoromethyl group appears as an apparent doublet at 103.2 ppm ($^{2}J_{CF}$ of 39.5 Hz), rather than a clear quartet. Besides these characteristic signals, the remaining three carbon signals are assigned to methylene carbon of C-6 at 34.5 ppm and quaternary carbons of C-3 at 172.2 ppm and C-5 at 163.7 ppm respectively.

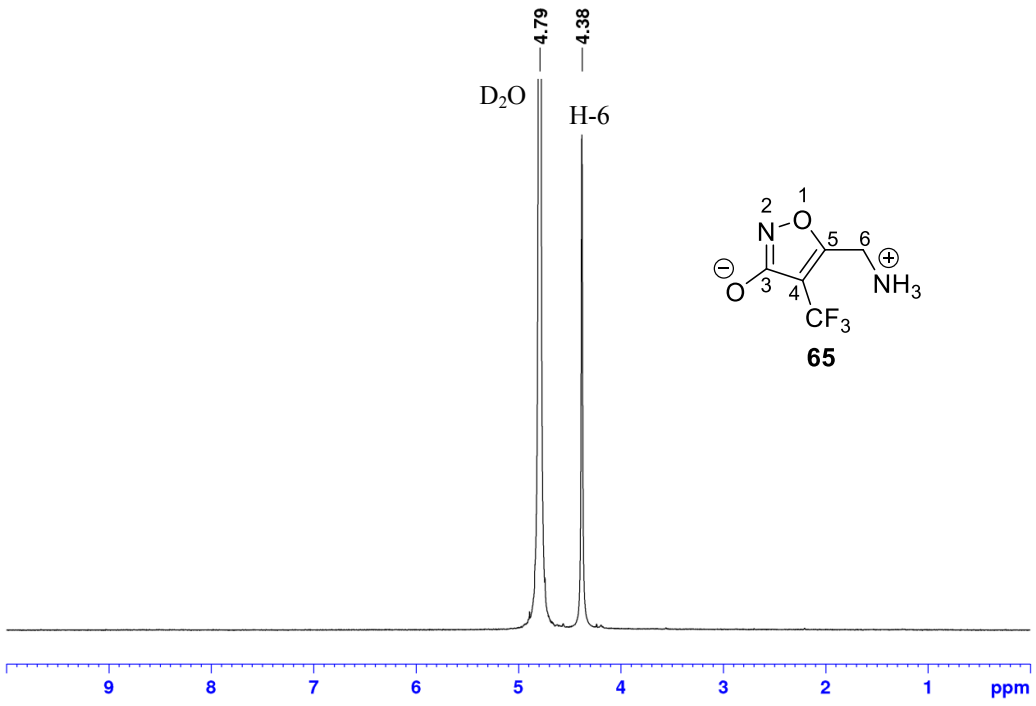

65

Figure **45**: ^{1}H NMR spectrum of trifluoromethylmuscimol (**65**).

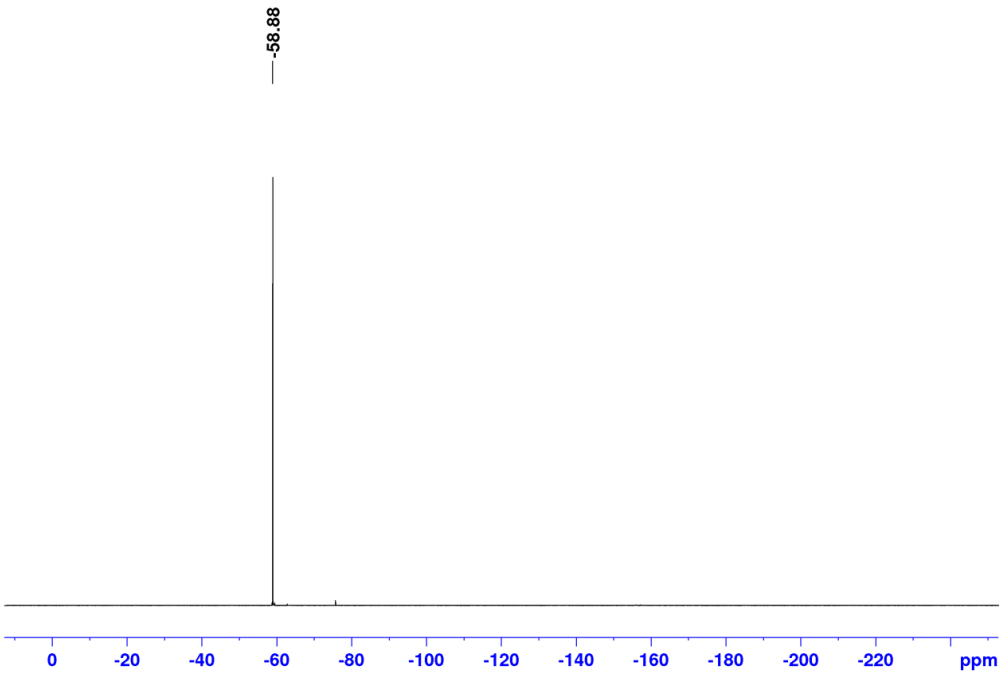

Figure **46**: ^{19}F NMR spectrum of trifluoromethylmuscimol (**65**).

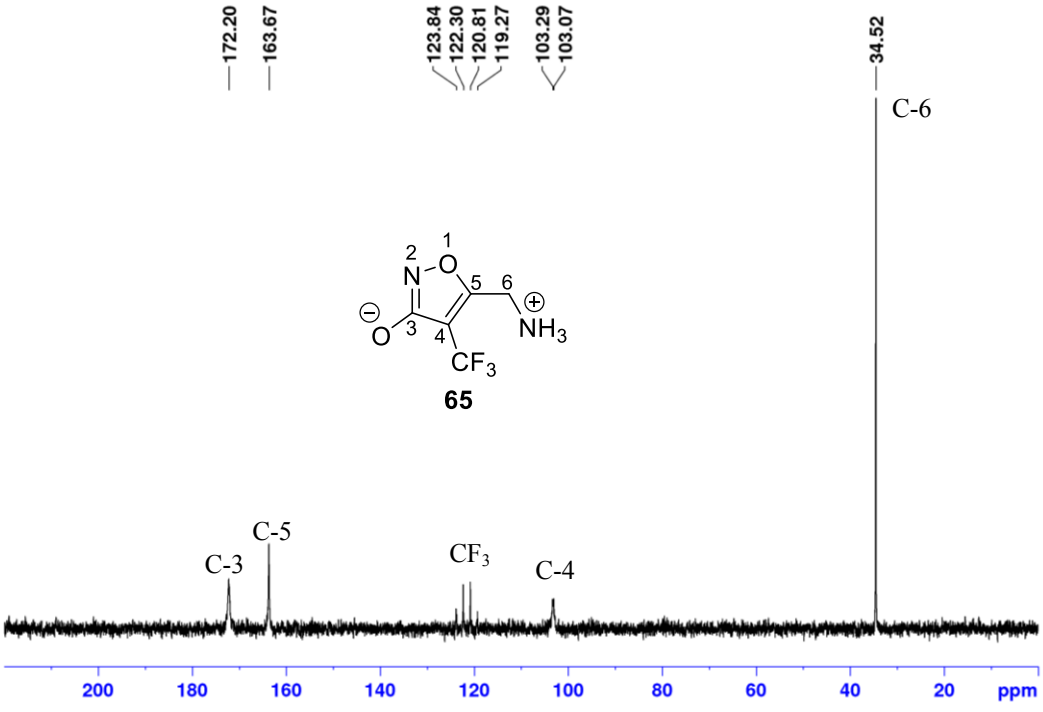

65

Figure **47**: ^{13}C NMR spectrum of trifluoromethylmuscimol (**65**).

2.4.6 Biological studies

Biological evaluation was performed at the Faculty of Pharmacy, the University of Sydney in Australia. Compounds were tested on human synaptic ($\alpha_1\beta_2\gamma_2$), extrasynaptic ($\alpha_4\beta_2\delta$) and (ρ_1) subunits of the $GABA_A$ receptor, expressed in *Xenopus laevis* frog oocytes. Oocytes were injected with a mixture of cRNAs encoding the desired $GABA_A$ receptor subunits and incubated for 3-7 days at 18 °C in modified Barth's solution (96 mM NaCl, 2.0 mM KCl, 1.0 mM $MgCl_2$, 1.8 mM $CaCl_2$, 5.0 mM HEPES, 2.5 mM sodium pyruvate, 0.5 mM theophylline, 100 μg/ml gentamycin, pH 7.4).

The activities of GABA agonists were measured by recording induced currents at a holding potential ranging from -60 to -80 mV using an Axon Geneclamp 500B amplifier (Molecular Devices). Responses and data acquisition were recorded by using two-electrode voltage-clamp electrophysiology. In the data presented in Table 11, E_{max} refers to the maximal current produced by a saturating concentration of the agonist and EC_{50} refers to the concentration of agonist that is required to produce 50% of the response in E_{max}.

GABA was reassayed as a control in this study. The potency of GABA was approximately 7-fold higher at the extrasynaptic ($\alpha_4\beta_2\delta$) than synaptic ($\alpha_1\beta_2\gamma_2$) receptors, with EC_{50} values of 2.8 and 20 μM respectively (Table 11, Figures 48a and 48b), and was found to be comparable with previous reports.[67–70] Synthetic muscimol was also compared with fluoromuscimol and trifluoromethylmuscimol. Fluoromuscimol (**64**) and muscimol (**11**) both evoked current responses at

synaptic ($\alpha_1\beta_2\gamma_2$) (Table 11, Figures 49a and 49b) and extrasynaptic ($\alpha_4\beta_2\delta$) (Table 11, Figures 49d and 49e) receptors that appeared similar to those of GABA (**12**). Fluoromuscimol (**64**) was between 9- and 17-fold less potent than GABA at both receptors types. However, it displayed higher efficacy at saturating concentrations than GABA at extrasynaptic ($\alpha_4\beta_2\delta$) receptors, with E_{max}(fluoromuscimol) 1.6-fold greater than E_{max}(GABA). The E_{max} was lowered at synaptic ($\alpha_1\beta_2\gamma_2$) receptors, reaching 77% of GABA. On the other hand, the introduction of fluorine increased the EC_{50} values of muscimol (**11**) by 56-fold for the synaptic ($\alpha_1\beta_2\gamma_2$) receptors and by 112-fold for the extrasynaptic ($\alpha_4\beta_2\delta$) receptors, thus reducing the potency, although the maximal efficacy (E_{max}) had been maintained for the extrasynaptic ($\alpha_4\beta_2\delta$) receptors, and a little reduced for the synaptic ($\alpha_1\beta_2\gamma_2$) receptors. The trifluoromethyl analogue of muscimol (**65**) was inactive and did not evoke any current responses at all the tested $GABA_A$ receptors at concentrations up to 300 μM (Figures 49c).

Agonist	$\alpha_1\beta_2\gamma_2$ Synaptic			$\alpha_4\beta_2\delta$ Extrasynaptic			ρ_1		
	EC_{50} (μM)	E_{Max} (%)	n_{exp}	EC_{50} (μM)	E_{Max} (%)	n_{exp}	EC_{50} (μM)	E_{Max} (%)	n_{exp}
GABA (**12**)	20	100	5	2.8	100	9	1.1	100	8
Muscimol (**11**)	3.1	120	6	0.43	160	9	1.6	75	6
Fluoromuscimol (**64**)	175	77	5	48	160	5	not active	not active	6
Trifluoromethyl muscimol (**65**)	not active	not active	3	not active	not active	3	not active	not active	3

Table **11**: Potency and relative efficacy of GABA (**12**), muscimol (**11**), fluoromuscimol (**64**) and trifluoromethylmuscimol (**65**) at synaptic ($\alpha_1\beta_2\gamma_2$), extrasynaptic ($\alpha_4\beta_2\delta$) and (ρ_1) $GABA_A$ receptors.

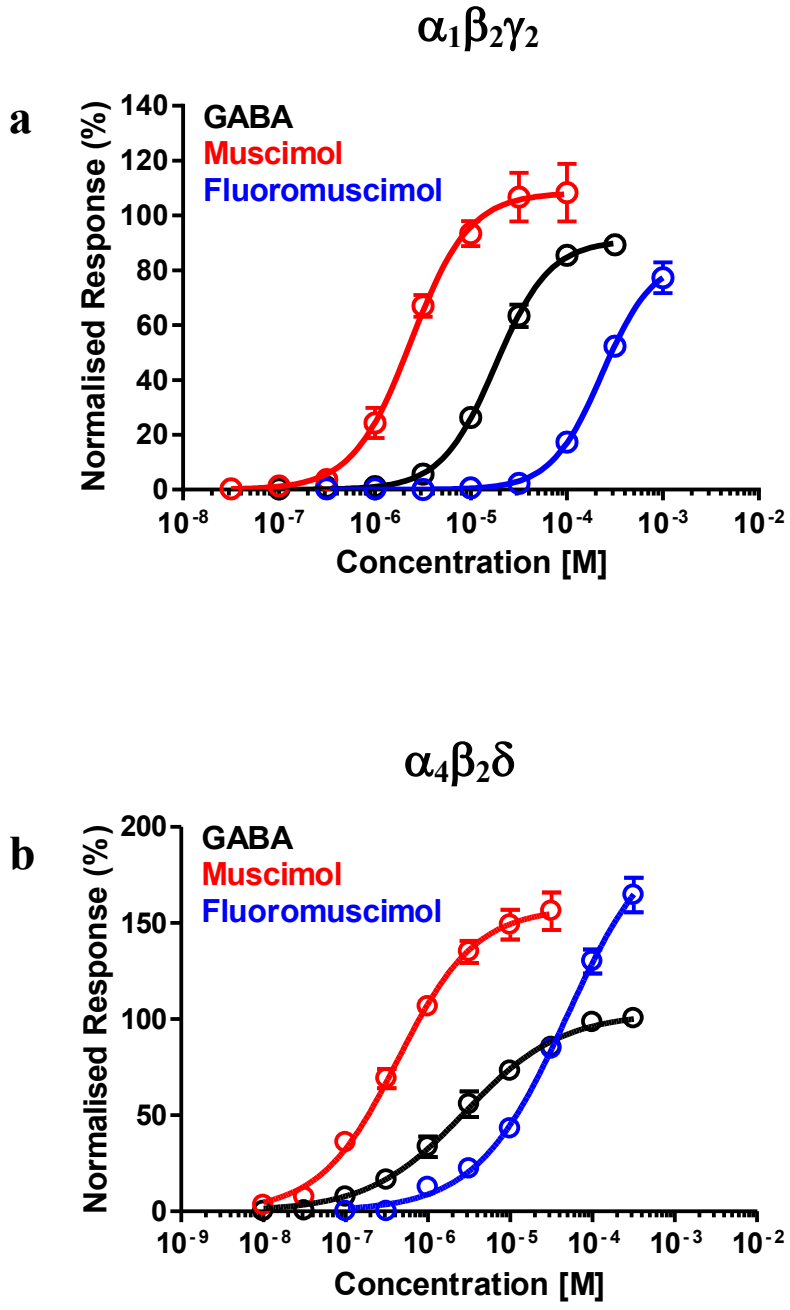

Figure **48**: Activities of GABA (**12**), muscimol (**11**) and fluoromuscimol (**64**) at synaptic (**a**)($\alpha_1\beta_2\gamma_2$) and extrasynaptic (**b**)($\alpha_4\beta_2\delta$) $GABA_A$ receptors.

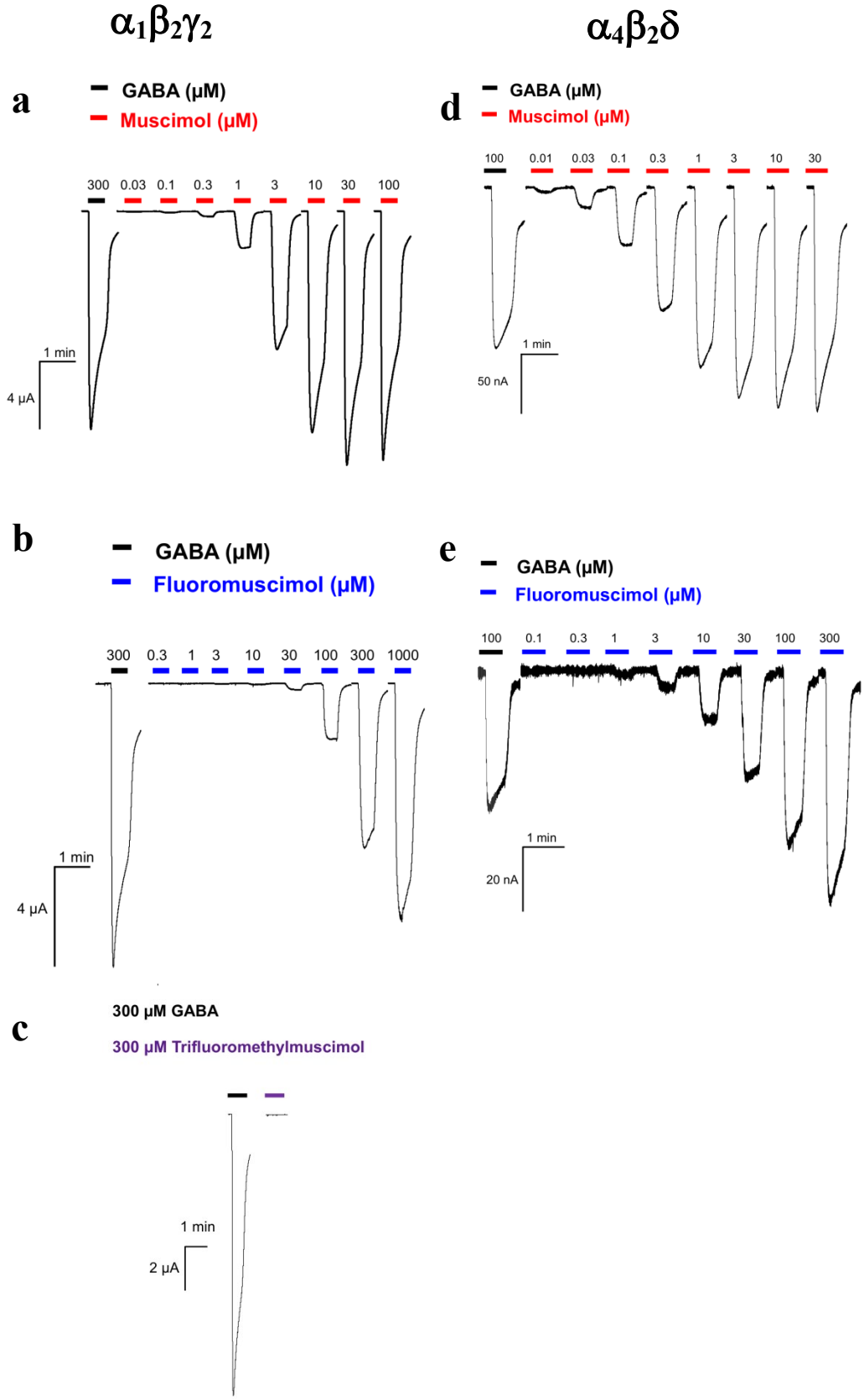

Figure **49**: Current responses of GABA (**12**), muscimol (**11**), fluoromuscimol (**64**) and trifluoromethylmuscimol (**65**) at synaptic (**a**)(**b**)(**c**)($\alpha_1\beta_2\gamma_2$) and extrasynaptic (**d**)(**e**)($\alpha_4\beta_2\delta$) $GABA_A$ receptors.

With respect to the ρ_1 $GABA_A$ receptors, both GABA (**12**) and muscimol (**11**) were characterised as full agonists, with EC values of 1.1 μM for GABA and 1.6 μM for muscimol respectively (Table 11 and Figure 50). Of the agonists tested, fluoromuscimol (**64**) was an inefficient agonist at ρ_1 $GABA_A$ receptors, only evoking 33% response at the highest tested concentration (1 mM) (Figure 50).

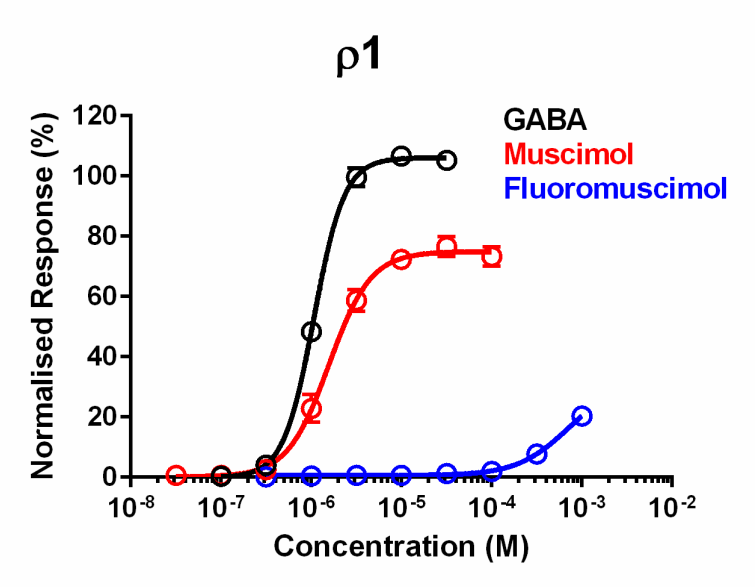

Figure **50**: Activities of GABA (**12**), muscimol (**11**) and fluoromuscimol (**64**) at ρ_1 $GABA_A$ receptors

The biological assessment has shown that, introduction of one fluorine atom or a trifluoromethyl group into muscimol (**11**) did not improve the potency at the $GABA_A$ receptors. The best result was achieved on the extrasynaptic ($\alpha_4\beta_2\delta$) receptors, where fluoromuscimol (**64**) showed higher potency than GABA (**12**) at saturating concentrations.

2.5 Conclusions

The first syntheses of fluoromuscimol (**64**) and trifluoromethylmuscimol (**65**) have been achieved in nine and eleven steps respectively. The key fluorination step in the synthesis of fluromuscimol (**64**) was achieved *via* lithiation of (**120**) with *n*-BuLi followed by addition of NFSI.

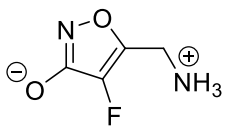

64

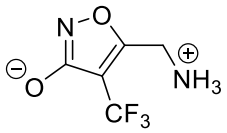

65

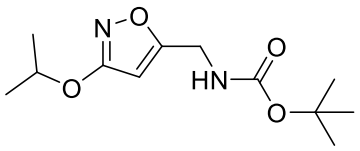

120

Fluoromuscimol (**64**) showed greater maximum response in comparison to GABA at the extrasynaptic $GABA_A$ receptors ($\alpha_4\beta_2\delta$), but lower overall potency. Therefore, the substitution of hydrogen atom by fluorine in muscimol resulted in a decrease in potency relative to reference compounds, GABA and muscimol.

The introduction of trifluoromethyl group onto muscimol was accomplished through the coupling of heteroaryl iodide (**129**) with trifluoromethylcopper species (**134**), which was generated in situ from MFSDA (**131**) in the presence of catalytic amounts of CuI. Trifluoromethylmuscimol (**65**) was inactive and did not evoke any current responses at all the tested $GABA_A$ receptors.

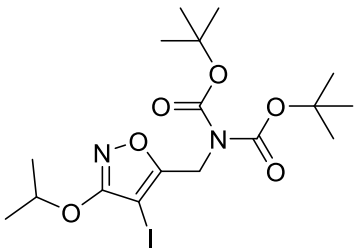

129

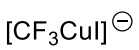

134

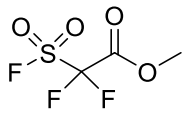

131

With the non-radioactive [^{19}F] reference compound (**64**) in hand, the immediate challenge is to develop a late stage synthesis suitable for PET studies. One of the approaches that could be employed is by using diaryliodonium salts as precursors. Alternatively, the iodination of muscimol may offer an alternative to fluoromuscimol (**64**), as this compound could be labelled using the longer half-life iodine-124. The syntheses of diaryliodonium salts and iodomuscimol are the subjects of Chapter 3.

2.6 References

1 M. Slifstein and A. Abi-Dargham, *Semin. Nucl. Med.*, 2016, **47**, 54–63.

2 A. Hoepping, M. Scheunemann, S. Fischer, W. Deuther-Conrad, A. Hiller, F. Wegner, M. Diekers, J. Steinbach and P. Brust, *Nucl. Med. Biol.*, 2007, **34**, 559–570.

3 A. Gaeta, J. Woodcraft, S. Plant, J. Goggi, P. Jones, M. Battle, W. Trigg, S. K. Luthra and M. Glaser, *Bioorg. Med. Chem. Lett.*, 2010, **20**, 4649–4652.

4 C. D'Hulst, I. Heulens, N. Van Der Aa, K. Goffin, M. Koole, K. Porke, M. Van De Velde, L. Rooms, W. Van Paesschen, H. Van Esch, K. Van Laere and R. F. Kooy, *PLoS One*, 2015, **10**, 1–12.

5 A. Kassenbrock, N. Vasdev and S. H. Liang, *Curr. Top. Med. Chem.*, 2016, **16**, 1830–1842.

6 P. Pevarello and M. Varasi, *Synth. Commun.*, 1992, **22**, 1939–1948.

7 B. E. Mccarry and M. Savard, *Tetrahedron Lett.*, 1981, **22**, 5153–5156.

8 V. Jäger and M. Frey, *Liebigs Ann. Chem.*, 1982, 817–820.

9 D. Chiarino, M. Napoletano and A. Sala, *Tetrahedron Lett.*, 1986, **27**, 3181–3182.

10 Y. Konda, H. Takahashi and M. Onda, *Chem. Pharm. Bull.*, 1985, **33**, 1083–1087.

11 P. Krogsgaard-Larsen and S.B. Christensen, *Acta Chem. Scand. B*, 1976, **30**, 281–282.

12 M. Frey and V. Jäger, *Synthesis*, 1985, 1100–1104.

13 G. Serdaroğlu, *Int. J. Quantum Chem.*, 2011, **111**, 3938–3948.

14 W. Sieghart and G. Sperk, *Curr. Top. Med. Chem.*, 2002, **2**, 795–816.

15 M. D. Moran, A. A. Wilson, C. S. Elmore, J. Parkes, A. Ng, O. Sadovski, A. Graff, Z. J. Daskalakis, S. Houle, M. J. Chapdelaine and N. Vasdev, *Bioorganic Med. Chem.*, 2012, **20**, 4482–4488.

16 P. Levêquel, S. Sanabria-Bohorquez, A. Bol, A. De Volder, D. Labar, K. Van Rijckevorsel and B. Gallez, *Eur. J. Nucl. Med. Mol. Imaging*, 2003, **30**, 1630–1636.

17 A. Lingford-Hughes, A. G. Reid, J. Myers, A. Feeney, A. Hammers, L. G. Taylor, L. Rosso, F. Turkheimer, D. J. Brooks, P. Grasby and D. J. Nutt, *J Psychopharmacol*, 2012, **26**, 273–281.

18 A. Jackson, M. R. Battle, D. M. O'Shea, W. F. Chau, A. Gaeta, S. L. Brown, A. L. Ewan, C. L. Jones, P. A. Jones, J. L. Woodcraft, D. R. Bouvet, B. B. Guilbert and W. Trigg, *Nucl. Med. Biol.*, 2014, **41**, 196–202.

19 R. Frantz, L. Hintermann, M. Perseghini, D. Broggini and A. Togni, *Org. Lett.*, 2003, **5**, 1709–1712.

20 D. P. Huber, K. Stanek and A. Togni, *Tetrahedron Asymmetry*, 2006, **17**, 658–664.

21 P. T. Nyffeler, S. G. Durón, M. D. Burkart, S. P. Vincent and C. H. Wong, *Angew. Chem. Int. Ed.*, 2005, **44**, 192–212.

22 K. Muniz, *Top. Organomet. Chem.*, 2010, **31**, 1–18.

23 S. Piana, I. Devillers, A. Togni and U. Rothlisberger, *Angew. Chem. Int. Ed.*, 2002, **41**, 979–982.

24 J. Breen, G. Sandford, B. Patel and J. Fray, *Synlett*, 2014, **26**, 51–54.

25 R. D. Chambers, J. Hutchinson, M. E. Sparrowhawk, G. Sandford, J. S. Moilliet and J. Thomson, *J. Fluor. Chem.*, 2000, **102**, 169–173.

26 R. D. Chambers, D. Holling, G. Sandford, A. S. Batsanov and J. A. K. Howard, *J. Fluor. Chem.*, 2004, **125**, 661–671.

27 C. E. Stephens and J. A. Blake, *J. Fluor. Chem.*, 2004, **125**, 1939–1945.

28 K. Sato, G. Sandford, K. Shimizu, S. Akiyama, M. J. Lancashire, D. S. Yufit, A. Tarui, M. Omote, I. Kumadaki, S. Harusawa and A. Ando, *Tetrahedron*, 2016, **72**, 1690–1698.

29 G. S. Lal, G. P. Pez and R. G. Syvret, *Chem. Rev.*, 1996, **96**, 1737–1756.

30 D. Edmond and O. Hans, *Synlett*, 1991, 187–189.

31 P. A. Champagne, J. Desroches, J. D. Hamel, M. Vandamme and J. F. Paquin, *Chem. Rev.*, 2015, **115**, 9073–9174.

32 R. E. Banks, M. K. Besheesh, S. N. Mohialdin-Khaffaf and I. Sharif, *J. Chem. Soc., Perkin Trans. 1*, 1996, 2069–2076.

33 R. E. Banks, S. N. Mohialdin-Khaffaf, G. S. Lal, I. Sharif and R. G. Syvret, *J. Chem. Soc. Chem. Commun.*, 1992, 595–596.

34 S. D. Taylor, C. C. Kotoris and G. Hum, *Tetrahedron*, 1999, **55**, 12431–12477.

35 R. A. Day, J. A. Blake and C. E. Stephens, *Synthesis*, 2003, 1586–1590.

36 G. Li, R. Kakarla and S. W. Gerritz, *Tetrahedron Lett.*, 2007, **48**, 4595–4599.

37 S. A. Shackelford, M. B. Anderson, L. C. Christie, T. Goetzen, M. C. Guzman, M. A. Hananel, W. D. Kornreich, H. Li, V. P. Pathak, A. K. Rabinovich, R. J. Rajapakse, L. K. Truesdale, S. M. Tsank and H. N. Vazir, *J. Org. Chem.*, 2003, **68**, 267–275.

38 F. Basuli, X. Zhang, E. M. Jagoda, P. L. Choyke and R. E. Swenson, *Nucl. Med. Biol.*, 2016, **43**, 770–772.

39 H. Xiong, A. T. Hoye, K. H. Fan, X. Li, J. Clemens, C. L. Horchler, N. C. Lim and G. Attardo, *Org. Lett.*, 2015, **17**, 3726–3729.

40 A. R. Studenov and M. S. Berridge, *Nucl. Med. Biol.*, 2001, **28**, 683–693.

41 M. C. Foti and C. Rocco, *Tetrahedron Lett.*, 2014, **55**, 1602–1607.

42 J. Duan, L. H. Zhang and W. R. Dolbier, Jr., *Synlett*, 1999, **8**, 1245–1246.

43 F. Péron, C. Fossey, J. Sopkova-de Oliveira Santos, T. Cailly and F. Fabis, *Chem. Eur. J.*, 2014, **20**, 7507–7513.

44 Y. Okada, M. Yokozawa, M. Akiba, K. Oishi, K. O-kawa, T. Akeboshi, Y. Kawamura, S. Inokuma, Y. Nakamura and J. Nishimura, *Org. Biomol. Chem.*, 2003, **1**, 2506–2511.

45 Y. Jeong, B.-I. Kim, J. K. Lee and J.-S. Ryu, *J. Org. Chem.*, 2014, **79**, 6444–6455.

46 S. B. Vogensen, K. Frydenvang, J. R. Greenwood, G. Postorino, B. Nielsen, D. S. Pickering, B. Ebert, U. Bølcho, J. Egebjerg, M. Gajhede, J. S. Kastrup, T. N. Johansen, R. P. Clausen and P. Krogsgaard-Larsen, *J. Med. Chem.*, 2007, **50**, 2408–2414.

47 B. Frølund, A. T. Jørgensen, L. Tagmose, T. B. Stensbøl, H. T. Vestergaard, C. Engblom, U. Kristiansen, C. Sanchez, P. Krogsgaard-Larsen and T. Liljefors, *J. Med. Chem.*, 2002, **45**, 2454–2468.

48 B. Frølund, L. S. Jensen, L. Guandalini, C. Canillo, H. T. Vestergaard, U. Kristiansen, B. Nielsen, T. B. Stensbøl, C. Madsen, P. Krogsgaard-Larsen and T. Liljefors, *J. Med. Chem.*, 2005, **48**, 427–439.

49 W. Fuhrer and H. W. Gschwend, *J. Org. Chem.*, 1979, **44**, 1133–1136.

50 J. A. Ma and D. Cahard, *J. Fluor. Chem.*, 2007, **128**, 975–996.

51 M. Schlosser, *Angew. Chem. Int. Ed.*, 2006, **45**, 5432–5446.

52 J. A. Ma and D. Cahard, *Chem. Rev.*, 2004, **104**, 6119–6146.

53 K. L. Kirk, *J. Fluor. Chem.*, 2006, **127**, 1013–1029.

54 K. Müller, C. Faeh and F. Diederich, *Science*, 2007, **317**, 1881–1886.

55 R. Betageri, Y. Zhang, R. M. Zindell, D. Kuzmich, T. M. Kirrane, J. Bentzien, M. Cardozo, A. J. Capolino, T. N. Fadra, R. M. Nelson, Z. Paw, D. T. Shih, C. K. Shih, L. Zuvela-Jelaska, G. Nabozny and D. S. Thomson, *Bioorganic Med. Chem. Lett.*, 2005, **15**, 4761–4769.

56 S. H. Watterson, J. Guo, S. H. Spergel, C. M. Langevine, R. V. Moquin, D. R. Shen, M. Yarde, M. E. Cvijic, D. Banas, R. Liu, S. J. Suchard, K. Gillooly, T. Taylor, S. Rex-Rabe, D. J. Shuster, K. W. McIntyre, G. Cornelius, C. D'Arienzo, A. Marino, P. Balimane, B. Warrack, L. Salter-Cid, M. McKinnon, J. C. Barrish, P. H. Carter, W. J. Pitts, J. Xie and A. J. Dyckman, *J. Med. Chem.*, 2016, **59**, 2820–2840.

57 S. Purser, P. R. Moore, S. Swallow and V. Gouverneur, *Chem. Soc. Rev.*, 2008, **37**, 320–330.

58 H.-J. Böhm, D. Banner, S. Bendels, M. Kansy, B. Kuhn, K. Müller, U. Obst-Sander and M. Stahl, *ChemBioChem*, 2004, **5**, 637–643.

59 W. K. Hagmann, *J. Med. Chem.*, 2008, **51**, 4359–4369.

60 S. Roy, B. T. Gregg, G. W. Gribble, V. D. Le and S. Roy, *Tetrahedron*, 2011, **67**, 2161–2195.

61 G. R. Villa, J. J. Hulce, C. Zanca, J. Bi, S. Ikegami, G. L. Cahill, Y. Gu, K. M. Lum, K. Masui, H. Yang, X. Rong, C. Hong, K. M. Turner, F. Liu, G. C. Hon, D. Jenkins, M. Martini, A. M. Armando, O. Quehenberger, T. F. Cloughesy, F. B. Furnari, W. K. Cavenee, P. Tontonoz, T. C. Gahman, A. K. Shiau, B. F. Cravatt and P. S. Mischel, *Cancer Cell*, 2016, **30**, 683–693.

62 M. Huiban, C. Coello, K. Wu, Y. Xu, Y. Lewis, A. P. Brown, M. Buraglio, C. Guan, S. Shabbir, R. Fong, J. Passchier, E. A. Rabiner and A. Lockhart, *Mol. Imaging Biol.*, 2016, **19**, 153–161.

63 M. Han, X. Ma, Y. Jin, W. Zhou, J. Cao, Y. Wang, S. Zhou, G. Wang and Y. Zhu, *Bioorganic Med. Chem. Lett.*, 2014, **24**, 5284–5287.

64 S. L. Clarke and G. P. McGlacken, *Chem. Eur. J.*, 2017, **23**, 1219–1230.

65 Q.-Y. Chen and S.-W. Wu, *J. Chem. Soc., Chem. Commun.,* 1989, 705–706.

66 Y. Nakamura, M. Fujiu, T. Murase, Y. Itoh, H. Serizawa, K. Aikawa and K. Mikami, *Beilstein J. Org. Chem.*, 2013, **9**, 2404–2409.

67 G. Akk, J. Bracamontes and J. H. Steinbach, *J. Physiol.*, 2004, **556**, 387–99.

68 N. Karim, P. Wellendorph, N. Absalom, G. A. R. Johnston, J. R. Hanrahan and M. Chebib, *Amino Acids*, 2013, **44**, 1139–1149.

69 H. J. Lee, N. L. Absalom, J. R. Hanrahan, P. Van Nieuwenhuijzen, P. K. Ahring and M. Chebib, *Brain Res.*, 2016, **1644**, 222–230.

70 L. Y. Hartiadi, P. K. Ahring, M. Chebib and N. L. Absalom, *Biochem. Pharmacol.*, 2016, **103**, 98–108.

Chapter 3: Towards the late stage fluorination of muscimol through diaryliodonium salts.

3.1 Introduction to hypervalent iodine compounds

The first organic hypervalent iodine compound, (dichloroiodo) benzene (**137**) was prepared in 1885 by German chemist Conrad Willgerodt by reacting iodobenzene (**136**) with ICl_3. One year later, Willgerodt reported an improved and high-yielding approach for the preparation of (dichloroiodo) benzene (**137**) by passing Cl_2 gas through a vessel containing an ice-cold iodobenzene solution. (Dichloroiodo) benzene (**137**) precipitated as yellow needles from the solution (Scheme 46).[1]

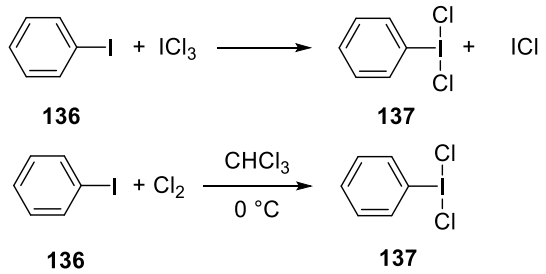

Scheme **46**: Willgerodt synthesis of (dichloroiodo) benzene (**137**).[1]

This was rapidly followed by the discovery of other new important hypervalent iodine compounds such as (diacetoxyiodo) benzene (**138**) and iodosylbenzene (**139**) in 1892,[2] 2-iodoxybenzoic acid (IBX) (**140**) in 1893[3] and diaryliodonium salts(**141**) in 1894.[4]

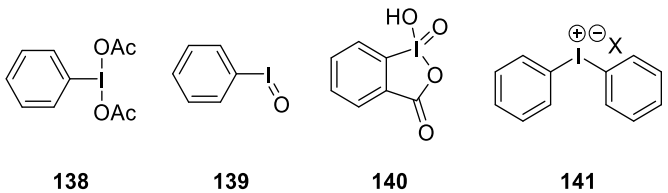

138 **139** **140** **141**

The next major contributor to the field was Beringer and co-workers, with their pioneering work to improve synthetic routes and applications of hypervalent iodine compounds for various organic transformations.[5] For example, the first synthetic application of hypervalent chemistry in the α-arylation of enolisable carbonyl compounds with diaryliodonium salts was reported Beringer and co-workers in 1960.[6] This synthesis involved the use of diphenyliodonoium chloride (**142**) in promoting the transformation of diketone (**143**) into the corresponding mono- and bis-phenylated products of (**144**) and (**145**) (Scheme 47).

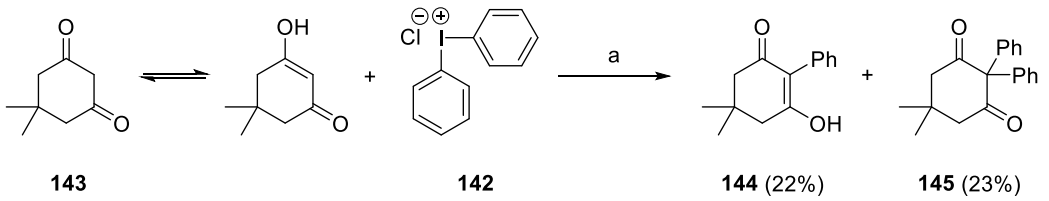

Scheme **47**: The first reported α-arylation of diketone (**143**) using diphenyliodonoium chloride (**142**).[6] Reagents and conditions: a) NaO*t*Bu, *t*-BuOH, 83 °C, 4 h.

The discovery of Dess-Martin periodinane (DMP) (**146**) as a mild and non-toxic oxidation reagent by Dess and Martin in the 1980s was a major breakthrough in hypervalent iodine chemsistry.[7] Since then, synthetic chemistry related to such compounds has received considerable attention. For example, although IBX was known since 1893, its utility in oxidation reactions was not unveiled until 1994.[8] Both DMP and IBX are frequently used in mild and selective oxidative transformations synthesis in organic and medicinal chemistry.[9,10] Recently, Wirth and co-workers developed a tetra-fluorinated analogue of FIBX (**147**).

This reagent exhibits greater solubility in organic solvent compared to IBX, thus improving the reactivity of a reaction.[11]

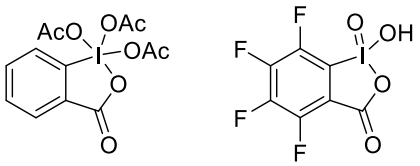

146 **147**

3.2 Nomenclature, oxidation state and bonding

The definition of a hypervalent state according to Musher is when an atom commonly in group 15-18 of the periodic table expands its valence shell beyond the limits of the Lewis octet rule.[12] The general oxidation process of iodine compounds is described according to the Martin-Arduengo *N-X-L* designation for hypervalent molecules and is shown in Scheme 48, where *N* is the number of valence electrons assignable to the valence shell of the central atom *X*, either as unshared pairs of electrons or as pairs of electrons in the sigma bonds joining a number, *L*, of ligands to the atom *X*.[13,14]

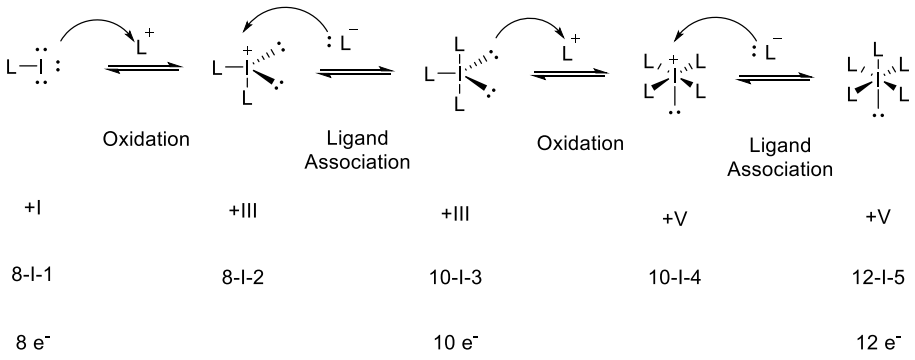

Scheme **48**: Oxidation levels of iodine compounds described according to the Martin-Arduengo *N-X-L* designation for hypervalent molecules.[13,14]

According to IUPAC nomenclature, hypervalent iodine compounds are generally classified according to the oxidation state of the iodine and are denoted with a lambda notation.[15] For examples, iodine compounds with the oxidation state of +III and +V are referred to as λ^3- and λ^5-iodanes respectively. The bonding in hypervalent iodine species can be demonstrated by using a λ^3-iodane (Figure 51). Iodine(III) compounds ($ArIL_2$) have 10 electrons at the iodine atom and the geometry is best depicted as a pseudotrigonal bipyramid (T-shape) with two of the heteroatom ligands L occupying the apical positions and the less electronegative aryl moiety and two free electron pairs occupy the equatorial positions.[16] The linear (L-I-L) bond in $ArIL_2$ is a three-centre four-electron (3c-4e) bond derived from the doubly occupied 5p orbital with two electrons from iodine and one each from the apical ligands. This results in a highly polarised, longer and weaker bond compared to others and the iodine is electrophilic.[16,17] Moreover, the electron withdrawing ligands also contribute to the electrophilicity of the iodine(III) centre.

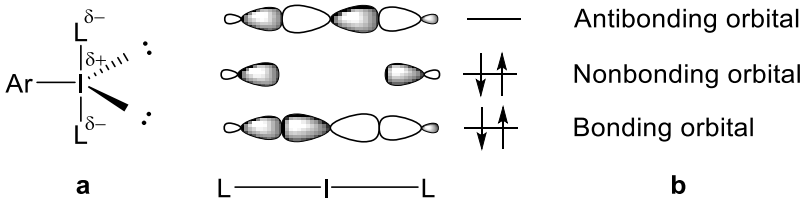

Figure **51**: (**a**) Pseudotrigonal bipyramid geometry of $ArIL_2$ λ^3-iodane. (**b**) Molecular orbitals of the hypervalent bond.

It follows that, hypervalent iodine(III) compounds react with nucleophiles by first forming the Nu-I bond with release of one of the ligands (Scheme 49). Subsequent nucleophilic substitution or reductive elimination yields the Nu-L product and releases ArI.[18]

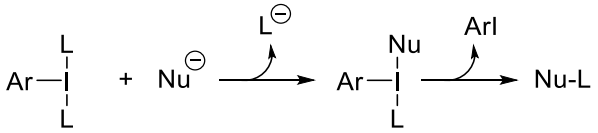

Scheme **49**: General reactivity of $ArIL_2$ λ^3-iodane with nucleophiles.[18]

3.3 Some of λ^3- and λ^5-iodane applications in organic transformations

Hypervalent iodine compounds exhibit attractive features of low cost, mild and selective reagents in organic synthesis.[19,20] These reagents serve as environmentally benign alternatives to toxic heavy-metal based oxidants and expensive organometallic catalysts.[21,22] The application of iodine(V) reagents such as DMP, IBX and their derivatives is vast, encompassing areas such as oxidations, C-C, C-heteroatom, heteroatom-heteroatom bond formation, rearrangements and radical reactions.[8,23–25] Unlike DMP, IBX is much more stable and less expensive than DMP. It has been widely employed as a precursor of DMP as a versatile reagent capable for (a) dehydrogenating aldehydes and ketones to their corresponding α,β-unsaturated carbonyl compounds,[26] (b) oxidising oximes to the corresponding carbonyl compounds,[27] (c) oxidising alcohols to carbonyl compounds,[8] (d) oxidising phenols to *o*-quinones,[28,29] (e) oxidising primary amides to the corresponding nitriles,[30] (f) deprotecting of thioketals to aldehydes,[31] (g) affecting the oxidation of benzylic sites[32] and (h) oxidising

sulfides to their sulfoxides counterparts.[33] The versatility of IBX reagent in organic transformations is illustrated in Figure 52.

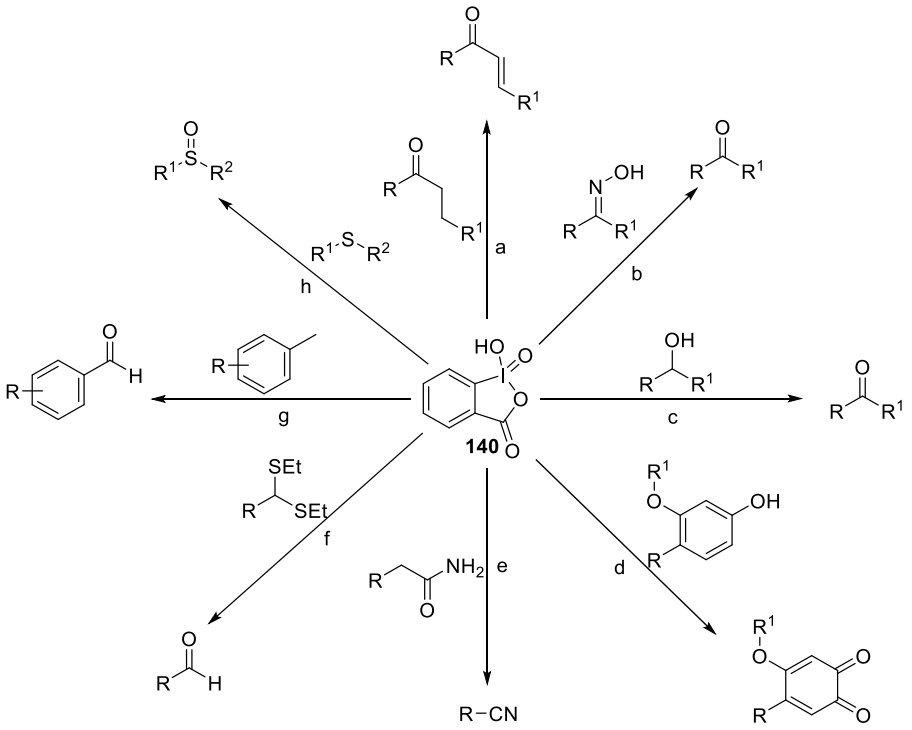

Figure **52**: Transformations of IBX reagent (**140**).

The first hypervalent iodine(III) compounds used as electrophilic trifluoromethylation reagents were developed in 2006 by Togni.[34] Two compounds, 1-(trifluoromethyl)1-2-benziodoxol-3(1*H*)-one (**148**) and trifluoromethyl-1,3-dihydro-3,3-dimethyl-1,2-benziodoxole (**149**) (Figure 53) have been widely employed as trifluoromethylation reagents for a variety of substrates.[35]

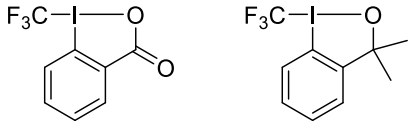

Figure **53**: Electrophilic trifluoromethylation iodine(III) reagents developed by Togni.[34]

Liu and co-workers recently utilised Togni's reagent in a one-pot, two-step process for the synthesis of trifluoromethylated isoxazoles. The reaction proceeds *via* copper catalysed trifluoromethylation of the Meyer-Schuster rearrangement. Addition of hydroxylamine to the reaction mixture led to the corresponding -CF_3 substituted compounds in acceptable yields (Scheme 50).[36]

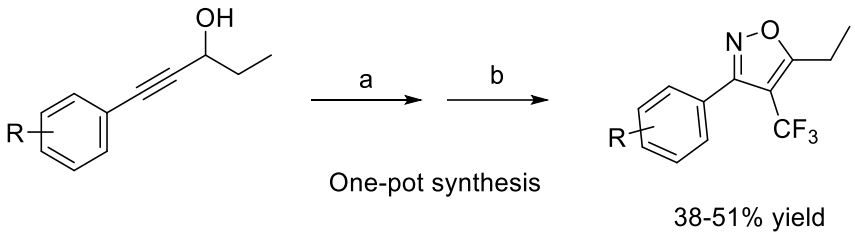

Scheme **50**: One-pot synthesis of trifluoromethylated isoxazoles from propargylic alcohols.[36] Reagents and condtions: a) (**148**) (1.8 eq), CuI (20 mol%), DCE, 80 °C; b) $NH_2OH{\cdot}HCl$, py, *t*-AmOH, 90 °C.

Diaryliodonium salts are one of the most important λ^3 hypervalent compounds. They have been widely employed as a precursors in fluorination reactions especially in the field of positron emission tomography.[37] The synthesis and application of these diaryliodonium salts for fluorination reactions is discussed in the following section.

3.4 Diaryliodonium salts

3.4.1 Structural features and reactivity

The general structure of λ^3-iodane diaryliodonium salts is shown in Figure 54. It is referred to as a symmetrical salt if $R^1 = R^2$ and unsymmetrical salt if $R^1 \neq R^2$ and can be classified as 8-I-2 cationic species according to the Martin-Arduengo *N-X-L* rule, with two aryl moieties associated with an anion X^-.[13,14]

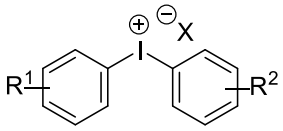

Figure **54**: General structure of diaryliodonium salts.

Since it has only 8 electrons in its valence shell, diaryliodonium salts are not formally hypervalent compounds. However, X-ray structural data demonstrate that they have similar features to a typical hypervalent iodine species exhibiting a pseudotrigonal bipyramid (T-shape) with a strong secondary interaction between the counterion and the iodine centre. Moreover, the L-I-L bond angle is about 90°, which is consistent with a hypervalent iodine species and they can be considered as 10-electron hypervalent compounds.[16]

3.4.2 Synthesis of diaryliodonium salts

Diaryliodonium salts can be prepared by several different approaches. The majority are carried out under acidic conditions and are summarised in Scheme 51. The most widely employed strategy requires two or three steps, with initial oxidation of the aryl iodide to an iodine(III) compound followed by ligand

exchange reaction with an arene or organometallic reagent to afford a diaryiodonium salt (strategy a). In many cases, anion exchange is required in order to obtain a suitable anion for further reaction.[5,38]

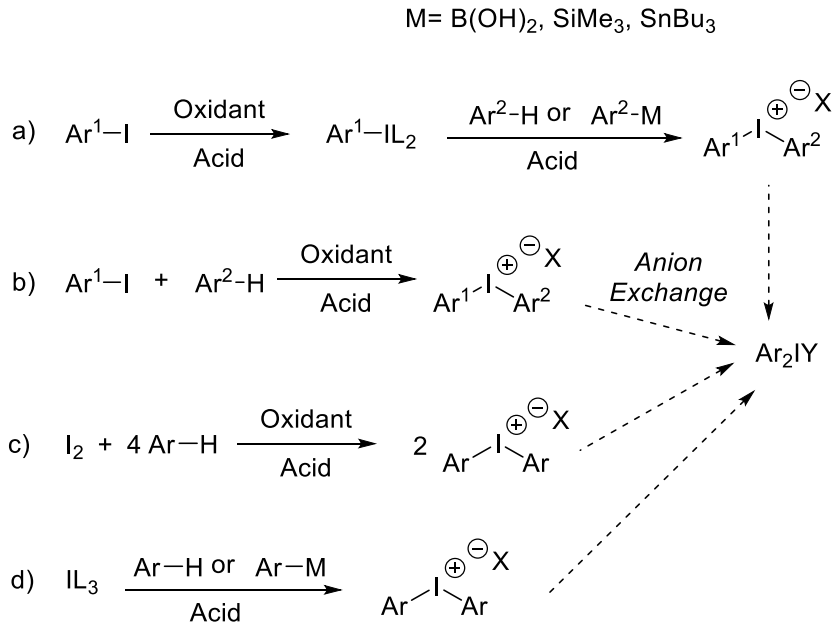

Scheme **51**: General strategies for synthesis of diaryiodonium salts.

Examples of how diphenyliodonium triflate (**151**) is prepared from iodobenzene (**136**) and benzene (**150**) *via* some of these strategies are illustrated in Scheme 52. (Diacetoxyiodo) benzene (**138**) was obtained in excellent yield and a short reaction time after oxidizing iodobenzene (**136**) with peracetic acid in acetic acid (route a).[39] Treatment of (**138**) in aqueous NaOH furnishes iodosylbenzene (**139**) (route b).[40] Kitamura and co-workers have successfully developed a route whereby this compound is converted to diphenyliodonium triflate (**151**), after treatment of (**139**) with TfOH, followed by the addition of benzene (route c and d).[41] Bielawski and co-workers reported that this route can be shortened by employing a one-pot oxidation and ligand exchange. They found that

iodobenzene (**136**) could be treated directly with *m*CPBA and TfOH before the addition of benzene (**150**) to obtain diphenyliodonium triflate (**151**) in excellent yield (route h). They also showed that the reaction of benzene (**150**) and iodine with the same oxidant (*m*CPBA) and acid (TfOH) could deliver diphenyliodonium triflate (**151**) in 93% yield (route g).[42] The same approach was also reported by Kitamura's group by employing $K_2S_2O_8$ as an oxidant. Diphenyliodonium triflate (**151**) was obtained in 78% yield after anion exchange with NaOTf (route e).[43] Alternatively, diphenyliodonium triflate (**151**) could also be obtained by treating benzene (**150**) in the presence of molecular iodine with $K_2S_2O_8$ (route f).[44]

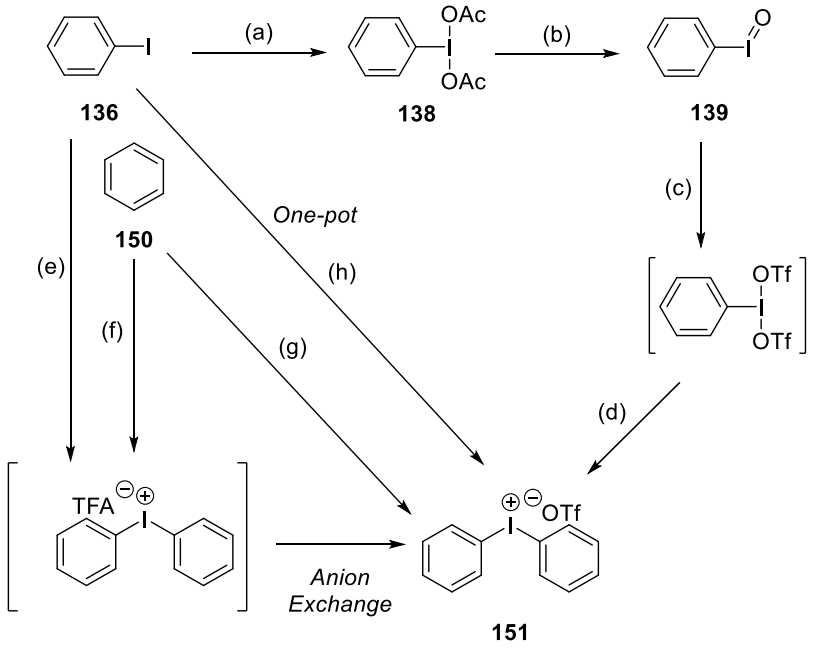

Scheme **52**: Example of how diphenyliodonium triflate (**151**) can be synthesised by employing the general strategies outlined in Scheme **51**. Reagents and conditions: a) AcOOH, AcOH, 25-30 °C, 4 h, 92%; b) NaOH(aq), rt, 1 h, 85-93%; c) TfOH, DCM, rt, 2 h; d) (**150**), rt, 17 h, 65%; e) $K_2S_2O_8$, TFA, (**150**), 36-38 °C, 20 h; f) I_2, $K_2S_2O_8$, TFA, 40 °C, 72 h; g) I_2, *m*CPBA, TfOH, 80 °C, 10 min, 93%; h) *m*CPBA, TfOH, (**150**), DCM, rt, 10 min, 92%.

The pre-formed iodine(III) compounds can also be employed as a starting materials and further reacted with silanes,[45,46] stannanes[46–48] or boron[49,50] reagents to yield diaryiodonium salts. The purpose of using these organometallic reagents is to provide a nucleophilic coupling partner for subsequent reaction with a diacetoxyiodoarene. Luke and co-workers recently demonstrated that by reacting the preoxidised diacetoxyiodo (**138**), with the corresponding stannanes and silanes reagents, iodonium trifalte (**152**) and trifluoroacetate (**153**) are obtained in acceptable yields (Scheme 53).[46]

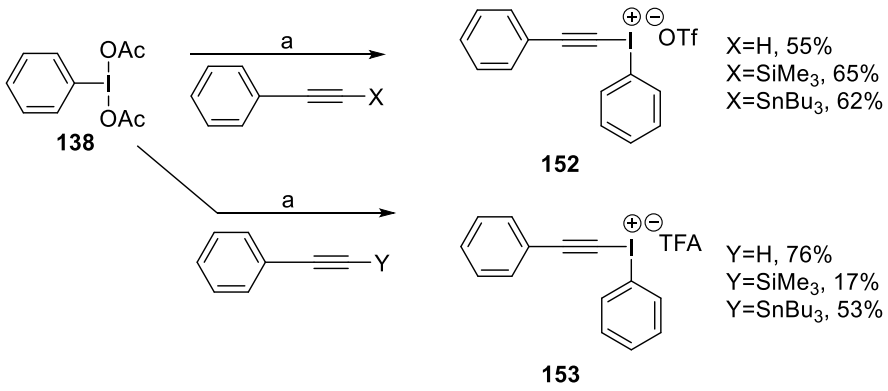

Scheme **53**: Route to iodonium triflate (**152**) and trifluoroacetate (**153**).[46] Reagents and conditions: a) TfOH, DCM -30 °C→rt.

3.4.3 Mechanism of nucleophilic substitution on iodonium salts

The selectivity of the nucleophilic substitutions of diaryliodonium salts tend to proceed according to the so-called "*ortho*-effect" (Scheme 54) with the most bulky and more sterically demanding aryl ligand and two electron lone pairs occupying equatorial positions for steric reasons. This effect results in the reductive elimination of PhI and preferential transfer of the nucleophile to the *ortho* substituted aryl group, situated in the equatorial position, even though if it is a more electron rich ring.[37,51,52]

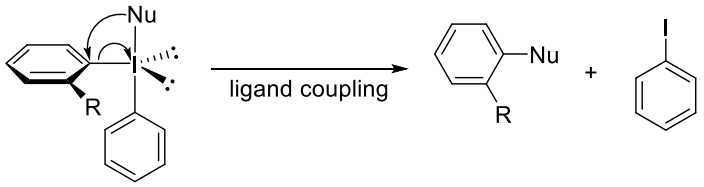

Scheme **54**: *Ortho*-effect of diaryliodonium salts.

If there is no *ortho* substituent present on either aryl ring, the ring with the lowest electron density will preferentially transfer to the nucleophile with varying selectivities. The initial ligand exchange gives rise to hypervalent iodine(III) intermediates (**154**) and (**155**) with the nucleophile occupying the axial position (Scheme 55). The fast pseudorotation of these intermediates lead to two different transition states (**156**) and (**157**).[37,53] Transition state (**157**) is more favourable than (**156**) due to stabilisation of the partial negative charge developed on the aromatic ring by the more electron-deficient aryl group. Moreover, the electron rich aryl group can also stabilise the enhanced positive charge on iodine(III) more effectively than an aryl substituent bearing an electron deficient group.[37,54,55]

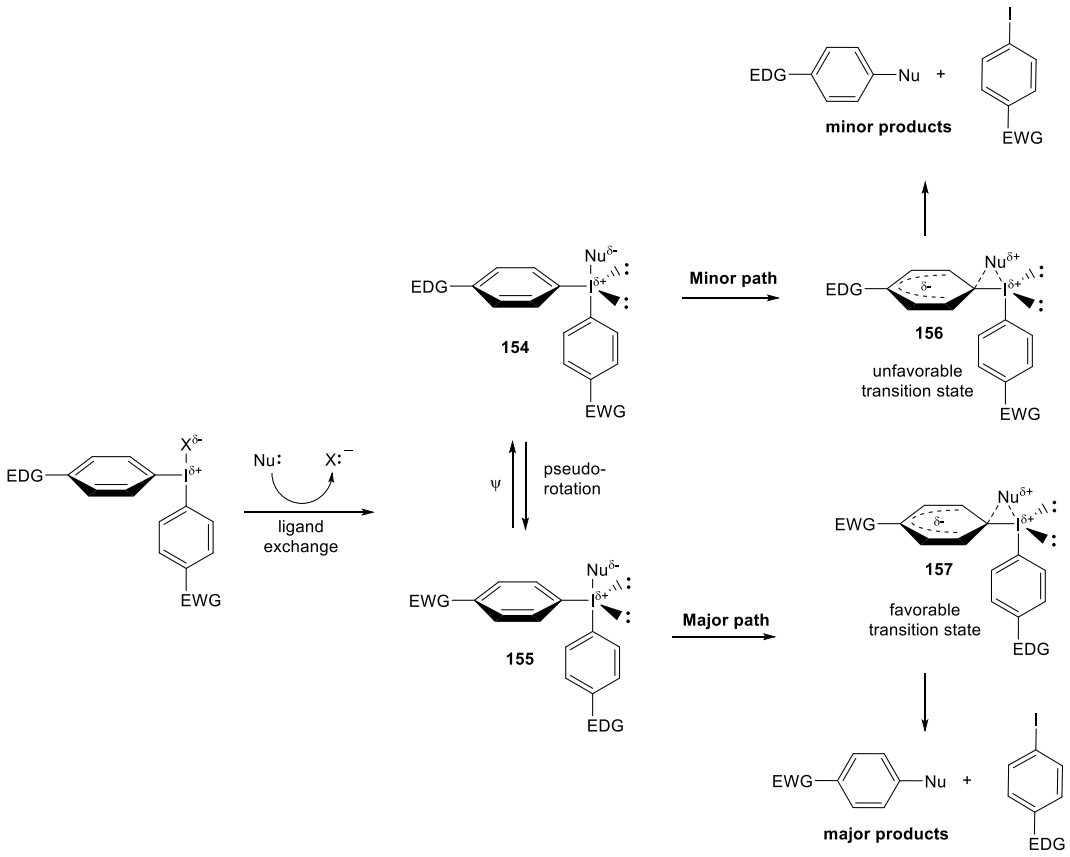

Scheme **55**: General mechanistic for the reactions of diarylidodonium salts with nucleophiles.

3.4.4 Application of iodonium salts as precursors for nucleophilic fluorination in PET

The first [^{18}F]radiofluorination using diaryliodonium salts as precursors was reported in 1995,[56] and since then they have become a valuable approach for the late stage introduction of fluorine into a diversity of aromatic compounds.[57] Furthermore, by using diaryliodonium salts, both electron-deficient and electron-rich rings can be fluorinated, allowing access to all regioisomers of a particular arene over standard S_NAr chemistry.[58] Moreover, these types of reactions typically require milder condition than standard S_NAr, and they can even take place in wet solvents.[59]

One of the limitations of nucleophilic aromatic substitution in the field of PET is that it is poor for labelling electron-rich arenes, and poor at accessing all regioisomers due to mechanistic considerations. This limitation can be circumvented using diarylidodonium salts as a precursor.[60] For example, the synthesis of *N*-(2,5-dimethoxybenzyl)-*N*-(5-[^{18}F]fluoro-2-phenoxyphenyl)acetamide ([^{18}F]DAA1106 (**159**), an imaging agent benzodiazepine receptors in the brain was achieved by nucleophilic radiofluorination of diphenyliodonium tosylate salt (**158**) as a precursor. [^{18}F]DAA1106 was produced in high chemical yield (65%) (Scheme 56).[61]

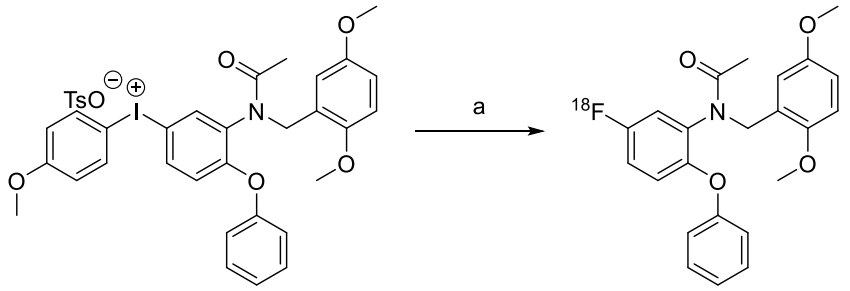

Scheme **56**: Synthesis of PET imaging [^{18}F]DAA1106, (**159**).[61] Reagents and conditions: a) $^{18}F^-$, nBu$_4$NHCO$_3$, DMSO, 80 °C, 20 min.

Recently, Manera and co-workers have reported the synthesis and evaluation of a potent and selective candidate marker of the CB2 cannabinoid receptor. [^{18}F]CB91 (**161**) is used to monitor the therapeutic efficacy of anti-inflammatory drugs in neurological diseases. The radioligand was obtained by nucleophilic fluorination of diaryliodonium salt (**160**) in good radiochemical yield (42%) (Scheme 57).[62]

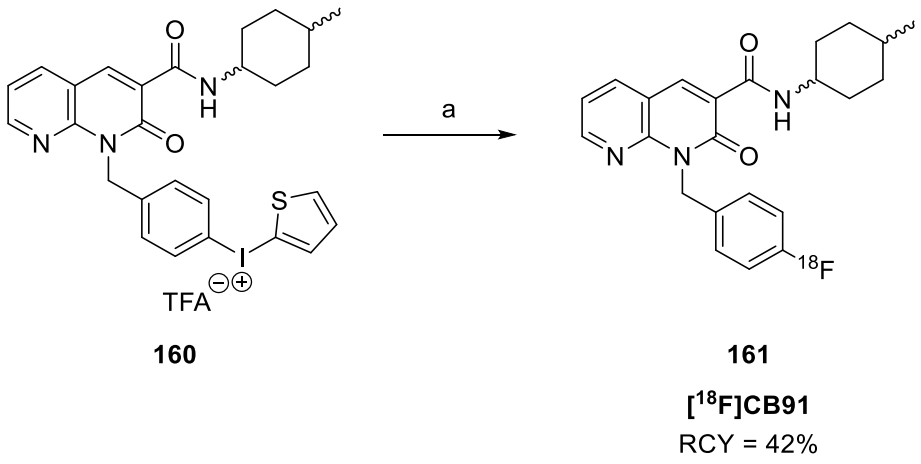

Scheme **57**: Radiosynthesis of [^{18}F]CB91 (**161**) from a diaryliodonium salt precursor (**160**).[62] Reagents and conditions: a) K^{18}F, kryptofix K$_{222}$, DMSO, 190 °C, 25 sec, microfluidics.

Despite extensive research dedicated to developing novel radiotracers, there have been few studies reported in the literature pertaining to the synthesise of imaging agents bearing *meta* substituents due to the difficulties associated with accessing these regioisomers by standard nucleophilic means. In this regard, diaryliodonium offer an opportunity and has been employed by Warnier and co-workers for the preparation of a fully automated cGMP compliant radiosynthesis of [^{18}F]UCB-H (**162**), a PET tracer for imaging synaptic vesicle glycoprotein 2A (SV2A). SV2A plays a pivotal role in neurotransmission processes and its role in epilepsy has rendered it an important PET target for neurological disorders related to epilepsy and Alzheimer's disease (Scheme 58).[37,63]

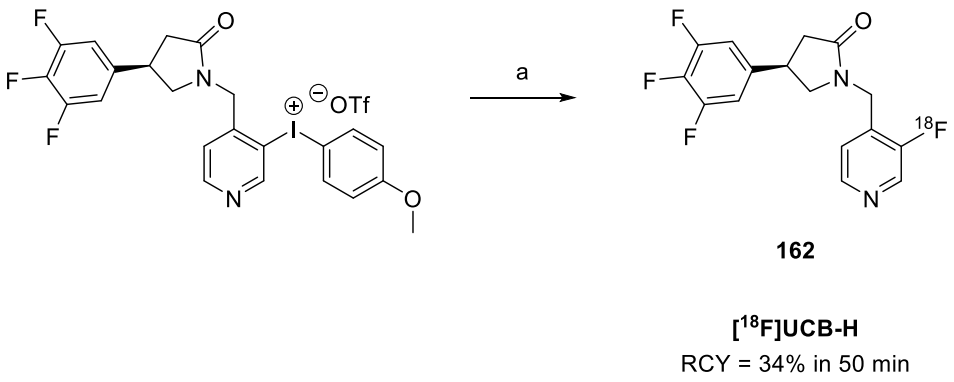

Scheme **58**: Automated cGMP compliant radiosynthesis of [^{18}F]UCB-H (**162**).[63] Reagent and condition: a) $^{18}F^-$, automated cGMP.

Practical radiofluorination using this approach has been demonstrated in the synthesis of *meta*-[^{18}F]fluorobenzylguanidine, ([^{18}F]MFBG) (**164**), which was achieved *via* a two-step automated method by thermolysis of diaryliodonium salt (**163**) and subsequent acid mediated deprotection. [^{18}F]MFBG was obtained in 31% radiochemical yield and is currently ongoing clinical imaging trials for neuroendocrine tumors (Scheme 59).[64]

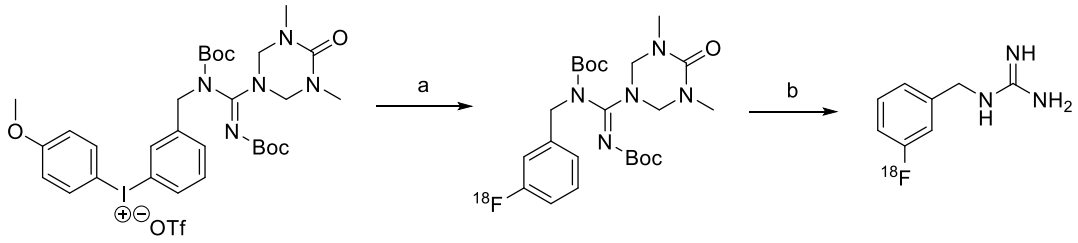

163 **164**

[^{18}F]MFBG

RCY = 31%

Scheme **59**: Two-step automated synthesis of [^{18}F]MFBG (**164**).[64] Reagents and conditions: a) K^{18}F, kryptofix K_{222}, toluene/MeCN, 120 °C; b) 6 M HCl, 120 °C.

3.5 Aims of this project

This aspect of the study can be divided into two objectives. The first involved the synthesis and late stage fluorination of diaryliodonium salts, as precursors to fluoromuscimol (**64**). The second objective focused on the synthesis of an iodinated analogue of muscimol (**11**) and to assess the agonist activity of this compound against $GABA_A$ receptors. Good agonist activity of iodomuscimol (**165**) would offer an alternative SPECT radiotracer to extend the tools for GABA receptor imaging.

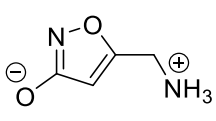

11

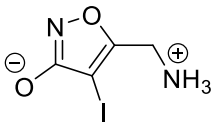

165

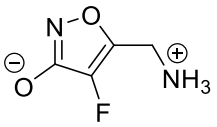

64

3.6 Results and Discussion

3.6.1 Synthesis of iodinated precursor (166)

The synthesis of (**166**) is illustrated in Scheme 60. Ester (**94**) was synthesised from the isoxazole (**77**). Protection of (**77**) as a methyl ether afforded methyl ester (**94**) which was then iodinated in good yield (80%) using NIS in TFA. Crystals suitable for X-ray studies of this product were obtained and the structure is shown in Figure 55.

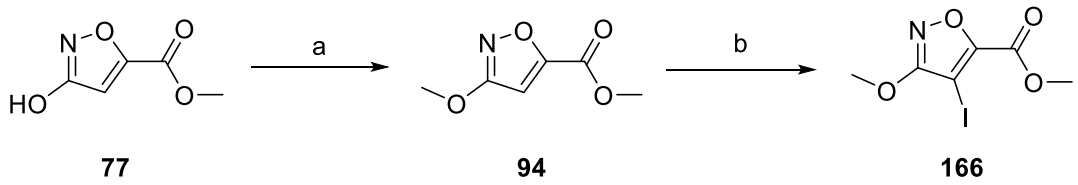

Scheme **60**: Synthesis of (**166**). Reagents and conditions: a) MeI, K_2CO_3, DMF, 14 h, 66%; b) NIS, TFA, MW, 50 W, 150 °C, 3h, 80%.

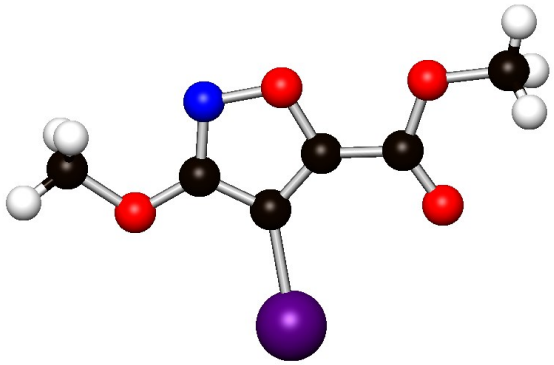

Figure **55**: Crystal structure of 4-iodo ester (**166**).

3.6.2 Synthesis of diacetoxyiodoarene (167)

There are many oxidising agents that have been widely employed in the transformation of iodoarenes to diacetoxyiodoarenes. These include sodium perborate tetrahydrate,[65,66] sodium periodate,[67] hydrogen peroxide-urea,[66,68] Selectfluor™,[66,69] and *m*-chloroperoxybenzoic acid.[66,70] The most general methodology for diacetoxyiodoarene preparation uses sodium perborate tetrahydrate as an oxidant in acetic at 45 °C.[65] The first attempt to synthesise diacetoxyarene (**167**) was carried out using this approach (Scheme 61). However, no consumption of aryliodide (**166**) was observed when following the reaction by ^{1}H NMR or TLC. Increasing the temperature of the reaction to 60 °C and with a reaction time of 24 h did not facilitate the reaction. Additional methods were explored, including changing the oxidant from sodium perborate tetrahydrate to hydrogen peroxide-urea and sodium periodate. However, these were also unsuccessful.

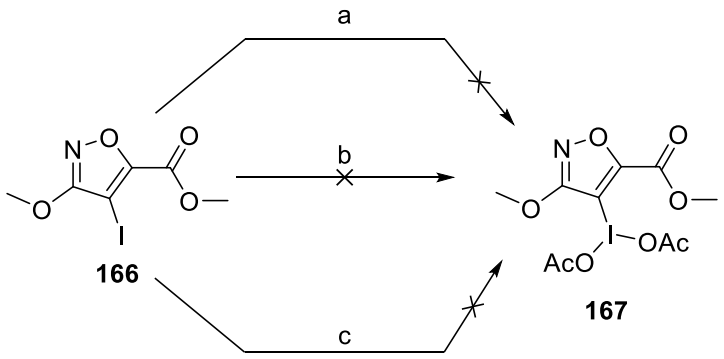

Scheme **61**: Attempted synthesis of diacetoxyiodo (**167**). Reagents and conditions: a) $NaBO_3{\cdot}4H_2O$, AcOH, 45 °C; b) $CO(NH_2)_2{\cdot}H_2O_2$, AcOH, Ac_2O, Na_2SO_4, 40 °C; c) $NaIO_4$, NaOAc, AcOH, Ac_2O, reflux.

A further method was considered using *m*CPBA in acetic acid as the oxidant (Scheme 62). This was successful, however, ^{1}H-NMR of the crude product mixture showed that it consisted of a 1.5:1 mix of starting material (**166**) and diacetoxyiodo compound (**167**) (Figure 56). Purification of diacetoxyiodo compound (**167**) by column chromatography or recrystallisation failed to separate the diacetoxyiodoarene as the product decomposed back to the starting material. Additionally, prolonged reaction times up to 96 h did not facilitate a complete conversion to the desired product (**167**).

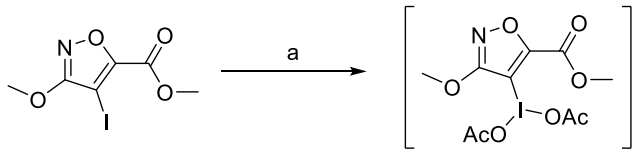

Scheme **62**: Synthesis of diacetoxyiodo compound (**167**). Reagents and conditions: a) *m*CPBA, AcOH, 55 °C, 96 h.

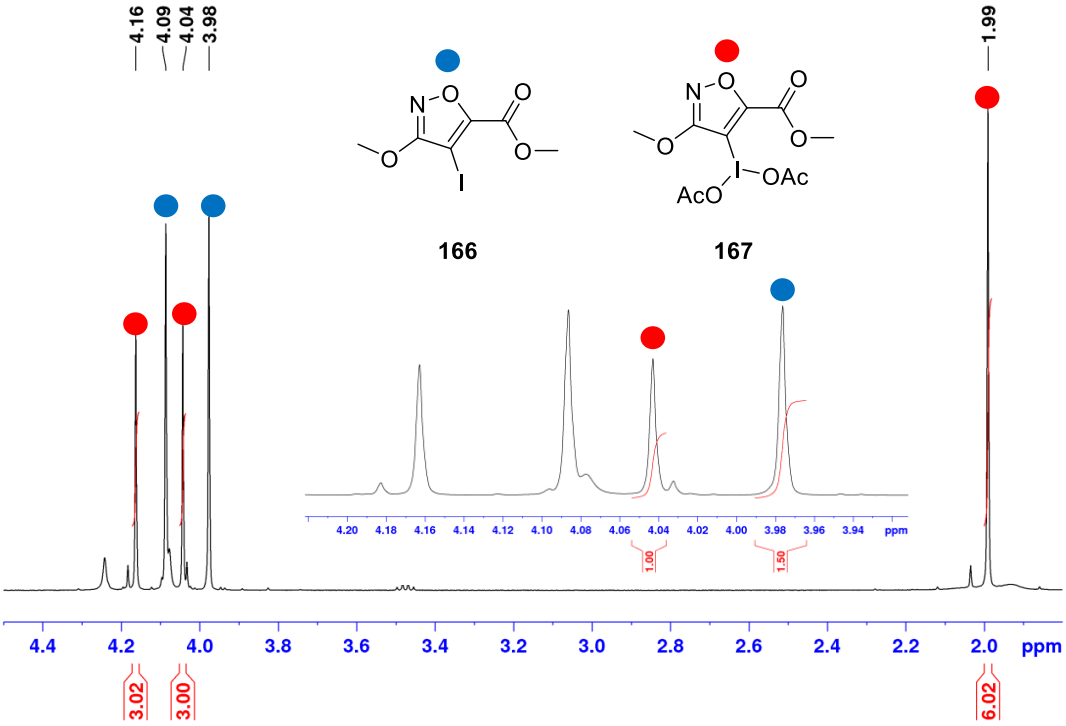

Figure **56**: Crude product NMR of diacetoxyiodo compound (**167**).

The mechanism for the synthesis of diacetoxyiodo (**167**) has not been fully established but a rationale is shown in Scheme 63. The iodoarene attacks the protonated *m*CPBA, forming a reactive iodine(III) species (**168**). Further activation of the OH of (**168**) in the acidic medium leads to the formation of oxonium intermediate (**169**), which enables a subsequent nucleophilic substitution with acetate to give diacetoxyiodo (**167**).

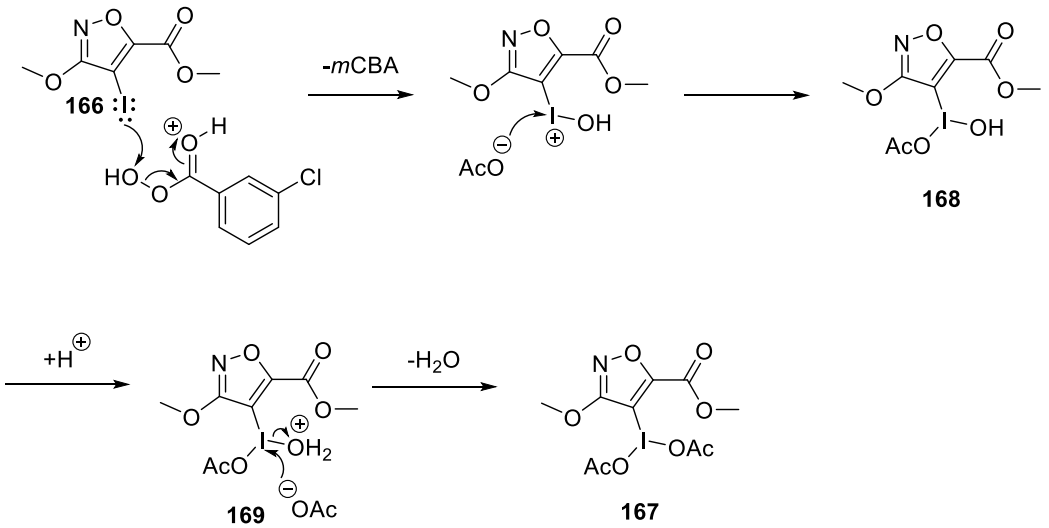

Scheme **63**: Proposed mechanism for diacetoxyiodo (**167**) formation.

3.6.3 Synthesis of diaryliodonium trifluoroacetate salt (171) from diacetoxyiodoarene (167)

The difficulty in purifying diacetoxyiodo (**167**), coupled with its apparent instability forced a direct synthesis approach to diaryliodonium salt (**171**). This synthesis was carried out by dissolving diacetoxyiodo (**167**) in dry DCM at -30 °C, followed by drop wise addition of TFA (2.0 eq). The resulting solution was stirred with the exclusion of light for another 30 min, followed by 1 h at room temperature. The solution was then re-cooled to -30 °C, when

tributyl(4-methoxyphenyl)stannane (**170**) (1.0 eq) was added. The solution was warmed to room temperature for a second time and left to stir overnight. The reaction solvent was then removed, followed by the addition of Et_2O to crystallise iodonium salt (**171**) (Scheme 64).

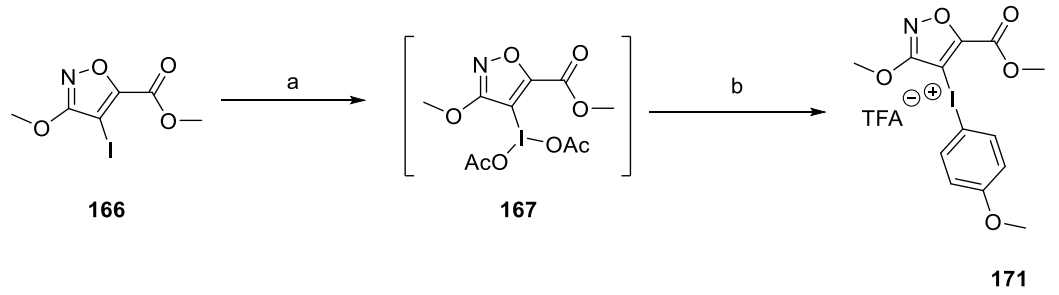

Scheme **64**: Direct synthesis of diaryliodonium salt (**171**). Reagents and conditions: a) *m*CPBA, AcOH, 55 °C, 96 h; b) TFA, (**170**), DCM, -30 °C→rt, overnight, 10%.

The nucleophilic coupling of arylstannene (**170**) with diacetoxyiodo (**167**) can be explained on the basis of the polarisation of the C-Sn bond. This polarisation enhances the reactivity of arylstannane towards the electrophilic iodine(III) centre. Subsequent TFA anion exchange, yielded diaryliodonium salt (**171**) (Scheme 65). The structure of the salt was confirmed by X-ray crystallography (Figure 57).

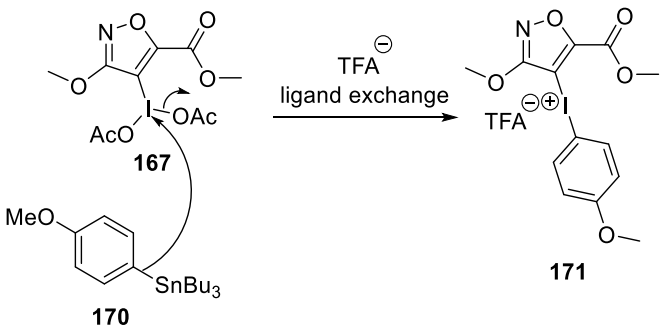

Scheme **65**: Nucleophilic coupling of arylstannane (**170**) with diacetoxyiodo (**167**).

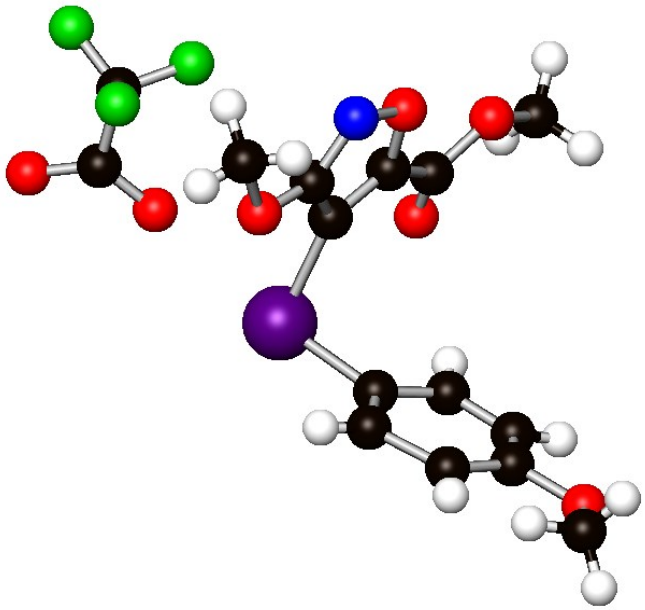

Figure **57**: X-ray structure of diaryliodonium salt (**171**).

3.6.4 Fluorination attempts on diaryliodonium trifluoroacetate salt (171)

As previously discussed, if there is no *ortho* substituent present on either ring, the most electron-deficient aryl moiety on the diaryliodonium salt will generally be fluorinated. In the context of diaryliodonium trifluoroacetate salt (**171**), the isoxazole moiety bearing the ester group, is clearly the most electron-deficient relative to the anisole counterpart. Therefore, it was anticipated that selective fluorination at C-4 of the isoxazole moiety should be observed.

Fluorination of diaryliodonium salt (**171**) (1.0 eq) was performed in DMF using caesium fluoride (2.0 eq) as a nucleophilic fluorination reagent (Scheme 66). Caesium fluoride was chosen on the basis of previous studies reported by Nairne *et al.*, on several fluorination reactions of trifluoroacetate diarylidodonium salt using various nucleophilic fluorination reagents. The yield of the fluorinated compounds obtained with respect to the reagents used

are as follow CsF>KF(18-crown-6)>KF(K_{222})>KF=TBAF.[71] However, despite exploring various sets of conditions (heating under microwave, addition of CuOTf as catalyst and addition of phase transfer reagent, kryptofix K_{222} to KF), none of the desired fluorinated isoxazole (**98**) could be isolated. ^{1}H NMR analysis of the crude mixture showed evidence of reductive degradation of the aryliodonium salt (**171**) to the corresponding isoxazoles (**94**), (**166**) and iodoanisole (**172**) in different ratios (Scheme 67).

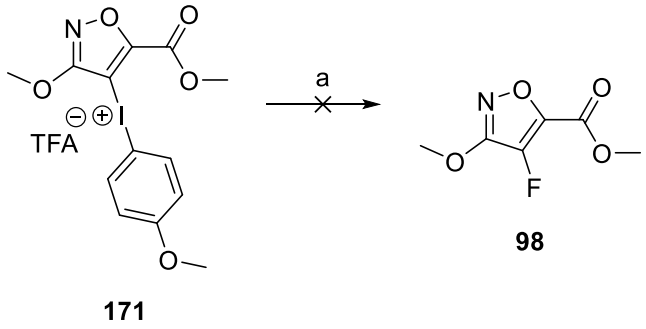

171 **98**

Scheme **66**: Fluorination attempts on diaryliodonium trifluoroacetate salt (**171**). Reagents and conditions: a) CsF, DMF, rt→130 °C.

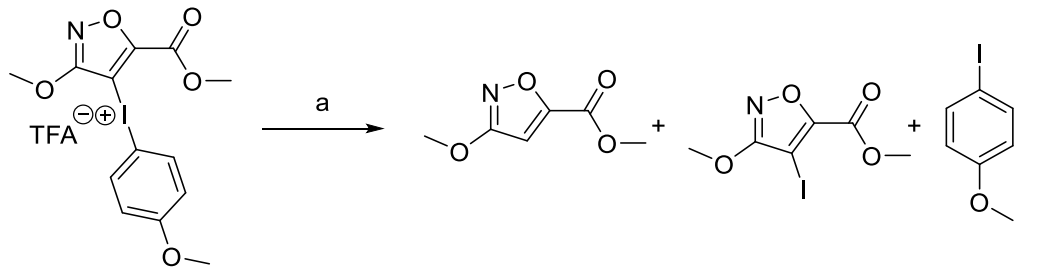

171 **94** (2) **166** (1) **172** (10)

Scheme **67**: Products from CsF treatment of (**171**). Reagents and conditions: a) CsF, DMF, rt→130 °C. The ratios are given in parentheses and were determined from ^{1}H NMR analysis of the crude mixture.

It has been reported that diaryliodonium salts can interact in an intra-molecular manner thus forming dimers, trimers and so on.[46] This is observed in the X-ray crystal structure of compound (**171**) (Figure 58). Furthermore, the presence of intra-molecular I···O interactions between the carbonyl of the ester attached to the isoxazole moiety and the iodine(III) centre could make the adduct more stable and thus less amenable to fluorination.

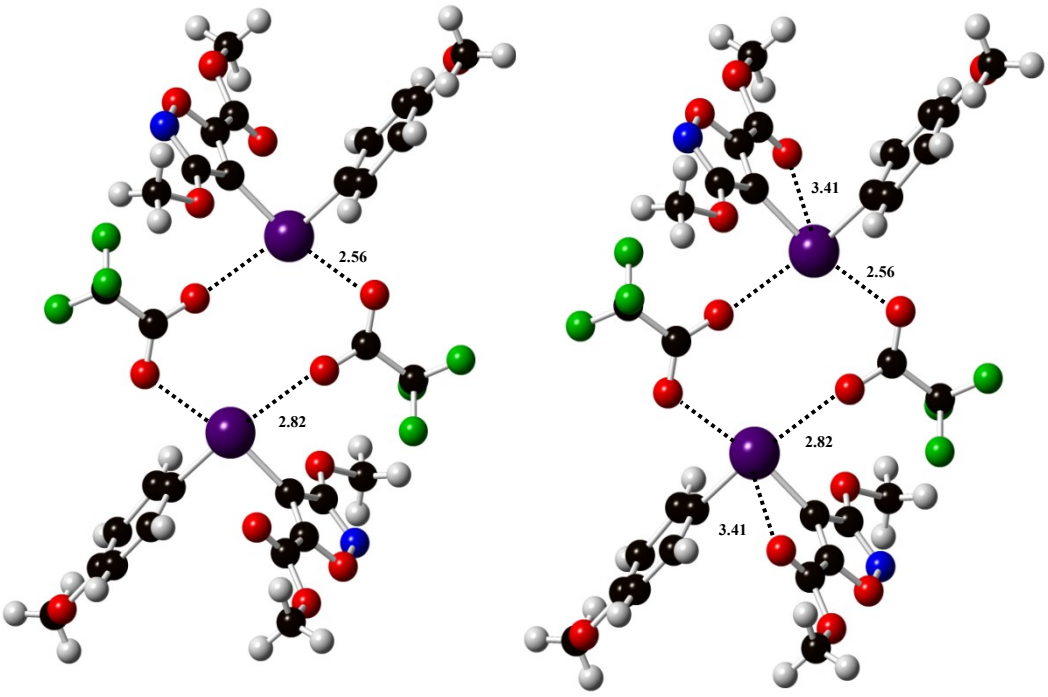

Figure **58**: X-ray crystal structure of (**171**) showing the formation of dimer (left) and the intra-molecular I···O interaction (right).

3.6.5 Synthesis of 4-iodo ether (173)

To address the limitation of carbonyl complexation, it was decided to prepare the iodonium salt from methyl ether (**96**). Scheme 68 shows the synthesis of iodoisoxazole (**173**), which was prepared starting from isoxazole (**77**). Iodination of methyl ether (**96**) was carried out again with NIS in TFA. The desired product (**173**) was isolated in good yield (88%) and its structure was confirmed by X-ray crystallography (Figure 59).

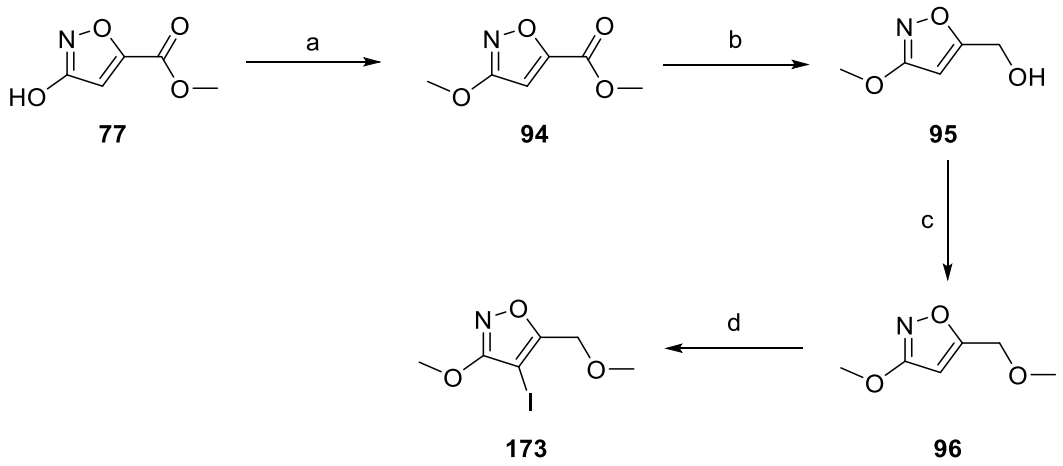

Scheme **68**: Synthesis of iodoisoxazole (**173**). Reagents and conditions: a) MeI, K_2CO_3, DMF, 14 h, 66%; b) $NaBH_4$, MeOH rt, overnight, 85%; c) NaH (60% dispersion oil), MeI, THF, 0 °C→rt, 1 h, 57%; d) NIS, TFA, rt, overnight, 88%.

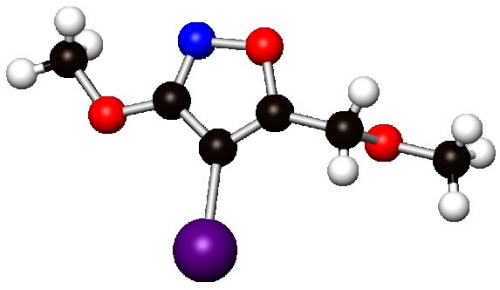

Figure **59**: Crystal structure of 4-iodo ether (**173**).

3.6.6 Attempted synthesis of diacetoxyiodoarene (174)

Attempts to oxidise (**173**) to the diacetoxyiodo (**174**) according to the standard condition outlined in Scheme 62 proved unsuccessful. Despite exploring various sets of reaction conditions as shown in Table 12, none of the desired product (**174**) could be isolated. Mass spectroscopy analysis of the crude mixture revealed the presence of iodoxy compound (**175**) along with unreacted starting material (**173**) (Scheme 69).

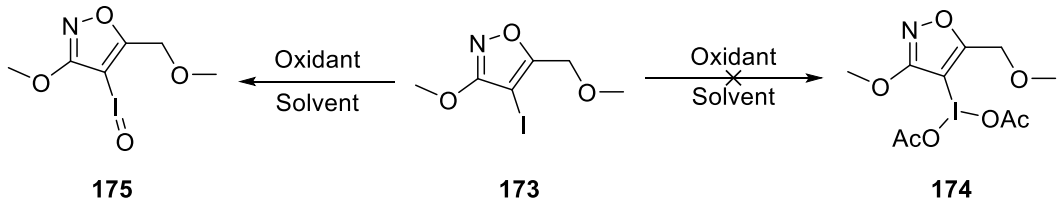

175 **173** **174**

Scheme **69**: Attempted synthesis of diacetoxyiodo compound (**174**).

Oxidant	Solvent	Additive	Temperature	Outcome
*m*CPBA	AcOH	-	55 °C	(**173**) + (**175**)
SPB	AcOH	-	55 °C	No reaction. Only (**173**) recovered
Oxone	TFA/$CHCl_3$	-	rt	No reaction. Only (**173**) recovered
*m*CPBA	AcOH	TFA	55 °C	(**173**) + (**175**)
*m*CPBA	AcOH	TfOH	55 °C	(**173**) + (**175**)
*m*CPBA	$CHCl_3$		rt	(**173**) + (**175**)

Table **12**: Conditions for oxidation of (**173**).

3.6.7 One-pot synthesis of diaryliodonium tetrafluoroborate salts (176) and (177)

A one-pot synthesis of the tetrafluoroborate iodonium salt was investigated. Such a protocol has been shown to be efficient in generating such salts without anion-exchange step.[72] Accordingly, a solution of *m*CPBA (1.3 eq) in DCM was treated with iodoisoxazole (**173**) (1.0 eq) and boronic acid precursors (1.1 eq) in the presence of boron trifluoride (2.5 eq) at room temperature. Diaryliodonium tetrafluoroborate salts (**176**) and (**177**) were obtained in acceptable yields upon precipitation with diethyl ether (Scheme 70).

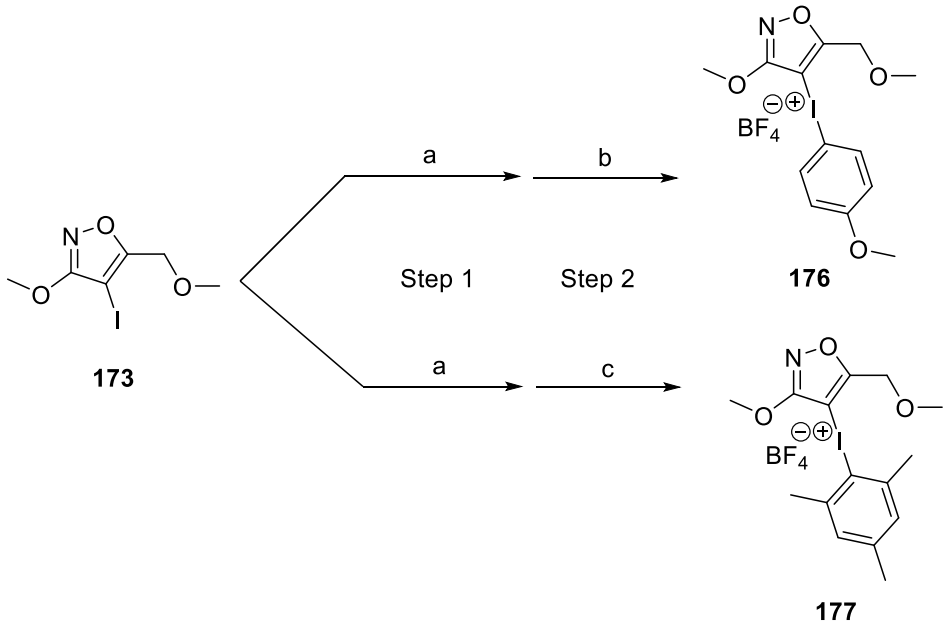

Scheme **70**: One-pot synthesis of iodonium tetrafluoroborate salts (**176**) and (**177**). Reagents and conditions: a) *m*CPBA, $BF_3{\cdot}OEt_2$, rt, 2 h; b) 4-OMePh-$B(OH)_2$, rt, 2 h, 50%; c) 2,4,6-TriMePh-$B(OH)_2$, rt, 2 h, 45%.

Despite a wide level of interest over many years in the one-pot synthesis of diaryliodonium salts, the exact mechanism remains unclear. A possible mechanism, shown in Scheme 71, starts with nucleophilic attack of iodoisoxazole

(**173**) on *m*CPBA to generate iodo oxide (**175**). Further activation of (**175**) by Lewis acid BF_3 followed by loss of fluoride of (**178**), leads to intermediate (**179**). The free fluoride can then attack BF_3 to generate BF_4^-. Intermediate (**179**) then undergoes nucleophilic addition at the electrophilic iodine centre to give (**180**) which then collapses to afford the desired iodonium tetrafluoroborate salts.

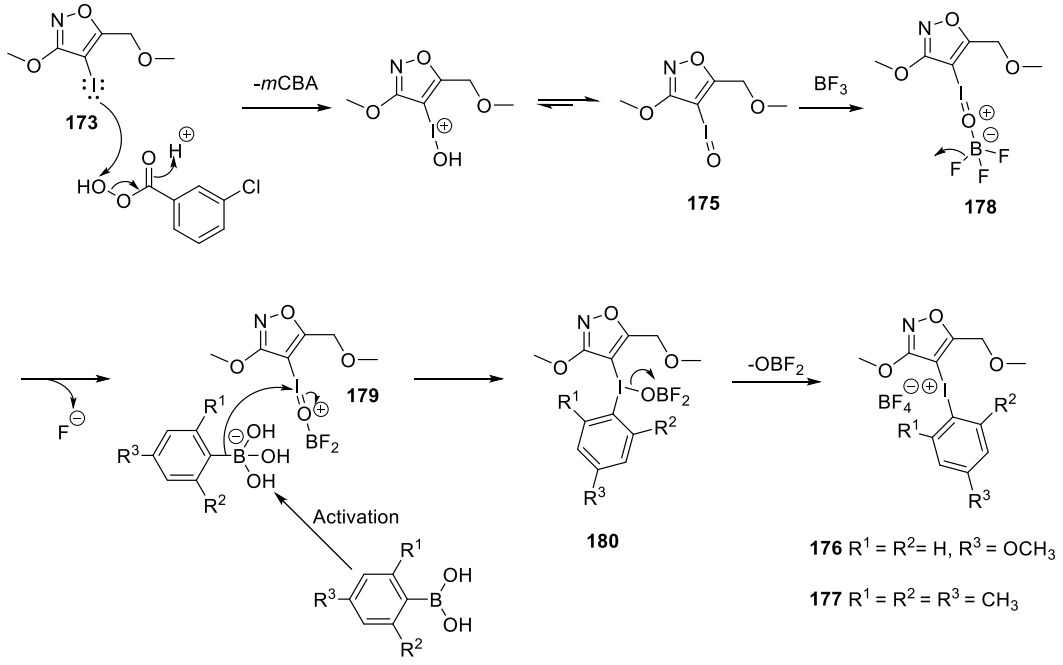

Scheme **71**: Putative mechanism for one-pot synthesis of diaryliodonium tetrafluoroborate salts (**176**) and (**177**).

Complete assignments of ^{1}H NMR, ^{13}C NMR and ^{19}F NMR spectra of diaryliodonium salts (**176**) and (**177**) are shown in Figures 60-63.

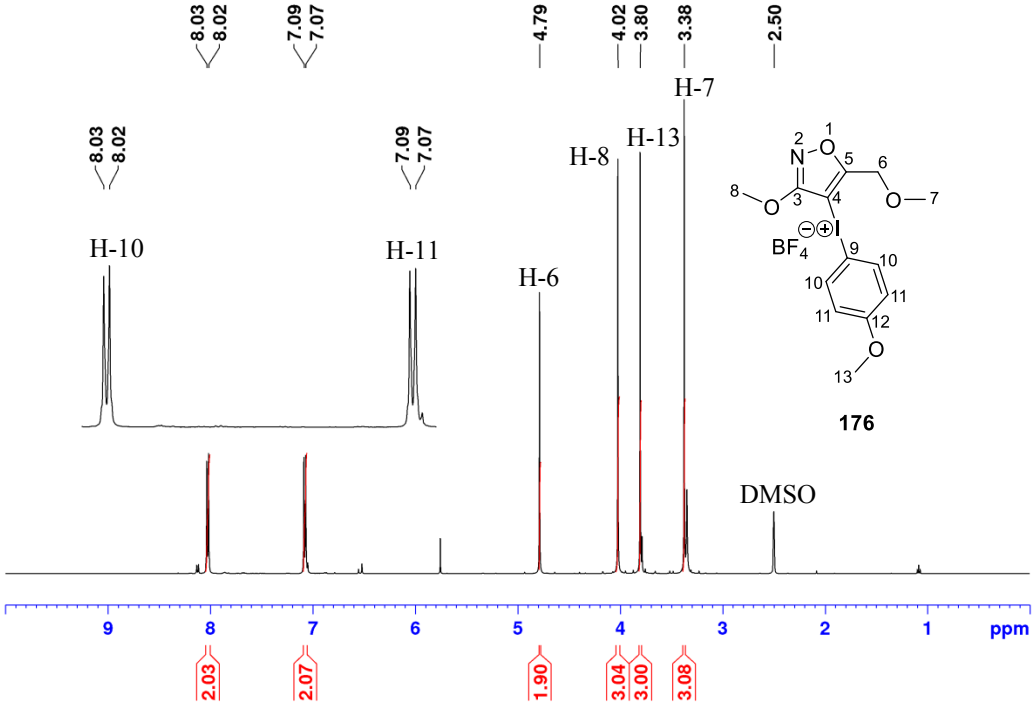

Figure **60**: ^{1}H NMR of iodonium salt (**176**).

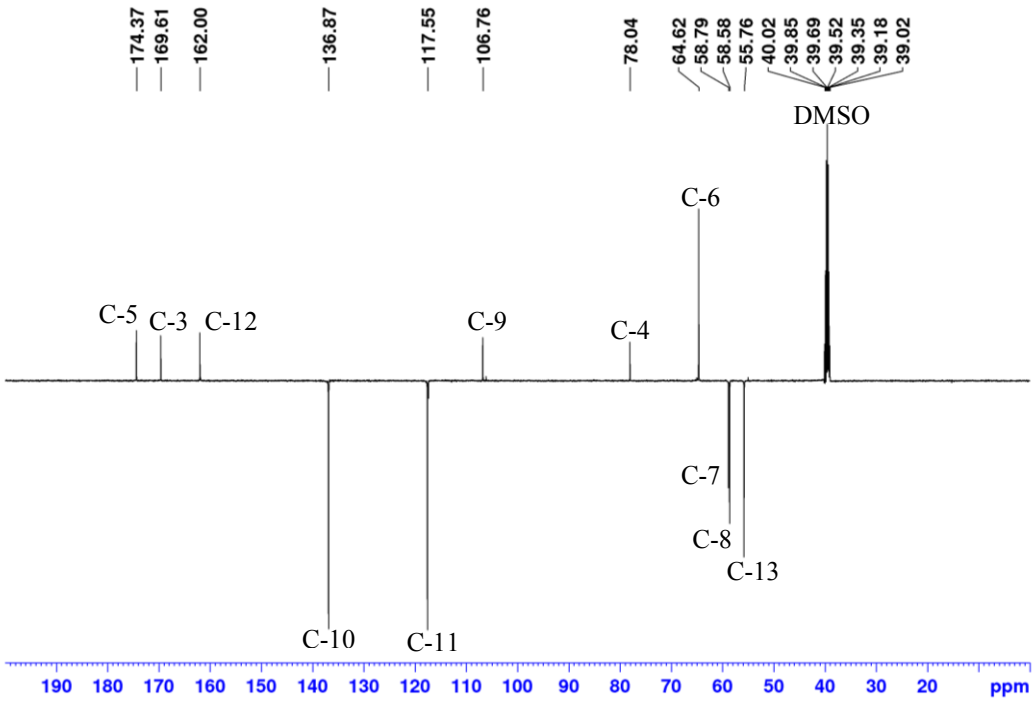

Figure **61**: ^{13}C NMR of iodonium salt (**176**).

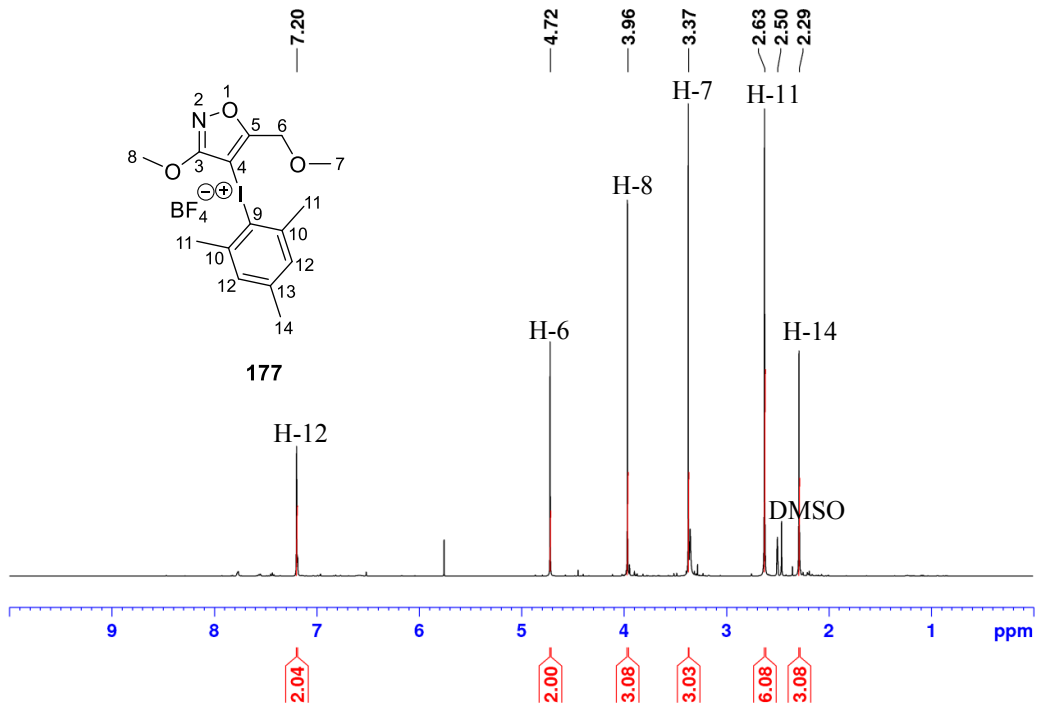

Figure **62**: ^{1}H NMR of iodonium salt (**177**).

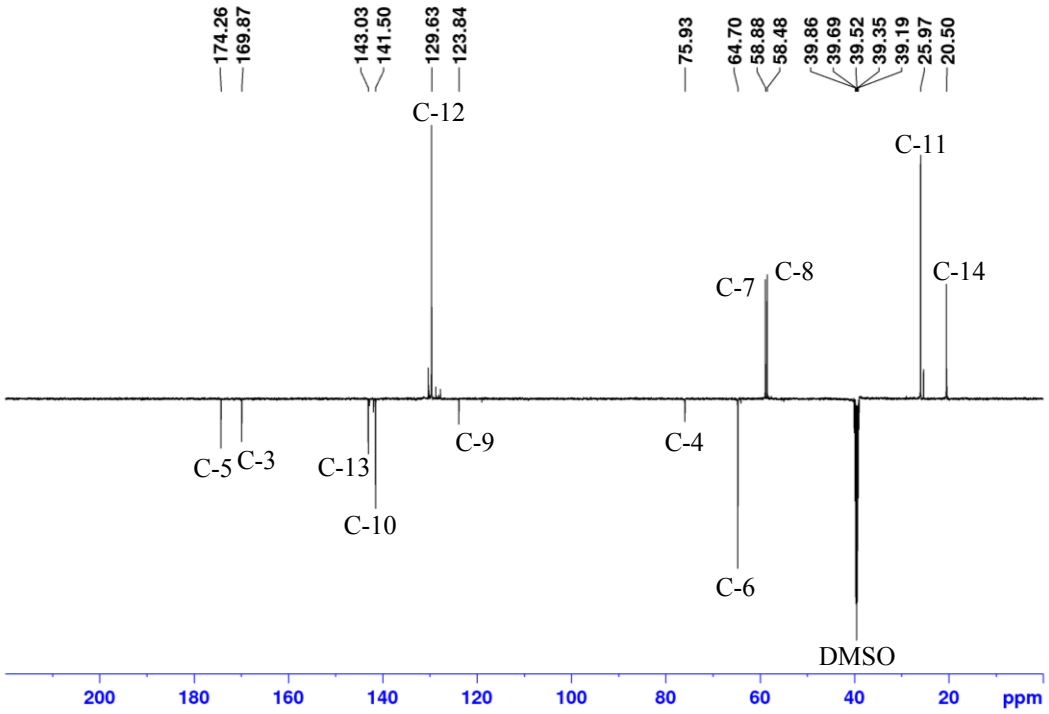

Figure **63**: ^{13}C NMR of iodonium salt (**177**).

^{19}F NMR spectra of (**176**) and (**177**) are shown to exhibit two fluorine signals with different intensities at (-148.17 and -148.23 ppm) for (**176**) and (–148.16 and -148.21 ppm) for (**177**). These signals correspond to the fluorines in the BF_4^- group. The different intensities of the resonances are due to different natural abundance of the two isotopes of boron (^{11}B and ^{10}B).[72–74] A representative ^{19}F NMR spectrum of (**176**) is shown in Figure 64.

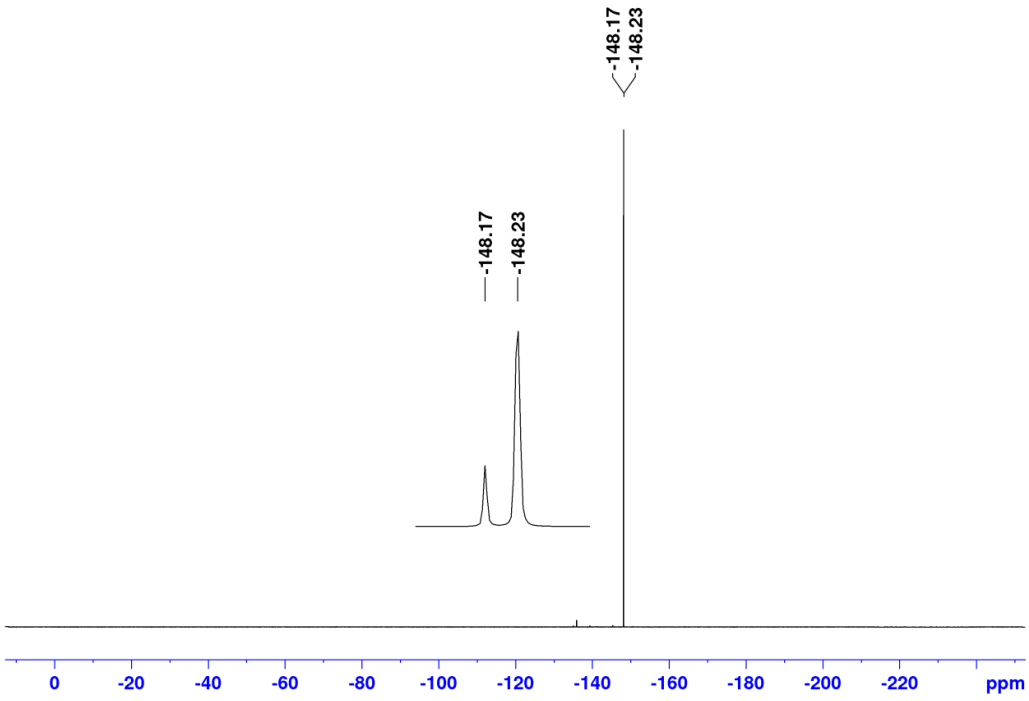

Figure **64**: ^{19}F NMR of iodonium salt (**176**).

3.6.8 Fluorination attempts on diaryliodonium salts (176) and (177)

Fluorinations of the diaryliodonium salts (**176**) and (**177**) were attempted according to the standard conditions outlined in Scheme 66. Unfortunately, despite exploring various sets of conditions (heating under microwave, addition of CuOTf as catalyst and addition of the phase transfer reagent, kryptofix K_{222} to KF), none of the attempted procedures furnished the desired fluorinated isoxazole (**99**) (Scheme 72). Again, ^{1}H NMR analyses of the crude mixtures showed evidence of reductive degradation of the aryliodonium tetrafluoroborate salts (**176**) and (**177**) to the corresponding iodoisoxazole (**173**) and 4-iodoanisole (**172**) or iodomesitylene (**181**) in different ratios (Scheme 73).

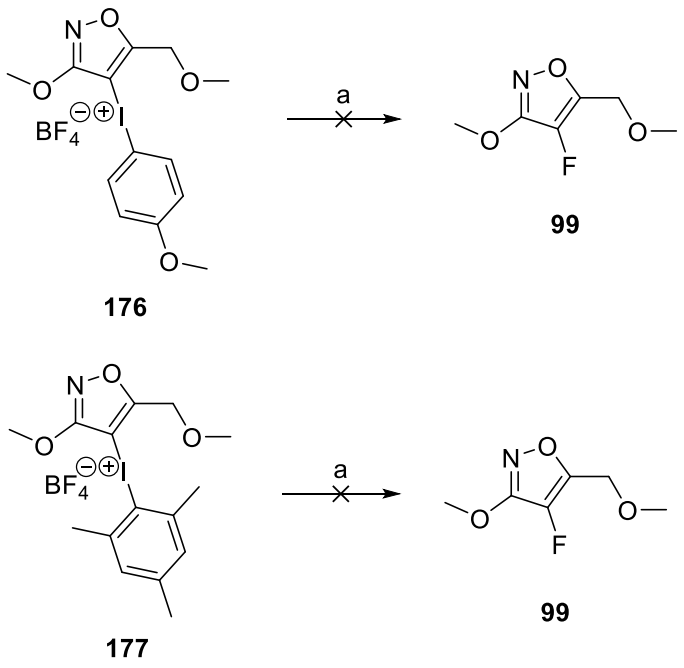

Scheme **72**: Fluorination attempts on diaryliodonium tetrafluoroborate salts (**176**) and (**177**). Reagents and conditions: a) CsF, DMF, rt→130 °C.

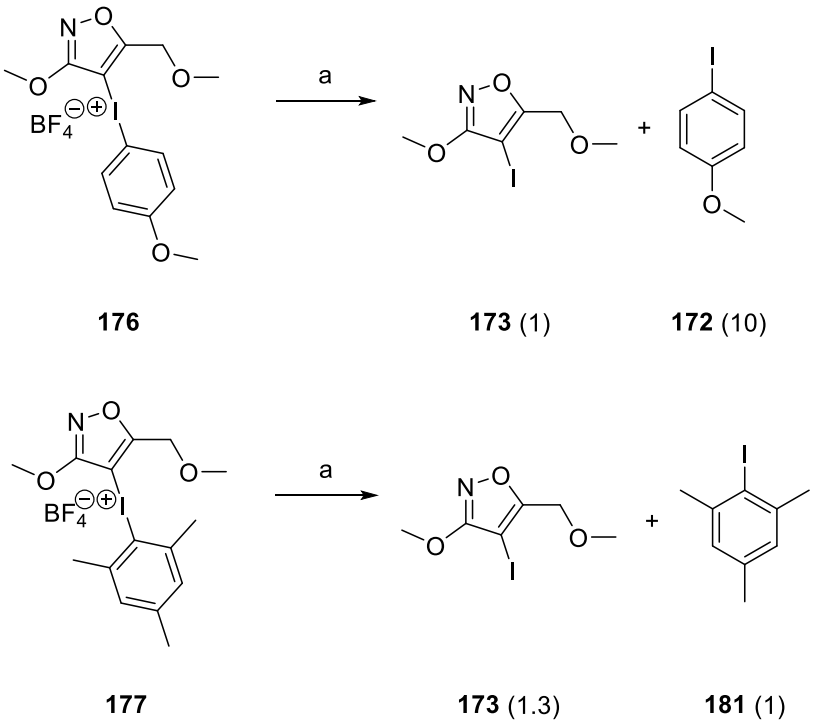

176 **173** (1) **172** (10)

177 **173** (1.3) **181** (1)

Scheme **73:** Products formed from fluorination of iodonium salts (**176**) and (**177**). Reagents and conditions: a) CsF, DMF, rt→130 °C. Ratios are given in parentheses and were determined from ^{1}H NMR analyses of crude mixtures.

It has been reported that the selectivity and distribution of the organofluorine compounds obtained from fluorination of non-symmetrical iodonium salts depends on the stereoelectronic properties of the aryl rings.[37] These results clearly suggest that diaryliodonium salts containing the isoxazole moiety do not meet the stereoelectronic requirements necessary for the fluorination reactions to occur. Moreover, the lack of precedent pertaining to the fluorination of these types of substrates perhaps reinforces their unsuitability.

3.6.9 Synthesis of iodomuscimol (165)

As discussed in Chapter 1, the most commonly employed radionuclides for PET imaging include ^{11}C and ^{18}F. These radiotracers suffer from a major limitation because of their short half-lives (20.4 min for ^{11}C and 110 min for ^{18}F) which may limit both the synthesis protocols and the time frame for PET studies. This limitation can be addressed by using iodine-124. With a half-life of 4.2 days, iodine-124 serves as an alternative PET radionuclide which allows extended radiosynthesis procedures and longitudinal PET imaging studies.[75] Therefore, it was decided to synthesise the iodo analogue of muscimol to investigate its agonist activity against GABA receptors. If good agonist activity is observed, a synthesis suitable for SPECT becomes an attractive prospect.

The synthesis of iodomuscimol (**165**) is illustrated in Scheme 74. It was developed based on the route to trifluoromethylmuscimol as described in Chapter 2. The synthesis was similar, except that the last two steps involved the reduction of compound (**126**) according to Staudinger conditions to form isopropyl protected iodomuscimol (**127**), followed by HBr deprotection to provide iodomuscimol (**165**), after preparative HPLC purification. A low yield was attributed to significant deiodination which was evident due to the recovery of muscimol (**11**) (Scheme 75). This product could result from competition between the rate of deiodination and the slower rate of the deprotection of the isopropyl group.

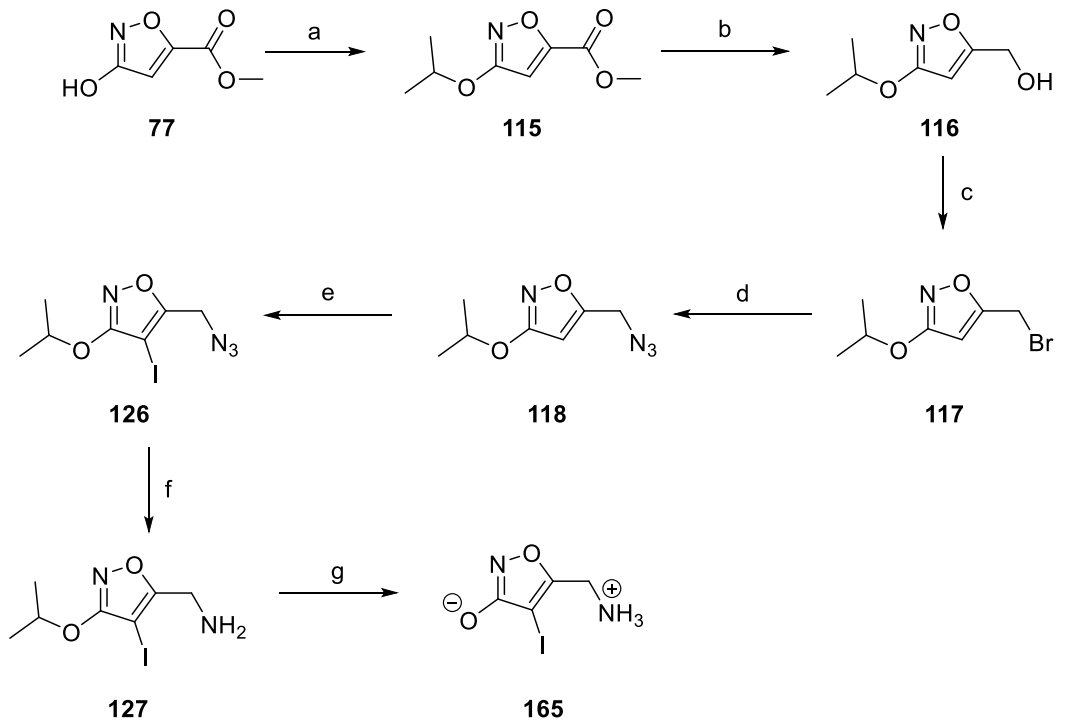

Scheme **74**: Successful route to iodomuscimol (**165**). Reagents and conditions: a) *i*-PrBr, K_2CO_3, DMF, 55 °C, overnight, 77%; b) $NaBH_4$, MeOH, 0 °C→rt, overnight, 90%; c) PPh_3, CBr_4, rt, 12 h, 58%; d) NaN_3, DMF, 80 °C, 3.5 h, 91%; e) NIS, TFA, rt, overnight, 86%; f) PMe_3, THF, H_2O, 0 °C, 1h, 83%; g) 33 % HBr in AcOH, 60 °C, 17 h, 19%.

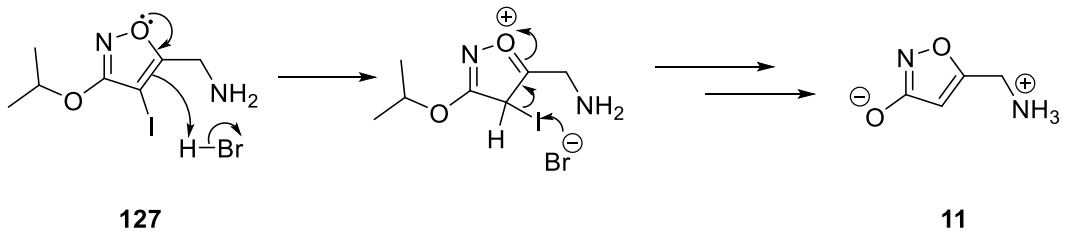

Scheme **75**: Putative mechanism for deiodination of isopropyl protected iodomuscimol (**127**) yielding muscimol (**11**), as a side reaction.

The purity of iodomuscimol (**165**) was determined by analytical HPLC on a reverse phase column. HPLC gave a single peak (t_r = 2.19 min), corresponding to iodomuscimol (**165**) and indicating high purity (>99%) (Figure 65).

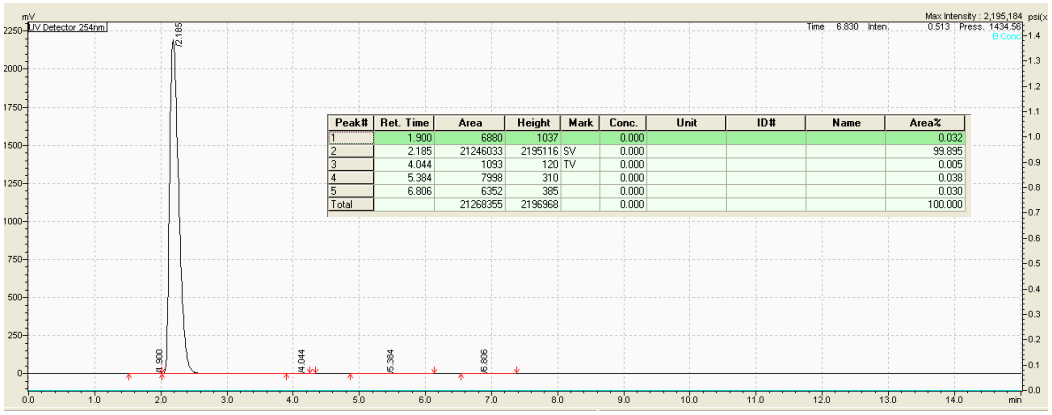

Peak#	Ret. Time	Area	Height	Mark	Conc.	Unit	ID#	Name	Area%
1	1.900	6880	1037		0.000				0.032
2	2.185	21246033	2195116	SV	0.000				99.895
3	4.044	1093	120	TV	0.000				0.005
4	5.384	7998	310		0.000				0.038
5	6.806	6352	385		0.000				0.030
Total		21268355	2196968		0.000				100.000

Figure **65**: HPLC chromatogram showing greater than 99 % purity iodomuscimol (**165**).

The ^{1}H-NMR spectrum of iodomuscimol (**165**) (Figure 66) shows the methylene signal at 4.21 ppm (H-6). Analysis of the ^{1}H-^{13}C HMBC spectrum (Figure 67) indicates that H-6 has ^{4}J correlation with δ_C 176.4 ppm (C-3), ^{3}J correlation with δ_C 61.6 ppm (C-4) and ^{2}J correlation with δ_C 163.2 ppm (C-5) respectively, as expected.

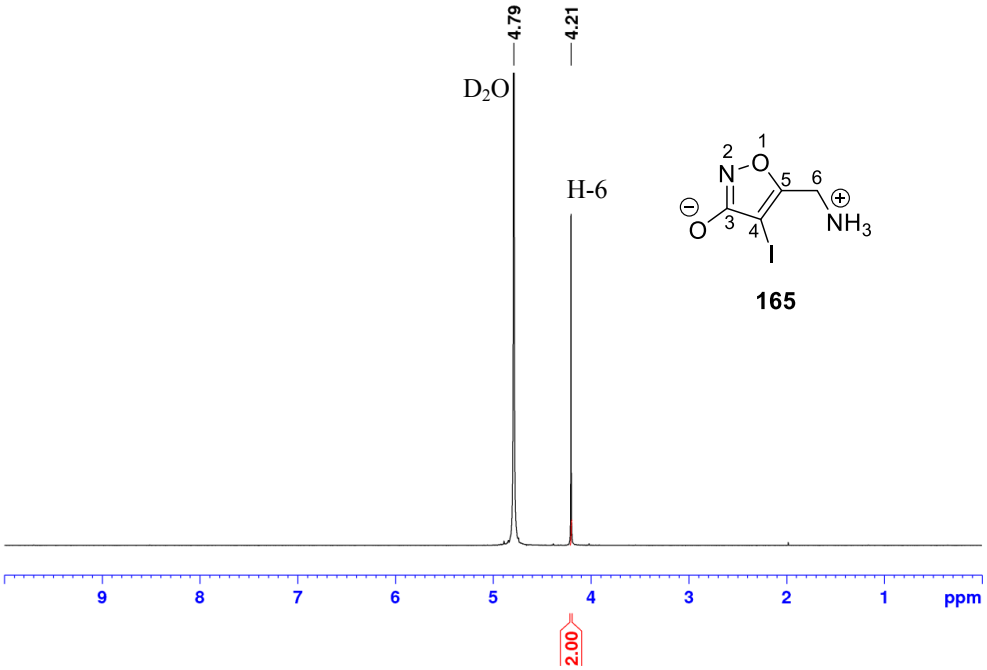

Figure **66**: ^{1}H NMR of iodomuscimol (**165**).

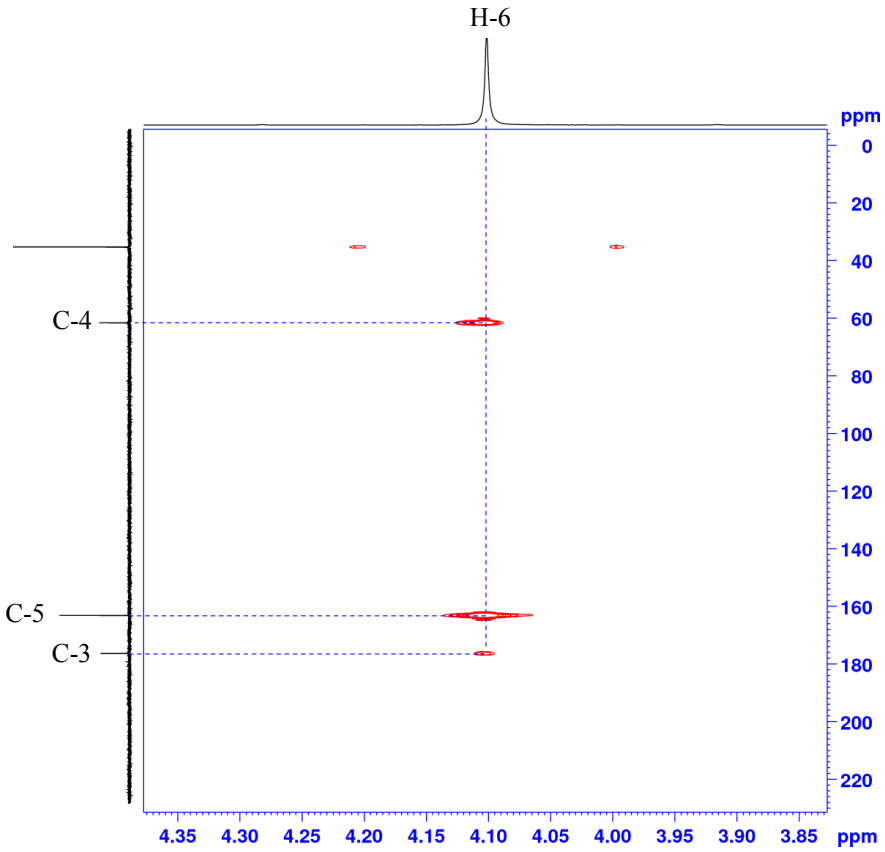

Figure **67**: ^{1}H-^{13}C HMBC spectrum of iodomuscimol (**165**).

The ^{13}C NMR spectrum (Figure 68) has the expected three heteroaromatic ring signals [176.4 ppm (C-3), 163.2 ppm (C-5) and 61.6 ppm (C-4)] and a methylene carbon [35.3 ppm (C-6)].

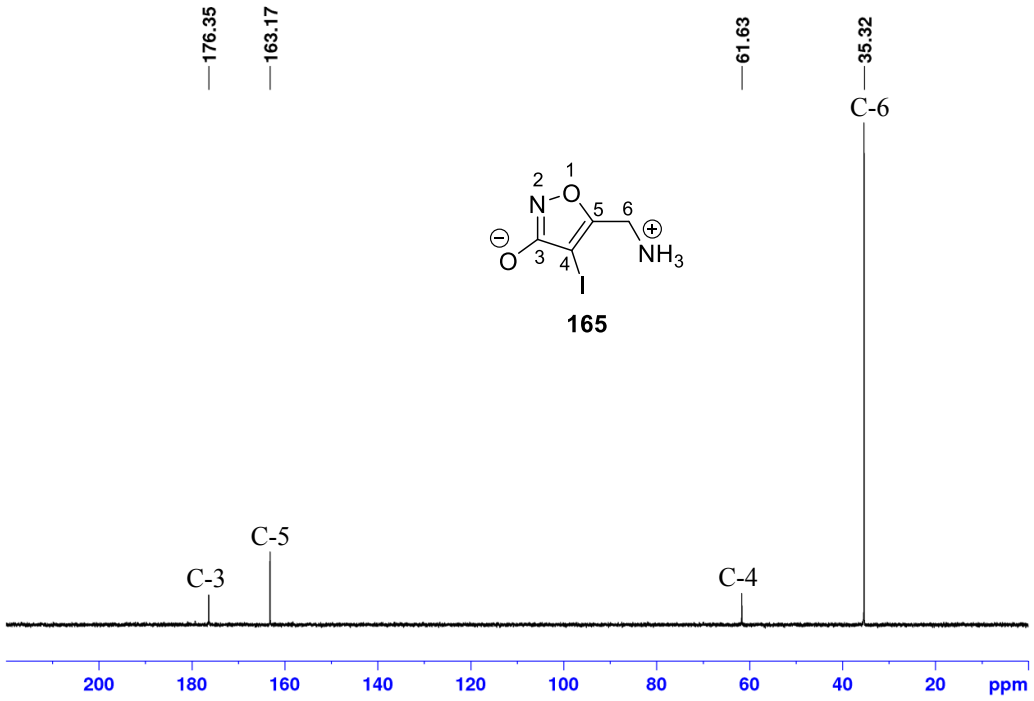

Figure **68**: ^{13}C NMR of iodomuscimol (**165**).

3.6.10 Biological results

Iodomuscimol (**165**) was sent to our collaborator, Professor Mary Collins at the Faculty of Pharmacy, University of Sydney, in Australia for biological evaluation against $GABA_A$ receptors in order to assess its agonist activity. Unfortunately, iodomuscimol (**165**) was inactive and did not evoke any current responses at all the tested $GABA_A$ receptors relative to the reference compounds, GABA (**12**) at concentrations up to 1000 μM (Figure 69).

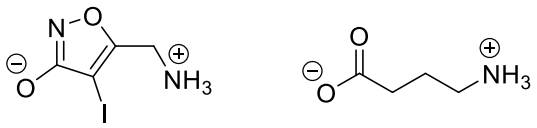

165 **12**

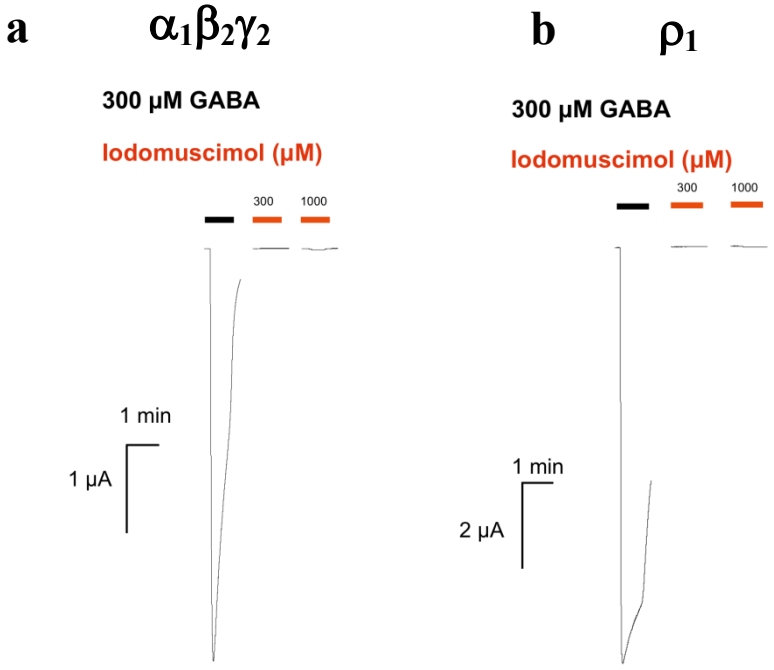

Figure **69**: Current responses of GABA (**12**) and iodomuscimol (**165**) at synaptic (**a**)($\alpha_1\beta_2\gamma_2$) and (**b**)(ρ_1) $GABA_A$ receptors.

3.7. Conclusions

The syntheses of three isoxazole diaryiodonium salts bearing anisole and mesitylene moieties were achieved. Diaryliodonium trifluoroacetate (**171**) was obtained by a direct synthesis of diacetoxyiodoarene (**167**) with aryl stannane (**170**) whereas the diaryliodonium tetrafluoroborate salts (**176**) and (**177**) were successfully prepared using a one-pot protocol from 4-iodo ether (**166**). Fluorination reactions of these compounds resulted in the reductive degradation to their corresponding isoxazole analogues and 4-iodoanisole or iodomesitylene in different ratios. Hence, these diaryliodonium salts are not suitable substrates for the preparation of fluoroisoxazole motifs.

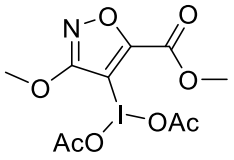

167

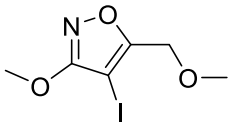

166

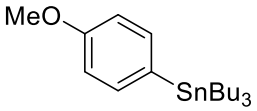

170

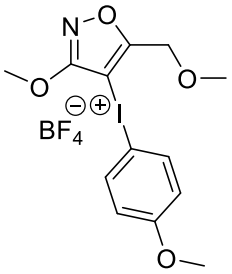

176

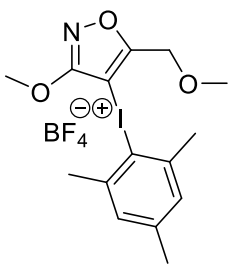

177

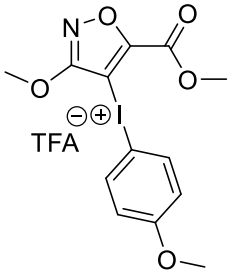

171

The first synthesis of iodomuscimol (**165**) was achieved in seven steps and high purity (>99%). Iodomuscimol (**165**) was inactive at all the tested $GABA_A$ receptors.

3.8 References

1 C. Willgerodt, *J. Prakt. Chem.*, 1886, **33**, 154–160.

2 C. Willgerodt, *Ber. Dtsch. Chem. Ges.*, 1892, **25**, 3494–3502.

3 C. Hartmann and V. Meyer, *Ber. Dtsch. Chem. Ges.*, 1893, **26**, 1727–1732.

4 C. Hartmann and V. Meyer, *Ber. Dtsch. Chem. Ges.*, 1894, **27**, 426–432.

5 E. A. Merritt and B. Olofsson, *Angew. Chem. Int. Ed.*, 2009, **48**, 9052–9070.

6 F. M. Beringer, P. S. Forgione and M. D. Yudis, *Tetrahedron*, 1960, **8**, 49–63.

7 D. B. Dess and J. C. Martin, *J. Org. Chem.*, 1983, **48**, 4155–4156.

8 M. Frigerio and M. Santagostino, *Tetrahedron Lett.*, 1994, **35**, 8019–8022.

9 R. Li, *Med. Res. Rev.*, 2016, **36**, 169–189.

10 L. F. Silva and B. Olofsson, *Nat. Prod. Rep.,* 2011, **28**, 1722–1754.

11 R. D. Richardson, J. M. Zayed, S. Altermann, D. Smith and T. Wirth, *Angew. Chem. Int. Ed.*, 2007, **46**, 6529–6532.

12 J. Musher, *Angew. Chem. Int. Ed.*, 1969, **8**, 54–68.

13 J. C. Martin, *Science*, 1983, **221**, 509–514.

14 C. W. Perkins, J. C. Martin, A. J. Arduengo, W. Lau, A. Alegria and J. K. Kochi, *J. Am. Chem. Soc.*, 1980, **102**, 7753–7759.

15 W. H. Powell, *Pure Appl. Chem.*, 1984, **56**, 769–778.

16 A. Yoshimura and V. V. Zhdankin, *Chem. Rev.*, 2016, **116**, 3328–3435.

17 V. V Zhdankin and P. J. Stang, *Chem. Rev.*, 2002, **102**, 2523–2584.

18 V. V Zhdankin, *Hypervalent iodine chemistry: preparation, structure, and synthetic applications of polyvalent iodine compounds*, John Wiley & Sons, Chichester, 2013, p. 13.

19 T. Wirth, *Angew. Chem. Int. Ed.*, 2005, **44**, 3656–3665.

20 R. D. Richardson and T. Wirth, *Angew. Chem. Int. Ed.*, 2006, **45**, 4402–4404.

21 V. Satam, A. Harad, R. Rajule and H. Pati, *Tetrahedron*, 2010, **66**, 7659–7706.

22 T. Wirth, *Angew. Chem. Int. Ed.*, 2001, **40**, 2812–2814.

23 V. V Zhdankin and P. J. Stang, *Chem. Rev.*, 2008, **108**, 5299–5358.

24 V. V Zhdankin, *Arkivoc*, 2009, **1**, 1–62.

25 V. V Zhdankin, *J. Org. Chem.*, 2011, **76**, 1185–1197.

26 K. C. Nicolaou, Y. Zhong and P. S. Baran, *J. Am. Chem. Soc.*, 2000, **122**, 7596–7597.

27 D. S. Bose and P. Srinivas, *Synlett*, 1998, 977–978.

28 D. Magdziak, A. A. Rodriguez, R. W. Van De Water and T. R. R. Pettus, *Org. Lett.*, 2002, **4**, 285–288.

29 Y. Huang, J. Zhang and T. R. R. Pettus, *Org. Lett.*, 2005, **7**, 5841–5844.

30 D. S. Bhalerao, U. S. Mahajan, K. H. Chaudhari and K. G. Akamanchi, *J. Org. Chem.*, 2007, **72**, 662–665.

31 N. S. Krishnaveni, K. Surendra, Y. V. D. Nageswar and K. R. Rao, *Synthesis*, 2003, 2295–2297.

32 K. C. Nicolaou, P. S. Baran and Y. L. Zhong, *J. Am. Chem. Soc.*, 2001, **123**, 3183–3185.

33 A. Ozanne-Beaudenon and S. Quideau, *Tetrahedron Lett.*, 2006, **47**, 5869–5873.

34 P. Eisenberger, S. Gischig and A. Togni, *Chem. Eur. J.*, 2006, **12**, 2579–2586.

35 J. Charpentier, N. Früh and A. Togni, *Chem. Rev.*, 2015, **115**, 650–682.

36 Y. P. Xiong, M. Y. Wu, X. Y. Zhang, C. L. Ma, L. Huang, L. J. Zhao, B. Tan and X. Y. Liu, *Org. Lett.*, 2014, **16**, 1000–1003.

37 M. S. Yusubov, D. Y. Svitich, M. S. Larkina and V. V. Zhdankin, *Arkivoc*, 2013, **1**, 364–395.

38 M. S. Yusubov, A. V. Maskaev and V. V. Zhdankin, *Arkivoc*, 2011, **1**, 370–409.

39 M. W. Justik and G. F. Koser, *Molecules*, 2005, **10**, 217–225.

40 H. Saltzman and J. G. Sharefkin, *Org. Synth.*, 1963, **43**, 60.

41 T. Kitamura, J. I. Matsuyuki, K. Nagata, R. Furuki and H. Taniguchi, *Synthesis*, 1992, 945–946.

42 M. Bielawski, M. Zhu and B. Olofsson, *Adv. Synth. Catal.*, 2007, **349**, 2610–2618.

43 M. D. Hossain and T. Kitamura, *Tetrahedron*, 2006, **62**, 6955–6960.

44 M. D. Hossain, Y. Ikegami and T. Kitamura, *J. Org. Chem.*, 2006, **71**, 9903–9905.

45 G. Koser and R. Wettach, *J. Org. Chem.*, 1980, **45**, 1543.

46 L. I. Dixon, M. A. Carroll, T. J. Gregson, G. J. Ellames, R. W. Harrington and W. Clegg, *Eur. J. Org. Chem.,* 2013, 2334–2345.

47 V. V. Zhdankin, M. C. Scheuller and P. J. Stang, *Tetrahedron Lett.*, 1993, **34**, 6853–6856.

48 V. W. Pike, F. Butt, A. Shah and D. A. Widdowson, *J. Chem. Soc., Perkin Trans. 1*, 1999, 245–248.

49 M. Ochiai, M. Toyonari, T. Nagaoka, D. W. Chen and M. Kida, *Tetrahedron Lett.*, 1997, **38**, 6709–6712.

50 M. A. Carroll, V. W. Pike and D. A. Widdowson, *Tetrahedron Lett.*, 2000, **41**, 5393–5396.

51 K. M. Lancer, G. H. Wiegand and M. Arx, *J. Org. Chem.*, 1976, **41**, 3360–3364.

52 Y. Yamada and M. Okawara, *Bull. Chem. Soc. Jpn.*, 1972, 45, 1860–1863.

53 M. Ochiai, Y. Takaoka, Y. Masaki and Y. Nagao, *J. Am. Chem. Soc.*, 1990, **112**, 5677–5678.

54 Masahito Ochiai, Y. Kitagawa and M. Toyonari, *Arkivoc*, 2003, **6**, 43–48.

55 N. Jalalian, PhD Thesis, Stockholm University, 2012.

56 V. W. Pike and F. I. Aigbirhio, *J. Chem. Soc., Chem. Commun.,* 1995, 2215–2216.

57 N. Ichiishi, A. J. Canty, B. F. Yates and M. S. Sanford, *Org. Lett.*, 2013, **15**, 5134–5137.

58 A. Shah, V. W. Pike and D. A. Widdowson, *J. Chem. Soc., Perkin Trans. 1*, 1998, 2043–2046.

59 J. H. Chun, S. Telu, S. Lu and V. W. Pike, *Org. Biomol. Chem.*, 2013, **11**, 5094–5099.

60 M. A. Carroll, J. Nairne and J. L. Woodcraft, *J. Label. Compd. Radiopharm.*, 2007, **50**, 452–454.

61 M. R. Zhang, K. Kumata and K. Suzuki, *Tetrahedron Lett.*, 2007, **48**, 8632–8635.

62 G. Saccomanni, G. Pascali, S. Del Carlo, D. Panetta, M. De Simone, S. Bertini, S. Burchielli, M. Digiacomo, M. Macchia, C. Manera and P. A. Salvadori, *Bioorg. Med. Chem. Lett.,* 2015, **25**, 2532–2535.

63 C. Warnier, C. Lemaire, G. Becker, G. Zaragoza, F. Giacomelli, J. Aerts, M. Otabashi, M. A. Bahri, J. Mercier, A. Plenevaux and A. Luxen, *J. Med. Chem.*, 2016, **59**, 8955–8966.

64 B. Hu, A. L. Vavere, K. D. Neumann, B. L. Shulkin, S. G. DiMagno and S. E. Snyder, *ACS Chem. Neurosci.*, 2015, **6**, 1870–1879.

65 A. McKillop and D. Kemp, *Tetrahedron*, 1989, **45**, 3299–3306.

66 B. H. Rotstein, N. A. Stephenson, N. Vasdev and S. H. Liang, *Nat. Commun.*, 2014, **5**, 1–7.

67 P. Kazmierczak, L. Skulski and L. Kraszkiewicz, *Molecules*, 2001, **6**, 881–891.

68 T. K. Page and T. Wirth, *Synthesis*, 2006, 3153–3155.

69 C. Ye, B. Twamley and J. M. Shreeve, *Org. Lett.*, 2005, **7**, 3961–3964.

70 H. Tohma, A. Maruyama, A. Maeda, T. Maegawa, T. Dohi, M. Shiro, T. Morita and Y. Kita, *Angew. Chem. Int. Ed.*, 2004, **43**, 3595–3598.

71 M. A. Carroll, J. Nairne, G. Smith and D. A. Widdowson, *J. Fluor. Chem.*, 2007, **128**, 127–132.

72 M. Bielawski, D. Aili and B. Olofsson, *J. Org. Chem.*, 2008, **73**, 4602–4607.

73 W. R. Dolbier, *Guide to fluorine NMR for organic chemists*, John Wiley & Sons, Hoboken, New Jersey, 2009.

74 L. Xiao and K. E. Johnson, *J. Electrochem. Soc.*, 2003, **150**, E307–E311.

75 L. Koehler, K. Gagnon, S. McQuarrie and F. Wuest, *Molecules*, 2010, **15**, 2686–2718.

Chapter 4: Experimental Section

4.1 General experimental protocol

4.1.1 Reagents, solvents and reaction conditions

All commercially available reagents were purchased from Acros UK, Sigma Aldrich, Fluorochem UK or Alfa Aesar UK and were used without further purification. *n*-BuLi was purchased from Sigma Aldrich as a 2.5 M solution in hexanes and was titrated against diphenylacetic acid prior to use. Anhydrous solvents (THF, DCM) were obtained from the MBraun MB SPS-800 solvent purification system, by passage through two drying columns and dispensed under an argon atmosphere. Anhydrous MeOH and MeCN were distilled from calcium hydride in recycling still.[1] Anhydrous DMF and dioxane were available commercially. If not stated otherwise, all non-aqueous reactions were performed in a flame-dried flask under an inert atmosphere of argon, using a double vacuum manifold with the argon passing through anhydrous calcium sulphate. Microwave reactions were performed using a CEM Discover microwave reactor with infrared pyrometer and pressure control system.

4.1.2 Chromatography and mass spectrometry

Thin layer chromatography (TLC) was performed using Merck silica gel $60F_{254}$ aluminium-supported thin layer chromatography sheets. Compounds were visualised by either UV light (254 nm) or thermal development after dipping in ethanolic solution of phosphomolybdic acid (PMA), basic aqueous solution of potassium permanganate ($KMnO_4$) or ninhydrin. Column chromatography was

performed using Merck Geduran silica gel 60 (250-400 mesh), eluting with solvents as supplied, under a positive pressure of compressed air. Reverse phase column chromatography was performed using C18 (Varian Mega Bond Elut C18) prepacked cartridges. High resolution mass spectra were recorded at the EPSRC National Mass Spectrometry Service, Swansea or at the University of St Andrews by Caroline Horsburgh on a Waters Micromass LCT time of flight mass spectrometer coupled to a Waters 2975 HPLC system. Values are reported as a ratio of mass to charge (*m/z*).

4.1.3 Nuclear magnetic resonance (NMR) spectroscopy

NMR spectra were acquired on either Bruker Avance 400 (^{1}H at 400 MHz, ^{13}C at 100 MHz, ^{19}F at 376 MHz) equipped with BBFO probe, Bruker Avance III HD 500 (^{1}H at 500 MHz, ^{13}C at 125 MHz, ^{19}F at 470 MHz) equipped with BBFO probe, Bruker Avance III 500 (^{1}H at 500 MHz, ^{13}C at 125 MHz) equipped with TCI cryoprobe or Bruker Avance III 700 (^{13}C at 176 MHz) equipped with a TCI cryoprobe. The chemical shifts (δ) are reported in parts per million (ppm) and are quoted relative to centre of the residual non-deuterated solvent peak for δ_H ($CDCl_3$: 7.26 ppm; MeCN: 1.94 ppm; D_2O: 4.79 ppm; DMSO: 2.50 ppm) and δ_C ($CDCl_3$: 77.16 ppm; MeCN: 1.32 ppm and 118.26 ppm; DMSO: 39.52 ppm). Chemical shifts δ_F are quoted relative to $CFCl_3$ (δ_F $CFCl_3$: 0.00 ppm). ^{13}C NMR spectra were recorded using the DEPT Q or UDEFT pulse sequence with broadband ^{1}H decoupling. ^{19}F{^{1}H} spectra were recorded with inverse-gating, to avoid errors on the integrals. Coupling constants (*J*) are given in Hertz (Hz). Signal splitting patterns are described as: br s (broad singlet), d (doublet),

s (singlet), sept (septet), t (triplet), dd (doublet of doublets), dm (doublet of multiplets) or m (multiplet). Spectroscopic data were assigned based on the combination of one- and two-dimensional experiments (HSQC and HMBC).

4.1.4 X-ray crystallography

Single crystal X-ray Diffraction analyses were carried out by Dr David B. Cordes and Professor Alexandra M. Z. Slawin at the University of St Andrews. All diffraction data except for (**122**) were collected by using a Rigaku FR-X Ultrahigh brilliance Microfocus RA generator/confocal optics and Rigaku XtaLAB P200 system, with Mo Kα radiation (λ = 0.71075 Å). Data for (**122**) were collected at 125 K by using a Rigaku MM-007HF High brilliance RA generator/confocal optics and Rigaku XtaLAB P200 system, with Cu Kα radiation (λ = 1.54187 Å). Intensity data for all samples were collected using ω steps accumulating area detector images spanning at least a hemisphere of reciprocal space. All data were corrected for Lorentz polarisation effects. A multiscan absorption correction was applied by using CrystalClear[2] or CrysAlisPro.[3] Structures were solved by Patterson (PATTY[4]) or direct (SIR2004,[5] SIR2011[6]) methods and refined by full-matrix least-squares against F^2 (SHELXL-2013[7]). Non-hydrogen atoms were refined anisotropically, and hydrogen atoms were refined using a riding model. All calculations were performed using the CrystalStructure[8] interface. The Crystallographic Information Files (CIF) were analysed using CrystalMaker software and are attached on a CD disc.

4.1.5 Other analysis

Melting points were obtained on an Electrothermal IA9100digital point apparatus without correction. IR spectra were recorded using the ATR technique on Shimadzu IRAffinity-1S FT-IR spectrometer with a diamond ATR attachment. HPLC analyses were performed using either a Waters system (600E multisolvent delivery system) or Shimadzu Prominence with reverse phase column as indicated in individual experiment. Amino acids (**11**), (**64**), (**65**) and (**165**) were freeze dried from solvent solution in water in a Chris Alpha 1-2 LO Plus freeze drier.

4.2 Experimental protocols

4.2.1 Methyl 4-azido-3-oxobutanoate (86)[9]

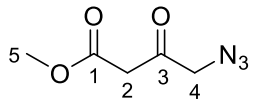

NaN_3 (1.4 g, 21.6 mmol, 1.3 eq) was added to a solution of methyl 4-chloroacetoacetate (2.5 g, 16.6 mmol, 1.0 eq) in THF/water (3:1 v/v mixture, 24 mL) at 0 °C. The mixture was stirred at rt overnight. Water (30 ml) was added and the product was extracted into EtOAc (3 x 100 ml). The combined organic layers were washed with a saturated aqueous solution of Na_2CO_3 (60 mL), dried over Na_2SO_4, filtered and concentrated under reduced pressure affording yellowish oil which was purified silica by gel column chromatography (DCM/petroleum ether, 80:20) to afford methyl 4-azido-3-oxobutanoate (**86**) (1.75 g, 67%) as a pale yellowish oil: $\mathbf{R_f}$ 0.82 (DCM/EtOAc, 90:10, PMA); δ_H (500 MHz, $CDCl_3$) 4.12 (2H, s, H-4), 3.76 (3H, s, H-5), 3.53 (2H, s, H-2); δ_C (125 MHz, $CDCl_3$) 197.1 (C-3), 166.8 (C-1), 57.7 (C-4), 52.9 (C-5), 46.4 (C-2); **HRMS** *m/z* (ES^+), found: $[M+Na]^+$ 180.0378, $C_5H_7N_3O_3Na$ requires $[M+Na]^+$ 180.0385. These data are in accordance with the literature.[9]

4.2.2 (±) Methyl 4-azido-2-fluoro-3-oxobutanoate (85)

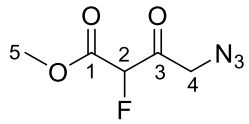

Selectfluor™ (1.52 g, 4.29 mmol, 1.5 eq) was added in single portion to a solution of methyl 4-azido-3-oxobutanoate (**86**) (450 mg, 2.86 mmol, 1.0 eq) in MeCN (20 mL). After complete dissolution of Selectfluor™, $TiCpCl_3$ (57 mg, 0.26 mmol, 0.1 eq) was added and the reaction mixture turned bright yellow. After 15 h stirring at rt, MTBE (10 mL) was added and the precipitate was removed by filtration. The filtrate was concentrated under reduced pressure, affording a dark yellowish oil which was purified by silica gel column chromatography (DCM, 100) to afford methyl 4-azido-2-fluoro-3-oxobutanoate (**85**) (185 mg, 37%) as a yellowish oil: $\mathbf{R_f}$ 0.69 (DCM/EtOAc, 90:10, PMA); **FT-IR** (ATR, cm^{-1}) 2922, 2108 (N_3), 1741 (C=O), 1456, 1440, 1287, 1231, 1138, 1099, 1015, 910; δ_H (500 MHz, $CDCl_3$) 5.39 (1H, d, $^2J_{HF}$ 48.4, H-2), 4.31 (1H, dd, $^2J_{HH}$ 19.2, $^4J_{HF}$ 2.2, H-4_a), 4.26 (1H, dd, $^2J_{HH}$ 19.2, $^4J_{HF}$ 1.6, H-4_b), 3.88 (3H, s, H-5); $^1H\{^{19}F\}$ (500 MHz, $CDCl_3$) 5.39 (1H, s, H-2), 4.31 (1H, d, $^2J_{HH}$ 19.2, H-4_a), 4.26 (1H, d, $^2J_{HH}$ 19.2, H-4_b), 3.88 (3H, s, H-5); δ_C (125 MHz, $CDCl_3$) 195.5 (d $^2J_{CF}$ 24.2, C-3) 163.7 (d, $^2J_{CF}$ 23.6, C-1), 90.5 (d, $^1J_{CF}$ 197.4, C-2), 55.1 (C-4), 53.8 (C-5), δ_F (470 MHz, $CDCl_3$) -199.5 (dm, $^2J_{HF}$ 48.4, 1F, CHF); $^{19}F\{^1H\}$ (470 MHz, $CDCl_3$) -199.5 (s, 1F, CHF); **HRMS** *m/z* ($APCI^+$), found: $[M+H]^+$ 176.0461, $C_5H_7N_3O_3F$ requires $[M+H]^+$ 176.0466.

4.2.3 Methyl 3-hydroxyisoxazole-5-carboxylate (77)[10]

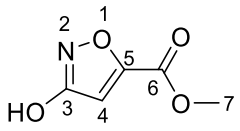

DBU (11.7 mL, 77.4 mmol, 1.1 eq) was slowly added to a solution of hydroxyurea (5.35 g, 70.4 mmol, 1.0 eq) in MeOH (85 mL) at 0 °C. After 15 min stirring at 0 °C, dimethyl acetylenedicarboxylate (8.6 mL, 70.4 mmol, 1.0 eq) was added dropwise to the reaction mixture. The resulting dark orange reaction mixture was stirred at rt for 2.5 h and concentrated under reduced pressure. The resulting red oil was diluted with water (120 mL), acidified with conc. HCl under ice-cooling to obtain pH<2 and extracted into Et_2O (3 × 80 mL). The aqueous layer was washed with saturated NaCl and extracted into Et_2O (2 × 80 mL). The combined organic layers were dried over $MgSO_4$, filtered and concentrated under reduced pressure to afford a yellow amorphous solid, which was purified by recrystallisation from $CHCl_3$ to give methyl 3-hydroxyisoxazole-5-carboxylate (**77**) (4.1 g, 41%) as colourless crystalline solid: $\mathbf{R_f}$ 0.57 (Et_2O/petroleum ether, 80:20, UV/$KMnO_4$); **mp** 165-166 °C [Lit.[10] 164-165 °C]; δ_H (500 MHz, $CDCl_3$) 6.61 (1H, s, H-4), 3.98 (3H, s, H-7); δ_C (125 MHz, $CDCl_3$) 170.8 (C-3), 160.1 (C-5), 156.9 (C-6), 101.4 (C-4), 53.2 (C-7); **HRMS** *m/z* (ESI^-), found: $[M-H]^-$ 142.0140, $C_5H_4NO_4$ requires $[M-H]^-$ 142.0146. These data are in accordance with the literature.[10]

4.2.4 Methyl 3-methoxyisoxazole-5-carboxylate (94)[11]

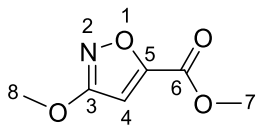

K_2CO_3 (2.9 g, 21.0 mmol, 1.5 eq) and CH_3I (1.3 mL, 21.0 mmol, 1.5 eq) were added to a solution of methyl 3-hydroxyisoxazole-5-carboxylate (**77**) (2.0 g, 13.9 mmol, 1.0 eq) in DMF (10 ml) at 0 °C. After 14 h stirring at rt, the mixture was poured into an ice-cold aqueous solution of HCl (0.5 M, 100 mL) and extracted into Et_2O (5 × 80 mL). The combined organic layers were washed with a saturated aqueous solution of Na_2CO_3 (80 mL), dried over $MgSO_4$, filtered and concentrated under reduced pressure to afford a light yellow crystalline solid, which was purified by silica gel column chromatography (petroleum ether/Et_2O, 80:20), affording methyl-3-methoxyisoxazole-5-carboxylate (**94**) (1.45 g, 66%) as colourless crystalline solid: $\mathbf{R_f}$ 0.71 (petroleum ether/Et_2O, 70:30, UV/$KMnO_4$); **mp** 72-73 °C [Lit.[11] 70 °C]; δ_H (500 MHz, $CDCl_3$) 6.53 (1H, s, H-4), 4.02 (3H, s, H-8), 3.94 (3H, s, H-7); δ_C (125 MHz, $CDCl_3$) 172.2 (C-3), 160.5 (C-5), 157.2 (C-6), 100.8 (C-4), 57.6 (C-8), 53.0 (C-7); **HRMS** *m/z* (ESI^+), found: $[M+Na]^+$ 180.0266, $C_6H_7NO_4Na$ requires $[M+Na]^+$ 180.0273. These data are in accordance with the literature.[11]

4.2.5 5-Hydroxymethyl-3-methoxyisoxazole (95)[12]

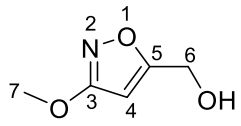

$NaBH_4$ (1.51 g, 40.0 mmol, 2.5 eq) was added to a solution of methyl 3-methoxyisoxazole-5-carboxylate (**94**) (2.50 g, 16.0 mmol, 1.0 eq) in MeOH (50 mL) at 0 °C. The mixture was stirred at rt overnight and quenched with saturated solution NH_4Cl (40 mL). The reaction mixture was partitioned between water (50 mL) and EtOAc (50 mL). The aqueous layer was extracted with EtOAc (3 x 50 mL). The combined organic layers were washed with brine (40 mL), dried over $MgSO_4$, filtered and concentrated under reduced pressure to afford a pale yellowish oil, which was purified by silica gel column chromatography (petroleum ether/EtOAc, 60:40) to afford 5-hydroxymethyl-3-methoxyisoxazole (**95**) (1.75 g, 85%) as colourless oil: $\mathbf{R_f}$ 0.65 (petroleum ether/EtOAc 50:50, $KMnO_4$); δ_H (500 MHz, $CDCl_3$) 5.88 (1H, s, H-4), 4.65 (2H, d, $^3J_{HH}$ 6.0, H-6), 3.96 (3H, s, H-7), 2.20 (br s, 1H, -OH); δ_C ($CDCl_3$, 125 MHz) 172.5 (C-3), 172.4 (C-5), 93.2 (C-4), 57.1 (C-6), 56.7 (C-7). **HRMS** *m/z* ($APCI^+$), found: $[M+H]^+$ 130.0496, $C_5H_8NO_3$ requires $[M+H]^+$ 130.0496. These data are in accordance with the literature.[12,13]

4.2.6 3-Methoxy-5-(methoxymethyl)isoxazole (96)[14]

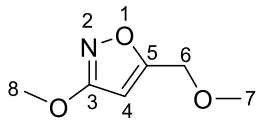

NaH (60% dispersion in mineral oil, 232 mg, 5.80 mmol, 1.1 eq) was added in single portion to a solution of 5-hydroxymethyl-3-methoxyisoxazole (**95**) (680 mg, 5.27 mmol, 1.0 eq) in THF (30 mL) at 0 °C. The reaction mixture was stirred at rt for 1 h, cooled to 0 °C and CH_3I (0.36 mL, 5.80 mmol, 1.1 eq) was added. After 1 h stirring at rt, the reaction was quenched by slow addition of ice-cold water (30 mL). The aqueous layer was extracted into EtOAc (4 × 20 mL). The combined organic layers were washed with brine (20 mL), dried over $MgSO_4$, filtered and concentrated under reduced pressure. The resulting yellow oil was purified by silica gel column chromatography (petroleum ether/Et_2O, 80:20) to afford 3-methoxy-5-(methoxymethyl)isoxazole (**96**) (473 mg, 57%) as a colourless oil: $\mathbf{R_f}$ 0.52 (petroleum ether/Et_2O, 70:30, $KMnO_4$); **FT-IR** (ATR, cm^{-1}) 2949, 1620, 1516, 1454, 1411, 1382, 1098, 1030, 966, 916, 795; δ_H (500 MHz, $CDCl_3$) 5.88 (1H, s, H-4), 4.42 (2H, s, H-6), 3.97 (3H, s, H-8), 3.42 (3H, s, H-7); δ_C ($CDCl_3$, 125 MHz) 172.5 (C-3), 170.3 (C-5), 94.4 (C-4), 65.8 (C-6), 58.9 (C-7), 57.2 (C-8); **HRMS** *m/z* (ESI^+), found: $[M+H]^+$ 144.0651, $C_6H_{10}NO_3$ requires $[M+H]^+$ 144.0661. These data are in accordance with the literature.[14]

4.2.7 Methyl 3-methoxy-4-nitroisoxazole-5-carboxylate (100)

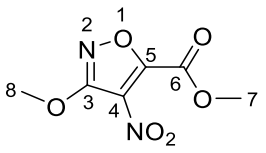

Triflic anhydride (5.9 g, 21.0 mmol, 3.0 eq) was added to solution of tetramethylammonium nitrate (2.9 g, 21.0 mmol, 3.0 eq) in DCM (3 mL) at rt. The suspension was stirred for 2 h, then a solution of methyl 3-methoxyisoxazole-5-carboxylate (**94**) (1.1 g, 7.0 mmol, 1.0 eq) in DCM (10 mL) was added. After 48 h stirring under reflux, the mixture was cooled down to rt and partitioned between water (30 mL) and DCM (40 mL). The organic layer was separated and washed with water (50 mL). The aqueous layer was extracted with DCM (3 x 50 mL). The combined organic layers were washed with brine (50 mL), dried over $MgSO_4$, filtered and concentrated under reduced pressure. The resulting yellow residue was purified by silica gel column chromatography (petroleum ether/DCM, 50:50) to afford methyl 3-methoxy-4-nitroisoxazole-5-carboxylate (**100**) (0.9 g, 70%) as yellowish oil: $\mathbf{R_f}$ 0.41 (petroleum ether/Et_2O, 80:20, UV/$KMnO_4$); **FT-IR** (ATR, cm^{-1}) 1751 (C=O), 1628, 1541 (NO_2), 1456, 1418, 1371, 1288, 1221, 1202, 1161, 1051, 964, 918, 831, 808; δ_H (500 MHz, $CDCl_3$) 4.14 (3H, s, H-8), 4.02 (3H, s, H-7); δ_C (125 MHz, $CDCl_3$) 164.0 (C-3), 157.4 (C-5), 155.0 (C-6), 127.7 (C-4), 58.9 (C-8), 54.2 (C-7); **HRMS** *m/z* ($APCI^+$), found: $[M+H]^+$ 203.0295, $C_6H_7N_2O_6$ requires $[M+H]^+$ 203.0299.

4.2.8 Methyl 4-amino-3-methoxyisoxazole-5-carboxylate (101)

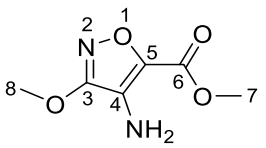

Fe powder (267 mg, 4.86 mmol, 5.0 eq) was added to a solution methyl 3-methoxy-4-nitroisoxazole-5-carboxylate (**100**) (196 mg, 0.97 mmol, 1.0 eq) in AcOH/H_2O (3:1 v/v mixture, 12 mL). After stirring at 50 °C for 2 h, the solution was cooled to rt and the solvent was removed under reduced pressure. The residue was partitioned between water (20 mL) and EtOAc (20 mL). The mixture was basified with a saturated aqueous solution of Na_2CO_3 and further extracted with EtOAc (3 x 20 mL). The combined organic layers were washed with brine (20 mL), dried over $MgSO_4$, filtered and concentrated under reduced pressure to afford a light pale yellow solid, which was purified by silica gel column chromatography (DCM, 100), affording methyl 4-amino-3-methoxyisoxazole-5-carboxylate (**101**) (139 mg, 83%) as colourless crystalline solid: $\mathbf{R_f}$ 0.74 (DCM/EtOAc, 90:10, UV/ninhydrin); **mp** 111-112 °C; **FT-IR** (ATR, cm^{-1}) 3499, 3397 (NH_2), 2957, 1711 (C=O), 1665, 1572, 1545, 1501, 1433, 1416, 1333, 1238, 1182, 1126, 1007, 986, 962, 901, 802, 764, 716; δ_H (400 MHz, $CDCl_3$) 4.15 (br s, 2H, -NH_2), 4.05 (3H, s, H-8), 3.92 (3H, s, H-7); δ_C ($CDCl_3$, 125 MHz) 164.5 (C-3), 159.1 (C-6), 138.4 (C-5), 125.6 (C-4), 57.5 (C-8), 51.9 (C-7); **HRMS** *m/z* (ESI^+), found: $[M+Na]^+$ 195.0373, $C_6H_8N_2O_4Na$ requires $[M+Na]^+$ 195.0382.

4.2.9 Methyl 4-bromo-3-methoxyisoxazole-5-carboxylate (105)

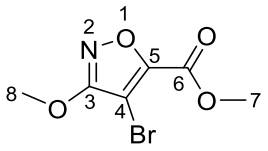

Methyl 3-methoxyisoxazole-5-carboxylate (**94**) (100 mg, 0.64 mmol, 1.0 eq), NBS (170 mg, 0.96 mmol, 1.5 eq) and TFA (3 mL) were placed in a 10 mL glass microwave vessel. The reaction vessel was sealed with a rubber lid (CEM) and heated under microwave irradiation at 150 °C (50 W) for 3 h. The solvent was removed under reduced pressure and the residue was purified by silica gel column chromatography (petroleum ether/Et_2O, 95:5), affording methyl 4-bromo-3-methoxyisoxazole-5-carboxylate (**105**) (128 mg, 85%) as colourless crystalline solid: $\mathbf{R_f}$ 0.56 (petroleum ether/Et_2O, 80:20, UV/$KMnO_4$); **mp** 103-104 °C; **FT-IR** (ATR, cm^{-1}) 2965, 1732 (C=O), 1527, 1450, 1433, 1414, 1277, 1217, 1206, 1172, 1105, 1038, 978, 947, 918, 808, 733, 700, 613; δ_H (500 MHz, $CDCl_3$) 4.10 (3H, s, H-8), 3.98 (3H, s, H-7); δ_C (125 MHz, $CDCl_3$) 169.7 (C-3), 156.5 (C-5), 156.3 (C-6), 91.7 (C-4), 58.1 (C-8), 53.0 (C-7); **HRMS** *m/z* (NSI^+), found: $[M+H]^+$ 235.9555, $C_6H_7NO_4{}^{79}Br$ requires $[M+H]^+$ 235.9553.

4.2.10 4-Bromo-3-methoxy-5-(methoxymethyl)isoxazole (107)

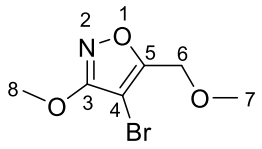

NBS (153 mg, 0.86 mmol, 2.0 eq) was added to a solution of 3-methoxy-5-(methoxymethyl)isoxazole (**96**) (61 mg, 0.43 mmol, 1.0 eq) in TFA (2 mL). After stirring at rt for 48 h, the solvent was removed under reduced pressure and the residue was purified by silica gel column chromatography (petroleum ether/Et_2O, 80:20), affording 4-bromo-3-methoxy-5-(methoxymethyl)isoxazole (**107**) (55 mg, 85%) as colourless crystalline solid: $\mathbf{R_f}$ 0.55 (petroleum ether/Et_2O, 70:30, UV/$KMnO_4$); **FT-IR** (ATR, cm^{-1}) 2994, 1624, 1530, 1452, 1413, 1375, 1283, 1192, 1101, 1057, 959, 947, 926, 781, 716, 689; **mp** 49-50 °C; δ_H (500 MHz, $CDCl_3$) 4.45 (2H, s,H-6) 4.03 (3H, s, H-8), 3.39 (3H, s, H-7); δ_C ($CDCl_3$, 125 MHz) 169.2 (C-3), 166.5 (C-5), 85.3 (C-4), 63.9 (C-6), 59.0 (C-7), 57.8 (C-8); **HRMS** *m/z* (NSI^+), found: $[M+H]^+$ 221.9762, $C_6H_9NO_3{}^{79}Br$ requires $[M+H]^+$ 221.9760.

4.2.11 5-Bromomethyl-3-methoxyisoxazole (109)[15]

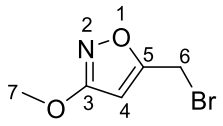

CBr_4 (4.44 g, 13.4 mmol, 1.04 eq) and PPh_3 (3.72 g, 14.2 mmol, 1.1 eq) were added to a solution of 5-hydroxymethyl-3-methoxyisoxazole (**95**) (1.66 g, 12.9 mmol, 1.0 eq) in DCM at 0 °C. The reaction was stirred at 0 °C for 2 h and concentrated under reduced pressure. The resulting residue was purified by silica gel column chromatography (petroleum ether/EtOAc, 90:10) to afford 5-bromomethyl-3-methoxyisoxazole (**109** (2.1 g, 83%) as a colourless oil: $\mathbf{R_f}$ 0.72 (petroleum ether/EtOAc, 80:20, UV/$KMnO_4$); δ_H (500 MHz, $CDCl_3$) 5.91 (1H, s, H-4), 4.30 (2H, s, H-6), 3.90 (3H, s, H-7); δ_C (125 MHz, $CDCl_3$) 172.2 (C-3), 168.2 (C-5), 95.1 (C-4), 57.1 (C-7), 19.1 (C-6); **HRMS** *m/z* (NSI^+), found: $[M+H]^+$ 191.9654, $C_5H_7NO_2{}^{79}Br$ requires $[M+H]^+$ 191.9655. These data are in accordance with the literature.[16]

4.2.12 5-Azidomethyl-3-methoxyisoxazole (110)

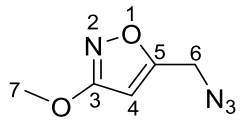

NaN_3 (1.56 g, 24.0 mmol, 5.0 eq) was added to a solution of 5-bromomethyl-3-methoxyisoxazole (**109**) (923 mg, 4.8 mmol, 1.0 eq) in DMF (21 mL). After stirring at 80 °C for 3.5 h, the resulting solution was diluted with water (50 mL), and the product was extracted into Et_2O (5 x 50 mL). The combined organic layers were washed with a saturated solution of Na_2CO_3 (50 mL), dried over $MgSO_4$, filtered and concentrated under reduced pressure. The resulting yellowish oil was purified by silica gel column chromatography (petroleum ether/EtOAc, 90:10) to afford 5-azidomethyl-3-methoxyisoxazole (**110**) (665 mg, 90%) as a colourless oil: $\mathbf{R_f}$ 0.62 (petroleum ether/EtOAc, 80:20, $KMnO_4$); **FT-IR** (ATR, cm^{-1}) 2949, 2100 (N_3), 1622, 1520, 1454, 1413, 1354, 1292, 1198, 1142, 1031, 914; δ_H (500 MHz, $CDCl_3$) 5.91 (1H, s, H-4), 4.32 (2H, s, H-6), 3.97 (3H, s, H-7); δ_C (125 MHz, $CDCl_3$) 172.4 (C-3), 167.5 (C-5), 94.9 (C-4), 57.3 (C-7), 45.9 (C-6); **HRMS** *m/z* (ESI^+), found: $[M+H]^+$ 155.0563, $C_5H_7N_4O_2$ requires $[M+H]^+$ 154.0569.

4.2.13 5-Azidomethyl-4-bromo-3-methoxyisoxazole (111)

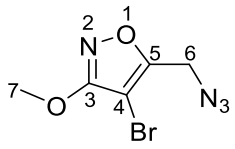

NBS (1.53 g, 8.6 mmol, 2.0 eq) was added to a solution of 5-azidomethyl-3-methoxyisoxazole (**110**) (665 mg, 4.3 mmol, 1.0 eq) in TFA (18 mL). After stirring at 30 °C for 27 h, the solvent was removed under reduced pressure and the residue was purified by silica gel column chromatography (petroleum ether/Et_2O, 95:5), affording 5-azidomethyl-4-bromo-3-methoxyisoxazole (**111**) (847 mg, 85%) as colourless oil: $\mathbf{R_f}$ 0.67 (petroleum ether/Et_2O, 80:20, UV/$KMnO_4$); **FT-IR** (ATR, cm^{-1}) 2957, 2097 (N_3), 1622, 1531, 1449, 1410, 1337, 1287, 1250, 1200, 1101, 1061, 961, 920, 881, 768; δ_H (500 MHz, $CDCl_3$) 4.36 (2H, s,H-6), 4.06 (3H, s, H-7); δ_C (125 MHz, $CDCl_3$) 169.4 (C-3), 164.6 (C-5), 85.5 (C-4), 57.9 (C-7), 44.4 (C-6); **HRMS** *m/z* ($APCI^+$), found: $[M+H]^+$ 232.9667, $C_5H_6N_2O_4{}^{79}Br$ requires $[M+H]^+$ 232.9669.

4.2.14 5-Aminomethyl-4-bromo-3-methoxyisoxazole (112)

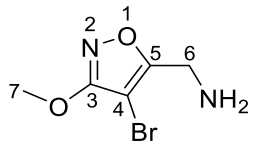

PMe_3 (1.0 M solution in THF, 4.5 mL, 4.5 mmol, 1.5 eq) was added to a solution of 5-azidomethyl-4-bromo-3-methoxyisoxazole (**111**) (700 mg, 3.0 mmol, 1.0 eq) in THF (20 mL) at 0 °C. The resulting mixture was stirred at 0 °C for 30 min and was quenched by slow addition of water (40 mL). The organic phase was separated and the aqueous phase was extracted into EtOAc (3 x 40 mL). The combined organic layers were washed with brine, dried over $MgSO_4$, filtered and concentrated under reduced pressure and the residue was purified by silica gel column chromatography (EtOAc, 100), affording 5-aminomethyl-4-bromo-3-methoxyisoxazole (**112**) (410 mg, 66%) as yellowish oil: $\mathbf{R_f}$ 0.20 (EtOAc, ninhydrin); **FT-IR** (ATR, cm^{-1}) 3375, 3320 (NH_2), 2955, 1614, 1530, 1451, 1408, 1194, 1099, 1032, 961, 939, 702; δ_H (500 MHz, $CDCl_3$) 4.02 (3H, s, H-7), 3.87 (2H, s, H-6), 1.58 (br s, 2H, $-NH_2$); δ_C ($CDCl_3$, 125 MHz) 170.6 (C-5), 169.4 (C-3), 81.8 (C-4), 57.7 (C-7), 37.7 (C-6); **HRMS** *m/z* (NSI^+), found: $[M+H]^+$ 206.9764, $C_5H_8N_2O_2{}^{79}Br$ requires $[M+H]^+$ 206.9764.

4.2.15 5-(*tert*-butyloxycarbonyl)aminomethyl-4-bromo-3-methoxyisoxazole (113)

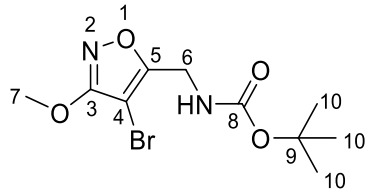

Et_3N (0.3 mL, 2.13 mmol, 1.1 eq) and di-*tert*-butyl dicarbonate (0.49 mL, 2.13 mmol, 1.1 eq) were added to a solution of 5-aminomethyl-4-bromo-3-methoxyisoxazole (**112**) (400 mg, 1.93 mmol, 1.0 eq) in DCM (30 mL). The resulting yellowish mixture was stirred at rt for 15 h, diluted with DCM (40 mL), and washed with water (50 mL). The aqueous layer was extracted into DCM (3 x 30 mL). The combined organic layers were combined, dried over $MgSO_4$, filtered and concentrated under reduced pressure. The resulting yellow residue was purified by silica gel column chromatography (petroleum ether/Et_2O, 70:30) to afford 5-(*tert*-butyloxycarbonyl)aminomethyl-4-bromo-3-methoxyisoxazole (**113**) (427 mg, 72%) as a colourless crystalline solid: $\mathbf{R_f}$ 0.41 (petroleum ether/Et_2O, 70:30, ninhydrin); **mp** 91-92 [Lit.[14] 91-92 °C]; **FT-IR** (ATR, cm^{-1}) 3314 (NH), 2978, 1678 (C=O), 1626, 1531 (NH), 1450, 1410, 1368, 1271, 1256, 1155, 1103, 1053, 976; δ_H (500 MHz, $CDCl_3$) 4.96 (br s, 1H, -NH), 4.37 (2H, d, $^3J_{HH}$ 5.5, H-6), 4.02 (3H, s, H-7), 1.44 (9H, s, H-10); δ_C (125 MHz, $CDCl_3$) 169.3 (C-3), 166.7 (C-5), 155.4 (C-8), 83.2 (C-4), 80.5 (C-9), 57.7 (C-7), 36.2 (C-6), 28.4 (C-10); **HRMS** *m/z* (NSI^+), found: $(M+NH_4)^+$ 324.0557, $C_{10}H_{19}N_3O_4{}^{79}Br$ requires $(M+NH_4)^+$ 324.0553. These data are in accordance with the literature.[14]

4.2.16 5-Di(*tert*-butyloxycarbonyl)aminomethyl-4-bromo-3-methoxyisoxazole (108)[14]

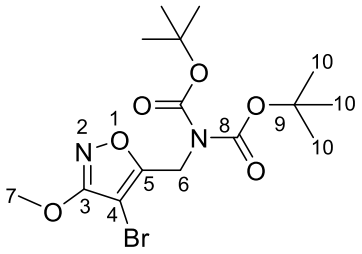

DMAP (32 mg, 0.26 mmol, 0.2 eq) and di-*tert*-butyl dicarbonate (0.60 mL, 2.6 mmol, 2.0 eq) were added to a solution of 5-(*tert*-butyloxycarbonyl)aminomethyl-4-bromo-3-methoxyisoxazole (**113**) (400 mg, 1.30 mmol, 1.0 eq) in MeCN (20 mL). The reaction mixture was heated under reflux for 3 h and allowed to cool to rt. The reaction was diluted with DCM (30 mL), and washed with water (40 mL). The aqueous layer was extracted into DCM (3 x 30 mL). The combined organic layers were combined, dried over MgSO4, filtered and concentrated under reduced pressure. The resulting brown oil was purified by silica gel column chromatography (petroleum ether/Et_2O, 80:20) to afford 5-di(*tert*-butyloxycarbonyl)aminomethyl-4-bromo-3-methoxyisoxazole (**108**) (497 mg, 91%) as a colourless crystalline solid: $\mathbf{R_f}$ 0.63 (petroleum ether/Et_2O, 70:30, ninhydrin); **mp** 73-74 °C [Lit.[14] 73-75 °C]; **FT-IR** (ATR, cm^{-1}) 2981, 1730 (C=O), 1694 (C=O), 1616, 1533, 1452, 1414, 1385, 1369, 1337, 1261, 1229, 1163, 1142, 1125, 1103, 1040, 968; δ_H (500 MHz, $CDCl_3$) 4.84 (2H, s, H-6), 4.02 (3H, s, H-7), 1.49 (18H, s, H-10); δ_C (125 MHz, $CDCl_3$) 169.3 (C-3), 166.2 (C-8), 151.6 (C-5), 83.6 (C-9), 82.2 (C-4), 57.7 (C-7), 41.8 (C-6), 28.1 (C-10); **HRMS** *m/z* (NSI^+), found: $[M+Na]^+$ 429.0631,

$C_{14}H_{17}N_9O_1{}^{79}BrNa$ requires $[M+Na]^+$ 429.0632. These data are in accordance with the literature.[14]

4.2.17 Methyl 3-isopropoxyisoxazole-5-carboxylate (115)[17]

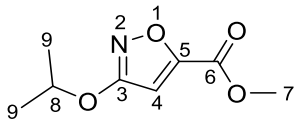

Isopropyl bromide (3.9 mL, 42.0 mmol, 1.5 eq) was added to a mixture of methyl 3-hydroxyisoxazole-5-carboxylate (**77**) (4.0 g, 28.0 mmol, 1.0 eq) and K_2CO_3 (4.3 g, 31.0 mmol, 1.1 eq) in DMF (50 mL). The mixture was stirred for 1 h at 60 °C then at 55 °C overnight. After cooling down to rt, water (80 mL) was added and the aqueous phase was extracted into Et_2O (3 x 50 mL). The combined organic layers were dried over $MgSO_4$, filtered and concentrated under reduced pressure. The resulting yellow residue was purified by silica gel column chromatography (petroleum ether/Et_2O, 90:10) to afford methyl 3-isopropoxyisoxazole-5-carboxylate (**115**) (4.0 g, 77%) as colourless oil: $\mathbf{R_f}$ 0.61 (petroleum ether/Et_2O, 80:20, UV/$KMnO_4$); δ_H (500 MHz, $CDCl_3$) 6.48 (1H, s, H-4), 4.93 (1H, sept, $^3J_{HH}$ 6.1, H-8), 3.92 (3H, s, H-7), 1.38 (6H, d, $^3J_{HH}$ 6.1, H-9); δ_C (125 MHz, $CDCl_3$) 170.9 (C-3), 160.0 (C-5), 157.3 (C-6), 101.5 (C-4), 74.2 (C-8), 52.9 (C-7), 21.9 (C-9); **HRMS** *m/z* (NSI^+), found: $[M+H]^+$ 186.0758, $C_8H_{12}NO_4$ requires $[M+H]^+$ 186.0761.The data were in good agreement with the literature values.[17]

4.2.18 5-Hydroxymethyl-3-isopropoxyisoxazole (116)

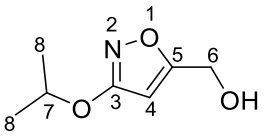

$NaBH_4$ (1.53 g, 40.5 mmol, 2.5 eq) was added to a solution of methyl 3-isopropoxyisoxazole-5-carboxylate (**115**) (3.00 g, 16.2 mmol, 1.0 eq) in MeOH (80 mL) at 0 °C. The mixture was stirred at rt overnight and quenched with a saturated solution NH_4Cl (50 mL). The reaction mixture was partitioned between water (60 mL) and EtOAc (60 mL). The aqueous layer was extracted into EtOAc (3 x 80 mL). The combined organic layers were washed with brine (50 mL), dried over $MgSO_4$, filtered and concentrated under reduced pressure to afford a pale yellowish oil, which was purified by silica gel column chromatography (petroleum ether/EtOAc, 80:20) to afford 5-hydroxymethyl-3-isopropoxyisoxazole (**116**) (2.29 g, 90%) as colourless oil: $\mathbf{R_f}$ 0.79 (petroleum ether/EtOAc, 70:30, $KMnO_4$); **FT-IR** (ATR, cm^{-1}) 3367 (OH), 2982, 1622, 1504, 1456, 1386, 1375, 1338, 1111; δ_H (500 MHz, $CDCl_3$) 5.83 (1H, s, H-4), 4.85 (1H, sept, $^3J_{HH}$ 6.1, H-7), 4.63 (2H, s, H-6), 2.61 (br s, 1H, -OH), 1.36 (6H, d, $^3J_{HH}$ 6.1, H-8); δ_C (125 MHz, $CDCl_3$) 171.9 (C-5), 171.2 (C-3), 94.1 (C-4), 73.5 (C-7), 56.9 (C-6), 22.0 (C-8); **HRMS** *m/z* (NSI^+), found: $[M+H]^+$ 158.0809, $C_7H_{12}NO_3$ requires $[M+H]^+$ 158.0812.

4.2.19 5-Bromomethyl-3-isopropoxyisoxazole (117)

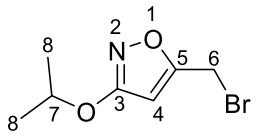

CBr_4 (7.26 g, 21.9 mmol, 2.2 eq) and PPh_3 (7.82 g, 29.8 mmol, 3.0 eq) were added to a solution of 5-hydroxymethyl-3-isopropoxyisoxazole (**116**) (1.56 g, 9.94 mmol, 1.0 eq) in DCM (100 mL) at 0 °C. The reaction mixture was stirred at rt for 12 h and concentrated under reduced pressure. The resulting residue was purified by silica gel column chromatography (petroleum ether/Et_2O, 95:5) to afford 5-bromomethyl-3-isopropoxyisoxazole (**117**) (1.27 g, 58%) as a colourless oil: $\mathbf{R_f}$ 0.66 (petroleum ether/Et_2O, 80:20 UV/$KMnO_4$); **FT-IR** (ATR, cm^{-1}) 2980, 1618, 1504, 1447, 1387, 1373, 1340, 1287, 1109, 1030, 916, 667; δ_H (500 MHz, $CDCl_3$) 5.90 (1H, s, H-4), 4.89 (1H, sept, $^3J_{HH}$ 6.1, H-7), 4.33 (2H, s, H-6), 1.38 (6H, d, $^3J_{HH}$ 6.1, H-8); δ_C (125 MHz, $CDCl_3$) 171.0 (C-3), 167.8 (C-5), 95.9 (C-4), 73.6 (C-7), 22.0 (C-8), 19.2 (C-6); **HRMS** *m/z* (ESI^+), found: $[M+H]^+$ 219.9969, $C_7H_{11}NO_2{}^{79}Br$ requires $[M+H]^+$ 219.9968.

4.2.20 5-Azidomethyl-3-isopropoxyisoxazole (118)

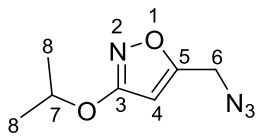

NaN_3 (1.6 g, 25.0 mmol, 5.0 eq) was added to a solution of 5-bromomethyl-3-isopropoxyisoxazole (**117**) (1.1 g, 5.0 mmol, 1.0 eq) in DMF (50 mL). After stirring at 80 °C for 3.5 h, the resulting solution was diluted with water (60 mL) and the product was extracted into Et_2O (5 x 60 mL). The combined organic layers were washed with a saturated solution of Na_2CO_3 (60 mL), dried over $MgSO_4$, filtered and concentrated under reduced pressure. The resulting yellowish oil was purified by silica gel column chromatography (petroleum ether/Et_2O, 95:5) to give 5-azidomethyl-3-isopropoxyisoxazole (**118**) (828 mg, 91%) as a colourless oil: $\mathbf{R_f}$ 0.64 (petroleum ether/Et_2O, 80:20, $KMnO_4$); **FT-IR** (ATR, cm^{-1}) 2980, 2100 (N_3), 1622, 1506, 1456, 1446, 1339, 1111, 1029; δ_H (500 MHz, $CDCl_3$) 5.87 (1H, s, H-4), 4.89 (1H, sept, $^3J_{HH}$ 6.1, H-7), 4.31 (2H, s, H-6), 1.38 (6H, d, $^3J_{HH}$ 6.1, H-8); δ_C ($CDCl_3$, 125 MHz) 171.1 (C-3), 166.9 (C-5), 95.5 (C-4), 73.7 (C-7), 45.9 (C-6), 22.0 (C-8); **HRMS** *m/z* (NSI^+), found: $[M+H]^+$ 183.0876, $C_7H_{11}N_4O_2$ requires $[M+H]^+$ 183.0877.

4.2.21 5-Aminomethyl-3-isopropoxyisoxazole (119)

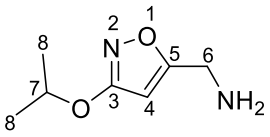

PMe_3 (1.0 M solution in THF, 13.2 mL, 13.2 mmol, 3.0 eq) was added to a solution of 5-azidomethyl-3-isopropoxyisoxazole (**118**) (800 mg, 4.40 mmol, 1.0 eq) in THF (30 mL) at 0 °C. The resulting mixture was stirred at 0 °C for 1 h and was quenched by slow addition of water (50 mL). The organic phase was separated and the aqueous phase was extracted into EtOAc (3 x 80 mL). The combined organic layers were washed with brine, dried over $MgSO_4$, filtered and concentrated under reduced pressure. The resulting residue was purified by silica gel column chromatography (EtOAc, 100) affording 5-aminomethyl-3-isopropoxyisoxazole (**119**) (446 mg, 65%) as yellowish oil: $\mathbf{R_f}$ 0.40 (EtOAc/MeOH, 80:20, ninhydrin); **FT-IR** (ATR, cm^{-1}) 3383, 3315 (NH_2), 2980, 1616, 1499, 1449, 1385, 1373, 1340, 1111, 1028; δ_H (500 MHz, $CDCl_3$) 5.70 (1H, t, $^4J_{HH}$ 0.7, H-4), 4.85 (1H, sept, $^3J_{HH}$ 6.1, H-7), 3.82 (2H, s, H-6), 1.56 (br s, 2H, -NH_2), 1.35 (6H, d, $^3J_{HH}$ 6.1, H-8); δ_C (125 MHz, $CDCl_3$) 174.3 (C-5), 171.2 (C-3), 92.6 (C-4), 73.2 (C-7), 38.8 (C-6), 22.0 (C-8); **HRMS** *m/z* (NSI^+), found: $[M+H]^+$ 157.0967, $C_7H_{13}N_2O_2$ requires $[M+H]^+$ 157.0972.

4.2.22 5-(*tert*-Butyloxycarbonyl)aminomethyl-3-isopropoxyisoxazole (120)[18]

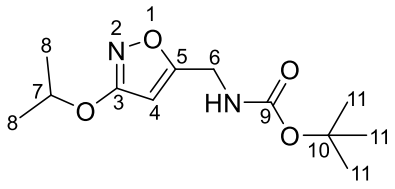

Na_2CO_3 (543 mg, 5.12 mmol, 2.0 eq) was added to a solution of 5-aminomethyl-3-isopropoxyisoxazole (**119**) (400 mg, 2.56 mmol, 1.0 eq) in dioxane/water (3:1 v/v mixture, 8 mL) at 0 °C, followed by dropwise addition of di-*tert*-butyl dicarbonate (0.65 mL, 2.82 mmol, 1.1 eq) in dioxane (2 mL). After stirring at rt overnight, dioxane was removed under reduced pressure and the residue was diluted with Et_2O (30 mL) and washed with water (50 mL). The aqueous layer was extracted into Et_2O (3 x 30 mL). The combined organic layers were combined, dried over $MgSO_4$, filtered and concentrated under reduced pressure. The resulting yellow residue was purified by silica gel column chromatography (petroleum ether/Et_2O, 70:30) to afford 5-(*tert*-butyloxycarbonyl)aminomethyl-3-isopropoxyisoxazole (**120**) (590 mg, 90%) as a colourless viscous oil that crystallised in time: $\mathbf{R_f}$ 0.74 (petroleum ether/Et_2O, 50:50, ninhydrin); **mp** 49-50 °C; **FT-IR** (ATR, cm^{-1}) 3306 (NH), 2980, 1712 (C=O), 1616, 1522 (NH), 1497, 1449, 1384, 1366, 1271, 1254, 1138, 1036, 901; δ_H (500 MHz, $CDCl_3$) 5.74 (1H, s, H-4), 5.00 (br s, 1H, -NH), 4.85 (1H, sept, $^3J_{HH}$ 6.1, H-7), 4.29 (2H, d, $^3J_{HH}$ 5.9, H-6), 1.44 (9H, s, H-11), 1.36 (6H, d, $^3J_{HH}$ 6.1, H-8); δ_C (125 MHz, $CDCl_3$) 171.2 (C-3), 170.2 (C-5), 155.6 (C-9), 94.0 (C-4), 80.4 (C-10), 73.4 (C-7), 37.1 (C-6), 28.4 (C-11), 22.0 (C-8); **HRMS** *m/z* (NSI^+), found: $[M+H]^+$ 257.1496, $C_{12}H_{21}N_2O_4$ requires $[M+H]^+$ 257.1496.

4.2.23 5-(*tert*-Butyloxycarbonyl)aminomethyl-4-fluoro-3-isopropoxyisoxazole (121)

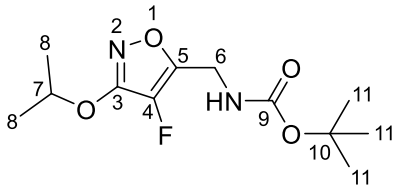

n-BuLi (1.7 mL, 2.5 M in hexanes, 4.29 mmol, 2.2 eq) was added dropwise to a solution of 5-(*tert*-butyloxycarbonyl)aminomethyl-3-isopropoxyisoxazole (**120**) (500 mg, 1.95 mmol, 1.0 eq) at -78 °C. The mixture was stirred for 1.5 h at -78 °C and added a solution of NFSI (676 mg, 2.15 mmol, 1.1 eq) in THF (2 mL). The mixture was stirred for 2 h at -78 °C and the temperature was allowed to warm to rt over 12 h. The reaction mixture was quenched with aqueous NH_4Cl (10 mL) and the organic phase was extracted into EtOAc (3 x 20 mL). The combined organic layers were dried over $MgSO_4$, filtered and concentrated under reduced pressure. The resulting residue was purified by silica gel column chromatography (petroleum ether/Et_2O, 80:20) to afford 5-(*tert*-butyloxycarbonyl)aminomethyl-4-fluoro-3-isopropoxyisoxazole (**121**) (160 mg, 30%) as a colourless viscous oil that crystallised in time: $\mathbf{R_f}$ 0.67 (petroleum ether/Et_2O, 50:50, ninhydrin); **mp** 63-65 °C; **FT-IR** (ATR, cm^{-1}) 3333 (NH), 2983, 1680 (C=O), 1612, 1526 (NH), 1285, 1269, 1252, 1107, 1078, 916, 907; δ_H (400 MHz, $CDCl_3$) 4.97 (br s, 1H, -NH, overlapped with H-7), 4.92 (1H, sept, $^3J_{HH}$ 6.1, H-7), 4.36 (2H, d, $^3J_{HH}$ 5.0, H-6), 1.44 (9H, s, H-11), 1.40 (6H, d, $^3J_{HH}$ 6.1, H-8); δ_C (125 MHz, $CDCl_3$) 161.5 (d, $^2J_{CF}$ 12.5, C-3), 155.5 (C-9), 152.3 (d, $^2J_{CF}$ 19.2, C-5), 134.3 (d, $^1J_{CF}$ 254.6, C-4), 80.5 (C-10), 74.6

(C-7), 35.0 (C-6), 28.4 (C-11), 22.0 (C-8); δ_F (376 MHz, $CDCl_3$) -188.0 (1F, s, CF); **HRMS** *m/z* (NSI^+), found: $[M+H]^+$ 275.1404, $C_{12}H_{20}N_2O_4F$ requires $[M+H]^+$ 275.1402.

4.2.24 5-Ammoniomethyl-4-fluoro-3-isopropoxyisoxazole trifluoroacetate (122)

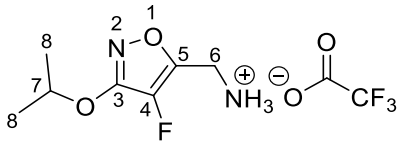

TFA (1.7 mL, 22.0 mmol, 40.0 eq) was added to a solution of 5-(*tert*-butyloxycarbonyl)aminomethyl-4-fluoro-3-isopropoxyisoxazole (**121**) (150 mg, 0.55 mmol, 1.0 eq) in DCM (8 mL). After stirring at rt overnight, the solvent was removed under reduced pressure and the resulting residue was purified by silica gel column chromatography (DCM/MeOH, 95:5) to afford 5-aminomethyl-4-fluoro-3-isopropoxyisoxazole trifluoroacetate salt (**122**) (155 mg, 98%) as light yellow solid: $\mathbf{R_f}$ 0.54 (DCM/MeOH, 90:10, ninhydrin); **mp** 116-118 °C; **FT-IR** (ATR, cm^{-1}) 2988, 2926, 2843, 2612, 1670 (C=O), 1541, 1516, 1508, 1435, 1381, 1352, 1339, 1290, 1242, 1120, 1177, 1138, 1103, 1064, 986; δ_H (400 MHz, CD_3CN) 6.76 (br s, 3H, $-NH_3$), 4.91 (1H, sept, $^3J_{HH}$ 6.1, H-7), 4.15 (2H, s, H-6), 1.38 (6H, d, $^3J_{HH}$ 6.1, H-8); δ_C (100 MHz, CD_3CN) 162.5 (q, $^2J_{CF}$ 30.5, TFA), 162.3 (d, $^2J_{CF}$ 12.5, C-3), 150.8 (d, $^2J_{CF}$ 20.4, C-5), 136.3 (d, $^1J_{CF}$ 255.7, C-4), 117.6 (q, $^1J_{CF}$ 291.9, TFA), 76.0 (C-7), 34.0 (C-6), 21.9 (C-8); δ_F (376 MHz, CD_3CN) -76.4 (3F, s, TFA), -186.5 (1F, s, CF);

HRMS *m/z* (ESI^+), found: $[M\text{-}TFA+H]^+$ 175.0876, $C_7H_{12}N_2O_2F$ requires $[M\text{-}TFA+H]^+$175.0877.

4.2.25 5-Aminomethyl-4-fluoro-3-hydroxyisoxazole (64)

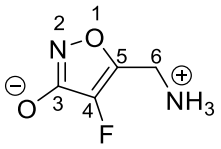

A solution of HBr 33% in AcOH (0.79 mL, 4.5 mmol, 25 eq) was added to 5-aminomethyl-4-fluoro-3-isopropoxyisoxazole trifluoroacetate (**122**) (53 mg, 0.18 mmol, 1.0 eq) and stirred at 60 °C for 17 h. The solvent was removed under vacuum and the residue was washed with water (3 x 2 mL). The residue was passed through a reverse phase C18 cartridge (Varian Mega Bond Elut C18, preconditioned with water) and the product was eluted with water (3 x 10 mL). The fractions were combined and concentrated under reduced pressure. The product was further purified by preparative HPLC (Waters system, using a Phenomenex Kingsorb C18 (250 x 21.2 mm, 5 μ) column equipped with security guard cartridge), with an isocratic mobile phase of H_2O at flow rate of 8.0 mL/min detected at 254 nm. Fractions containing product (t_R = 7.80 min) were collected and concentrated under reduced pressure. Fluoromuscimol (**64**) was obtained as a colourless solid after freeze drying (11 mg, 36%). Analytical HPLC analysis was performed using Shimadzu system (Phenomenex Kingsorb C18 (150 x 4.6 mm, 5 μ) column), with an isocratic mobile phase of H_2O at flow rate of 0.8 mL/min detected at 254 nm (t_R = 1.97 min, purity >99%); **mp** >200 °C (dec.); **FT-IR** (ATR, cm^{-1}) 3429, 2982, 2621 (br), 2237, 2099 (br),

1521, 1458, 1273, 1219, 1144, 1088, 1069, 988; δ_H (400 MHz, D_2O) 4.21 (2H, d, $^4J_{HF}$ 1.5, H-6); $^1H\{^{19}F\}$ (400 MHz, D_2O) 4.21 (2H, s, H-6); δ_C (176 MHz, D_2O) 167.8 (d, $^2J_{CF}$ 11.0, C-3), 145.6 (d, $^2J_{CF}$ 21.8, C-5), 139.1 (d, $^1J_{CF}$ 257.1, C-4), 32.5 (d, $^3J_{CF}$ 3.1, C-6); δ_F (376 MHz, D_2O) -185.2 (1F, s, CF); **HRMS** *m/z* (ESI^+), found: $[M+H]^+$ 133.0407, $C_4H_6N_2O_2F$ requires $[M+H]^+$133.0413.

4.2.26 5-Aminomethyl-3-hydroxyisoxazole (11)

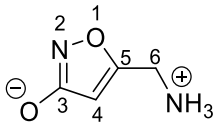

A solution of HBr 33% in AcOH (1.8 mL, 10.3 mmol, 25 eq) was added to 5-aminomethyl-3-isopropoxyisoxazole (**119**) (64 mg, 0.41 mmol, 1.0 eq) and stirred at 60 °C for 17 h. The solvent was removed under vacuum and the residue was washed with water (3 x 2 mL). The residue was passed through a reverse phase C18 cartridge (Varian Mega Bond Elut C18, preconditioned with water) and the product was eluted with water (3 x 10 mL). The fractions were combined and concentrated under reduced pressure. The product was further purified by preparative HPLC (Waters system, using a Phenomenex Kingsorb C18 (250 x 21.2 mm, 5 μ) column equipped with security guard cartridge), with an isocratic mobile phase of H_2O at flow rate of 8.0 mL/min detected at 254 nm. Fractions containing product (t_R = 7.95 min) were collected and concentrated under reduced pressure. Muscimol (**11**) was obtained as a colourless solid after freeze drying (16 mg, 34%). Analytical HPLC analysis was performed using

Shimadzu system (Phenomenex Kingsorb C18 (150 x 4.6 mm, 5 μ) column), with an isocratic mobile phase of H_2O at flow rate of 0.8 mL/min detected at 254 nm (t_R= 1.98 min, purity >99%); **mp** 171-173 °C (dec.) [Lit.[19] 170-172 °C (decomp)]; δ_H (400 MHz, D_2O) 4.15 (s, 2H, H-6), 5.87 (s, 1H, H-4); δ_C (176 MHz, D_2O) 176.2 (C-3), 165.8 (C-5), 98.9 (C-4), 34.9 (C-6); **HRMS** *m/z* (ESI^+), found: $[M+H]^+$ 115.0501, $C_4H_7N_2O_2$ requires $[M+H]^+$ 115.0508. These data are in accordance with the literature.[19]

4.2.27 5-Azidomethyl-4-iodo-3-isopropoxyisoxazole (126)

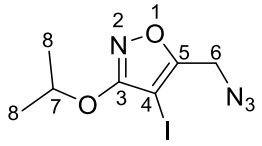

NIS (202 mg, 0.90 mmol, 1.5 eq) was added to a solution of 5-azidomethyl-3-isopropoxyisoxazole (**118**) (110 mg, 0.60 mmol, 1.0 eq) in TFA (5 mL) at rt. After stirring at rt overnight, the solvent was removed under reduced pressure and the residue was purified by silica gel column chromatography (petroleum ether/Et_2O, 95:5), affording 5-azidomethyl-4-iodo-3-isopropoxyisoxazole (**126**) (159 mg, 86%) as yellowish oil: $\mathbf{R_f}$ 0.87 (petroleum ether/Et_2O, 90:10, UV/$KMnO_4$); **FT-IR** (ATR, cm^{-1}) 2980, 2095 (N_3), 1607, 1506, 1427, 1387, 1373, 1333, 1287, 1182, 1109, 1087, 914, 839, 768, 700; δ_H (500 MHz, $CDCl_3$) 4.95 (1H, sept, $^3J_{HH}$ 6.2, H-7), 4.37 (2H, s, H-6), 1.42 (6H, d, $^3J_{HH}$ 6.2, H-8); δ_C (125 MHz, $CDCl_3$) 170.3 (C-3), 167.4 (C-5), 74.9 (C-7), 53.2 (C-4), 45.3 (C-6), 21.9 (C-8); **HRMS** *m/z* (NSI^+), found: $[M+H]^+$ 308.9846, $C_7H_{10}N_4O_2{}^{127}I$ requires $[M+H]^+$ 308.9843.

4.2.28 5-Aminomethyl-4-iodo-3-isopropoxyisoxazole (127)

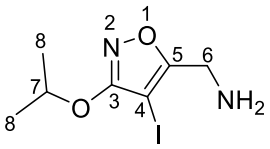

PMe_3 (1.0 M solution in THF, 1.47 mL, 1.47 mmol, 3.0 eq) was added to a solution of 5-azidomethyl-4-iodo-3-isopropoxyisoxazole (**126**) (150 mg, 0.49 mmol, 1.0 eq) in THF (8 mL) at 0 °C. The resulting mixture was stirred at 0 °C for 1 h and was quenched by slow addition of water (10 mL). The organic phase was separated and the aqueous phase was extracted into EtOAc (3 x 20 mL). The combined organic layers were washed with brine, dried over $MgSO_4$, filtered and concentrated under reduced pressure and the residue was purified by silica gel column chromatography (EtOAc, 100), affording 5-aminomethyl-4-iodo-3-isopropoxyisoxazole (**127**) (114 mg, 83%) as yellowish oil: $\mathbf{R_f}$ 0.50 (EtOAc/MeOH, 90:10, UV/ninhydrin); **FT-IR** (ATR, cm^{-1}) 3397, 3377 (NH_2), 2978, 1593, 1502, 1431, 1385, 1373, 1335, 1107, 1084, 916, 837, 754, 721, 691; δ_H (500 MHz ,$CDCl_3$) 4.91 (1H, sept, $^3J_{HH}$ 6.2, H-7), 3.85 (2H, s, H-6), 1.53 (br s, 2H, -NH_2), 1.39 (6H, d, $^3J_{HH}$ 6.2, H-8); δ_C (125 MHz, $CDCl_3$) 173.2 (C-5), 170.2 (C-3), 74.4 (C-7), 49.2 (C-4), 38.5 (C-6), 21.9 (C-8); **HRMS** *m/z* (NSI^+), found: $[M+H]^+$ 282.9935, $C_7H_{12}N_2O_2{}^{127}I$ requires $[M+H]^+$ 282.9938.

4.2.29 5-(*tert*-Butyloxycarbonyl)aminomethyl-4-iodo-3-isopropoxyisoxazole (128)

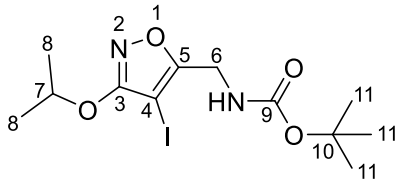

Na_2CO_3 (541 mg, 5.10 mmol, 2.0 eq) was added to a solution of 5-aminomethyl-4-iodo-3-isopropoxyisoxazole (**127**) (720 mg, 2.55 mmol, 1.0 eq) in dioxane/water (3:1 v/v mixture, 16 mL) at 0 °C, followed by dropwise addition of di-*tert*-butyl dicarbonate (0.65 mL, 2.81 mmol, 1.1 eq) in dioxane (2 mL). After stirring at rt overnight, dioxane was removed under reduced pressure and the residue was diluted with Et_2O (40 mL) and washed with water (50 mL). The aqueous layer was extracted into Et_2O (3 x 40 mL). The combined organic layers were combined, dried over $MgSO_4$, filtered and concentrated under reduced pressure. The resulting yellow residue was purified by silica gel column chromatography (petroleum ether/Et_2O, 70:30) to afford 5-(*tert*-butyloxycarbonyl)aminomethyl-4-iodo-3-isopropoxyisoxazole (**128**) (788 mg, 81%) as a colourless viscous oil: $\mathbf{R_f}$ 0.53 (petroleum ether/Et_2O, 60:40, UV/ninhydrin); **FT-IR** (ATR, cm^{-1}) 3352 (NH), 2980, 1699 (C=O), 1603, 1506 (NH), 1433, 1387, 1368, 1337, 1281, 1250, 1167, 1090, 916; δ_H (500 MHz, $CDCl_3$) 4.98 (br s, 1H, -NH), 4.90 (1H, sept, $^3J_{HH}$ 6.2, H-7), 4.37 (2H, d, $^3J_{HH}$ 5.9, H-6), 1.44 (9H, s, H-11), 1.39 (6H, d, $^3J_{HH}$ 6.2, H-8); δ_C (125 MHz, $CDCl_3$) 170.3 (C-3), 169.3 (C-5), 155.4 (C-9), 80.4 (C-10), 74.5 (C-7), 50.5 (C-4), 37.1 (C-6), 28.5 (C-11), 21.9 (C-8); **HRMS** *m/z* (ESI^+), found: $[M+Na]^+$ 405.0273, $C_{12}H_{19}N_2O_4{}^{127}INa$ requires $[M+Na]^+$ 405.0282.

4.2.30 5-Di(*tert*-butyloxycarbonyl)aminomethyl-4-iodo-3-isopropoxyisoxazole (129)

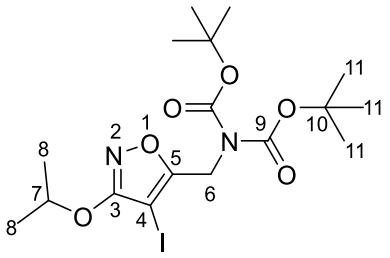

DMAP (34.2 mg, 0.28 mmol, 0.2 eq) and di-*tert*-butyl dicarbonate (0.65 mL, 2.82 mmol, 2.0 eq) were added to a solution of 5-(*tert*-butyloxycarbonyl)aminomethyl-4-iodo-3-isopropoxyisoxazole (**128**) (540 mg, 1.41 mmol, 1.0 eq) in MeCN (25 mL). The reaction mixture was heated under reflux for 3 h and allowed to cool to rt. The reaction was diluted with DCM (20 mL), and washed with water (30 mL). The aqueous layer was extracted into DCM (3 x 30 mL). The combined organic layers were combined, dried over $MgSO_4$, filtered and concentrated under reduced pressure. The resulting brown oil was purified by silica gel column chromatography (petroleum ether/Et_2O, 90:10) to afford 5-di(*tert*-butyloxycarbonyl)aminomethyl-4-iodo-3-isopropoxyisoxazole (**129**) (592 mg, 87%) as a colourless viscous oil: $\mathbf{R_f}$ 0.68 (petroleum ether/Et_2O, 70:30, UV/ninhydrin); **FT-IR** (ATR, cm^{-1}) 2986, 1730 (C=O), 1688 (C=O), 1601, 1510, 1435, 1416, 1383, 1368, 1337, 1227, 1165, 1140, 1121, 1090, 918, 858, 849, 791, 760; δ_H (500 MHz, $CDCl_3$) 4.90 (1H, sept, $^3J_{HH}$ 6.2, H-7), 4.83 (2H, s, H-6), 1.48 (18H, s, H-11), 1.39 (6H, d, $^3J_{HH}$ 6.2, H-8); δ_C (125 MHz, $CDCl_3$) 171.0 (C-3), 169.7 (C-9), 151.7 (C-5), 83.5 (C-10), 74.4 (C-7), 48.8 (C-4), 42.7 (C-6),

28.2 (C-11), 21.9 (C-8); **HRMS** *m/z* (ESI^+), found: $[M+Na]^+$ 505.0796, $C_{17}H_{27}N_2O_6{}^{127}INa$ requires $[M+Na]^+$ 505.0806.

4.2.31 5-Di(*tert*-butyloxycarbonyl)aminomethyl-4-trifluoromethyl-3-isopropoxyisoxazole (130)

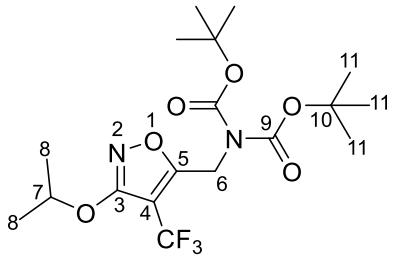

Methyl 2,2-difluoro-2-(fluorosulfonyl) acetate (MFDSA) (945 mg, 4.92 mmol, 4.0 eq) was added to a preformed solution of 5-di(*tert*-butyloxycarbonyl)aminomethyl-4-iodo-3-isopropoxyisoxazole (**129**) (592 mg, 1.23 mmol, 1.0 eq), copper(I) iodide (47.6 mg, 0.25 mmol, 0.2 eq) and HMPA (1 ml) in DMF (8 ml). The reaction mixture was heated under reflux at 80 °C for 24 h. The clear, dark orange reaction mixture was cooled to room temperature and diluted with Et_2O (10 ml), washed with a saturated aqueous solution of NH_4Cl (15 ml) and brine (15 ml). The aqueous layer was back-extracted into Et_2O (3 x 20 ml) and the combined organic layers were combined, dried over $MgSO_4$, filtered and concentrated under reduced pressure. The resulting yellowish oil was purified by silica gel column chromatography (petroleum ether/Et_2O, 90:10) to afford 5-di(*tert*-butyloxycarbonyl)aminomethyl-4-trifluoromethyl-3-isopropoxyisoxazole (**130**) (177 mg, 34%) as a colourless viscous oil: $\mathbf{R_f}$ 0.66 (petroleum ether/Et_2O, 80:20, ninhydrin);

FT-IR (ATR, cm^{-1}) 2982, 1761 (C=O), 1699 (C=O), 1647, 1516, 1472, 1718, 1369, 1333, 1308, 1260, 1227, 1130, 1109, 1078, 1036, 918, 854, 843.764; δ_H (400 MHz, $CDCl_3$) 4.97 (2H, q, $^5J_{HF}$ 1.0, H-6), 4.91 (1H, sept, $^3J_{HH}$ 6.2, H-7), 1.49 (18H, s, H-11), 1.40 (6H, d, $^3J_{HH}$ 6.2, H-8); **^{1}H{^{19}F}** (400 MHz, $CDCl_3$) 4.97 (2H, s, H-6), 4.91 (1H, sept, $^3J_{HH}$ 6.2, H-7), 1.49 (18H, s, H-11), 1.40 (6H, d, $^3J_{HH}$ 6.2, H-8); δ_C (176 MHz, $CDCl_3$) 169.4 (C-9), 167.4 (C-3), 151.6 (C-5), 121.2 (q, $^1J_{CF}$ 254.6, CF_3), 99.2 (q, $^2J_{CF}$ 39.4, C-4), 83.8 (C-10), 74.9 (C-7), 42.2 (C-6), 28.1 (C-11), 21.8 (C-8); δ_F (376 MHz, $CDCl_3$) -57.7 (3F, t, $^5J_{HF}$ 1.0, CF_3); **^{19}F{^{1}H}** (376 MHz, $CDCl_3$) -57.7 (s, CF_3);. **HRMS** *m/z* (ESI^+), found: $[M+Na]^+$ 447.1704, $C_{18}H_{27}N_2O_6F_3Na$ requires $[M+Na]^+$ 447.1713.

4.2.32 5-Aminomethyl-4-trifluoromethyl-3-hydroxyisoxazole (65)

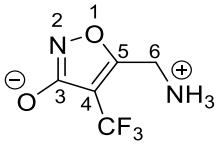

TFA (0.17 mL, 2.2 mmol, 20.0 eq) was added to a solution of 5-di(*tert*-butyloxycarbonyl)aminomethyl-4-trifluoromethyl-3-isopropoxyisoxazole (**130**) (45 mg, 0.11 mmol, 1.0 eq) in DCM (5 mL). After stirring at rt for 6 h, the solvent was removed under reduced pressure to afford a hygroscopic colourless crystalline solid contained (**135**) (35 mg), which was used in the subsequent step without further purification. A solution of HBr 33% in AcOH (0.9 mL, 5.0 mmol, 50 eq) was added to crude (**135**) (35 mg, 0.10 mmol, 1.0 eq) and stirred at 60 °C for 48 h. The solvent was removed under vacuum and the residue was washed

with water (3 x 2 mL). The residue was passed through a reverse phase C18 cartridge (Varian Mega Bond Elut C18, preconditioned with water) and the product was eluted with water (3 x 10 mL). The fractions were combined and concentrated under reduced pressure. The product was further purified by preparative HPLC (Waters system, using a Phenomenex Kingsorb C18 (250 x 21.2 mm, 5 μ) column equipped with security guard cartridge) with an isocratic mobile phase of H_2O at flow rate of 8.0 mL/min detected at 254 nm. Fractions containing product (t_R = 9.10 min) were collected and concentrated under reduced pressure. Trifluoromethylmuscimol (**65**) was obtained as a colourless solid after freeze drying (7.2 mg, 36% over 2 steps). Analytical HPLC analysis was performed using Shimadzu system (Phenomenex Kingsorb C18 (150 x 4.6 mm, 5 μ) column), with an isocratic mobile phase of H_2O at flow rate of 0.8 mL/min detected at 254 nm (t_R = 2.27 min, purity >98%); **mp** 165-168 °C (dec); **FT-IR** (ATR, cm^{-1}) 2997, 2891, 2631 (br), 1667, 1491, 1425, 1371, 1344, 1161, 1109, 1042, 978, 745; δ_H (400 MHz, D_2O) 4.38 (s, H-6); δ_C (176 MHz, D_2O) 172.2 (C-3), 163.7 (C-5), 121.6 (q, $^1J_{CF}$ 267.8, CF_3), 103.2 (q, $^2J_{CF}$ 39.5, C-4), 34.5 (C-6); δ_F (376 MHz, D_2O) -58.9 (s, CF_3); **HRMS** *m/z* (ESI^+), found: $[M+H]^+$ 183.0373, $C_5H_6N_2O_2F_3$ requires $[M+H]^+$ 183.0381.

4.2.33 Methyl 4-iodo-3-methoxyisoxazole-5-carboxylate (166)

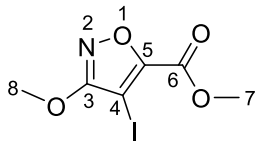

Methyl-3-methoxyisoxazole-5-carboxylate (**94**) (680 mg, 4.33 mmol, 1.0 eq), NIS (1.95 g, 8.66 mmol, 2.0 eq), and TFA (19 mL) were placed in a 10 ml glass microwave vessel. The reaction vessel was sealed with a rubber lid (CEM) and heated under microwave irradiation at 150 °C (50 W) for 3 h. The solvent was removed under reduced pressure and the residue was purified by silica gel column chromatography (petroleum ether/Et_2O, 90:10), furnishing methyl 4-iodo-3-methoxyisoxazole-5-carboxylate (**166**) (980 mg, 80%) as colourless crystalline solid: $\mathbf{R_f}$ 0.47 (petroleum ether/Et_2O, 80:20, UV/$KMnO_4$); **mp** 140-141 °C; **FT-IR** (ATR, cm^{-1}) 2963, 1730 (C=O), 1518, 1445, 1431, 1406, 1269, 1211, 1204, 1169, 1090, 1032, 978, 945, 918, 808, 773, 698, 606; δ_H (500 MHz, $CDCl_3$) 4.08 (3H, s, H-8), 3.97 (3H, s, H-7); δ_C (125 MHz, $CDCl_3$) 172.1 (C-3), 159.2 (C-5), 156.7 (C-6), 58.2 (C-8), 57.9 (C-4), 53.0 (C-7); **HRMS** *m/z* (NSI^+), found $[M+H]^+$ 283.9419, $C_6H_7NO_4{}^{127}I$ requires $[M+H]^+$ 283.9414.

4.2.34 Tributyl(4-methoxyphenyl)stannane (170)[20]

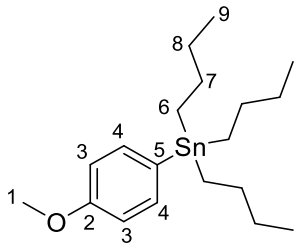

4-Methoxyphenylmagnesium bromide (0.50 M in THF, 8.0 mL, 4.0 mmol, 2.0 eq) was added to a solution of tributyltin chloride (652 mg, 2.00 mmol, 1.0 eq) in THF (2 mL). After stirring for 2 h at 60 °C, the reaction mixture was cooled to 0 °C and quenched with saturated aqueous solution of NH_4Cl (10 mL) and Et_2O (10 ml) was added. The phases were separated and the aqueous phase was extracted with Et_2O (3 x 10 mL). The combined organic layers were washed with brine (20 mL), dried over Na_2SO_4, filtered and concentrated under reduced pressure. The residue was purified by fractional distillation to afford tributyl(4-methoxyphenyl)stannane (**170**) (630 mg, 79%) as a colourless oil: δ_H (500 MHz, $CDCl_3$) 7.43-7.28 (m, 2H, H-3), 6.93-6.90 (m, 2H, H-4), 3.81 (s, 1H, H-1), 1.57-1.51 (m, 6H, H-7), 1.37-1.30 (m, 6H, H-8), 1.04-1.02 (m, 6H, H-6), 0.89 (t, $^3J_{HH}$ 7.3, H-9); δ_C (100 MHz, $CDCl_3$) 159.8 (C-2), 137.6 (C-3), 132.1 (C-5), 114.1 (C-4), 55.1 (C-1), 29.2 (C-7), 27.5 (C-8), 13.8 (C-9), 9.7 (C-6). These data are in accordance with the literature.[20]

4.2.35 (3-Methoxy-5-(methoxycarbonyl)isoxazol-4-yl) (4-methoxyphenyl)iodonium trifluoroacetate (171)

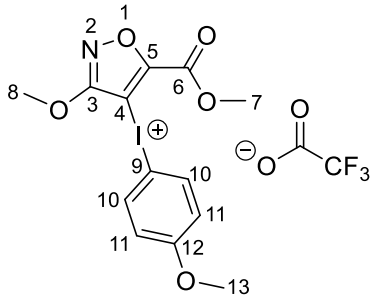

*m*CPBA (70% active oxidant, 791 mg, 3.21 mmol, 1.3 eq) was added to a solution of methyl 4-iodo-3-methoxyisoxazole-5-carboxylate (**166**) (700 mg, 2.47 mmol, 1.0 eq) in AcOH (20 ml). After stirring at 55 °C for 96 h, water (30 ml) was added to the reaction mixture and it was extracted into DCM (3 x 20 ml). The combined organic layers were washed with a saturated aqueous solution of Na_2CO_3 (60 mL), dried over Na_2SO_4, filtered and concentrated under reduced pressure to afford a colourless solid, which was used without further purification.

Methyl (4-diacetoxyiodo)-3-methoxyisoxazole-5-carboxylate (**167**) (281 mg, 0.7 mmol, 1.0 eq as a 40% mixture determined by ^{1}H-NMR with methyl 4-iodo-3-methoxyisoxazole-5-carboxylate (**166**)), was dissolved in DCM (10 ml) and cooled to -30 °C, followed by dropwise addition of TFA (110 µL, 1.40 mmol, 2.0 eq). The solution was stirred with exclusion of light for 30 min, followed by 1 h at rt. The reaction mixture was re-cooled to -30 °C and tributyl(4-methoxyphenyl)stannane (**170**) (278 mg, 0.70 mmol, 1.0 eq) was added. The reaction was warmed to rt for the second time and left to stir overnight. The solvent was removed under *vacuo*, leaving the addition of Et_2O to afford (3-methoxy-5-(methoxycarbonyl)isoxazol-4-yl)(4-methoxyphenyl)iodonium TFA

salt (**171**) (35 mg, 10%) as colourless crystalline solid: **mp** 150-153 °C (dec.); **FT-IR** (ATR, cm^{-1}) 1732 (C=O), 1655, 1523, 1487, 1294, 1260, 1145, 1132, 1028, 819, 797, 719; δ_H (500 MHz, d_6-DMSO) 8.00 (2H, d, $^3J_{HH}$ 7.2, H-10), 7.06 (2H, d, $^3J_{HH}$ 7.2, H-11), 4.07 (3H, s, H-7), 4.01 (3H, s, H-8), 3.80 (3H, s, H-13); δ_C (125 MHz, d_6-DMSO) 170.1 (C-6), 162.0 (C-12), 161.0 (C-5), 155.3(C-3), 137.0 (C-10), 117.5 (C11), 107.0 (C-9), 83.9(C-4), 59.0(C-7), 55.7(C-13), 54.0 (C-8); δ_F (470 MHz, d_6-DMSO) -73.6 (3F, s, TFA); **HRMS** *m/z* (ESI^+), found $[M\text{-}TFA]^+$ 389.9819, $C_{13}H_{13}NO_5{}^{127}I$ requires $[M\text{-}TFA]^+$ 389.9833.

4.2.36 4-Iodo-3-methoxy-5-(methoxymethyl)isoxazole (173)

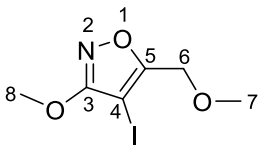

NIS (997 mg, 4.43 mmol, 1.5 eq) was added to a solution of 3-methoxy-5-(methoxymethyl)isoxazole (**96**) (422 mg, 2.95 mmol, 1.0 eq) in TFA (10 mL). After stirring at rt overnight, the solvent was removed under reduced pressure and the residue was purified by silica gel column chromatography (petroleum ether/Et_2O, 90:10), affording 4-iodo-3-methoxy-5-(methoxymethyl)isoxazole (**173**) (696 mg, 88%) as colourless crystalline solid: $\mathbf{R_f}$ 0.50 (petroleum ether/Et_2O, 70:30, UV/$KMnO_4$); **mp** 88-89 °C; **FT-IR** (ATR, cm^{-1}) 2990, 1609, 1526, 1447, 1408, 1371, 1277, 1192, 1105, 1086, 1053, 959, 947, 928, 783, 716, 546; δ_H (500 MHz, $CDCl_3$) 4.47 (2H, s, H-6) 4.03 (3H, s, H-8), 3.40 (3H, s, H-7); δ_C (125 MHz, $CDCl_3$) 171.5 (C-3), 169.8 (C-5), 64.8 (C-6), 59.0 (C-7), 57.8

(C-8), 51.7 (C-4); **HRMS** *m/z* (ESI^+), found: $[M+H]^+$ 269.9619, $C_6H_9NO_3{}^{127}I$ requires $[M+H]^+$ 269.9627.

4.2.37 (3-Methoxy-5-(methoxymethyl)isoxazol-4-yl) (4-methoxyphenyl)iodonium tetrafluoroborate (176)

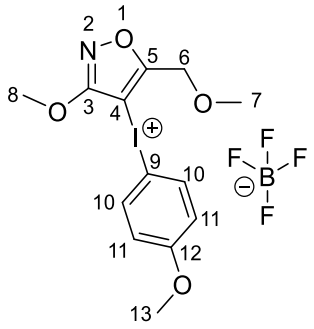

4-Iodo-3-methoxy-5-(methoxymethyl)isoxazole (**173**) (70 mg, 0.26 mmol, 1.0 eq) and $BF_3{\cdot}Et_2O$ (80 μL, 0.65 mmol, 2.5 eq) were added to a solution of *m*CPBA (70% active oxidant, 83 mg, 0.34 mmol, 1.3 eq) in DCM (1.5 mL) at rt. The resulting yellow solution was stirred at rt for 2 h and cooled to 0 °C, 4-methoxyphenylboronic acid (43 mg, 0.29 mmol, 1.1 eq) was added and the temperature was allowed to warm to rt. After 2 h of stirring, the crude mixture was applied on silica plug (0.8 g) and eluted with DCM (10 mL) to remove unreacted ArI (**173**) and *m*CBA followed by (DCM/MeOH) (20:1 v/v mixture, 42 mL) to elute the product, leaving any boronic acid derivatives on the column. The latter solution was concentrated and Et_2O (1 mL) was added to the residue to induce precipitation. The ether phase was decanted and the solid was washed twice more with Et_2O (2 x 1 mL) and dried in *vacuo* to give (3-methoxy-5-(methoxymethyl)isoxazol-4-yl)(4-methoxyphenyl)iodonium tetrafluoroborate salt (**176**) in (60 mg, 50%) as a pale yellow solid: **mp** 161-163 °C (dec.);

FT-IR (ATR, cm^{-1}) 2945, 1601, 1497, 1408, 1246, 1088, 1039, 756, 692; δ_H (500 MHz, d_6-DMSO) 8.00 (2H, d, $^3J_{HH}$ 8.9, H-10), 7.08 (2H, d, $^3J_{HH}$ 8.9, H-11), 4.79 (2H, s, H-6), 4.02 (3H, s, H-8), 3.80 (3H, s, H-13), 3.38 (3H, s, H-7); δ_C (125 MHz, d_6-DMSO) 174.4 (C-5), 169.6 (C-3), 162.0 (C-12), 136.9 (C-10), 117.6 (C-11), 106.7 (C-9), 78.0 (C-4), 64.6 (C-6), 58.8 (C-7), 58.6 (C-8), 55.8 (C-13); δ_F (470 MHz, d_6-DMSO) -148.17, -148.23 (4F, s, BF_4^-); **HRMS** *m/z* (ESI^+), found: $[M\text{-}BF_4]^+$ 376.0028, $C_{13}H_{15}NO_4{}^{127}I$ requires $[M\text{-}BF_4]^+$ 376.0040].

4.2.38 Mesityl(3-methoxy-5-(methoxymethyl)isoxazol-4-yl)iodonium tetrafluoroborate (177)

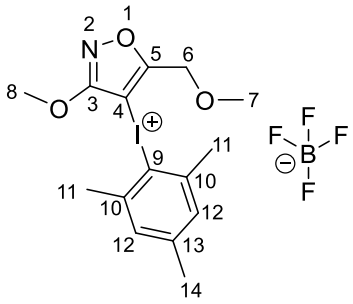

4-Iodo-3-methoxy-5-(methoxymethyl)isoxazole (**173**) (70 mg, 0.26 mmol, 1.0 eq) and $BF_3{\cdot}Et_2O$ (80 μL, 0.65 mmol, 2.5 eq) were added to a solution of *m*CPBA (70% active oxidant, 83 mg, 0.34 mmol, 1.3 eq) in DCM (1.5 mL) at rt. The resulting yellow solution was stirred at rt for 2 h and cooled to 0 °C, 2,4,6-trimethylphenylboronic acid (48 mg, 0.29 mmol, 1.1 eq) was added and the temperature was allowed to warm to rt. After 2 h of stirring, the crude mixture was applied on silica plug (0.8 g) and eluted with DCM (10 mL) to remove unreacted ArI (**173**) and *m*CBA followed by (DCM/MeOH) (20:1 v/v mixture, 42 mL) to elute the product, leaving any boronic acid derivatives on the column.

The latter solution was concentrated, and Et_2O (1 mL) was added to the residue to induce precipitation. The ether phase was decanted and the solid was washed twice more with Et_2O (2 x 1 mL) and dried in *vacuo* to give mesityl(3-methoxy-5-(methoxymethyl)isoxazol-4-yl)iodonium tetrafluoroborate salt (**177**) in (55 mg, 45%) as a pale yellow solid: ; **mp** 157-160 °C (dec.); **FT-IR** (ATR, cm^{-1}) 2916, 1607, 1470, 1377, 1032, 1003, 962, 835, 687; δ_H (500 MHz, d_6-DMSO) 7.20 (2H, s, H-12), 4.72 (2H, s, H-6), 3.96 (3H, s, H-8), 3.37 (3H, s, H-7), 2.63 (6H, s, H-11), 2.29 (3H, s, H-14); δ_C (125 MHz, d_6-DMSO) 174.3 (C-5), 169.9 (C-3), 143.0 (C-13), 141.5 (C-10), 129.6 (C-12), 123.9 (C-9), 75.9 (C-4), 64.7 (C-6), 58.9 (C-7), 58.5 (C-8), 26.0 (C-11), 20.5 (C-14); δ_F (470 MHz, d_6-DMSO) -148.16, -148.21 (4F, s, BF_4^-); **HRMS** *m/z* (ESI^+), found: $[M\text{-}BF_4]^+$ 388.0392, $C_{15}H_{19}NO_3{}^{127}I$ requires $[M\text{-}BF_4]^+$ 388.0404.

4.2.39 5-Aminomethyl-4-iodo-3-hydroxyisoxazole (165)

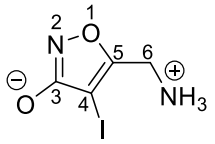

A solution of HBr 33% in AcOH (1.7 mL, 9.5 mmol, 25 eq) was added to 5-aminomethyl-4-iodo-3-isopropoxyisoxazole (**127**) (107 mg, 0.38 mmol, 1.0 eq) and stirred at 60 °C for 17 h. The solvent was removed under vacuum and the residue was washed with water (3 x 2 mL). The residue was passed through a reverse phase C18 cartridge (Varian Mega Bond Elut C18, preconditioned with water) and the product was eluted with water (3 x 10 mL). The fractions were combined and concentrated under reduced pressure. The product was further

purified by preparative HPLC (Waters system, using a Phenomenex Kingsorb C18 (250 x 21.2 mm, 5 μ) column equipped with security guard cartridge), with an isocratic mobile phase of H_2O at flow rate of 8.0 mL/min detected at 254 nm. Fractions containing product (t_R = 8.97 min) were collected and concentrated under reduced pressure. Iodomuscimol (**165**) was obtained as a colourless solid after freeze drying (17.3 mg, 19%). Analytical HPLC analysis was performed using Shimadzu system (Phenomenex Kingsorb C18 (150 x 4.6 mm, 5 μ) column), with an isocratic mobile phase of H_2O at flow rate of 0.8 mL/min detected at 254 nm (t_R = 2.19 min, purity >99%); **mp** 161-162 °C; **FT-IR** (ATR, cm^{-1}) 3350, 2990, 2637 (br), 2363, 1616, 1487, 1358, 1254, 1077, 1037, 968; δ_H (400 MHz, D_2O) 4.21 (s, 2H, H-6); δ_C (176 MHz, D_2O) 176.4 (C-3), 163.2 (C-5), 61.6 (C-4), 35.3 (C-6); **HRMS** *m/z* (ESI^+), found: $[M+H]^+$ 240.9466, $C_4H_6N_2O_2{}^{127}I$ requires $[M+H]^+$ 240.9474.

4.3 References

1 W. L. F. Armarego and C. L. L. Chai, *Purification of Organic Chemicals*, Butterworth-Heinemann, London, 6th edn., 2009.

2. *CrystalClear-SM Expert* v2.0 and v2.1. Rigaku Americas, The Woodlands, Texas, USA, and Rigaku Corporation, Tokyo, Japan, 2010-2013.

3. *CrysAlisPro* v1.171.38.41. Rigaku Oxford Diffraction, Rigaku Corporation, Oxford, U.K. 2015.

4 P. T. Beurskens, G. Beurskens, R. de Gelder, S. Garcia-Granda, R. O. Gould, R. Israel and J. M. M. Smits, *DIRDIF-99*, Crystallography Laboratory, University of Nijmegen, The Netherlands, 1999.

5 M. C. Burla, R. Caliandro, M. Camalli, B. Carrozzini, G. L. Cascarano, L. De Caro, C. Giacovazzo, G. Polidori and R. Spagna, *J. Appl. Crystallogr.*, 2005, **38**, 381–388.

6 M. C. Burla, R. Caliandro, M. Camalli, B. Carrozzini, G. L. Cascarano, C. Giacovazzo, M. Mallamo, A. Mazzone, G. Polidori and R. Spagna, *J. Appl. Crystallogr.*, 2012, **45**, 357–361.

7 G. M. Sheldrick, *Acta Crystallogr. Sect. C*, 2015, **71**, 3–8.

8. *CrystalStructure* v4.2. Rigaku Americas, The Woodlands, Texas, USA, and Rigaku Corporation, Tokyo, Japan, 2013.

9 E. Sahin, N. Kishali, L. Kelebekli, E. Mete, H. Secen, R. Altundas and Y. Kara, *Org. Prep. Proced. Int.*, 2007, **39**, 509–513.

10 M. Frey and V. Jäger, *Synthesis*, 1985, 1100–1104.

11 A. Melikian, G. Schlewer, J. P. Chambon and C. G. Wermuth, *J. Med. Chem.*, 1992, **35**, 4092–4097.

12 E. Falch, P. Krogsgaard-Larsen, P. Jacobsen, A. Engesgaard, C. Braestrup and D. R. Curtis, *Eur. J. Med. Chem.*, 1985, **20**, 447–453.

13 D. J. Kempf, H. L. Sham, K. C. Marsh, C. A. Flentge, D. Betebenner, B. E. Green, E. McDonald, S. Vasavanonda, A. Saldivar, N. E. Wideburg, W. M. Kati, L. Ruiz, C. Zhao, L. Fino, J. Patterson, A. Molla, J. J. Plattner and D. W. Norbeck, *J. Med. Chem.*, 1998, **41**, 602–617.

14 R. Wadoux, MPhil Thesis, University of St Andrews, 2013.

15 A. Plant, J. E. Boehmer, J. Black and T. D. Sparks, WO2006/024820 A1, 2006.

16 J. J. Hansen and P. Krogsgaard-Larsen, *J. Chem. Soc. Perkin Trans. 1*, 1980, 1826–1833.

17 S. B. Vogensen, R. P. Clausen, J. R. Greenwood, T. N. Johansen, D. S. Pickering, B. Nielsen, B. Ebert and P. Krogsgaard-Larsen, *J. Med. Chem.*, 2005, **48**, 3438–3442.

18 J. G. Petersen, R. Bergmann, H. A. Møller, C. G. Jørgensen, B. Nielsen, J. Kehler, K. Frydenvang, J. Kristensen, T. Balle, A. A. Jensen, U. Kristiansen and B. Frølund, *J. Med. Chem.*, 2013, **56**, 993–1006.

19 T. A. Oster and T. M. Harris, *J. Org. Chem.*, 1983, **48**, 4307–4311.

20 T. Ritter, T. Furuya and P. Tang, *WO2010/59943 A2*, 2010.

Appendix 1.1-Crystallographic information for (101)

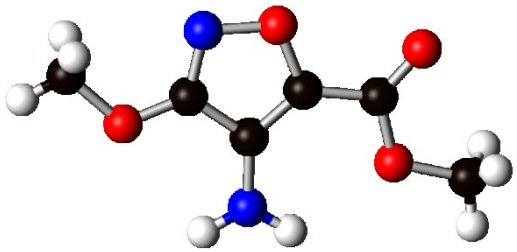

	mmdh7 (101)
Formula	$C_6H_8N_2O_4$
Molecular weight	172.14
Crystal description	Colourless prism
Crystal dimensions (mm)	0.27×0.06×0.06
Crystal system	Monoclinic
Space group	$P2_1/c$
a (Å)	7.0425(18)
b (Å)	11.555(3)
c (Å)	9.654(2)
α (°)	
β (°)	106.629(6)
γ (°)	
Volume (Å^3)	752.7(3)
Z	4
Calculated density (g cm^{-3})	1.519
Temperature (K)	173
μ (mm^{-1})	0.129
F(000)	360
Reflections collected	9048
Unique reflections (R_{int})	1388 (0.0511)
Max./min. transmission	0.992, 0.695
R_1, wR_2 [I>2σ(I)]	0.0300, 0.0813
R_1, wR_2 (all data)	0.0345, 0.0833
Goodness of fit	1.086
Data/restraints/parameters	1388/2/119
Max. difference peak/hole (e A^{-3})	0.17, -0.20

Appendix 1.2-Crystallographic information for (105)

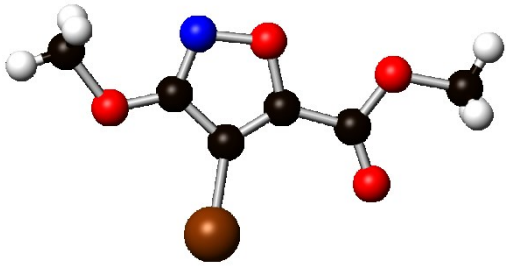

	mmdh1 (105)
Formula	$C_6H_6BrNO_4$
Molecular weight	236.03
Crystal description	Colourless platelet
Crystal dimensions (mm)	0.17×0.03×0.01
Crystal system	Monoclinic
Space group	$P2_1/n$
a (Å)	3.9658(10)
b (Å)	15.912(4)
c (Å)	12.881(3)
α (°)	
β (°)	94.979(7)
γ (°)	
Volume (Å^3)	809.8(3)
Z	4
Calculated density (g cm^{-3})	1.936
Temperature (K)	173
μ (mm^{-1})	5.064
F(000)	464
Reflections collected	8194
Unique reflections (R_{int})	1468 (0.1382)
Max./min. transmission	0.951, 0.457
R_1, wR_2 [I>2σ(I)]	0.0605, 0.1401
R_1, wR_2 (all data)	0.0826, 0.1505
Goodness of fit	0.925
Data/restraints/parameters	1468/0/111
Max. difference peak/hole (e A^{-3})	1.49, -0.83

Appendix 1.3-Crystallographic information for (107)

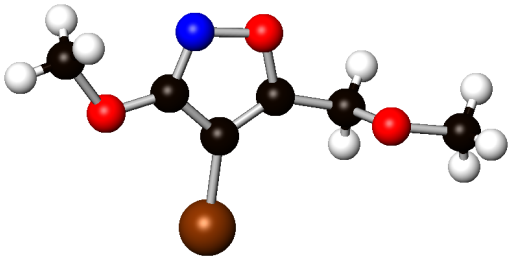

	mmdh5 (107)
Formula	$C_6H_8BrNO_3$
Molecular weight	222.04
Crystal description	Colourless prism
Crystal dimensions (mm)	0.06×0.06×0.04
Crystal system	Orthorhombic
Space group	$P2_12_12_1$
a (Å)	4.0901(5)
b (Å)	7.0548(10)
c (Å)	28.194(4)
α (°)	
β (°)	
γ (°)	
Volume (Å^3)	813.53(19)
Z	4
Calculated density (g cm^{-3})	1.813
Temperature (K)	173
μ (mm^{-1})	5.025
F(000)	440
Reflections collected	9749
Unique reflections (R_{int})	1489 (0.0580)
Max./min. transmission	0.818, 0.602
R_1, wR_2 [I>2σ(I)]	0.0233, 0.0549
R_1, wR_2 (all data)	0.0249, 0.0551
Goodness of fit	0.976
Data/restraints/parameters	1489/0/102
Max. difference peak/hole (e A^{-3})	0.73, -0.22

Appendix 1.4-Crystallographic information for (108)

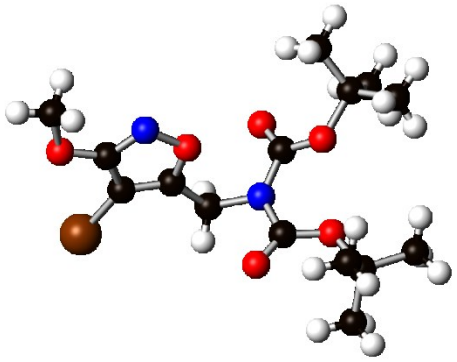

	mmdh14 (108)
Formula	$C_{15}H_{23}BrN_2O_6$
Molecular weight	407.26
Crystal description	Colourless platelet
Crystal dimensions (mm)	0.18×0.09×0.02
Crystal system	Monoclinic
Space group	$P2_1/c$
a (Å)	11.3612(13)
b (Å)	9.2489(11)
c (Å)	18.561(2)
α (°)	
β (°)	97.991(3)
γ (°)	
Volume (Å^3)	1931.4(4)
Z	4
Calculated density (g cm^{-3})	1.400
Temperature (K)	173
μ (mm^{-1})	2.164
F(000)	840
Reflections collected	23120
Unique reflections (R_{int})	3536 (0.0246)
Max./min. transmission	0.958, 0.830
R_1, wR_2 [I>2σ(I)]	0.0255, 0.0620
R_1, wR_2 (all data)	0.0315, 0.0648
Goodness of fit	1.019
Data/restraints/parameters	3536/0/224
Max. difference peak/hole (e A^{-3})	0.36, -0.37

Appendix 1.5-Crystallographic information for (120)

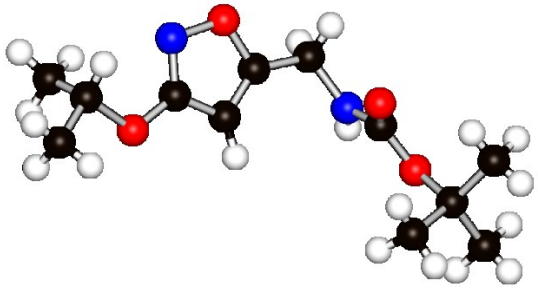

	mmdh17 (120)
Formula	$C_{12}H_{20}N_2O_4$
Molecular weight	256.30
Crystal description	Colourless chip
Crystal dimensions (mm)	0.04×0.04×0.02
Crystal system	Orthorhombic
Space group	*Pbcn*
a (Å)	14.177(12)
b (Å)	8.920(8)
c (Å)	22.562(19)
α (°)	
β (°)	
γ (°)	
Volume (Å^3)	2853(4)
Z	8
Calculated density (g cm^{-3})	1.193
Temperature (K)	173
μ (mm^{-1})	0.090
F(000)	1104
Reflections collected	32287
Unique reflections (R_{int})	2606 (0.6336)
Max./min. transmission	0.998, 0.515
R_1, wR_2 [I>2σ(I)]	0.0926, 0.0953
R_1, wR_2 (all data)	0.1442, 0.3157
Goodness of fit	1.065
Data/restraints/parameters	2606/19/187
Max. difference peak/hole (e A^{-3})	0.21, -0.19

Appendix 1.6-Crystallographic information for (121)

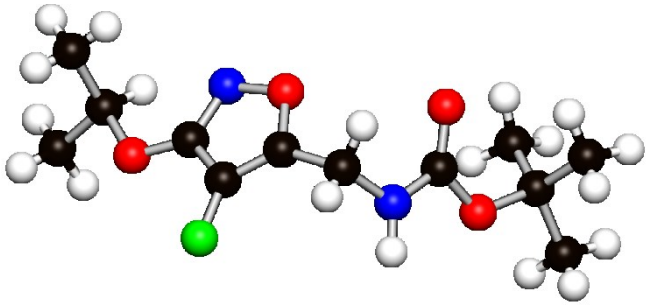

	mmdh20 (121)
Formula	$C_{12}H_{19}FN_2O_4$
Molecular weight	274.29
Crystal description	Colourless platelet
Crystal dimensions (mm)	0.17×0.07×0.01
Crystal system	Monoclinic
Space group	$P2_1/c$
a (Å)	29.944(18)
b (Å)	9.572(6)
c (Å)	9.989(6)
α (°)	
β (°)	99.228(12)
γ (°)	
Volume (Å^3)	2826(3)
Z	8
Calculated density (g cm^{-3})	1.289
Temperature (K)	173
μ (mm^{-1})	0.105
F(000)	1168
Reflections collected	43304
Unique reflections (R_{int})	5154 (0.3362)
Max./min. transmission	0.999, 0.796
R_1, wR_2 [I>2σ(I)]	0.1049, 0.1219
R_1, wR_2 (all data)	0.3055, 0.1761
Goodness of fit	1.040
Data/restraints/parameters	5154/2/361
Max. difference peak/hole (e A^{-3})	0.24, -0.23

Appendix 1.7-Crystallographic information for (122)

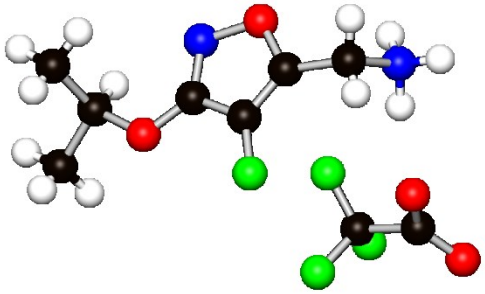

	mmdh23 (122)
Formula	$C_9H_{12}F_4N_2O_4$
Molecular weight	288.20
Crystal description	Colourless platelet
Crystal dimensions (mm)	0.05×0.05×0.01
Crystal system	Monoclinic
Space group	$P2_1/c$
a (Å)	12.7513(10)
b (Å)	10.6475(5)
c (Å)	10.3803(8)
α (°)	
β (°)	112.145(9)
γ (°)	
Volume (Å^3)	1305.37(18)
Z	4
Calculated density (g cm^{-3})	1.466
Temperature (K)	125
μ (mm^{-1})	1.342
F(000)	592
Reflections collected	14808
Unique reflections (R_{int})	2669 (0.0678)
Max./min. transmission	0.987, 0.536
R_1, wR_2 [I>2σ(I)]	0.0571, 0.1846
R_1, wR_2 (all data)	0.0671, 0.2025
Goodness of fit	0.830
Data/restraints/parameters	2669/3/184
Max. difference peak/hole (e A^{-3})	0.19, -0.33

Appendix 1.8-Crystallographic information for (64)

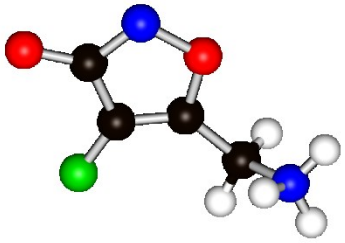

	mmdh24 (64)
Formula	$C_4H_5FN_2O_2$
Molecular weight	132.09
Crystal description	Colourless prism
Crystal dimensions (mm)	0.12×0.03×0.02
Crystal system	Monoclinic
Space group	$P2_1/n$
a (Å)	6.8563(18)
b (Å)	6.6807(13)
c (Å)	10.937(3)
α (°)	
β (°)	92.905(7)
γ (°)	
Volume (Å^3)	500.3(2)
Z	4
Calculated density (g cm^{-3})	1.754
Temperature (K)	173
μ (mm^{-1})	0.164
F(000)	272
Reflections collected	5826
Unique reflections (R_{int})	913 (0.0250)
Max./min. transmission	0.997, 0.930
R_1, wR_2 [I>2σ(I)]	0.0301, 0.0807
R_1, wR_2 (all data)	0.0354, 0.0844
Goodness of fit	1.066
Data/restraints/parameters	913/3/94
Max. difference peak/hole (e A^{-3})	0.27, -0.20

Appendix 1.9-Crystallographic information for (135)

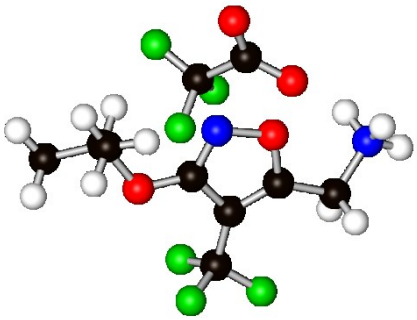

	mmdh26 (135)
Formula	$C_{10}H_{12}F_6N_2O_4$
Molecular weight	338.21
Crystal description	Colourless platelet
Crystal dimensions (mm)	0.16×0.12×0.02
Crystal system	Monoclinic
Space group	$P2_1/c$
a (Å)	17.240(4)
b (Å)	10.355(2)
c (Å)	7.9889(17)
α (°)	
β (°)	101.840(6)
γ (°)	
Volume (Å^3)	1395.8(5)
Z	4
Calculated density (g cm^{-3})	1.609
Temperature (K)	173
μ (mm^{-1})	0.172
F(000)	688
Reflections collected	16782
Unique reflections (R_{int})	2552 (0.0896)
Max./min. transmission	0.997, 0.833
R_1, wR_2 [I>2σ(I)]	0.0473, 0.0768
R_1, wR_2 (all data)	0.1056, 0.0958
Goodness of fit	1.035
Data/restraints/parameters	2554/3/213
Max. difference peak/hole (e A^{-3})	0.21, -0.22

Appendix 1.10-Crystallographic information for (166)

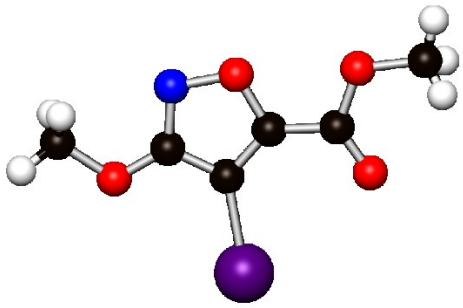

	mmdh2 (166)
Formula	$C_6H_6INO_4$
Molecular weight	283.02
Crystal description	Colourless platelet
Crystal dimensions (mm)	0.21×0.12×0.02
Crystal system	Monoclinic
Space group	$P2_1/n$
a (Å)	4.1252(13)
b (Å)	15.712(4)
c (Å)	13.231(4)
α (°)	
β (°)	95.941(9)
γ (°)	
Volume (Å^3)	853.0(4)
Z	4
Calculated density (g cm^{-3})	2.204
Temperature (K)	173
μ (mm^{-1})	3.731
F(000)	536
Reflections collected	9717
Unique reflections (R_{int})	1549 (0.1853)
Max./min. transmission	0.928, 0.181
R_1, wR_2 [I>2σ(I)]	0.0964, 0.2438
R_1, wR_2 (all data)	0.1131, 0.2514
Goodness of fit	0.985
Data/restraints/parameters	1549/0/112
Max. difference peak/hole (e A^{-3})	3.89, -1.97

Appendix 1.11-Crystallographic information for (171)

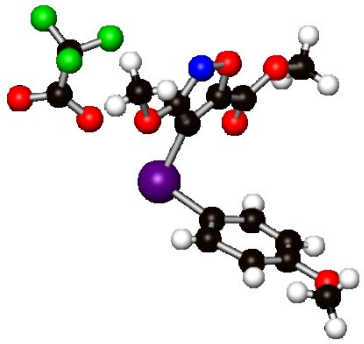

	mmdh10 (171)
Formula	$C_{15}H_{13}F_3INO_7$
Molecular weight	503.17
Crystal description	Colourless platelet
Crystal dimensions (mm)	0.16×0.03×0.01
Crystal system	Triclinic
Space group	$P\bar{1}$
a (Å)	8.436(2)
b (Å)	10.750(3)
c (Å)	11.338(3)
α (°)	113.913(5)
β (°)	97.392(4)
γ (°)	98.975(5)
Volume (Å^3)	907.2(4)
Z	2
Calculated density (g cm^{-3})	1.842
Temperature (K)	173
μ (mm^{-1})	1.833
F(000)	492
Reflections collected	11079
Unique reflections (R_{int})	3270 (0.0528)
Max./min. transmission	0.982, 0.862
R_1, wR_2 [I>2σ(I)]	0.0602, 0.1317
R_1, wR_2 (all data)	0.0925, 0.1456
Goodness of fit	1.045
Data/restraints/parameters	3270/0/246
Max. difference peak/hole (e A^{-3})	1.49, -0.66

Appendix 1.12-Crystallographic information for (173)

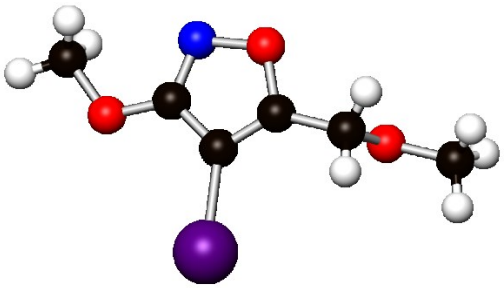

	mmdh11 (173)
Formula	$C_6H_8INO_3$
Molecular weight	269.04
Crystal description	Colourless platelet
Crystal dimensions (mm)	0.12×0.04×0.01
Crystal system	Orthorhombic
Space group	$P2_12_12_1$
a (Å)	4.1851(10)
b (Å)	7.2364(19)
c (Å)	28.331(8)
α (°)	
β (°)	
γ (°)	
Volume (Å^3)	858.0(4)
Z	4
Calculated density (g cm^{-3})	2.083
Temperature (K)	173
μ (mm^{-1})	3.694
F(000)	512
Reflections collected	13556
Unique reflections (R_{int})	1560 (0.1144)
Max./min. transmission	0.964, 0.629
R_1, wR_2 [I>2σ(I)]	0.0657, 0.1427
R_1, wR_2 (all data)	0.0833, 0.1498
Goodness of fit	1.103
Data/restraints/parameters	1560/0/102
Max. difference peak/hole (e A^{-3})	1.99, -0.78